# The Role of the Group Environment in Galaxy Evolution

by

Sean Liam McGee

A thesis
presented to the University of Waterloo
in fulfillment of the
thesis requirement for the degree of
Doctor of Philosophy
in
Physics

Waterloo, Ontario, Canada, 2010

I hereby declare that I am the sole author of this thesis. This is a true copy of the thesis, including any required final revisions, as accepted by my examiners.

I understand that my thesis may be made electronically available to the public.

**Abstract**

The majority of typically sized galaxies in the local Universe reside in a common dark matter halo with other similar galaxies known as a galaxy group. However, this was not always the case. Nine billion years ago, when the universe was one third its current age, these galaxies were almost exclusively the only massive galaxy in their dark matter haloes. In this thesis, I use both observational and theoretical methods to attempt to understand the effect these galaxy groups have on the evolution of galaxy properties.

I examine the morphological and star formation properties of galaxies in redshift selected samples of galaxy groups at two redshift epochs, z=0 and z=0.4. Galaxy groups contain fewer disk galaxies, as determined by quantitative morphology measures, than similar luminosity field galaxies at both redshift epochs. Furthermore, the difference, at fixed luminosity, grows from 6% at z=0.4 to 19% at z=0. The fraction of passive galaxies, as determined from spectral energy distribution fitting of UV and optical photometry, shows similar behaviour. However, at neither redshift do we find that the disk dominated and star forming galaxies in groups have properties which are significantly different from those in the field. The disks in both environments show similar scaling relations and similar distributions of asymmetry. While both group and field star forming galaxies have similar average star formation rates at fixed stellar mass and redshift. These results argue in favor of a relatively gentle physical mechanism of transformation, like strangulation, which removes the hot halo of a galaxy as it falls into a more massive halo.

I use a semi-analytic galaxy formation to understand the accretion histories of galaxies which reside in galaxy groups and clusters at different redshift epochs. The use of a simple model for environmental effects finds that the evolution seen in our observations of passive galaxies can be explained if a galaxy becomes passive 3 Gyrs after falling into a dark matter halo which has a mass of greater than $10^{13}$ $M_{\odot}$.

Finally, I use two novel methods for exploring how diffuse stellar mass and dust is distributed in and around galaxy groups. These are important probes of the environmental influence on galaxy evolution. By correlating the positions of hostless type Ia supernovae with galaxy groups, I find that as much as half of a galaxy's stellar mass is in a diffuse form outside of galaxies. These means that processes which shred or harass galaxies must be particularly strong in the group environment. I also find that dust is destroyed by the hot gas contained within groups and clusters. Dust is a necessary component of star formation,

and its destruction could be an additional mechanism to suppress the production of stars in galaxy groups.

**Acknowledgements**

I would like to thank my supervisor, Michael Balogh, for his guidance and support through the past five years. His unique ability to instill confidence, along with his unwavering open door, have been a huge benefit both personally and professionally. I have had a great time working with him and hope to continue to do so.

I have been fortunate to have a great group of eager collaborators. David Wilman deserves special mention both for immediately accepting me as a collaborator and for his enthusiasm. I would also like to thank the rest of the GEEC team; Richard Bower, John Mulchaey, Gus Oemler, Laura Parker, Alexis Finoguenov, Jen Connelly, Krystal Tyler and George Rieke. Each have made a distinct impression on me about what it means to be a researcher and a collaborator. I have also enjoyed my collaborations with Andreea Font, Ian McCarthy and David Gilbank. I would like to thank James Taylor, Mike Hudson, Mike Waite, James Sloan and Luc Simard for serving on my PhD committee and for advice at various stages of my research.

Thanks to Louise Edwards, who has been a collaborator and a friend for a long time. It is through her that I was exposed to astrophysics research, an experience which lead me to attempt it myself. The students of the Physics and Astronomy Department have made this journey enjoyable. In particular, I'd like to thank Ting Lu, who shared every step from the note-taking days of the third floor to the postdoc job search. The various inhabitants of 208B made every day interesting, especially Steve Allanson, Chad Greene, and Mike Hillier. I've enjoyed getting to know Clif Kirkpatrick, Carolyn McCoey, Farbod Kamiab, Farnoud Kazemzadeh, Brad Krane and Grant Salton. While not purely academic, I'd also like to thank the motley crew of Roslin Avenue and CLV, Chess Records, McGinnis and the Schwebs Acoustic Duo.

To my parents, thanks are not enough. Their ability to be proud and supportive while always maintaining that my happiness is most important is awe-inspiring. It is not hard to see this thesis as the natural extension of light pollution experiments with Dad, or the math problems set by Mom. Their love of learning, reading and thinking have affected my life in the most profound way. Thanks for being amazing parents. Thanks to Danny, who has been an inspiration for so long, our conversations through the years have been a keystone for me. Also, to both Danny and Jill, thanks for all the support, especially in the first years in Halifax. Sincere thanks to Sharon and Gary, and Trudy and Mike for making

their respective cities feel like home. As always, thanks to Gunnar and Riley for, among other things, reminding me that sometimes you just have to frap.

And to Abbey, Hannah and Mya, who have only known me as a graduate student, and who have, on occasion, asked an important question: 'Why are you still in school?' Hopefully, this thesis is an appropriate response.

## Dedication

This thesis is dedicated to my grandparents, Annie & Angus Dan McGee and Araminta & Harold Crossman.

# Contents

# List of Tables

# List of Figures

# Chapter 1

# Introduction

Our understanding of what the Universe is made of and how it evolves has been revolutionized within the past 20 years. Extraordinary advances in probing the cosmic microwave background, large scale galaxy clustering and recessional velocity of "standard candle" supernovae have led to a model of our Universe called the Concordance Model. In this model, also known as a $\Lambda$ Cold Dark Matter ($\Lambda$CDM ) universe, the energy/mass density of the Universe roughly consists of 5% baryons, 25 % cold dark matter and 70 % dark energy (Riess et al., 1998; Perlmutter et al., 1999; Tegmark et al., 2004; Komatsu et al., 2009).

Over the same timescale, new observational techniques and instruments have allowed a characterization of the build-up of stellar mass within galaxies from a time of 2 billion years after the Big Bang until today. It appears that the star formation rate density of the universe, a fundamental measure of how quickly galaxies form, varies greatly over this time. It rises gradually to a peak of activity at redshift of $\sim 1$ or 2 and declines by a factor of 10 to the present day (Lilly et al., 1996; Madau et al., 1996; Hopkins, 2004; Bouwens et al., 2009).

Far from being a static universe, the cosmos is constantly evolving. Understanding the nature and causes of this evolution and how it relates to the structure of the Universe is a fundamental goal of modern astronomy. It is only with the dual advances in cosmology and observations of galaxies that these questions can even be asked.

It is the purpose of this thesis to investigate how our understanding of the Universe and

its development with time affects the evolution of the galaxy population within. In this introduction, I will discuss what we know about the growth of structure in a ΛCDM universe and how we can select samples of massive dark matter haloes. I will then discuss observations which suggest that this structure does affect galaxies and finally I will introduce physical processes which may be causing this.

## 1.1 Growth of Structure

In the early universe, the typical perturbations in the mass density were very small, on the order of $10^{-5}$ of the size of the background density. Through gravitational interaction, as the Universe ages, these small perturbations grow in size. Eventually these perturbations become large enough that the matter within collapses into a well defined dark matter halo. Baryonic material falls into these dark matter haloes and begins to cool. This cooling material becomes unstable and fragments to form stars into centrally concentrated galaxies.

In some locations, the resulting gravitational attraction grows so large that other dark matter haloes are attracted towards it. Numerical simulations, and some observations, suggest that dark matter haloes are attracted into filaments which are gradually drained into central nodes. These nodes contain the remnants of multiple dark matter halos and their galaxies, which eventually virialize into larger haloes. When a halo contains a mass above $\sim 10^{12}$-$10^{13}$ $h^{-1}$ $M_\odot$_it is called a group, owing to its appearance as a group of luminous galaxies. More massive collections of matter, above $\sim 10^{14}$ $h^{-1}$ $M_\odot$, are called clusters of galaxies.

Assuming that our model for the Universe is correct, the growth and evolution of these dense environments, groups and clusters, is very well determined. Analytic models, such as extended Press-Schecter and Sheth-Tormen formalisms, largely agree with N-body simulations about the mass function of halos and its evolution with redshift (Press & Schechter, 1974; Lacey & Cole, 1993; Bower, 1991; Sheth & Tormen, 2002; Jenkins et al., 2001; Warren et al., 2006).

Figure 1.1 shows the halo mass function as determined by the extended Press-Schecter formalism (Bower & Balogh, 2004). This figure shows the cumulative fraction of the mass of the universe which is in haloes of a given mass and above. Importantly, this figure shows

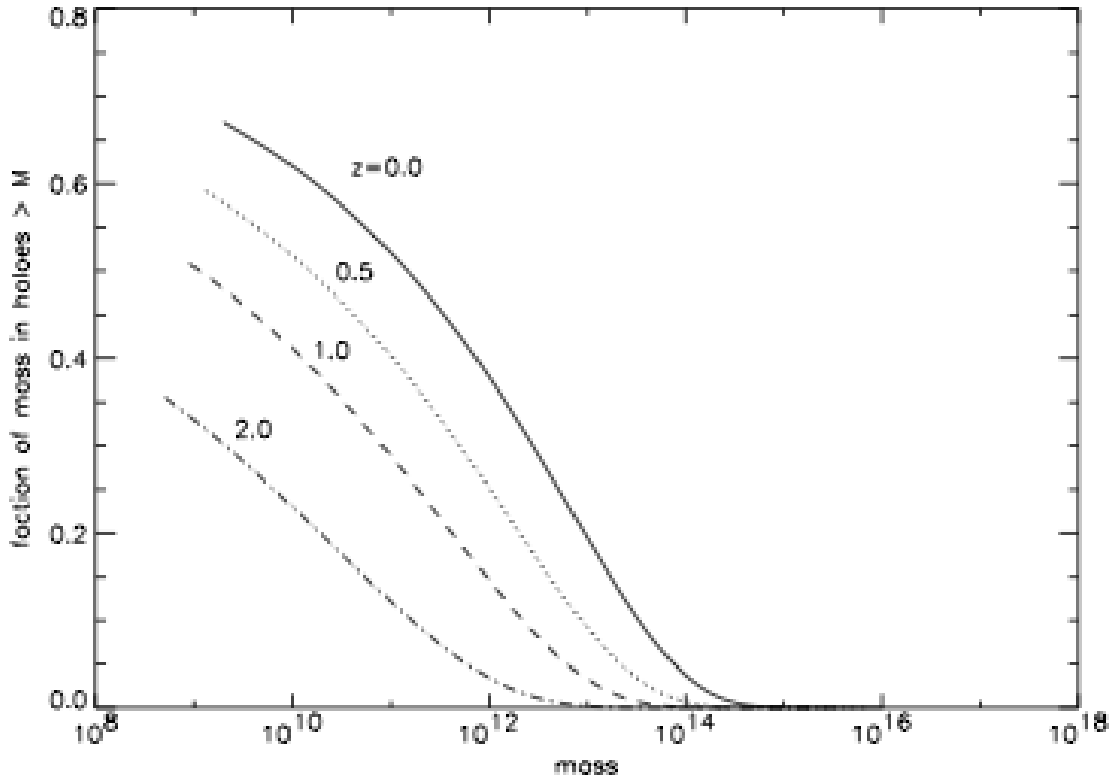


Figure 1.1: The cumulative fraction of mass in dark matter haloes of a given mass as a function of halo mass. This is shown for four different redshift epochs. Between z=0.5 and z=0, the fraction of mass in group haloes almost doubles. (Adapted from Bower & Balogh (2004))

that the fraction of mass within group sized haloes almost doubles between redshift 0.5 and 0, while at redshift 2 there is a negligible fraction of mass in these haloes. Evidently, galaxy groups are not a static entity, but grow hierarchically with time.

Figure 1.1 also shows that the fraction of mass in galaxy clusters is never more than $\sim$ 5% at any epoch. In other words, the galaxies within galaxy clusters are a small percentage of the total population. In contrast, galaxy groups contain $\sim$ 40-50 % of the total mass of the universe at z=0. Thus, the influence of groups is expected to be a fundamental piece of how galaxies form and evolve.

## 1.2 Selection of environment

As the largest gravitationally bound structures in the Universe, galaxy groups and clusters have been the subject of intense study for many years. The principal components of galaxy clusters and groups are dark matter and baryons. As in the rest of the Universe, dark matter makes up the majority of the mass of both clusters and groups. The baryons are largely in the form of hot gas, galaxies, dust and intragroup, or intracluster, stellar mass. The baryon to total mass ratio ($f_{\rm B}$) in galaxy clusters is thought to be equal to the universal value of $\sim$ 17% (Spergel et al., 2007; White et al., 1993; McCarthy et al., 2007). Although still a matter of debate, galaxy groups may have a lower $f_{\rm B}$ owing to their smaller potential wells, which may allow AGN or other heating processes to eject gas outside the group (Bower et al., 2008).

The majority of the baryons in a cluster are in the form of hot gas. This gas is heated to the virial temperature of the halo upon infall. The stellar mass in galaxy groups and clusters is expected to be in the range of 2 to 6% of the total mass of the halo (Gonzalez et al., 2007). These values are somewhat controversial (eg. Balogh et al., 2008), partly because of the difficulty in measuring the stars which reside outside the galaxies, ie. within the intragroup medium.

There are many ways to select samples of galaxy groups or clusters for study. For galaxy formation and evolution studies, the ideal method would be to select a sample based only on system mass. In this way we would be certain that results for the selected sample could be extended to the population of groups and clusters in the Universe as a

whole. Unfortunately, there is no clear method yet for achieving this. Some of the more common methods, along with their drawbacks, are:

- **Optical galaxy overdensity:** The first samples of galaxy clusters were discovered by visual examination of photographic plates (Abell, 1958). These methods have evolved, so that they no longer rely on visual examination, but rather detailed numerical methods. In addition, this may involve the pre-selection of 'red' galaxies, which form a tight sequence and thus increase the contrast with the background (Gladders & Yee, 2000). The optical overdensity is likely a real tracer of the system mass, although with a large scatter (Rykoff et al., 2008b; Becker et al., 2007). However, for galaxy groups of the type studied in this thesis, only the most concentrated and those with the most bright galaxies would be found using current observational limitations without also introducing many spurious groups. This may be a major problem for galaxy evolution studies as a high concentration and high abundance of bright galaxies may lead to a sample biased towards relaxed dynamical states, or older formation ages, of the group (Smith & Taylor, 2008; Dariush et al., 2010). This method may be able to produce unbiased measurements of samples with extremely large surveys, and techniques which account for this bias.

- **X-ray emission:** As mentioned above, galaxy clusters are filled with hot gas which has been shock heated to the cluster virial temperature on infall. Because this hot plasma emits radiation in the X-ray, surveys of the sky with X-ray telescopes can lead to a sample of clusters. This is a very effective method for finding clusters, however, the X-ray properties of galaxy groups are wildly varying (Rasmussen et al., 2006). X-rays can only be effectively observed from space. Because of this, observations in the X-ray are difficult to obtain in large quantities. We are only beginning to accumulate data in blank fields to sufficient depth which may find large samples of unbiased galaxy groups (Finoguenov et al., 2009). A primary concern of this method is that x-ray emission is a tracer of the density and temperature of a group. A sample of only the most dense galaxy groups could overestimate the efficiency of environmental effects.

- **Gravitational lensing:** Light moves through straight paths in space-time, or rather, on smooth geodesics. However, because space-time is warped by mass, light can appear to bend around massive structures like galaxy groups and clusters. Viewed

from the right angle, light from a background galaxy can be bent into a large arc in the sky. The appearance of these large arcs can be visually striking and thus identified in photometric surveys (Cabanac et al., 2007). The radius of the circle from which the arc is a segment correlates with the mass within it, and thus can be a useful probe of the dark matter. This type of lensing, 'strong lensing', has been used in limited cases to identify previously unknown galaxy groups (Momcheva et al., 2006; Thanjavur et al., 2010). However, on average, this will produce a sample of galaxy groups which are more concentrated than the typical galaxy groups (Broadhurst et al., 2005; Oguri et al., 2009).

A second way of selecting groups and clusters using gravitational lensing is through weak lensing surveys. Detections of sheared background galaxies could lead to the identification of mass-selected clusters. There have been successfully detected clusters via shear alone (Wittman et al., 2001; Hetterscheidt et al., 2005; Miyazaki et al., 2007). However, this requires very high quality data, which has so far limited the size of these surveys. Additionally, this detection method is sensitive to the entire line of sight mass overdensity, so extension into the halo mass range of galaxy groups may result in primarily detecting projected structure rather than true halos.

- **Sunyaev-Zel'dovich Effect:** The Sunyaev-Zel'dovich (SZ) effect is caused by the interaction of energetic electrons with the photons of the cosmic microwave background (CMB) (Sunyaev & Zeldovich, 1972). The electron boosts the energy of the CMB photon via inverse Compton scattering. Galaxy clusters, as they contain lots of high energy electrons, create a significant thermal SZ effect. This boost of energy, and thus frequency, allows radio telescopes to efficiently search for SZ influenced CMB photons. This selection method is mainly sensitive to the quantity and energetics of free electrons (density and temperature), as opposed to x-ray emission, which is sensitive to the square of the density. And thus, it could be a very useful technique as it is independent of redshift for the same gas properties. Large surveys searching for these SZ clusters are currently being done with the goal of making cosmological measurements (Staniszewski et al., 2009). Unfortunately, the signal of SZ may be significantly hindered by the background before reaching the sensitivity to needed to detect typical galaxy groups (Holder et al., 2007).

- **Redshift surveys:** One of the most common methods currently being used is to

search for overdensities in spectroscopic redshift surveys. Large surveys such as SDSS and 2dF have made this an extremely efficient technique (Eke et al., 2004; Miller et al., 2005; Yang et al., 2007). Accurate spectroscopic redshifts allow for essentially a 3-dimensional search for galaxy overdensities. Although this is not a perfect method, largely because the high velocities of galaxies in groups and clusters leads to a loss of precision of the position in the line of sight. This makes it difficult to separate galaxies in the foreground or background of the cluster from true members and leads to 'contamination' such that 15-20% of so-called cluster and group members actually reside outside the virial radius (Berlind et al., 2006; McGee et al., 2008). However, when the goal is galaxy evolution studies, all of the previous methods require spectroscopic follow-up to determine galaxy membership and suffer from the same problems. For these reasons, for studies of galaxy groups, this is currently the most effective and unbiased method of selection. In this thesis, I only use galaxy groups and clusters selected in redshift space. This is expected to allow an extrapolation of our results to galaxy groups as a whole.

## 1.3 Galaxy properties of the local Universe

Extraordinary progress has been made in understanding the distribution of galaxy properties in the low redshift universe. In particular, we have come to understand that the mass (both stellar and gas), star formation rate, morphology and dust are the key parameters of galaxy formation and evolution. Despite the large number of possible combinations of these parameters, in broad terms, galaxies in the local universe belong to one of two classes. One class, often called late types, are actively forming stars, have a strong disk component with large amounts of dust and cold HI gas and tend to be less massive than the other class. Due to their young stellar population, late types emit most of their visual light in the blue part of the spectrum. On the contrary, the other class, known as early types, have essentially stopped forming stars and appear spherical or ellipsoidal in shape. They also tend to be massive, dust poor and contain little cold gas. These galaxies are red, because of their old stellar population (Humason, 1936; Strateva et al., 2001).

In Figure 1.2, we show a compilation of galaxy properties from Blanton & Moustakas (2009). These show the distribution of galaxy types as a function of (a) $r$ band magnitude,

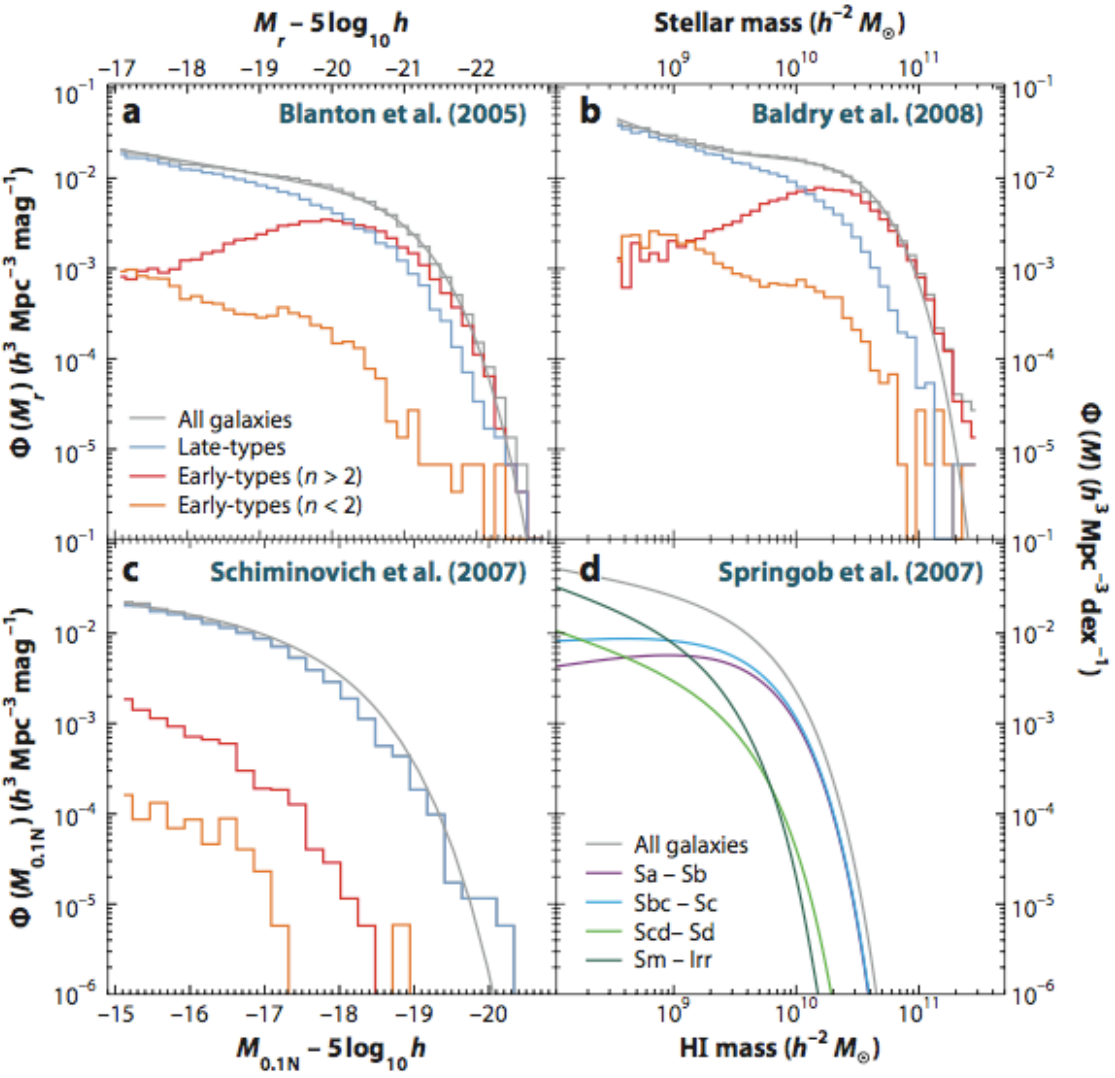


Figure 1.2: The distribution of different galaxy types as a function of (a) $r$ band luminosity, (b) stellar mass, (c) $NUV$ luminosity and (d) HI mass. (Adapted from Blanton & Moustakas (2009))

(b) stellar mass, (c) near ultraviolet ($NUV$) luminosity and (d) HI mass. In panels (a), (b) and (c), the late type galaxies are defined as any galaxies with ongoing star formation, while the remaining two types are both non-star forming galaxies which are divided by the sersic index, a measure of how concentrated the galaxy light is. In panel (d) the galaxy types are different types of disk galaxy, going from most disk-like to disk and bulge combinations. This plot summarizes the main properties of the two classes. As we can see, early type galaxies dominate the demographics at large stellar mass, but this difference is not as large at high $r$ band luminosity. $r$ band luminosity is slightly sensitive to the recent star formation history of the galaxy, so it makes the late types brighter at fixed stellar mass. In panel (c), we see that the late types are by far the brightest galaxies in the $NUV$ band, because this is very sensitive to the light from young stars. Finally, the HI mass or the cold gas, which is a measure of the fuel which is available for future star formation, is completely dominated by late type galaxies.

The galaxies which have some properties of both classes are very important for understanding how these classes came to be. However, they are rare enough, that especially in early studies, they were essentially ignored. Thus, the fraction of spiral galaxies or the fraction of blue galaxies was assumed to be equivalent.

## 1.4 Environmental influence on galaxy formation

### 1.4.1 Historical observations

Much of the early thinking about the effect a galaxy's environment has on its properties was driven by a few key observations. While it is now apparent that these observations were complicated by many factors, they still contain a key trend which has proven to be important. There are three historical ideas which especially deserve attention.

(i) From the very first observations of "clusters and clouds" of galaxies, it was apparent that the shapes of the highly clustered galaxies were different from the galaxies that were weakly clustered (Zwicky, 1939, 1951). The central parts of clusters are rich in spherical, or elliptical galaxies, while the lower-density regions between the clusters are populated with spiral galaxies. In 1980, Dressler (1980) attempted to quantify this

trend by assembling a sample of photometric observations for 55 rich galaxy clusters in the low redshift universe ($z_{max} = 0.066$). Dressler quantified the local environment by using the projected number density of galaxies around a given galaxy. Using this metric, he found that the elliptical and S0 fraction strongly increased and the spiral and irregular fraction decreased with increasing density. Thus, galaxies at least show a correlation between morphology and environment.

(ii) Several studies, beginning with Oemler (1974), have shown that the galaxy population depends on the type of host galaxy cluster. Oemler divided a sample of 15 rich clusters into spiral-rich, spiral-poor and cD-dominated classes. The cD-dominated clusters were rich in ellipticals, highly concentrated and had spherical galaxy distributions. The spiral-poor clusters, which were dominated by S0 galaxies, were slightly less concentrated, but still maintained a spherical galaxy distribution. In contrast, the spiral-rich clusters had irregular galaxy distributions and were not centrally concentrated. One interpretation of this is that the clusters represent an evolutionary sequence, and the spiral-rich clusters will eventually relax into cD or spiral-poor clusters, thereby also necessitating a transformation in the galaxies. This is evidence that the accretion history of galaxies plays an important role in their evolution.

(iii) A revolutionary discovery was made in 1978 by Harvey Butcher and Augustus Oemler. They found that the fraction of blue galaxies in two rich clusters at intermediate redshift, C1 0024+1645 (z=0.39) and 3C 295 (z=0.46), was significantly higher than in a similar sample of low redshift clusters (Butcher & Oemler, 1978a,b). In other words, the galaxy content of clusters changes with cosmic time.

Although these observations have existed for some time now, the physical origin of these correlations are still largely uncertain.

### 1.4.2 A modern perspective

With more systematic study of galaxy evolution, it has become apparent that there are at least three key factors which determine a galaxy's properties. As we have discussed, the environment and the redshift of the galaxy are important aspects. However, the galaxy's own stellar mass is also plays a key role in determining the galaxy's properties.

Part of the reason that the historical observations are difficult to interpret is likely that essentially all early studies of galaxy environments were mixing several effects. It is now known that galaxy clusters have different stellar mass functions than the general field (Balogh et al., 2001; Lin et al., 2004). It is also known that there are significant morphological trends with the stellar mass of the galaxy regardless of the environment (e.g. Allen et al., 2006; Bamford et al., 2009). Thereby comparing morphologies as a function of density without removing the stellar mass difference naturally leads to a correlation.

The observation that dense environments have different stellar mass functions than the general field is interesting, but often not what we mean by an "environmental effect". In this thesis, we define an environmental effect as an active process which changes the properties of galaxies when compared to the field at fixed stellar mass and redshift. It is by studying this "differential" effect of galaxy environment that we hope to isolate the "transforming" galaxy population.

Accordingly, the key environmental effects which were known at the onset of this thesis are below.

(i) At low redshift, morphology at fixed stellar mass does show density dependence (Bamford et al., 2009; van der Wel et al., 2010). It is important to recall that the Dressler (1980) results were only for densities within clusters, while Postman & Geller (1984) had extended it to the group regime.

Morphology at higher redshift requires either space based imaging or adaptive optics. Both are difficult to obtain for large samples and thus the morphology trend has only been measured in clusters at higher redshift, where there is a weaker correlation.

(ii) Red fraction or passive fraction, at fixed stellar mass is elevated in groups and clusters when compared to the general field at low redshift (Weinmann et al., 2006a; Baldry et al., 2006; Kimm et al., 2009). These trend continues to higher redshift (at least to z$\sim$ 1.), but the difference between the dense environments and the field becomes smaller (Gerke et al., 2007; Balogh et al., 2009; Kovac et al., 2009).

(iii) Galaxy groups at low redshift seem to have early type galaxy fractions and passive fractions between those of clusters and those of the field (Hansen et al., 2007; Kimm et al., 2009). Therefore, since clusters are built at least partially from galaxy groups, environmental effects rely heavily on what occurs in galaxy groups.

The quantification of these correlations has been important, but ultimately has not lead to a definitive understanding of environment. One approach which is likely to aid our understanding is by studying the redshift evolution of typical galaxy groups. It is this approach which is the bulk of the thesis.

## 1.5 Physical processes in dense environments

Theoretical understanding of the possible mechanisms responsible for the observed environmental correlations is critical. While there are very many possible explanations, below I describe four of the most plausible and well-developed ideas.

### 1.5.1 Galaxy Mergers

A natural consequence of hierarchical structure formation is galaxy mergers. There are clear examples of galaxies which are undergoing interaction, or merging with each other (e.g. the Antennae Galaxies (NGC 4038/NGC 4039) or the Mice Galaxies (NGC 4676a/b)). However, much of the understanding of the timescales and transformational properties of mergers is drawn from numerical simulations. Early n-body simulations suggested that the merging of two spiral-like galaxies could produce ellipsoidal-like galaxies (Toomre & Toomre, 1972; Barnes & Hernquist, 1992).

The stars themselves are essentially collisionless because the distances between them are large compared to their own cross-section. However, the gas in the galaxies is compressed causing shock waves (Mihos & Hernquist, 1996; Barnes & Hernquist, 1996). This shocked gas may be driven towards the galaxy center, cool rapidly and undergo a burst of star formation. This may also fuel the central AGN, causing it to light up in a "quasar" mode and stifling future star formation (Kauffmann & Haehnelt, 2000; Hopkins et al., 2006).

There is no question that galaxy mergers are an important part of galaxy formation overall. Their ability to explain environmental correlations would require a substantial enhancement of the galaxy merger rate within dense environments. Theoretical models of dark matter evolution do find that the halo merger rate is enhanced in these environments (Gottlöber et al., 2001; Fakhouri & Ma, 2009). However, semi-analytic models which attempt to quantify the galaxy merger rate find that mergers do not occur frequently enough

in groups and clusters to explain environmental correlations (Bundy et al., 2009). Unfortunately, the actual galaxy merger rates in groups and clusters are difficult to determine observationally because of the higher fraction of chance superpositions (van Dokkum et al., 1999; Lin et al., 2010).

The role of galaxy mergers is also complicated by increasing theoretical suggestions that gas-rich mergers may actually reform into spiral galaxies (Hopkins et al., 2009; Stewart et al., 2009). However, observational evidence for such a process is rare (Hau et al., 2008; Kannappan et al., 2009). Nonetheless, perhaps the gas poor galaxies which inhabit dense environments leads to an increased efficiency of turning mergers into spheroidal galaxies. However, galaxy mergers become ineffective when the velocity difference of the colliding galaxies is larger than their internal velocity dispersions. Thus in galaxy clusters, colliding galaxies will not spiral together to form a final galaxy.

### 1.5.2 Galaxy Harassment

A high speed encounter between galaxies is unlikely to lead to a full merger. However, it does still lead to an impulsive heating event, often called 'galaxy harassment' (Moore et al., 1996). Repeated heating events, like those which may occur in galaxy groups or clusters may case a morphological transformation from a spiral into a spheroid (Moore et al., 1998).

The energy imparted during galaxy harassment is found, via the impulse approximation, to depend on the square of the perturbing mass, $m_{\rm perturb}$ (Spitzer, 1958). While the frequency of these heating events depends on density of perturbing galaxies (or subhaloes), $\rho_{\rm gal}$. Thus, the efficiency of galaxy harassment, $\xi_{\rm harass}$ can be expressed as

$$\xi_{\rm harass} \propto \rho_{\rm gal} m_{\rm perturb}^2 \tag{1.1}$$

If we assume that mass of the perturber, $m_{\rm perturb}$, is tidally limited then the mass varies linearly with the cluster radius ($m_{\rm perturb} \propto r_{\rm cluster}$). Meanwhile, the galaxy density, $\rho_{\rm gal}$ scales approximately as $r_{\rm cluster}^{-2}$. Therefore, the efficiency of galaxy harassment should be approximately independent of cluster/group radius. Unfortunately, radial trends in environmentally affected galaxies are observed (Balogh et al., 2000; Ellingson et al., 2001; Hansen et al., 2007).

### 1.5.3 Ram Pressure Stripping

As baryonic material falls into dark matter haloes it is thought to shock heat to the virial temperature of the halo. In small halos, this temperature is low enough that it can quickly cool into stars. However, in galaxy groups and clusters, the virial temperature is so high that it can not cool efficiently. Thus, galaxy clusters are filled with hot, dense and X-ray emitting gas (Forman et al., 1972; Cavaliere & Fusco-Femiano, 1976). As a galaxy falls into this massive cluster, it can experience a significant drag force from this intracluster medium (Gunn & Gott, 1972). If the drag force is great enough it may remove the cold gas from the infalling galaxy, and thus reduce the amount of possible future star formation (Abadi et al., 1999). While this scenario does not necessarily induce a morphological transformation, shutting off star formation within the disk may allow it to fade enough to appear as an S0 galaxy (Abraham et al., 1996; Quilis et al., 2000).

Observations of galaxies infalling into the Virgo and Coma clusters seems to support this process. Several galaxies appear to have truncated HI gas disks while maintaining undisturbed stellar disks (Kenney & Koopmann, 1999; Vollmer et al., 2004). In other galaxies, HI reveals extended tails apparently being dragged away from the host galaxy (Oosterloo & van Gorkom, 2005). There is also some evidence that gas being stripped from galaxies is forming stars in their wake, as seen by extended H$\alpha$ tails (Sun et al., 2007a). Despite this, definite examples of ram pressure stripping are still rare.

Ram pressure occurs when the restoring force per unit area of the infalling galaxy ($F_{res}/A$), is less than the pressure of the drag force from the intracluster medium $P_{drag}$. The restoring force is simply due to the self-gravity of the infalling galaxy disk, of the form

$$F_{\rm res}/A = C\Sigma_{\rm gas}\Sigma_{\rm stars} \tag{1.2}$$

where $\Sigma$ is the surface density of the gas or stars and $C$ is a constant. If we make the assumption that the gas and stars are distributed the same way throughout the disk, then $\Sigma_{gas} = f_{gas}\ \Sigma_{disk}$ and $\Sigma_{star} = f_{star}\ \Sigma_{disk}$. $f_{gas}$ is the fraction of the disk made of gas and $f_{star}$ is the fraction made of stars. Further, galaxy formation models suggest that the disk surface density is directly related to its total mass, $m$ such as $\Sigma_{disk} \propto m^{1/3}$. Thus, the restoring force is

$$F_{\rm res}/A = Cf_{\rm star}f_{\rm gas}\Sigma_{\rm disk}^2 = Cf_{\rm star}f_{\rm gas}m^{2/3} \tag{1.3}$$

The drag pressure, $P$, caused by the intracluster medium is proportional to the hot gas density, $\rho_{\rm hot}$ and the square of the relative velocity between the galaxy and the ICM, $V_{\rm orb}$. However, because halos at a given epoch have the same average density, the hot gas density is simply proportional to the fraction of hot gas, $f_{\rm hot}$.

$$P \propto \rho_{\rm hot} V_{\rm orb}^2 \propto f_{\rm hot} M^{2/3} \tag{1.4}$$

Therefore, at a given halo mass, ram pressure stripping is more likely to occur in less massive galaxies. As we have mentioned, this is in qualitative agreement with observations of galaxy clusters. However, in group scale halos, both $M$ and $f_{\rm hot}$ are lower which reduces the efficiency of ram pressure stripping in these environments.

### 1.5.4 Strangulation

The current star formation of a galaxy occurs from the fragmenting and collapse of cold gas held within it. However, it is also believed that isolated galaxies maintain a hot halo of gas (White & Rees, 1978; White & Frenk, 1991). This gas is thought to replenish the cold gas which is used in star formation and also gas which is heated from supernova feedback. Without this refueling of cold gas, a typical galaxy disk is only able to sustain star formation for a fraction of its life (Kennicutt, 1998).

As we have seen, ram pressure stripping of the cold gas of a galaxy is likely to become inefficient in group scale halos. However, the drag force from the intragroup medium may still be effective at removing this hot halo. This process is called "strangulation" and until recently, was the standard technique of dealing with environmental effects in semi-analytic galaxy formation models (Larson et al., 1980; Balogh et al., 2000; White & Frenk, 1991; Kauffmann et al., 1993).

Balogh et al. (2000) used n-body simulations to track the orbits of galaxies as they were accreted into and orbit within galaxy clusters. In their model, they assumed that galaxies are accreted into a group or cluster with the field rate of star formation and this star formation rate declines according to a Kennicutt Schmidt law, assuming no additional gas accretion. This model is an excellent match to radial gradient of star formation rates within observed clusters.

However, implementing this scheme into semi-analytic galaxy formation models found that the simulated fraction of passive galaxies was much too high in galaxy groups (Weinmann et al., 2006b; Gilbank & Balogh, 2008). This is because star formation within the hot halo-stripped galaxy caused additional gas, which was originally cold, to be ejected due to supernova feedback. In essence, completely stripping the hot halo of infalling galaxies actually leaves only a fraction of its cold gas for future star formation.

Subsequent numerical simulations showed that the infalling hot halo is not completely stripped (Kawata & Mulchaey, 2008; McCarthy et al., 2008b). This allows gas to be ejected but then recycled into the remaining hot halo and re-cool into the disk. X-ray observations suggest that these partially removed haloes do remain around cluster/group galaxies for some time (Sun et al., 2007b; Jeltema et al., 2008). Unfortunately, implementing this phenomenon into galaxy formation models introduces a large population of "green valley" galaxies not seen in observations (Font et al., 2008a; Balogh et al., 2009).

## 1.6 Outline and goals of the thesis

The general goal of these thesis is to shed light on the environmental processes which occur in galaxy groups. I will do this with a combination of theoretical and observational studies.

In Chapter 2, I use semi-analytic models of galaxy formation to attempt to understand how galaxies are accreted into groups and clusters. This is purely theoretical work and informs the remainder of the largely observational efforts of the rest of the thesis. We use simple models of environmental effects to produce the expected evolution of the general population.

In Chapters 3 and 4, I make a direct comparison of the morphology and star formation properties of group galaxies selected from two unbiased redshift surveys with the general field. By making this comparison at two epochs we directly probe the evolution of group galaxies.

In Chapter 5, I use a novel technique of correlating type Ia supernova with low redshift galaxy groups. Quantifying the number of hostless supernova allows a direct probe of the observationally difficult intragroup stellar mass. This is an important constraint on the processes of galaxy harassment and stripping which are likely to occur in groups.

In Chapter 6, I examine the effect of galaxy groups on the dust content of the universe. Dust is an important component in star formation and how it is distributed on large scales is a direct probe of its creation and destruction.

Chapters 2, 3, 5, and 6 represent largely unchanged versions of papers which were each published in the Monthly Notices of the Royal Astronomical Society (MNRAS), a refereed astronomical journal (McGee et al., 2009, 2008; McGee & Balogh, 2010a,b, respectively). The work which constitutes Chapter 4 will also be submitted to MNRAS in the near future.

The co-authors of the paper which resulted in Chapter 2 were Michael Balogh, Richard Bower, Andreaa Font and Ian McCarthy. As with all papers in this thesis, Michael Balogh provided ideas, inspiration and the 'first line of defense'. The remaining authors were key members in constructing the semi-analytic models used in the paper. The co-authors of the paper from Chapter 3 were Michael Balogh, Robert Henderson, David Wilman, Richard Bower, John Mulchaey and Augustus Oemler. All, except for Robert Henderson, are key members of the GEEC survey (known at the time as CNOC2 groups team), and will also be co-authors of the work resulting from Chapter 4. Each member was instrumental in obtaining the data and in processing the redshifts and photometry used in both chapters. Robert Henderson developed an algorithm, based on Allen et al. (2006), which determined if galaxies were fit with a pure bulge or disk, or both.

# Chapter 2

# The accretion of galaxies into groups and clusters

## 2.1 Introduction

In recent years, an extraordinary confluence of independent measurements of the cosmological parameters has resulted in the concordance model of the Universe ($\Lambda$CDM), in which the mass density is dominated by cold dark matter. In this model, the initial distribution of density perturbations has the greatest power on small scales, which causes low mass dark matter haloes to form first at high redshift. Larger haloes form later through the merging, or accretion, of smaller halos. Eventually, this 'hierarchical structure formation' leads to the formation of galaxy groups and clusters, which become more common with time. The mass assembly of dark matter halos has been extensively studied analytically (Press & Schechter, 1974; Bond et al., 1991; Bower, 1991; Lacey & Cole, 1993; Sheth & Tormen, 2002; van den Bosch, 2002; Benson et al., 2005) and through numerical simulations (e.g. Davis et al., 1985; Li et al., 2008). Consistent with these studies, Berrier et al. (2009, hereafter B09) used n-body simulations to show that the mass assembly of clusters is dominated by the most massive accretion events; in effect, the merging of groups with clusters. However, by associating dark matter subhalos with galaxies, they show that the *galaxy* assembly of clusters is dominated by lower mass halos, or the infalling of isolated galaxies. This distinction could be of great importance since there are a variety of physical processes that depend on the mass of the host dark matter halo and which could affect the properties

of a galaxy, such as ram pressure stripping, strangulation and galaxy harassment.

Indeed, detailed observations of dense environments, galaxy groups, and clusters in the local universe have shown that the galaxies which inhabit these environments have properties substantially different from galaxies in low density or field environments. In particular, galaxy groups and clusters have lower average galaxy star formation rates (Lewis et al., 2002; Gómez et al., 2003), lower fractions of disk galaxies (Dressler et al., 1997; McGee et al., 2008), and higher red fractions (Balogh et al., 2004b; Weinmann et al., 2006a) than field galaxies. Despite this wealth of observational data, there is no consensus on the dominant physical mechanism responsible for these differences, mainly because large populations of "transition" objects have avoided detection. In particular, there is no large excess in the fraction of galaxies between the red sequence and the blue cloud in dense environments (Balogh et al., 2004b; Weinmann et al., 2006a). While there are specific examples of transitioning spiral galaxies which are in the process of having their HI gas stripped due to ram pressure in local clusters (Kenney et al., 2004; Vollmer et al., 2004), the X-ray temperatures and pressures, as well as the infalling velocity of the galaxies, required for such a transformation mechanism are probably too high to be effective in low mass groups.

Strangulation, the process in which the more loosely bound hot halo of a galaxy is stripped by the group or cluster halo, leaving a reduced amount of gas available for future star formation (Balogh et al., 2000), is an attractive candidate because it is still effective in low mass groups (McCarthy et al., 2008b; Kawata & Mulchaey, 2008). However, it is not clear if such a gentle mechanism can account for the dramatic effect seen in clusters. Zabludoff & Mulchaey (1998) have proposed that the extreme properties of galaxy clusters may result from the "pre-processing" of galaxies in group environments before accretion into the cluster. This is supported by observations of reduced star formation rates in the outskirts of clusters, well past the virial radius (Balogh et al., 1999; Lewis et al., 2002). However, B09 have claimed that "pre-processing" is not a large effect. They find only $\sim$ 12 % of galaxies are accreted in to the final cluster environment as members of groups with five or more galaxies. While the B09 clusters are relatively low mass, their work shows the importance of distinguishing the accretion of galaxies from that of dark matter mass.

A complementary approach to trying to isolate "transition galaxies" is to study the properties of galaxies in groups and clusters as a function of redshift. As first shown by Butcher & Oemler (1978a) and confirmed by many others (eg. Lavery & Henry, 1986;

Couch & Sharples, 1987; Ellingson et al., 2001), the fraction of blue galaxies in clusters increases with redshift, the so called Butcher-Oemler effect. Despite this, the fraction of star forming galaxies in groups and clusters is still lower than the coeval field fraction at least to z=1 (Wilman et al., 2005a; Gerke et al., 2007; Balogh et al., 2009). The need to explain the Butcher-Oemler effect, as well as the local properties of galaxy clusters provides important constraints for the nature of the transformation mechanism. Essentially, if the transformation mechanism only occurs in very massive clusters, then the fraction of blue galaxies is simply the fraction of galaxies which have fallen into the cluster within the time scale of transformation.

The time scale for transformation of galaxy properties to occur is a significant uncertainty in attempting to link the growth of structure to the Butcher-Oemler effect. Previous attempts using cluster assembly histories adopted relatively short time scales of $\sim 1$ Gyr and, while complicated by uncertain cosmological parameters, showed that a direct infall model alone did not produce enough evolution in the blue fraction (Bower, 1991; Kauffmann, 1995). Kodama & Bower (2001) combined the evolving star formation properties of field galaxies with a cluster infall model to successfully reproduced the scatter in the red sequence of low redshift clusters. Similarly, Ellingson et al. (2001) found that the radial distribution of early type galaxies in galaxy clusters at two redshift epochs could best be explained if the galaxy infall into clusters decreased by a factor of $\sim 3$ between $z > 0.8$ and $z \sim 0.5$.

In this chapter, we examine the *galaxy* assembly properties of groups and clusters over a wide mass range and at four redshift epochs. We investigate the mass of halos through which groups and clusters gain their galaxies and the extent to which preprocessing in the group environment is important at four redshift epochs. By making simple assumptions, we investigate the predictions for the fraction of galaxies in groups and clusters which are "environmentally affected" for a range of relevant timescales and the halo mass thresholds which those effects begin. Using these models we try to gain insight into the dominant physical processes necessary to reproduce observations of group and cluster galaxies, as well make predictions for future observations. In §2.2, we present the details of our simulated clusters and some of their properties and present our results in §2.3. We discuss these results and conclude in §2.4. In this chapter, we assume a cosmology with $\Omega_m = 0.25$, $\Omega_\Lambda = 0.75$, $\sigma_8$=0.9 and $H_0 = 100h$ km s$^{-1}$ Mpc$^{-1}$ unless mentioned otherwise.

## 2.2 Simulations

To interpret observations of galaxy properties as a function of environment, we need to know the accretion history of those galaxies; as shown by B09 this can be subtly different from the total mass assembly history. But galaxy formation has proven to be a difficult problem, and it is not clear, given that the dark matter halo mass function has a very different shape from the galaxy luminosity function, if the approach of B09 of simply associating subhalos with galaxies includes all of the relevant physics. At the least, this approach does not allow for the robust identification of the stellar masses of galaxies. Unfortunately, an obvious alternative — the direct simulation of the baryonic processes of galaxies — is difficult on the scale of the cosmological volumes needed to study large samples of groups and clusters.

Semi-analytic galaxy formation models provide a good tool to encapsulate the essential physical processes of gas cooling, star formation and feedback (e.g. White & Frenk, 1991; Kauffmann et al., 1993; Somerville & Primack, 1999; Croton et al., 2006; Bower et al., 2006). Dark matter simulations, on which modern semi-analytic models are based, are now large enough to allow the study of the growth of the groups and clusters over a wide range of redshifts. We make use of one such semi-analytic model by Font et al. (2008a, hereafter F08), which is a recent modification to the Durham semi-analytic model (GALFORM) of Bower et al. (2006). The basic prescriptions for gas cooling and star formation in the GALFORM model was laid out by Cole et al. (2000), and subsequently modified for modern cosmological parameters by Benson et al. (2003). The model of Bower et al. (2006) introduced a method for parameterizing the effect of AGN feedback on the gas in massive galaxies to correct for the "overcooling" problem.

The Bower et al. (2006) model, as in essentially all previous semi-analytic models, implements a relatively simple treatment of environmental effects, in which the hot gas reservoirs of galaxies are removed upon becoming a satellite galaxy. Many authors have since shown that this approach produces an unphysically high fraction of red galaxies in groups and clusters (Weinmann et al., 2006a; Baldry et al., 2006; Gilbank & Balogh, 2008). The F08 model implements a more realistic "strangulation" model in which the hot gas halo of galaxies falling into more massive halos are removed according to a prescription of McCarthy et al. (2008b). However, a careful examination of cluster and group data with this model at a range of redshifts reveal that there are important discrepancies.

In particular, the model overpopulates the green valley between the blue cloud and red sequence (Balogh et al., 2009). We emphasize that despite this difficulty in reproducing galaxy colours, the stellar masses of galaxies in the F08 and Bower et al. models are much better understood. In particular, the Bower et al. model reproduces the observed evolution of the stellar mass function out to at least z=5.

In this chapter, our analysis relies primarily on the GALFORM prediction of the stellar mass function of galaxies in different environments. This is insensitive to the problem noted above, as the star formation rate of galaxies declines rapidly with redshift, so the bulk of a galaxy's stellar mass is already in place before it ever becomes a satellite. Thus, the details of the strangulation procedure adopted in GALFORM are unimportant for our analysis and, indeed, all our conclusions are independent of the choice of either the Bower et al. model or the F08 model.

### 2.2.1 Cluster and group sample

The F08 model, from which our simulated galaxy clusters and groups are drawn, is based on merger trees derived from the dark matter Millennium simulation (Springel et al., 2005b), a ΛCDM cosmological box with $500/h$ Mpc sides. The Millennium simulation uses GADGET2 (Springel, 2005), a TREE-PM N-body code, and an initial power spectrum calculated using CMBFAST (Seljak & Zaldarriaga, 1996). The merger trees are generated as described in Helly et al. (2003) and Harker et al. (2006), and are complete down to halos which host $\sim 10^8\ h^{-1}\ \mathrm{M}_\odot$ galaxies. In this chapter, we are principally concerned with selecting samples of galaxies which are observationally accessible, and thus specify a single fixed stellar mass cut of $M > 10^9\ h^{-1}\ \mathrm{M}_\odot$, much higher than the completeness limit.

We analyze all the groups and clusters in the F08 model more massive than $M = 10^{12.9}\ h^{-1}\ \mathrm{M}_\odot$ at four redshift epochs (z=0, 0.5, 1 and 1.5). The key properties of the cluster samples are shown in Tables 2.1 and 2.2. In particular, we show the number of clusters, and the average number of galaxies with stellar masses above $M = 10^9\ h^{-1}\ \mathrm{M}_\odot$ at the epoch of observation, in each of the mass bins which will be used in the remainder of the chapter.

In Figure 2.1, we present the cumulative distribution of galaxies which reside within the virial radius of host halos of a given mass. We plot this for four stellar mass ranges at

z=0. In the F08 model, $\sim 50\%$ of z = 0 $L_*$ galaxies are in host halos with masses above $10^{12.5}\ h^{-1}\ M_\odot$. This compares very well with observational results: Berlind et al. (2006) found that $\sim 56$ % of $M_r < -20.5$ galaxies in the SDSS are linked to groups containing at least one other member, a result that is completely consistent with independent analysis using the 2dFGRS Eke et al.. We also see that 25% of $L_*$ galaxies are in relatively large groups or clusters with halo masses above $10^{13}\ h^{-1}\ M_\odot$. This is much larger than the $\sim 10$ % claimed by B09, likely a result of the way they assign galaxies to subhalos, as discussed further in §2.3.6. In particular, B09 assign a galaxy to a subhalo if the subhalo mass is $> 10^{11.5}\ h^{-1}\ M_\odot$ when it is accreted into a more massive host. However, the mass in a subhalo begins to be tidally stripped significantly before reaching the virial radius of a more massive host, even without significantly disturbing the galaxy within (Natarajan et al., 2007).

## 2.3 Results

We now look in detail at how the cluster galaxies end up in the clusters, and what insights this might give into the processes which might affect those galaxies.

### 2.3.1 Cluster and group accretion history

Galaxies which have been in massive halos prior to joining the final environment may have been environmentally pre-processed. Thus, we begin by examining the host halo masses of galaxies just prior to their accretion into the final group or cluster halo. To acheive this, we trace the most massive progenitor of every galaxy, back through each snapshot in the simulation. We record the halo mass of this progenitor in the timestep just before it becomes a member of the final cluster, which defines its environment at the time of accretion.

Here we will examine the most important insights which can be drawn from those accretion histories. Figure 2.2 shows the fraction of galaxies in the final cluster which were accreted through haloes at least as massive as $10^{13}\ h^{-1}\ M_\odot$ (large groups). We show this as a function of the final cluster mass for each of four redshift epochs. We first consider relatively low-mass clusters, with $M \sim 10^{14.2} M_\odot$ at z=0. We find that 32 per cent of

| Redshift | Number of clusters | Mass range Log($h^{-1}$ $M_\odot$) | Median mass Log($h^{-1}$ $M_\odot$) | Average number of galaxies per cluster |
|---|---|---|---|---|
| 0 | 40 | 15.0-15.6 | 15.14 | 1161 |
| | 189 | 14.7-15.0 | 14.82 | 569 |
| | 673 | 14.4-14.7 | 14.53 | 297 |
| | 1822 | 14.1-14.4 | 14.24 | 156 |
| | 4404 | 13.8-14.1 | 13.94 | 78 |
| | 9325 | 13.5-13.8 | 13.64 | 41 |
| | 18730 | 13.2-13.5 | 13.34 | 20 |
| | 36265 | 12.9-13.2 | 13.04 | 10 |
| 0.5 | 4 | 15.0-15.6 | 15.16 | 1161 |
| | 29 | 14.7-15.0 | 14.79 | 536 |
| | 212 | 14.4-14.7 | 14.51 | 289 |
| | 786 | 14.1-14.4 | 14.23 | 156 |
| | 2471 | 13.8-14.1 | 13.93 | 80 |
| | 6325 | 13.5-13.8 | 13.68 | 42 |
| | 14440 | 13.2-13.5 | 13.34 | 22 |
| | 30124 | 12.9-13.2 | 13.04 | 11 |

Table 2.1: Properties of the cluster sample derived from Font et al. (2008a). The first column lists the redshift snapshot from which the clusters were selected and the second column gives the total number of clusters used for analysis in each bin. Columns 3 and 4 list the cluster halo mass range and median mass of clusters in that range. We use these halo mass bins extensively in the rest of the chapter. Column 5 lists the average number of galaxies per cluster with stellar masses above $M = 10^9\ h^{-1}\ M_\odot$ at the epoch of observation.

| Redshift | Number of clusters | Mass range Log($h^{-1}$ $M_\odot$) | Median mass Log($h^{-1}$ $M_\odot$) | Average number of galaxies per cluster |
|---|---|---|---|---|
| 1.0 | 0 | 15.0-15.6 | – | – |
| | 3 | 14.7-15.0 | 14.82 | 532 |
| | 40 | 14.4-14.7 | 14.51 | 252 |
| | 275 | 14.1-14.4 | 14.22 | 137 |
| | 1134 | 13.8-14.1 | 13.92 | 72 |
| | 3643 | 13.5-13.8 | 13.63 | 38 |
| | 9820 | 13.2-13.5 | 13.34 | 21 |
| | 23388 | 12.9-13.2 | 13.04 | 11 |
| 1.5 | 0 | 15.0-15.6 | – | – |
| | 1 | 14.7-15.0 | 14.81 | 381 |
| | 2 | 14.4-14.7 | 14.41 | 178 |
| | 55 | 14.1-14.4 | 14.19 | 119 |
| | 322 | 13.8-14.1 | 13.92 | 66 |
| | 1528 | 13.5-13.8 | 13.62 | 35 |
| | 5465 | 13.2-13.5 | 13.33 | 19 |
| | 15134 | 12.9-13.2 | 13.03 | 10 |

Table 2.2: Properties of the high redshift cluster sample derived from Font et al. (2008a). Columns are the same as Table 2.1

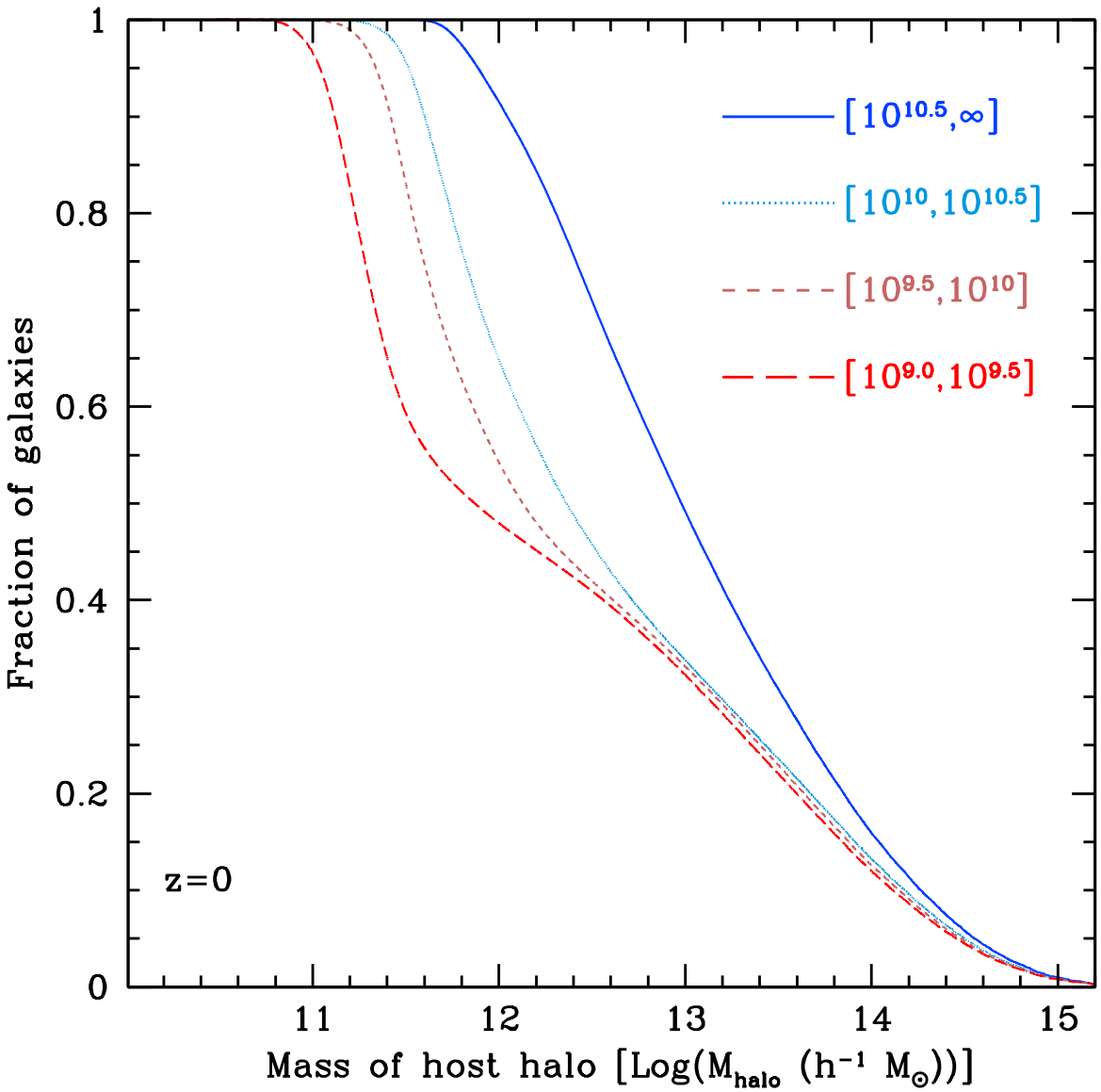


Figure 2.1: The cumulative distribution of the host halo mass of galaxies at z=0. The distribution is shown for four ranges in the galaxy's stellar mass at $z = 0$, shown in the upper right corner in units of $h^{-1}$ $M_{\odot}$.

galaxies in these clusters were accreted through such group-sized halos. This is somewhat higher than the 24 per cent found by B09; the small difference can be related to the difference in the way haloes are populated with galaxies, as we discuss in § 2.3.6.

However, such clusters are fairly poor systems; they are less massive than all 16 clusters observed extensively by the CNOC1 collaboration (Carlberg et al., 1996), and an order of magnitude smaller than the nearby Coma cluster ($M_{200} = 1.88\ ^{+0.65}_{-0.56} \times 10^{15}\ h^{-1}\ M_\odot$, (Kubo et al., 2007)). Figure 2.2 shows that the fraction of galaxies which are accreted through group sized halos is strongly dependent on the mass of the final halo. This is because massive haloes are not surrounded by an average patch of the universe, but tend to be strongly clustered with other massive halos (eg. Kaiser, 1984). At z=0, we see that 45 % of galaxies accreted into a cluster of Coma's mass have been accreted from haloes with $M > 10^{13}\ h^{-1}\ M_\odot$. This suggests that pre-processing in group environments before cluster accretion may be significant. Interestingly, the fraction of galaxies accreted through massive haloes has only a weak dependence on the redshift of observation of the cluster. In other words, a Coma-sized cluster at z=0.5 would accrete 40 % of its galaxies from $M > 10^{13}\ h^{-1}\ M_\odot$ halos. The galaxy assembly histories are remarkably similar, with the dominant difference being simply that Coma-sized clusters do not exist in the relatively small volume of the Millennium simulation at $z = 1.0$ or 1.5.

In Figure 2.3, we show the fraction of stellar mass which is accreted through halos at least as massive as $10^{13}\ h^{-1}\ M_\odot$. This figure is quite similar to Figure 2.2. However, notice that the fraction of *stellar mass* accreted by the most massive clusters through groups is larger than the fraction of *galaxies* accreted through such systems. Indeed, the stellar mass accretion history closely matches the expected behavior of the dark matter accretion. The extended Press Schechter formalism and n-body simulations of dark matter roughly agree that $\sim$ 30 % of the mass of a halo is accreted from halos with masses a tenth the mass of the final halo (Bond et al., 1991; Bower, 1991; Lacey & Cole, 1993; Stewart et al., 2008). We find this same fraction for all our stellar mass accretion histories, while the fraction of galaxies accreted is smaller at high cluster mass. This implies there are are fundamental differences in how galaxies are accreted as a function of their stellar mass. This is illustrated in Figure 2.4, where we show the accretion histories of galaxies which end up in a $M = 10^{15.0}\ h^{-1}\ M_\odot$ cluster at z=0, binned by their final stellar mass. There is a large difference in the masses of the host halos prior to accretion for low and high mass galaxies. While $\sim$ 52 % of the most massive galaxies are accumulated from haloes

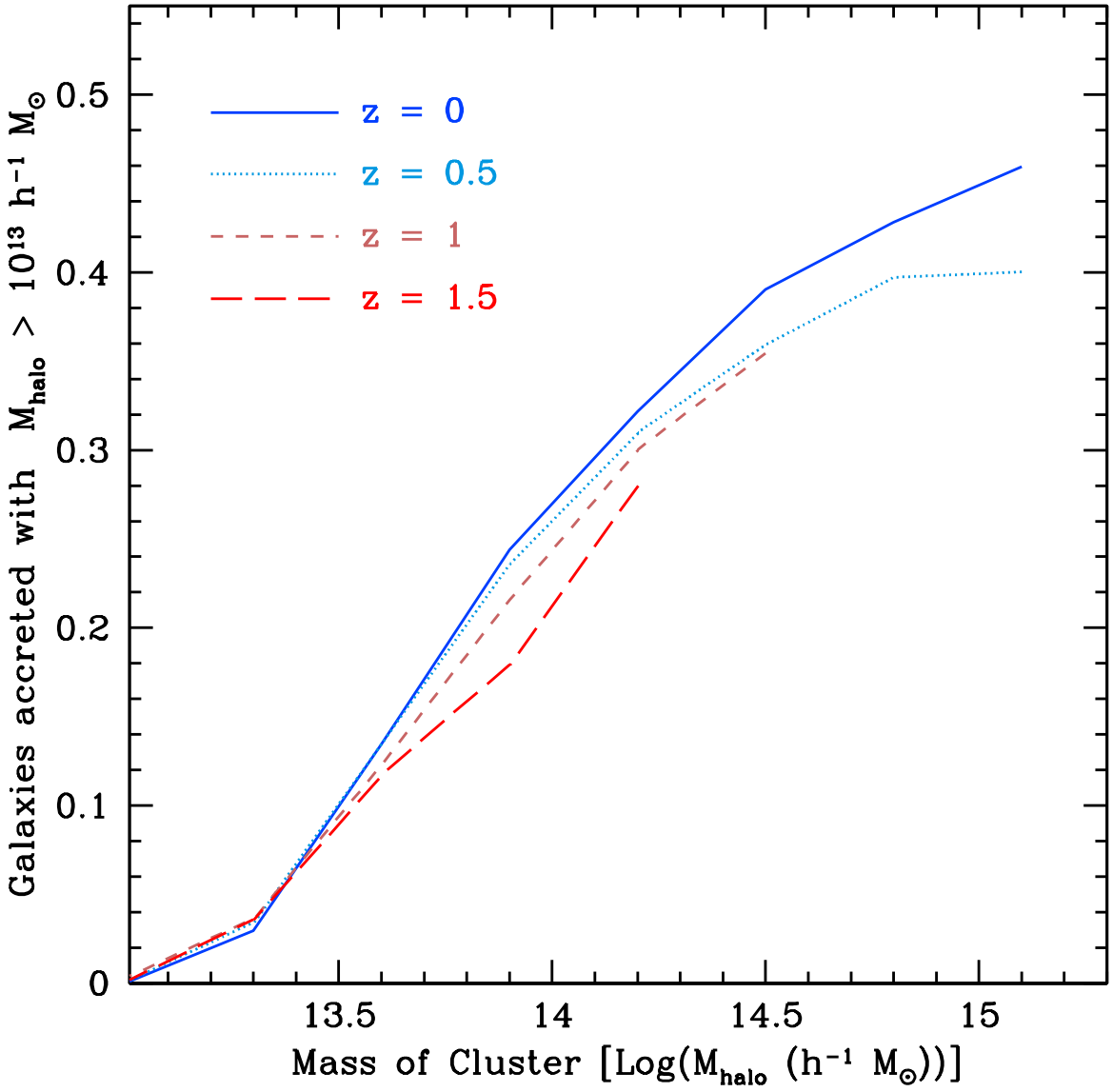


Figure 2.2: The fraction of cluster galaxies which were accreted into the final cluster halo as a member of a halo with $M > 10^{13}$ $h^{-1}$ $M_\odot$. This is shown as a function of the final cluster mass at the epoch of observation, for four redshifts. All cluster galaxies have final stellar masses of $M > 10^9 M_\odot$. The mass range bins were defined in Table 1, and are shown for all bins containing more than two clusters.

with $M > 10^{13}$ $h^{-1}$ $M_\odot$, this is only the case for $\sim$ 45 % of the least massive galaxies we consider. This discrepancy is much larger if we consider accretion through poorer groups, with $M > 10^{12}$ $h^{-1}$ $M_\odot$. The more massive galaxies are more likely to have been accumulated from group mass halos, and thus more likely to have been pre-processed prior to accretion into a cluster.

Now that we have seen that the degree of group preprocessing depends on both the stellar mass of the galaxy and the mass of the final cluster, we would like to examine how this varies as a function of redshift. In Figure 2.5 we show the fraction of cluster galaxies which were accreted into the final cluster halo as a member of a halo with $M > 10^{13}$ $h^{-1}$ $M_\odot$ halo. This is broken up into three bins, which represent the redshift at the time of the galaxy's accretion into the cluster. From this we see that the degree of preprocessing is significantly dependent on the time the galaxies were accreted. Galaxies which are accreted recently into the cluster are more likely to have been in a group environment than ones accreted into the cluster at high redshift. In particular, since $z = 0.5$ the most massive clusters today have accreted most of their new galaxies via infalling groups.

### 2.3.2 Cluster and group assembly histories

We have seen that the accretion history of clusters varies with final cluster mass, is a function of the stellar mass of the accreted galaxy and is dependent on the redshift of accretion. However, this does not address the state of the cluster itself. The importance of pre-processing depends not only on the accretion history but also on the amount of time the main cluster progenitor itself had the mass of a group.

Therefore, to get a complete picture of the assembly of galaxy clusters and groups and the halo masses which are important for the properties of their galaxies we present Figure 2.6. This shows the distribution of halo masses in which the most massive progenitors of final z=0 cluster galaxies reside, as a function of lookback time and for four bins of final z=0 cluster mass. The panels in Figure 2.6 show distinctly different assembly histories for very massive clusters, smallish clusters, and groups. In particular, the relative importance of the group environment varies tremendously for these three types of structures. The most massive cluster never has more than 17 % of galaxies in group sized halos ($10^{13}$ $h^{-1}$ $M_\odot$< $M_{\rm halo} < 10^{14}$ $h^{-1}$ $M_\odot$) while as many as 44% of the galaxies in a $M \sim 10^{14.2}$ $h^{-1}$ $M_\odot$ cluster today have spent some time within such haloes in the past. In fact, for a period of 2 Gyrs,

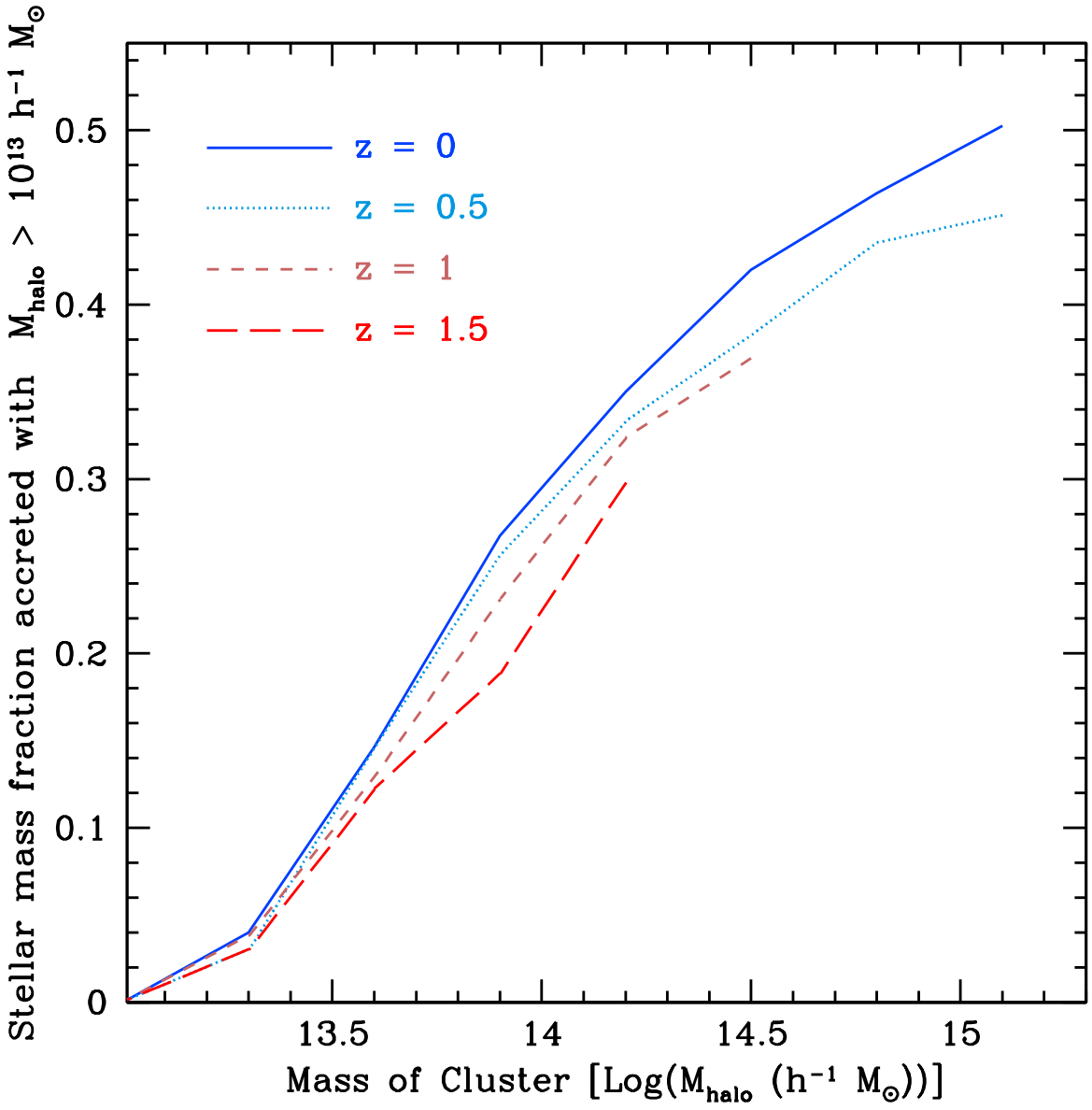


Figure 2.3: As Figure 2.2, but showing the fraction of accreted *stellar mass* which resides in a $M > 10^{13}\ h^{-1}\ \mathrm{M}_{\odot}$ halo at the time of accretion.

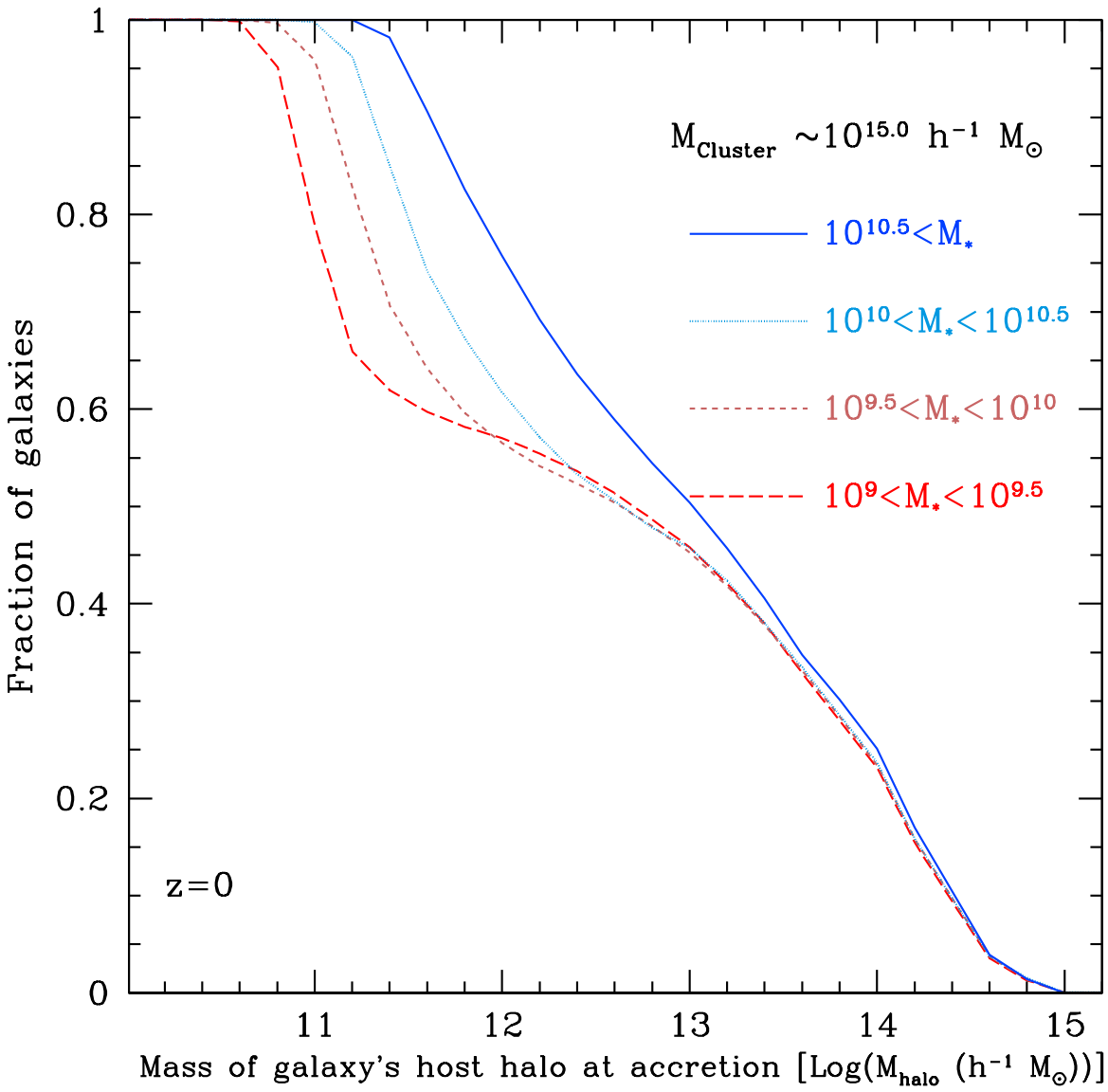


Figure 2.4: The cumulative distribution of accreted cluster galaxies as a function of host halo mass at the time of accretion into the final cluster. The distribution is shown in three stellar mass bins at z=0, for a final cluster with $M = 10^{15}h^{-1}$ $M_{\odot}$.

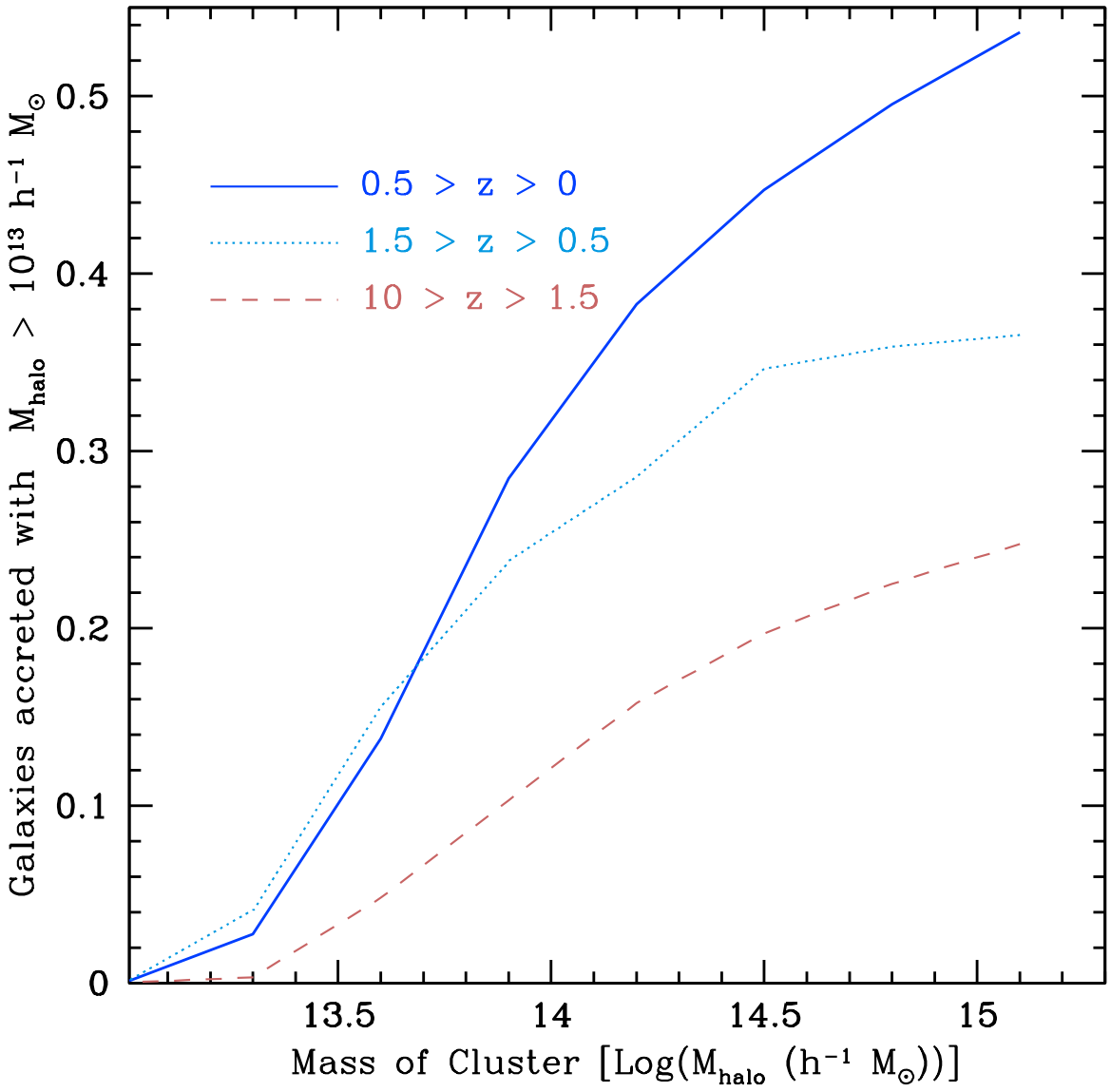


Figure 2.5: The fraction of cluster galaxies which were accreted into the final cluster halo as a member of a $10^{13}$ $h^{-1}$ $M_{\odot}$ halo or greater. This is shown as a function of the final cluster mass z=0 and for three bins in accretion redshift. All cluster galaxies have final stellar masses of $M > 10^{9} M_{\odot}$.

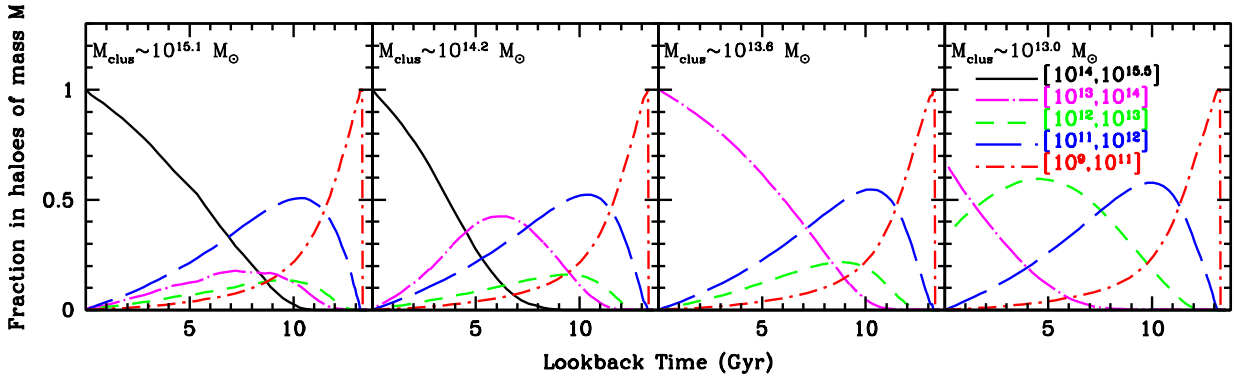


Figure 2.6: The fraction of galaxies residing in z=0 clusters that are found in halos of mass $M$ at a previous time $t$. We only consider the most massive progenitor of each cluster galaxy. Each curve shows a range of M, indicated by the legend, in units of $h^{-1}$ $M_\odot$. Each panel represents clusters of different final masses, as indicated in the top-left corner. Note that the curve corresponding to haloes with $10^{11} < M/h^{-1}$ $M_\odot < 10^{12}$ is very similar in all cases, indicating that the accretion rate of "isolated" galaxies is roughly independent of final cluster mass.

groups are the most common environment of the galaxy progenitors; this is because during this time the main cluster progenitor itself has the mass of a group. Thus, considering only the haloes of galaxies prior to accretion into the main cluster may underestimate the role of the group environment, as already noted by B09.

Given the distinctly different assembly histories of these clusters and massive groups, it is perhaps surprising that observations of large samples of galaxy clusters in the local universe show that the fraction of red galaxies is approximately constant in clusters more massive than $10^{13.8}$ $h^{-1}$ $M_\odot$ (Hansen et al., 2007). Therefore, it is useful to look for some common trait in the assembly histories of clusters which may point to the reason for this uniformity. It is interesting that the population of 'isolated' galaxies, those in $10^{11}$ $h^{-1}$ $M_\odot < M_{\rm halo} < 10^{12}$ $h^{-1}$ $M_\odot$, shows a similar distribution in the four different panels. At a lookback time of 10 Gyrs, $\sim 55$ % of cluster galaxy progenitors were in this halo mass regime, and that percentage has declined at a nearly constant rate of $5-6$ % per Gyr until the current epoch, regardless of the final cluster mass. In other words, the distribution of galaxies not in 'isolated' halos is similar regardless of final cluster mass, and supports the hypothesis that the galaxy transformation mechanism begins to occur as galaxies leave

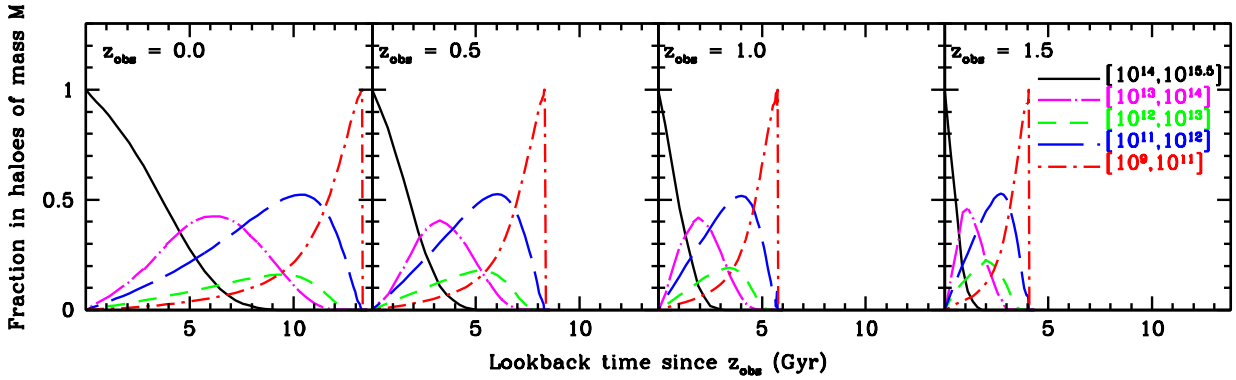


Figure 2.7: As in Figure 2.6, but for a cluster of mass $10^{14.5}$ ($h^{-1}$ $M_\odot$) observed at four redshift epochs as indicated at the top of each panel. Clusters of a given mass at higher redshift must assemble their mass more quickly, and thus the time available for pre-processing through group-sized haloes is decreased.

their 'isolated' halos.

Finally, we examine the assembly histories of galaxy clusters of a given mass at each redshift epoch. In Figure 2.7 we show the distributions of halo masses for the most massive progenitors of $10^{14.5}$ $h^{-1}$ $M_\odot$ cluster galaxies as a function of lookback time at all four redshift epochs. While the final cluster mass is the same (at each epoch), the higher redshift clusters must assemble their mass more quickly and thus their galaxies have not been in massive halos for as long. For instance, 5 Gyrs prior to the observation epoch, $\sim$ 50% of z=0 galaxies were in $10^{14}$ $M_\odot$ $h^{-1}$ haloes, while none of the z=1 or z=1.5 cluster galaxies were even in $10^{13}$ $h^{-1}$ $M_\odot$ haloes yet. Environmental processes have had a much longer timescale over which to affect low redshift groups and clusters than higher redshift ones.

There are two interesting points when comparing Figure 2.7 with Figure 2.6. First, we see that the maximum fraction of galaxies in each halo mass bin is the same in clusters of the same final mass but seen at different redshifts. For instance, the maximum fraction of galaxies which reside in halos of $10^{13}$ $h^{-1}$ $M_\odot$$< M_{\rm halo} <$ $10^{14}$ $h^{-1}$ $M_\odot$ at any time is 40 % regardless of the redshift epoch. The lookback time at which these maximum fractions occur varies significantly with redshift, but it would appear their path through the hierarchy is similar. Essentially, clusters of fixed mass at different redshift epochs have assembly histories which become more stretched out at lower redshift. The assembly

histories would look almost identical if the lookback time was divided by the age of the universe at that redshift epoch. This result was hinted at in Figure 2.2, which showed that the fraction of galaxies accreted through massive haloes was approximately the same at all redshift epochs for a cluster of given mass.

This leads to the second interesting observation to be made from Figure 2.7. The rate at which galaxies leave their 'isolated' halos increases significantly with redshift. At z=0, as before, for the 10 Gyrs prior to observation the fraction of galaxies in halos of $10^{11}$ $h^{-1}$ $M_{\odot}$< $M_{\rm halo}$ < $10^{12}$ $h^{-1}$ $M_{\odot}$decreases by about 5-6% per Gyr, while 10% (15%) [20%] of galaxies leave their 'isolated' halos per Gyr at a constant rate for 5(3.5)[2.5] Gyrs prior to observation at z=0.5(1)[1.5]. Therefore, the accretion rate of galaxies from isolated environments into groups and clusters is higher at higher redshift. Again, this result is a direct result of the reduced time between the epoch of observation and the beginning of the universe. The assembly histories at higher redshift are just compressed, leading to a higher accretion rate, even though the total number accreted from isolated environments is constant at each epoch of observation. The effect this has on the galaxy properties of galaxy clusters as a function of redshift will be discussed in the following section.

### 2.3.3 Cluster to cluster variation in environmental effects

We have established the galaxy accretion history and galaxy assembly history of galaxy clusters at a range of epochs. We would now like to assess how these galaxy histories affect the final properties of galaxies at each redshift epoch. To this end, we examine the fraction of galaxies in each cluster, which have been within dense environments long enough to expect that environmental effects might be important. By examining the fraction of environmentally affected galaxies in each cluster, we can quantify both the total numbers of affected galaxies, and their variation from cluster to cluster.

In a simple way, we can parametrize the length of time it takes for a galaxy to display an environmental effect, $T_{\rm trunc}$, after falling into a halo with a mass above a characteristic mass threshold, $M_{\rm trunc}$. Although it is not obvious that there is a single main physical mechanism which causes the environmental effects displayed in both groups and clusters, we explore the predictions of such a model and discuss the limitations of this approach in the following section.

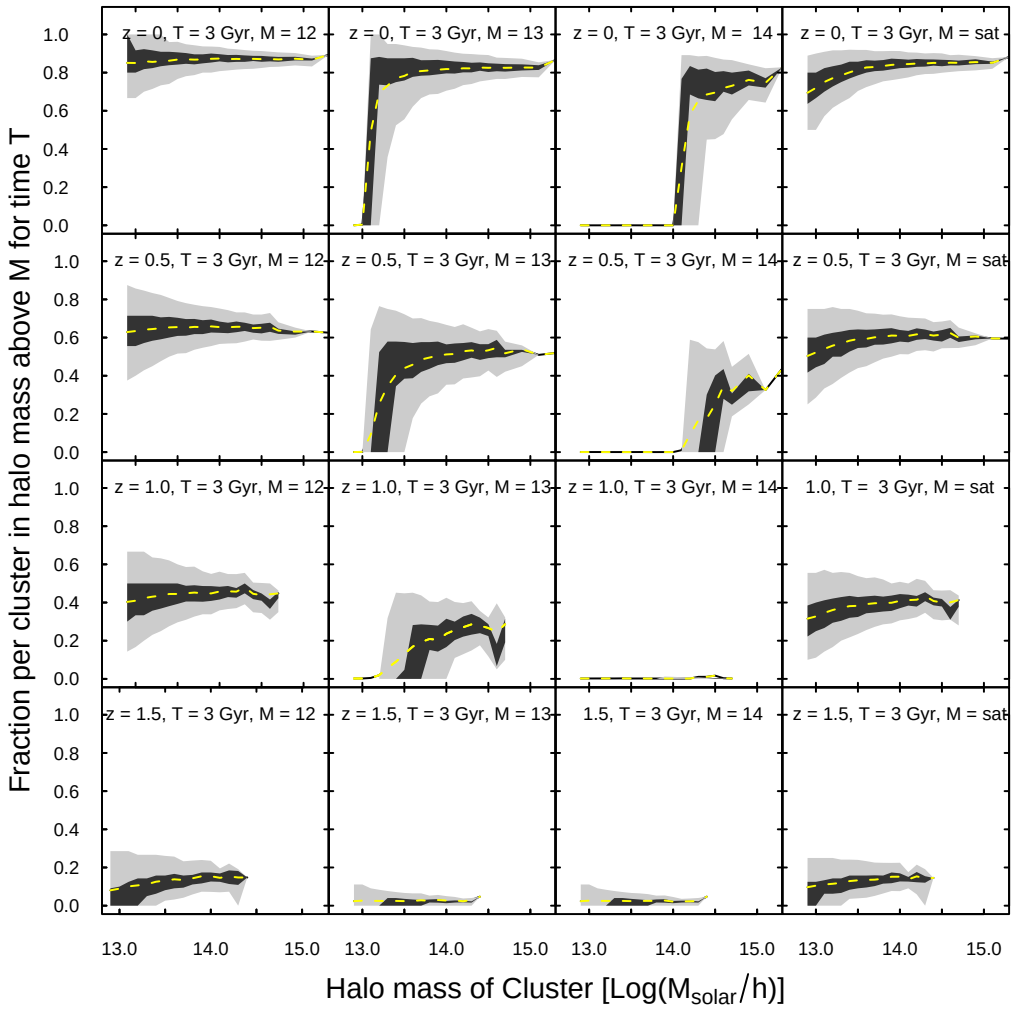


Figure 2.8: The fraction of cluster galaxies with $M > 10^9 h^{-1}$ $M_\odot$ that have resided within a halo of mass $M \geq M_{\rm trunc}$ for a time $t \geq T_{\rm trunc}$ is shown as a function of final cluster mass. We interpret this as the fraction of "environmentally–affected" population in our simple model. The panels contain four contour lines marking the 10, 33, 67 and 90 percentiles of the distribution in this fraction, while the dashed yellow line represents the average. The truncation time is fixed at $T_{\rm trunc}$= 3 Gyr, and each column shows a different assumption for $M_{\rm trunc}$, as indicated. Different rows correspond to clusters at a different redshift, as indicated.

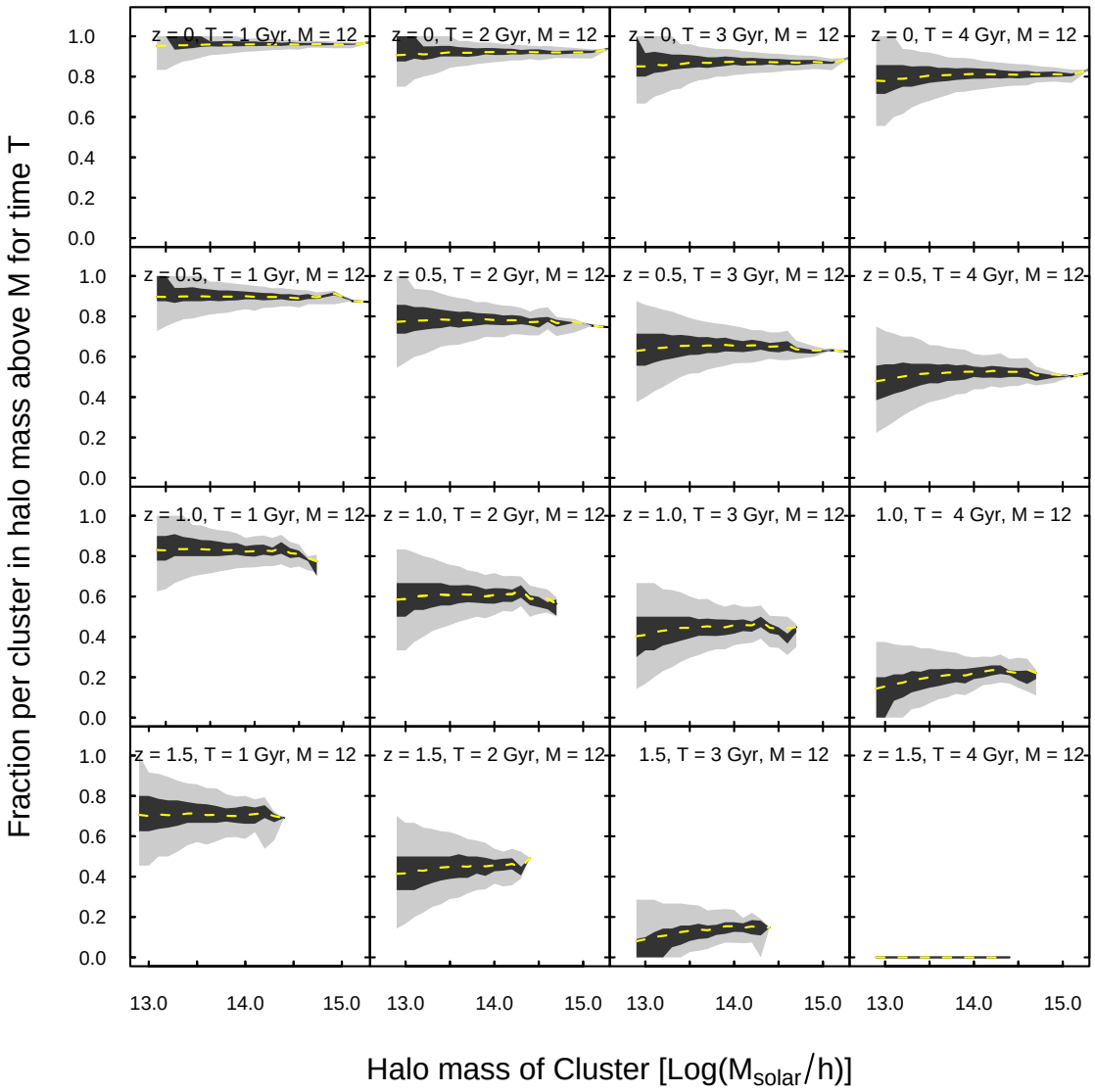


Figure 2.9: As Figure 2.8, but where the characteristic halo mass threshold is fixed at $M_{\rm trunc}= 10^{12}\ h^{-1}\ {\rm M}_{\odot}$, and the truncation times $T_{\rm trunc}$ are varied along rows of the figure, from 1–4 Gyr as indicated.

Given this model we can explore how varying the truncation time, $T_{\rm trunc}$, and the characteristic mass threshold, $M_{\rm trunc}$, alters the implied environmental effects on galaxies. In Figure 2.8, we show the predicted average fraction of galaxies in each cluster which are subject to environmental effects in our simple model; the distribution of this fraction is reflected in the four contour lines marking the 10, 33, 67 and 90 percentiles. Here we fix the truncation time, $T_{\rm trunc}$, to be 3 Gyr and allow the characteristic mass threshold, $M_{\rm trunc}$, to vary from $10^{12}$ $h^{-1}$ $M_{\odot}$ to $10^{14} M_{\odot}$. In other words, in this figure, a galaxy has felt an "environmental effect" if it has been within a halo of mass $M \geq M_{\rm trunc}$ for at least 3 Gyrs. In addition, we allow a fourth category, in which the expression of an environmental effect occurs 3 Gyrs after the galaxy has become a satellite galaxy in a larger dark matter halo, regardless of its mass.

This figure has some noteworthy features. First, for massive clusters (M $> 10^{14.5}$ $h^{-1}$ $M_{\odot}$) at z=0, the mean number of environmentally affected galaxies in this model is similar ($\sim$ 80-85 %) regardless of $M_{\rm trunc}$. The implication of this for low redshift observational studies is that it is difficult to discern the value of the characteristic mass threshold by observing systems above that mass threshold. This highlights the importance of studies of low mass galaxy groups. Observations at low and intermediate redshift show that group galaxies with a given stellar mass have properties distinct from the average field galaxy; if our simple model of environment-driven transformation is correct, this indicates a characteristic mass threshold of at least this scale (M $\approx 10^{12.5}$ - $10^{13}$ $h^{-1}$ $M_{\odot}$) (Wilman et al., 2005a; Weinmann et al., 2006a).

Indeed, as previously mentioned, low redshift observations show that the fraction of red galaxies in clusters is essentially uniform, for clusters with $M > 10^{13.8}$ $h^{-1}$ $M_{\odot}$ (Hansen et al., 2007). Given this, it is also worth noting that in Figure 2.8, our model also produces a strikingly flat fraction of environmentally affected galaxies per cluster as a function of cluster mass. This is a direct result of the behavior noted in Figure 2.6, that the fraction of galaxies infalling from isolated halos is independent of halo mass.

Although it may be difficult to use the average properties of massive clusters at a given epoch to discern the characteristic mass threshold, one possible method would be to observe the variation in their properties. The predicted scatter in the fraction of environmentally affected galaxies per cluster is quite small ($\sim$ 5 %) for $10^{14.5}$ $h^{-1}$ $M_{\odot}$ clusters at z=0 when $M_{\rm trunc}$= $10^{12}$ $h^{-1}$ $M_{\odot}$, but close to 40 % when $M_{\rm trunc}$= $10^{14}$ $h^{-1}$ $M_{\odot}$. The scatter in, for instance, the fraction of early type galaxies or optical line emitting galaxies in clusters

at z=0 is much smaller than 40 % (Dressler, 1980; Poggianti et al., 2006; Finn et al., 2008). We will examine the scatter in red fractions of galaxies in clusters at z=0 in an seperate paper (Balogh & McGee, 2010). Unfortunately, the scatter at z=0 of a model where $M_{\rm trunc}$= $10^{12}$ $h^{-1}$ $M_{\odot}$ is not that different from a model where $M_{\rm trunc}$= $10^{13}$ $h^{-1}$ $M_{\odot}$. However, notice that the scatter in these two models becomes more significant at z > 0. Intriguingly, Dressler et al. (1997) showed that, while the morphology-density relation was equally strong in all clusters at low redshift, the relation was stronger in centrally–concentrated clusters than irregular clusters at z $\sim$ 0.5.[1] In effect, this suggests that the scatter in the fraction of environmentally affected galaxies of each cluster is significant at z $\sim$ 0.5. Although not definitive, this may point to a characteristic mass threshold which is somewhat larger than $10^{12}$ $h^{-1}$ $M_{\odot}$, given that scatter in that model is still quite small at z=0.5 ($\sim$ 13 % at $10^{14.5}$ $h^{-1}$ $M_{\odot}$). Notice that a model where the environmental effects begin to occur when a galaxy becomes a satellite behaves very similarly to a model with $M_{\rm trunc}$= $10^{12}$ $h^{-1}$ $M_{\odot}$. We discuss this similarity further in §2.3.7.

Examining the redshift evolution of any of the given models shows that they all predict a significant Butcher-Oemler effect. That is, they predict that there are fewer environmentally affected galaxies in clusters with increasing redshift. In particular, by z= 1.5 all of the models predict a very small or non-existent fraction of environmentally affected galaxies. Indeed, the $10^{14}$ $h^{-1}$ $M_{\odot}$ model leads to the prediction that, by $z = 1$, no galaxies will be environmentally affected.

Our choice of $T_{\rm trunc}$= 3 Gyrs in the models presented above is ad hoc, and we would like to quantify how changing the timescale affects the predictions. In Figure 2.9, we explore a model in which the characteristic halo mass, $M_{\rm trunc}$, is kept fixed at $10^{12}$ $h^{-1}$ $M_{\odot}$, and allow $T_{\rm trunc}$to vary from 1 Gyr to 4 Gyrs. We show the fraction of environmentally affected galaxies for each of the four redshift epochs of our clusters. Although $M_{\rm trunc}$ is held constant, we note that the results and our interpretation are similar for any choice of $M_{\rm trunc}$ within the range $10^{12}$–$10^{13}$ $h^{-1}$ $M_{\odot}$, which seems the most likely value given the arguments above.

Similarly to Figure 2.8, for each $T_{\rm trunc}$, we see a significant Butcher-Oemler effect, such that clusters at higher redshift have fewer galaxies affected by environmental processes.

[1]While the Dressler et al. results, and many intermediate redshift results, have limiting stellar mass on the order of $10^{10}$ $h^{-1}$ $M_{\odot}$compared with our limit of $10^{9}$ $h^{-1}$ $M_{\odot}$, we have verified that the scatter in the cluster red fractions is constant with a limiting mass change to $10^{10}$ $h^{-1}$ $M_{\odot}$.

However, the size of the effect even between $z = 0$ and $z = 0.5$ is dramatically altered by the choice of time scale. With a short timescale of only 1 Gyr, the fraction of environmentally-affected galaxies evolves little, from ∼85% at $z = 0.5$ to ∼ 95% today. On the other hand, a long timescale of $T_{\rm trunc}$= 4 Gyr results in a much stronger evolution over this redshift range, from 50% to 80%. Compare this evolution with that observed in the red fraction of cluster galaxies, which indicate an evolution of ∼ 25 % over a similar redshift range, from 0.9 at z=0.2 to 0.65 at z=0.5 (Ellingson et al., 2001). This seems to indicate that a relatively long time scale for the expression of environmental effects (> 2 Gyr) would be required to match this quick evolution. A similar timescale is necessary to explain the radial gradient of passive galaxies in galaxy clusters (Ellingson et al., 2001; Balogh et al., 2000).

The predicted scatter from cluster to cluster is also noteworthy. Recall that in Figure 2.8 we saw that the scatter was sensitive to the characteristic halo mass used. In this plot, for the majority of the time, the scatter is similar at each redshift regardless of the timescale for truncation. This strengthens our previous argument that a well-defined measure of the scatter in cluster properties at a given redshift could allow one to discern the characteristic halo mass for truncation.

We have provided strong evidence, which we summarize in §2.3.5, that the dominant environmental processes at work in galaxy groups and clusters begin to become effective at a halo mass scale of $10^{12}$ - $10^{13}$ $h^{-1}$ $M_{\odot}$, and are active for a timescale of at least a few Gyrs. Given these constraints, we see that figure 2.9 predicts that by z=1.5 there should be little to no environmental effect on galaxies. Remarkably, this prediction has some observational evidence to suggest it is correct. Cooper et al. (2007) showed, using galaxies selected from the DEEP2 redshift survey, that the red fraction only weakly correlates with overdensity at z ∼ 1.3. While the comparison to our predictions is complicated because the Cooper et al. sample only includes massive galaxies, this is not a trivial agreement; in fact, assuming the timescale was 1 Gyr, this would lead us to predict that 70 % of galaxies at z=1.5 are still environmentally affected. This fraction would be even higher when we used the same limiting stellar mass as Cooper et al., as is discussed in the next section. Additionally, the DEEP2 survey is complicated by their rest frame blue magnitude limit which causes them to naturally detect fewer and fewer red galaxies at higher redshifts. Further, DEEP2 does not cover a wide enough area to have massive clusters within it, so targeted, stellar mass limited studies of the extreme cluster environments are still needed at this redshift

to quantify the size of the environmental effects. Although, given our results, they may be difficult to find using the popular and efficient red sequence method (Gladders & Yee, 2000; Lu et al., 2009).

### 2.3.4 Stellar mass dependence of environmental effects

Observations suggest that the fraction of galaxies which are passive or red, depends greatly on their own stellar mass (Baldry et al., 2006; Haines et al., 2006). It is thought that this is at least partially due to secular influences, ie. AGN feedback, which primarily occur in massive galaxies (Kauffmann et al., 2003a). We can use our simple model for environmental effects to examine the fraction of cluster galaxies (those with $M_{halo} > 10^{14}\ h^{-1}\ \mathrm{M}_{\odot}$) which may also be subject to environmental effects. This is presented in Figure 2.10 for a model which has $M_{\mathrm{trunc}} = 10^{12}\ h^{-1}\ \mathrm{M}_{\odot}$ and $T_{\mathrm{trunc}} = 3$ Gyr at all four redshift epochs.

The fraction of environmentally affected galaxies is a strong function of stellar mass in this model, and the gradient becomes stronger with increasing redshift. The most massive galaxies have resided within group-sized haloes since at least $z = 1.5$; thus any environmental effects would have manifested themselves a long time prior to observation, and we expect to see little signature of cluster growth in their properties. On the other hand, galaxies with lower stellar mass are a better tracer of the recent mass accretion history of the cluster, hence we see a strong evolution in the fraction of environmentally–affected galaxies.

### 2.3.5 Observational constraints

It is now useful to review the observational constraints on our model parameters, $M_{\mathrm{trunc}}$and $T_{\mathrm{trunc}}$. The halo mass threshold at which environmental effects become important must be at least as low as $10^{13}\ h^{-1}\ \mathrm{M}_{\odot}$ because there are observations of systems at this mass with significant environmental effects (Wilman et al., 2005a; Weinmann et al., 2006a). For this reason, we investigated a model with a low halo mass threshold, $10^{12}\ h^{-1}\ \mathrm{M}_{\odot}$, in Figure 2.9. Well defined samples of galaxy clusters show a significant Butcher-Oemler effect, such that the fraction of red galaxies decreases from $\sim 0.9$ at z=0.2 to $\sim 0.65$ at z=0.5 (Ellingson et al., 2001). This evolution is much quicker than predicted by a model with a $T_{\mathrm{trunc}}$of 2 Gyrs or less. Thus a model with $M_{\mathrm{trunc}}$ of $\sim 10^{12}\ h^{-1}\ \mathrm{M}_{\odot}$ and a $T_{\mathrm{trunc}}$of $\sim 3$ Gyrs is the

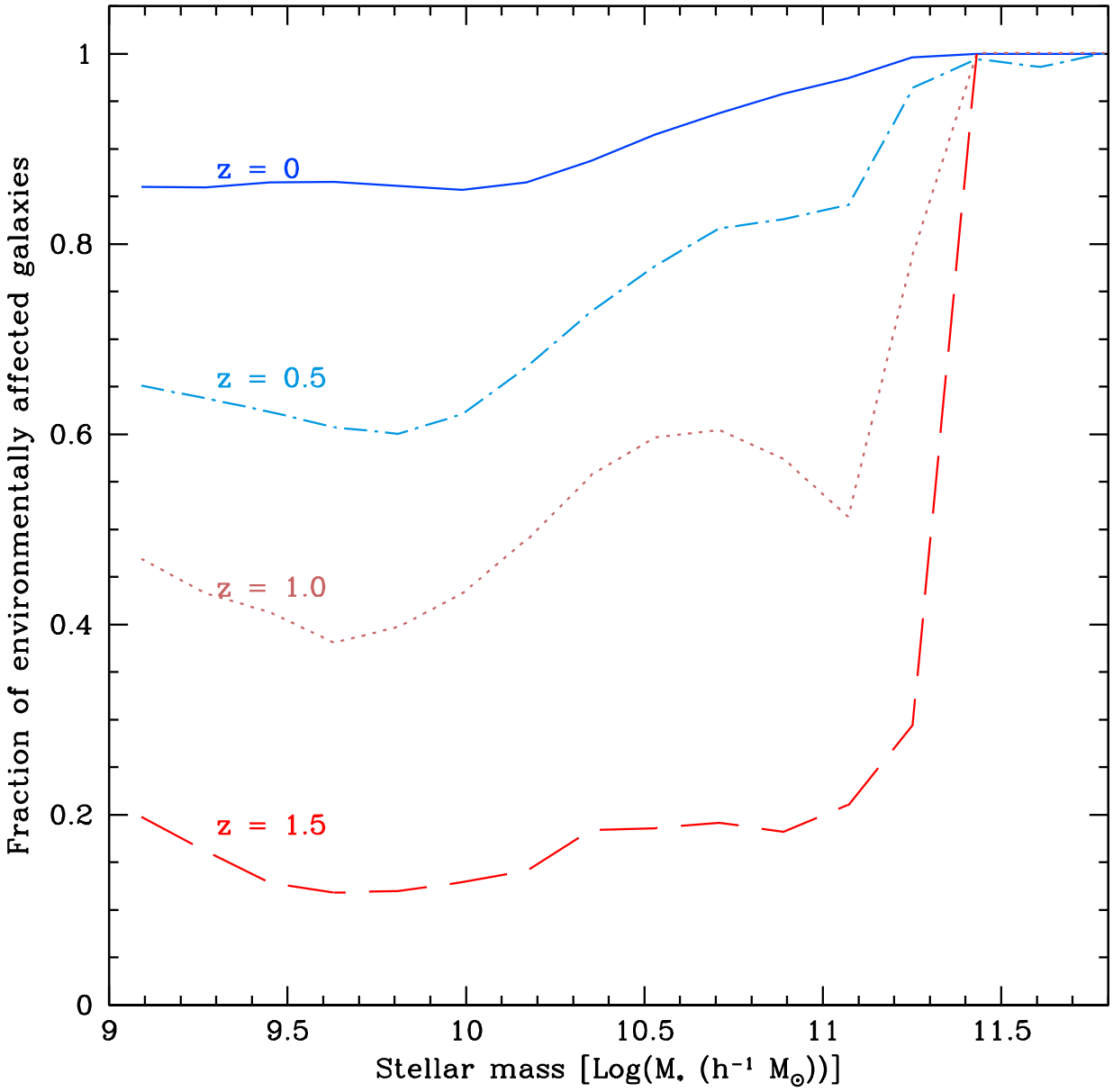


Figure 2.10: The fraction of environmentally affected galaxies in clusters at all four redshift epochs as a function of galaxy stellar mass. Cluster galaxies have host halo masses greater than $10^{14}$ $h^{-1}$ $M_{\odot}$at the epoch of observation. This model assumes $M_{trunc}$=$10^{12}h^{-1}$ $M_{\odot}$ and $T_{\rm trunc}$= 3 Gyrs as in Figure 2.8.

most favored model. As suggested previously, this leads to the prediction that by z=1.5, little or no environmental effects are felt by the galaxy population.

Recall §2.3.4, in which we investigated the stellar mass dependence of the galaxy population using our most favored model. We found that while the most massive galaxies are environmentally affected at all redshifts, the lower mass galaxies become more affected with time. Gilbank & Balogh (2008) used a compilation of the observational literature to show that the ratio of red bright galaxies to red faint galaxies steadily increases with redshift, the same qualitative behaviour we see in the simple model.

It is difficult to observationally quantify the extent to which massive galaxies are environmentally affected. This is largely because the visual colours of galaxies are not very sensitive to low levels of star formation. Mid-IR observations are more sensitive to low levels of star formation and thus are better at establishing the environmental influence of massive galaxies. Observations at z $\sim$ 0.4 suggest that only 10 % of massive galaxies ($> 10^{10}\ h^{-1}\ \mathrm{M}_{\odot}$) in groups have IR emission indicative of activity, while the global fraction is much higher ($\sim$ 40%, Wilman et al., 2008). Additionally, Wolf et al. (2009) find that massive galaxies are uniformly old and red in the cluster cores, while having a significant population of dusty, star-forming red galaxies in the infall regions. Both of these studies suggests that significant environmental effects are felt even by massive galaxies, as assumed in our model.

We emphasize that this observational comparison is qualitative, yet highly suggestive. In a future paper we investigate the quantitative behavior of these models with a direct comparison to the best available cluster, group and field data to z$\sim$ 1.

### 2.3.6 Comparison to Previous Work

In an attempt to explain observations of the fraction of cluster members with [OII] emission at z=0 and z=0.6, Poggianti et al. (2006) have presented a similar, but more complex model. The observations they present (their Figure 4) show that while, at z=0.6, higher mass clusters have lower average fractions of [OII] emitting galaxies, this is largely because of an upper envelope which decreases with increasing cluster velocity dispersion. In contrast, they notice that at z=0, the fraction of [OII] emitting galaxies is constant with cluster velocity dispersion above 550 km/s ($\sim 10^{14}\ h^{-1}\ \mathrm{M}_{\odot}$), but the scatter is large below that value.

In effect, to explain the observations, Poggianti et al. (2006) introduces two $M_{\rm trunc}$ and two $T_{\rm trunc}$ parameters to match the observed behavior. The first set of $M_{\rm trunc}$ and $T_{\rm trunc}$ are meant to represent 'primordially' passive galaxies, and are associated with elliptical galaxies. They claim that galaxies within $3{\times}10^{12}$ $h^{-1}$ $M_{\odot}$ groups at $z = 2.5$ represent these primordially passive galaxies. The second set of parameters are associated with quenched galaxies or S0 galaxies, and are set to have $M_{\rm trunc}{=}10^{14}$ $h^{-1}$ $M_{\odot}$ and $T_{\rm trunc}{=}$ 3 Gyrs. However, observations of galaxy groups with masses less than $10^{14}$ $h^{-1}$ $M_{\odot}$show a significant population of S0 galaxies and passive spiral galaxies (Wilman et al., 2009, McGee et al., in prep), which are hard to reconcile with their model. On the other hand, the lower value of $M_{\rm trunc}{\sim}$ $10^{13}h^{-1}$ $M_{\odot}$ that we advocate might have trouble explaining the large fraction of galaxies with [OII] emission in the Poggianti et al. (2006) clusters at $z \sim 0.5$. Undoubtedly both models are greatly oversimplified and, moreover, there are important systematic uncertainties in the current data (especially in determining cluster masses and galaxy star formation rates) and statistical limitations resulting from small sample sizes.

Similar constraints have also been derived in the past from observations of radial gradients in clusters. Balogh et al. (2000) used n-body simulations of the infall of substructure into clusters and concluded that, to match the radial gradients of star formation rates, the star formation rates in cluster galaxies must decline on the timescale of a few Gyrs after entering the cluster. Significantly, they also found that the best match to radial gradients was provided if the star formation rate in the galaxy began to decline as soon as it was found in a dark matter structure of group-size or larger. Ellingson et al. (2001) took this a step further and investigated the evolution of such gradients. They determined that 'field-like' galaxies became early type galaxies on a 2-3 Gyr timescale. Ellingson et al. also inferred that if galaxies were transformed on the 3 Gyr timescale, than the galaxy infall rate into clusters between z $\sim$ 1.5 and z $\sim$ 0.5 must have declined by $\sim$ 20 %. Our results suggest that the infall rate of galaxies into clusters over the same span fell by $\sim$ 15 %. This is a surprisingly good agreement given the large observational uncertainties at each step in this analysis.

Finally, it is instructive to reexamine the results of B09 in the context of our results. We have previously shown that B09 finds a lower fraction of galaxies within groups and clusters than we do (§2.2.1). This is likely due to a subhalo completeness level which varies as a function of environment. They use the global number density of subhalos above

their mass threshold and compare it against SDSS number densities to conclude that their global magnitude limit is $\sim 0.3$ $L_*$. However, when they compare number densities of their subhalos within clusters with cluster observations, they find that their cluster magnitude limit is $\sim 0.5$ $L_*$. Using the red galaxy luminosity function derived from a large sample of galaxy clusters by Lu et al. (2009), a magnitude cut of 0.5 $L_*$ instead of 0.3 $L^*$ reduces the number of cluster galaxies by $\sim$ 40 %. In other words, groups falling into their clusters could have $\sim$ 40 % fewer galaxies than would be expected from a consistent luminosity cut. Indeed, we find that this is on the order of the discrepancy between our results and those of B09. For instance, we have shown that, for $10^{14.2}$ $h^{-1}$ $M_\odot$ clusters, $\sim$ 35 % of galaxies have been accreted through $10^{13}$ $h^{-1}$ $M_\odot$ halos at z=0, while B09 find only 24%. While this disagreement is significant for evaluating the role of preprocessing in cluster assembly, a bigger factor is that the B09 clusters are not very massive. Indeed, these are smaller than the bulk of well studied clusters at intermediate and high redshift. We have extended their analysis to more massive clusters and find, as B09 themselves anticipated, that group pre-processing is potentially much more important for more massive clusters.

### 2.3.7 Towards a physically motivated model

We have shown, by following the accretion of galaxies into groups and clusters, and making simple assumptions about the nature of environmental effects on galaxies, that the halo mass at which environmental effects begin to be induced on galaxies is approximately $10^{12}$ – $10^{13}$ $h^{-1}$ $M_\odot$, and the time those effects take to manifest themselves is quite long (> 2 Gyr). Here, we address some of the more important simplifications we have made in constructing this model.

The first simplification is that we have assumed that an environmental effect will have a unique signature on the properties of galaxies. However, in comparing our model to, for instance, the fraction of red galaxies in clusters, we must acknowledge that there is more than one process which can make a galaxy red. In the local Universe, observations suggest that nearly all galaxies with stellar masses above $10^{10}$ $h^{-1}$ $M_\odot$ are red regardless of their environment (Baldry et al., 2006). However, as shown in Figure 2.10, in our simple model the most massive cluster galaxies would still be red, a consequence of the fact that they have resided within massive dark haloes for a long time. This, combined with the fact that the more numerous low mass galaxies dominate the fraction of galaxies in a cluster,

indicate that this is not a large complicating factor.

Secondly, we have assumed that all galaxies display environmental effects after a specific time $T_{\rm trunc}$, regardless of their incoming orbit. However, McCarthy et al. (2008b) has shown in simulations that the environmental effect on an infalling galaxy is dependent on the orbit of that galaxy. McCarthy et al. also showed that the bulk of the environmental effect on an infalling galaxy occurs when the satellite is at its pericentre. The size of this effect can be quantified by the variation in the time it takes a galaxy to fall from the virial radius to the pericentre of its orbit. In Figure 2.11, we show the distribution of times for a realistic distribution of infalling dark matter substructure from Benson (2005), randomly sampled 10,000 times. The distribution is shown as a mass-independent quantity, along with the best fit gaussian. A cluster of $10^{14}$ $h^{-1}$ $M_{\odot}$ has a $R_{vir}$= 1.26 $h^{-1}$ Mpc and $V_{\rm circ}$=400 km/s, which translates to a quite narrow distribution, with a dispersion of only $\sim$ 0.2 Gyrs. This will not have significant implications for a timescale which is greater than 2 Gyrs. It is worth noting that the simulations of Benson were not adequate to quantify the effect of any host halo mass dependence of the orbital distribution, but the indications are that this will not have a significant impact for our purposes. Additionally, we have assumed that all galaxies entering a massive halo feel similar environmental effects, however, galaxies with large pericentric distances may not feel strong effects, and thus predictions for the red fraction scatter and its mass dependence will still benefit from proper tracing of orbits in the future.

Thirdly, we have assumed that the mass of a halo is the important quantity driving any environmental effects. In fact, most of the physical processes which could produce environmental effects are likely more sensitive to X-ray gas density or temperature ($T_x$). For galaxy clusters and massive groups the scatter in the M–$T_x$ relation is actually quite small ($\pm$ 30 % at $M = 10^{14.5}$ $h^{-1}$ $M_{\odot}$). However, the Mass – X-ray Luminosity (M – L) relation, which is more sensitive to the gas density, does show significant scatter at cluster mass scales (McCarthy et al., 2004; Balogh et al., 2006). But this scatter is driven by properties of the group and cluster cores, while at the radius of a typical galaxy pericentre (0.2-0.3 times the virial radius), the scatter from system to system is quite small (McCarthy et al., 2008a; Sun et al., 2008). So the bulk of ram pressure stripping will occur at radii where the gas density has little scatter from system to system. However, this analysis is limited to fairly massive groups and clsuters, as measurement of X-ray properties for typical $10^{12}$ $h^{-1}$ $M_{\odot}$ haloes is quite difficult (Reiprich & Böhringer, 2002).

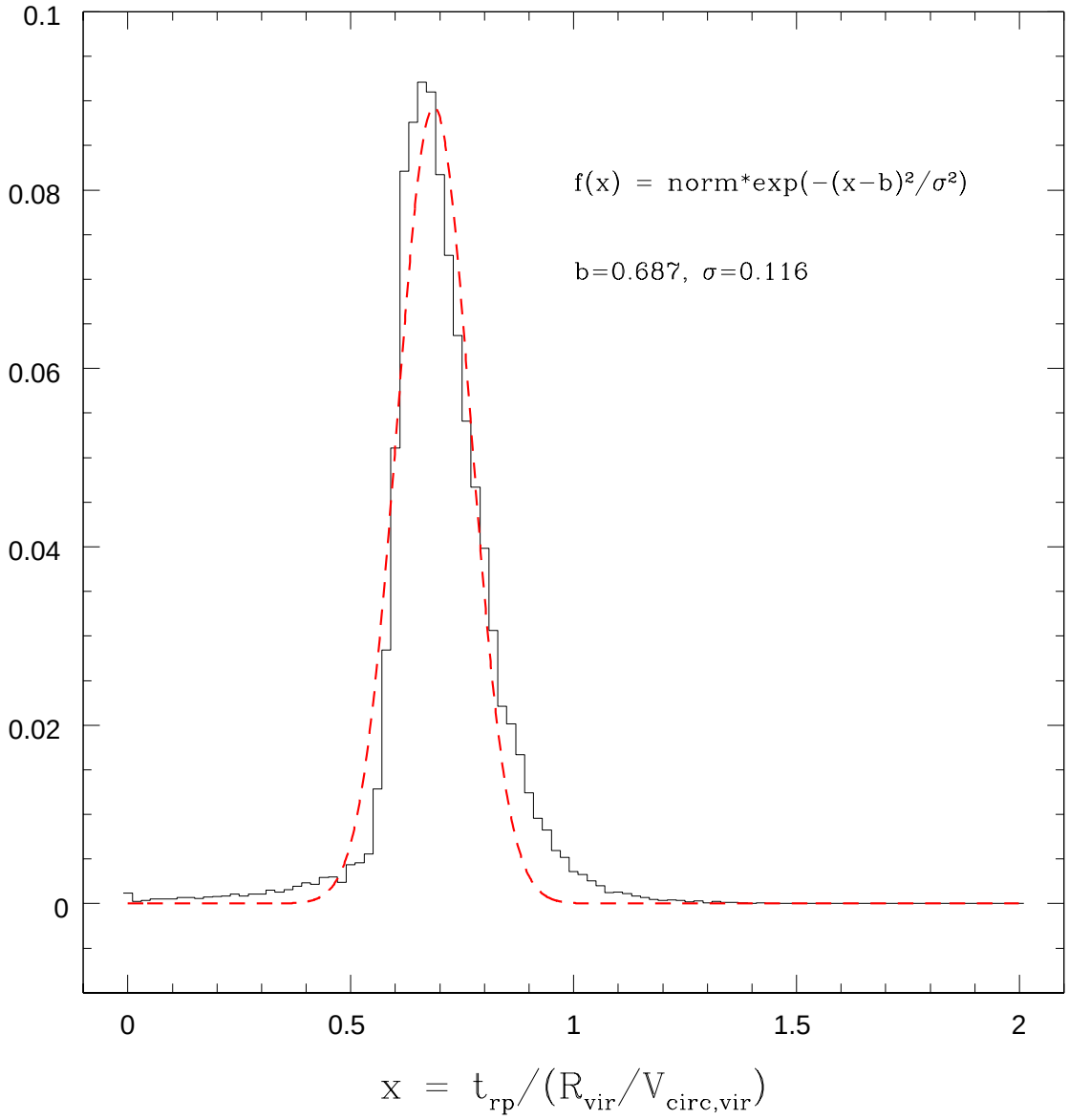


Figure 2.11: The distribution of times, $t_{rp}$ for an infalling dark matter substructure to reach its pericentre from the virial radius, $R_{vir}$, of a halo with circular velocity $V_{circ,vir}$. The black line is the distribution of $10^5$ randomly sampled orbits from Benson (2005) and the dotted red line is the best fit gaussian.

One theoretical indication of the size of this effect in low-mass groups comes from the scatter in the virial mass – circular velocity relation, which is approximately ± 15 % at M $= 10^{12}\ h^{-1}\ \mathrm{M}_{\odot}$(Bullock et al., 2001a). The circular velocity is more indicative of the depth of the dark matter potential, and thus is likely more closely correlated with the gas density. Despite this, the size of this scatter is likely not a huge source of uncertainty in our model, given that we only make broad statements about the characteristic halo mass scale. Given all of these results, it is encouraging that our model does not appear too simple to give important insights to the behavior of environmental effects.

The next step is to put this ad hoc model on a more physical basis. In particular, in our model we have specified that galaxies within a host halo are equally affected by environmental processes regardless of their position within the halo. But because the cooling rate of gas in a halo is density dependent, semi-analytic models treat galaxies at the center of halos (centrals) different from those not in the center (satellites). While this distinction is still a simplification (Simha et al., 2008), we point out the similarity between a model with a $M_{\mathrm{trunc}}$ of $10^{12}\ h^{-1}\ \mathrm{M}_{\odot}$ and one where the environmental effect begins to occur when a galaxy becomes a satellite, as shown in Figure 2.8 . Our most favored $M_{\mathrm{trunc}}$ model is essentially equivalent to choosing a physically motivated central/satellite model.

We have also employed a fixed timescale for environmental effects to occur. Ideally, we would like to link this timescale to a physically motivated quantity, such as the orbital timescale of a galaxy in a cluster or group. This mean timescale is approximately constant for the groups and clusters in our mass range at a given redshift epoch. However, because of the decreasing universe density with time, at high redshift the orbital timescale is actually smaller by a factor of $\sim (1+\mathrm{z})^{3/2}$. A timescale based on this would suggest that at z=1.5 the timescale is $\sim 4$ times shorter than the timescale at z=0. Unfortunately, directly implementing a timescale based on the orbital timescale would ignore several other complicating factors such as the evolution of cluster gas density profiles and the evolution of galaxy sizes and densities. Exploring these issues in a full semi-analytic galaxy model is the important next step forward.

## 2.4 Discussion and Conclusions

We have used the stellar mass and merger trees produced by the semi-analytic galaxy catalogues of F08 to follow the accretion of galaxies into groups and clusters at four different redshift epochs (z=0,0.5,1.0 and 1.5) for samples of galaxies with stellar mass $M > 10^9 h^{-1}$ $M_\odot$. By tracking galaxies through the hierarchy of structure formation we are able to examine the effect that environmental processes may have on the galaxy population of groups and clusters. Further, by adopting a simple model for the environmental effects, we are able to make strong claims about the timescale and mass threshold on which environmental effects occur. Our main results are summarized as follows:

- Clusters at all redshifts examined have had a significant fraction of their galaxies accreted through galaxy groups. For instance, $10^{14.5}$ $h^{-1}$ $M_\odot$ mass clusters at z=0 have had $\sim 40\%$ of their galaxies ($M_{\rm stellar} > 10^9$ $h^{-1}$ $M_\odot$) accreted through halos with masses greater than $10^{13}$ $h^{-1}$ $M_\odot$. At higher redshifts fewer galaxies are accreted through massive halos. Only $\sim$ 25 % of galaxies have been accreted through $10^{13}$ $h^{-1}$ $M_\odot$ into $10^{14.5}$ $h^{-1}$ $M_\odot$ mass clusters at z=1.5.

- We find only a moderate difference in the stellar mass accretion history and the galaxy accretion history at high cluster mass. That is, more massive galaxies are accreted preferentially through groups. While 45% of galaxies in $10^{15}$ $h^{-1}$ $M_\odot$ mass clusters at z=0 are accreted through halos with masses greater than $10^{13}$ $h^{-1}$ $M_\odot$, 50% of the stellar mass is accreted through the same halo mass range. Contrary to the study of Berrier et al. (2009), we do not see a large difference between the galaxy assembly of clusters and the mass assembly of clusters.

- Following from the previous point, we find that the extent to which galaxies are pre-processed in groups before falling into clusters depends on the stellar mass of the infalling galaxy. For a $10^{14.5}$ $h^{-1}$ $M_\odot$ mass cluster, 73 % of galaxies with stellar masses greater than $10^{10.5}$ $h^{-1}$ $M_\odot$ are accreted through $10^{12}$ $h^{-1}$ $M_\odot$ systems, while only 50% of $10^9$ to $10^{10}$ $h^{-1}$ $M_\odot$ are accreted through the same systems. Further, we find that in the accretion through group sized halos increases at late times when compared to the accretion into the cluster during early times.

- We have shown that the fraction of isolated galaxies infalling into z=0 groups and clusters is remarkably independent of the final cluster mass. 5-6 % of the final cluster

galaxies are accreted per Gyr for the last 10 Gyrs. Thus if a galaxy begins to be affected by its environment soon after becoming a satellite galaxy, and the time it takes for that effect to manifest itself is constant with halo mass, then a similar fraction of galaxies are affected in each cluster above a halo mass of $10^{13}$ $h^{-1}$ $M_{\odot}$.

- Despite the previous result, observing a cluster of the same halo mass at each redshift epoch implies different accretion rates of isolated galaxies, from 5-6 % per Gyr at z=0 to 15% per Gyr at z=1.5. Thus, in effect, the Butcher Oemler effect may be qualitatively explained by the shorter time available for cluster assembly at higher redshift.

- We find that combining the simple observations of the existence of a significant Butcher Oemler effect at z=0.5 and the observations that galaxies within groups display significant environmental effects with galaxy accretion histories justifies striking conclusions. Namely, that the dominant environmental process must begin to occur in halos of $10^{12}$ – $10^{13}$ $h^{-1}$ $M_{\odot}$ and act over timescales of $> 2$ Gyrs. This supports a long lifetime, gentle mechanism like strangulation.

- This simple model predicts that by z=1.5 galaxy groups and clusters will display little to no environmental effects. This conclusion may have limit the effectiveness of red sequence cluster finding methods at high redshift.

In essence, we have seen that systematic observations of intermediate and high redshift clusters and groups have the power to strongly constrain the mechanisms which induce environmental transformations on galaxies. However, because of the significant cluster to cluster variations in environmental effects, it is important that the method for selecting galaxy clusters and groups for observation must be easily and accurately reproducible in cosmological simulations. Only this will allow the careful testing of models against observations. In a future paper we will compare the best available data on groups and clusters at a variety of redshift epochs to further constrain the dominant environmental processes.

Significant progress on the implications of strangulation and the physical processes involved will need more extensive hydrodynamical simulations. The simulations of ram pressure stripping of the hot haloes of infalling galaxies by McCarthy et al. (2008b) is a significant step forward. However, there are important unknowns. In particular, how

effective are low mass group halos in stripping the infalling galaxies? Unfortunately, this is sensitively dependent on how the gas is distributed in both the infalling galaxy and the group halos. Indeed, the effectiveness of strangulation is also dependent on the strength of star formation feedback, and how reheated galaxy gas is distributed and stripped from the galaxy. The behavior of galaxies within small groups which subsequently fall into massive clusters is also unclear. To what extent are galaxies "shielded" by their local group from further gas stripping? Encouragingly, large scale hydrodynamical simulations are beginning to be able to address some of these questions (e.g. Crain et al., 2009).

So, while there is much room for improvement in understanding the details of galaxy – environment interactions, our results have shown that the galaxy accretion histories of groups and clusters combined with a simple model strongly suggest that the dominant environmental effect occurs over long time scales and is effective in low mass halos. In a future paper, we will examine these insights by making a quantitative comparison between semi-analytic models and the best available cluster, group and field data to $z \sim 1$.

# Chapter 3

# Evolution in the disks and bulges of group galaxies since $z = 0.4$

## 3.1 Introduction

Galaxies, at a simple level, are a mixture of two fundamental and distinct components: a bulge and a disk. In the local universe, bulge dominated galaxies are generally red and quiescent, while disk dominated galaxies are generally blue and actively forming stars (Blanton et al., 2003a). Thus, the morphology of galaxies may be important when trying to explain the observations that show the cosmic star formation density has rapidly declined from a peak at z$\sim$1-1.5 (Lilly et al., 1996; Madau et al., 1996; Hopkins, 2004), and that the fraction of red galaxies has rapidly increased over the same time (Faber et al., 2007; Bell et al., 2004). Indeed, these observations suggest that the process which transforms galaxies from disk-dominated to bulge-dominated is also the process which transforms them from the blue cloud to the red sequence (eg., Bell et al., 2007). However, studies of red, disk-dominated galaxies (Wolf et al., 2005) and blue, bulge-dominated galaxies (Abraham et al., 1991; Menanteau et al., 2006) suggest this model may be too general. In addition, the large fractions of passive spirals at intermediate redshift suggests that the truncation of star formation may happen before the morphological transformation mechanism (Poggianti et al. 1999, but see Wilman et al. 2008).

The local environment of a galaxy is an important factor in its evolution. Observations

of galaxy clusters have shown that galaxies within clusters have lower star formation rates than the general field (eg. Balogh et al., 1999). The rapid structure growth associated with ΛCDM cosmology, which increases the fraction of galaxies within galaxy groups, may be the key driver of the decline of galaxy star formation rates. Indeed, analogous to the lower star formation rates in clusters, there is a correlation between the local galaxy surface density and the morphology of galaxies (Dressler, 1980). At low redshift, the percentage of early type galaxies increases, and the percentage of late types decreases, with increasing density. Interestingly, Dressler (1980) found that this relation was equally strong in centrally-concentrated, relaxed clusters and in irregular, less centrally-concentrated clusters. At higher redshift, z $\sim$ 0.5, Dressler et al. (1997) showed that this *morphology-density relation* is stronger in highly concentrated clusters than in less concentrated clusters.

Although these studies point to the crucial role clusters play in the morphological transformation of galaxies, they are rare environments, and thus cannot have a large enough effect on the properties of galaxies to explain the decline of the star formation density of the universe as a whole. However, the less dense environment of optically selected groups is the most common environment for galaxies in the local universe (Eke et al., 2004). Indeed, Postman & Geller (1984) found that the morphology-density relation extends smoothly into the group scale environments. Further supporting the integral role of groups, suppressed galaxy star formation rates in group-scale environments of the local universe is now well-established (eg., Balogh et al., 2004a). Wilman et al. (2005a) have shown that the fraction of galaxies with [OII]$\lambda$3727Å emission, a measure of star formation, is much higher in group galaxies at intermediate redshift, z $\sim$ 0.4, than in the local universe; however, the group galaxies still exhibit suppressed star formation relative to the field at the same epoch.

The physical cause of the suppression of star formation since z$\sim$1 isn't clear, but there are many candidates, each with their own morphological signatures. Within the context of ΛCDM cosmology, galaxy mergers are often thought to be a dominant mechanism (Hopkins et al., 2007). Simulations suggest that a major merger between two gas-rich and star-forming spiral galaxies produces a gas-poor, passively evolving elliptical galaxy (Toomre & Toomre, 1972; Mihos & Hernquist, 1996). If dominant, this scenario suggests that quiescent spiral galaxies should be rare, and that the transformation of morphological type should precede or happen at the same time as the complete suppression of star-formation. Group environments are thought to be the ideal place for galaxy mergers because of their high density and small relative velocities.

Recently, driven by dual observations of large bubbles seen in the hot X-ray gas of the intracluster medium (McNamara et al., 2000; Fabian et al., 2000) and the correlation between the mass of the galactic bulge and the size of the central supermassive black hole (Magorrian et al., 1998; Ferrarese & Merritt, 2000), feedback from active galactic nuclei has become a popular explanation for the suppression of star formation rates in massive galaxies. Semi-analytic galaxy formation models have successfully introduced these mechanisms in a parametrised way (Bower et al., 2006; Croton et al., 2006), but the details are still uncertain. Such energy feedback mechanisms may not directly alter the galaxy morphology, but reduced star formation may result in significant fading of the disk component.

Meaningful morphological measurements are necessary to break the degeneracy of physical explanations of star formation truncation. Visual classification of galaxies onto a Hubble (or similar) system has proven to be very useful for the study of galaxy evolution. However, the high resolution and uniform quality of large galaxy surveys has given rise to automated morphology systems which attempt to make more quantitative measurements than a visual system will allow. Non-parametric morphology systems (eg. Abraham et al., 2003; Lotz et al., 2004) are robust, but are not easily linked to physical quantities such as bulge or disk scale lengths. For this reason, in this chapter we use a popular code, GIM2D (Simard et al., 2002), to fit parametric models to the surface brightness profiles. Parametric systems suffer because they fit an *a priori* model to the galaxy surface brightness and, as such, are prone to giving non-physical results in some cases. We therefore adopt the logical filtering system proposed by Allen et al. (2006), to help mitigate some of these effects.

In this chapter, we examine the morphological properties of optically selected samples of group galaxies at z=0.4 and z=0.1. In §3.2 we describe our data samples and our morphological measurements. In §3.3 we present the main data results and in §3.4 we discuss what the data tells us about galaxies in transformation and compare our data results with the semi-analytic galaxy catalogue of Bower et al. (2006). We summarize our main results in §3.5. Throughout this chapter we assume a cosmology with matter density $\Omega_m = 0.3$, energy density $\Omega_\Lambda = 0.7$, and present-day Hubble constant $H_0 = 100h$ km s$^{-1}$ Mpc$^{-1}$ with $h = 0.75$ (or $h_{75} = 1$).

## 3.2 The Data

### 3.2.1 The $0.3 \leqq z \leqq 0.55$ Sample

Our moderate-redshift galaxy sample is derived from the Canadian Network for Observational Cosmology Field Galaxy Redshift Survey (CNOC2), a spectroscopic and photometric survey completed with the Multi-Object Spectrograph instrument at the 3.6-m Canada France Hawaii telescope (Yee et al., 2000). The survey was designed to study galaxy clustering and evolution. It targeted galaxies in the redshift range $0.1 < z < 0.6$ over four different patches of sky totaling about 1.5 square degrees. The survey consists of 5 colour (U,B,V,$R_C$, $I_C$) photometry of ∼40,000 galaxies to a limiting magnitude of $R_C$=23.0 mag. Spectroscopic redshifts of ∼6000 galaxies were obtained with an overall sampling rate of 48% to $R_C$=21.5. This large survey allowed Carlberg et al. (2001) to identify a set of 200 groups using a friends-of-friends redshift-space group finder.

Wilman et al. (2005b) followed the CNOC2 survey with deeper spectroscopy of a set of 26 groups (20 targeted, 6 serendipitous) drawn from the Carlberg et al. catalogue using the Low Dispersion Survey Spectrograph (LDSS2) at the 6.5m Baade telescope at Las Campanas Observatory in Chile. These groups were chosen to lie within $0.3<z<0.55$, and galaxies brighter than $R_C$=22.0 were targeted for spectroscopy. This additional spectroscopy was designed to give near full completeness at bright magnitudes ($R_C<20$; for details, see Wilman et al., 2005b).

For each of the 20 targeted groups, we obtained single orbit *Hubble Space Telescope (HST)* Advanced Camera for Surveys (ACS) pointings in the F775W filter during Cycle 12. These data were processed with the ACS pipeline as described by Pavlovsky et. al (2005). The images were further processed with the *Multidrizzle* task in *pyraf* to remove cosmic rays and hot pixels.

Sources were detected in the *HST* ACS images using the SExtractor software v2.3.2 (Bertin & Arnouts, 1996). For a source to be accepted, the signal in at least 10 of its ACS pixels (0.5 arcsec$^2$) had to be a minimum of 1.3 $\sigma$ above the background. The faintest sources that are reliably detected using these criteria have $R_{775} \approx 23.9$. In this chapter we restrict the analysis to sources with redshifts ($R_C < 22$) and are therefore insensitive to these detection parameters. However, we are sensitive to the deblending parameters as the automated surface brightness fits use the segmentation image produced by SExtractor

to identify which pixels belong to the galaxy. We used 32 deblending subthresholds, with a minimum contrast parameter of $9.0 \times 10^{-4}$. By trial and error, these parameters gave the best deblending upon visual inspection of the output segmentation images.

We have used a suite of Bruzual & Charlot (2003) population synthesis models to k-correct our *HST* magnitudes. We have chosen to avoid large k-corrections by correcting all galaxies to the nearest restframe waveband, $V$. Figure 3.1 shows the models used. The k-correction is mainly sensitive to the star formation history and dust attenuation of the galaxy, and is insensitive to the initial mass function and the metallicity. We add a correction of $k' = -0.75\ z + 0.65$, shown by the red dashed line, to each of our galaxies. This was chosen to minimize bias for any single galaxy type, but dominates the uncertainty in the magnitudes to $\pm$ 0.1. In all cases, our statistical uncertainties dominate over this source of systematic error. All *HST* magnitudes are quoted in the k-corrected rest frame $V$ band.

**The Group and Field Samples**

The group catalogue of Carlberg et al. (2001) originally identified virialized galaxy groups in redshift space using an iterative friends-of-friends algorithm on the CNOC2 redshift catalog. They found over 200 groups, with an average of 3.8 confirmed members per group. To take advantage of the deeper and more complete LDSS2 spectroscopy available to us, we redefine the CNOC2 groups following Wilman et al. (2005b). Briefly, an iterative procedure is used, which initially selects galaxies within two times the velocity dispersion of the mean group redshift, and with a transverse distance from the group centre within 1/5 of the dispersion distance. In each iteration, the velocity dispersion is recomputed using the Gapper estimator (Beers et al., 1990) and the centre is recomputed as the luminosity-weighted geometric centre of the group. The iterations are continued until a stable group membership is reached.

Using these group centers and velocity dispersions, we restrict the membership of our group sample to galaxies within two velocity dispersions of the group redshift and within $500h_{75}^{-1}$kpc of the group center in the transverse direction. To obtain a true sample of group-sized halos we further restrict our group sample to have velocity dispersions $< 700$ km/s within $500h_{75}^{-1}$kpc of the group center.

Field samples of galaxies are commonly defined in one of two ways: as an "isolated"

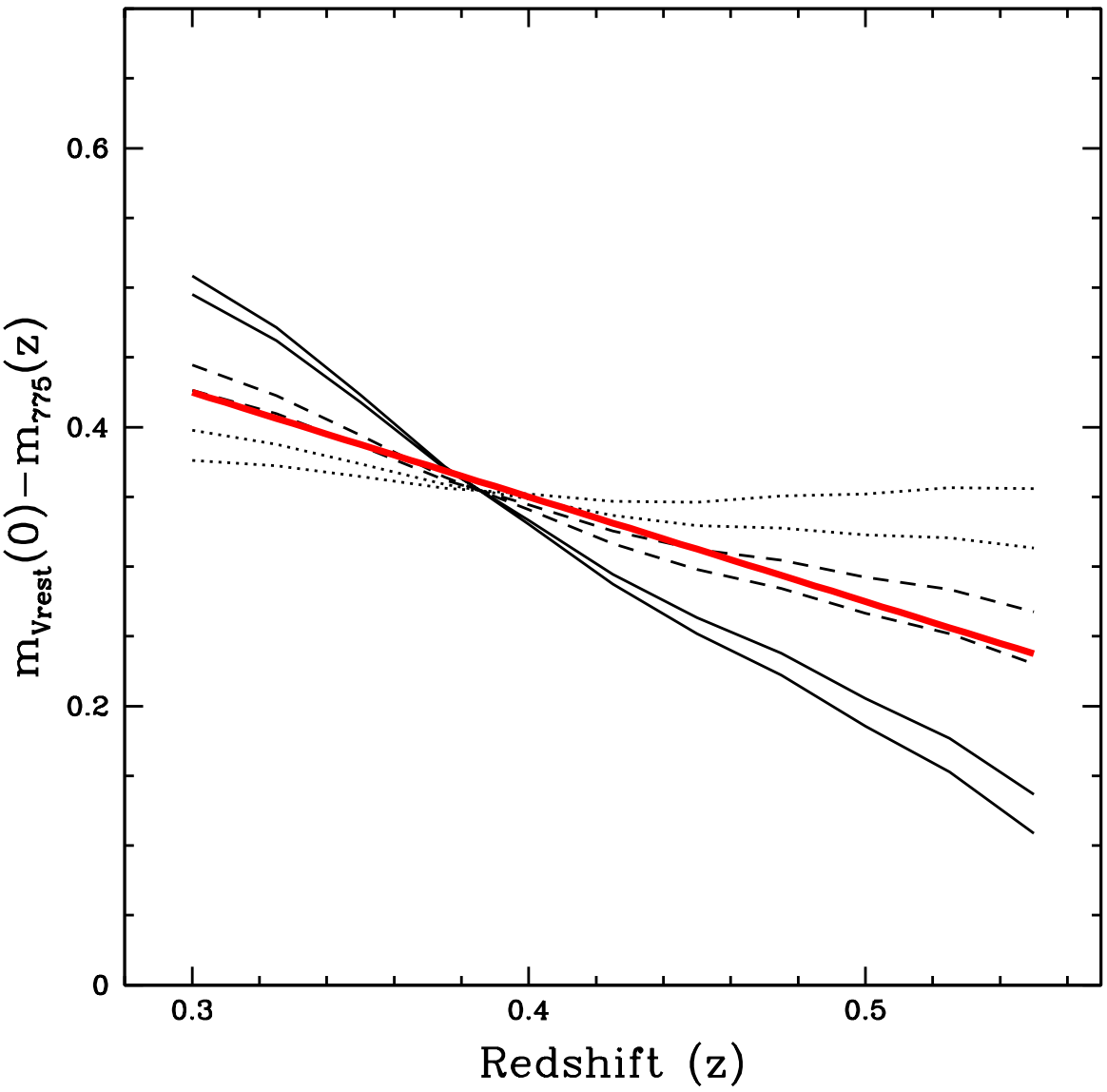


Figure 3.1: We show k-corrections to rest frame V band magnitudes, derived from a suite of Bruzual & Charlot (2003) population synthesis models. The solid lines indicate a constant star formation rate; the dashed lines are models with an exponentially declining star formation rate; and the dotted lines represent single stellar population models created at $z = 4$. All models are shown with and without one magnitude of dust extinction. The thick red line indicates the adopted k-correction of $k' = -0.75\ z + 0.65$.

sample, in which galaxies within groups and clusters are removed, or as a "global" sample, which includes all galaxies regardless of their environment. In practice, the removal of all group and cluster galaxies is not possible in our sample. Incomplete redshift sampling and the observational uncertainties associated with group membership would lead to an "isolated" field sample which still contained some group galaxies. Therefore, we prefer to define a field sample that contains all galaxies, regardless of their group or cluster membership. However, our follow-up spectroscopy focused on regions that have groups identified in the CNOC2 survey, and our morphologies are derived from small ACS images centered on our each of 20 targeted groups. To avoid the bias toward groups that would otherwise be present, we define our field sample to include only those galaxies that are not in groups as identified by the Carlberg et al. algorithm. As discussed in §3.2.2, because of the incompleteness of the CNOC2 survey, and the strict group finding algorithm of Carlberg, this leaves a field sample which is only slightly depleted in group galaxies when compared to the universe as a whole at z=0.4. A similar selection in the semi-analytic group catalogues discussed later (§3.4.3) shows that the field sample will have only $\sim 8\%$ fewer group galaxies than a true global field sample. We could correct for this bias by creating a true field sample which is an admixture made of 92% observed field sample and 8% group sample. However, all of our conclusions are insensitive to this correction, and for the sake of simplicity, we do not apply it to our results.

Using these definitions yields a sample of 114 group galaxies and 128 field galaxies with $0.3 \leq z \leq 0.55$ and $M_V < -19$.

### 3.2.2 The z $\sim$ 0.1 Sample

Our sample of low redshift galaxies is derived from the Millennium Galaxy Catalog (MGC). The MGC is a 37.5 square degree B-band imaging survey carried out using the Wide Field Camera on the Isaac Newton Telescope (Liske et al., 2003). The survey is a long, 35 arcmin wide strip, fully contained within both the Two Degree Field Galaxy Redshift Survey (2dFGRS) and the Sloan Digital Sky Survey (SDSS). The photometric catalogs are complete to B<24 mag, and the imaging is of sufficient quality to allow for the decomposition of galaxies into a bulge and disk component.

MGCz, the redshift survey component of the MGC, was designed to obtain AAT/2dF spectra of B<20 galaxies which were not covered by either 2dFGRS or SDSS (Driver et al.,

2005). This gives a redshift completeness of 96% for B<20 galaxies.

### The Group and Field Samples

There exist many low redshift group catalogues derived from either the SDSS or 2dF surveys. However, we wish to create a catalogue that can be compared directly and fairly with our higher-redshift group sample. The latter was derived from a two-step process — the initial survey and the targeted group follow-up — applied to an incomplete redshift survey. This method is not the most direct or efficient way to find groups in our lower-redshift sample, but it does accurately reproduce our higher-redshift selection and the possible biases within.

The primary goal of our low redshift group finding algorithm is to reproduce the selection criteria applied to our high redshift groups. Thus, our algorithm is not the most efficient method possible, but it does accurately reproduce our selection and the possible biases within. Further, this method will not result in a complete sample of groups in the MGC strip.

We first find groups in the SDSS main galaxy sample using the original method of Carlberg et al. (2001). The MGC strip is a narrow region, $\sim$ 35 arcmins across, which makes group finding within the strip itself difficult. For this reason, we first find groups in the SDSS, in a region 2 degrees across and centered on the MGC. We define our SDSS galaxy sample to be directly analogous to the CNOC2 sample. There are two areas of particular relevance to this work where these differ: completeness and depth. Because the SDSS has a much higher completeness ($\sim$ 90%) than the CNOC2 redshift survey ($\sim$ 48 %), we randomly remove half the SDSS galaxies. Further, we use the same absolute magnitude cut as Carlberg et al., $M_R = -18.5$, with an additional evolution correction of 1 magnitude per unit redshift.

Carlberg et al.'s primary goal was to find virialized groups in overdense environments, so they estimate the overdensity of each galaxy and restrict their group finding algorithm to galaxies in dense environments. A cylinder of $0.33h_{75}^{-1}$ Mpc radius and $\pm 6.67h_{75}^{-1}$ Mpc line-of-sight depth is centered around each galaxy and the number of galaxies within the cylinder is counted. If there are fewer than 3 neighbors in this cylinder, the process is repeated with a cylinder 1.5 times larger. A background estimate is then obtained by randomly drawing points from a redshift distribution fit to the entire sample. Figure 3.2

shows the redshift distribution of galaxies in our sample and our analytic fit. If the number of neighbours in the cylinder is greater than the background estimate then the main galaxy is kept as a possible group member.

Starting with the galaxy with the greatest overdensity, we begin a trial group by adding any galaxies within the original cylinder, and any of their friends. When we run out of friends we have a trial group, for which the geometric position, redshift and velocity dispersion are computed. Galaxies are trimmed or added within $1.5R_{200}$ and three velocity dispersions, where $R_{200}$ is the radius at which the density is 200 times the critical density. This process is iterated four times with the requirement that the last two iterations are identical. A group is moved to the next stage if it has more than two members. This concludes the Carlberg et al. algorithm.

The next stage is to emulate the process in Wilman et al. (2005b), to account for the targeted spectroscopic follow-up, which resulted in a more nearly complete redshift sampling around selected groups. We do this by including the complete SDSS catalogue. We use the Carlberg initial centres but set the velocity dispersion equal to 500 km/s, as was done by Wilman et al. This was done to remove any bias in the starting velocity dispersions, which were only based on very few galaxies. We again iterate on these positions using the entire SDSS catalogue and recompute the luminosity weighted centres. We compute the velocity dispersion at each step using the Gapper estimator and remove galaxies outside two velocity dispersions and $500h_{75}^{-1}$kpc. Finally, we keep only those groups which lie completely within the MGC strip. Using this method we have 19 groups with velocity dispersions between 100 km/s and 700 km/s, and which lie within $0.04 < z < 0.12$. Using a volume-limited sample of $M_B < -18$, we have a sample containing 99 group members and 3022 field galaxies. As discussed in § 3.2.1, a true field sample would contain all group members and field galaxies. However, to maintain consistency between the CNOC2 and MGC samples we do not exclude the small number of group galaxies from our field sample. In practice, due to the size of the field sample ($\sim 3000$), adding or removing the 99 group galaxies has no effect on the bulk properties of the field.

There exist a large number of group and cluster catalogues based on the SDSS and 2DF surveys with which we can compare. This is especially important to calibrate the systematic effects which may be present in our high redshift sample, which doesn't have sufficient completeness to quantify within the survey itself. One of the more popular group finding algorithms, and the most direct analogue to our method, is that of Berlind et al.

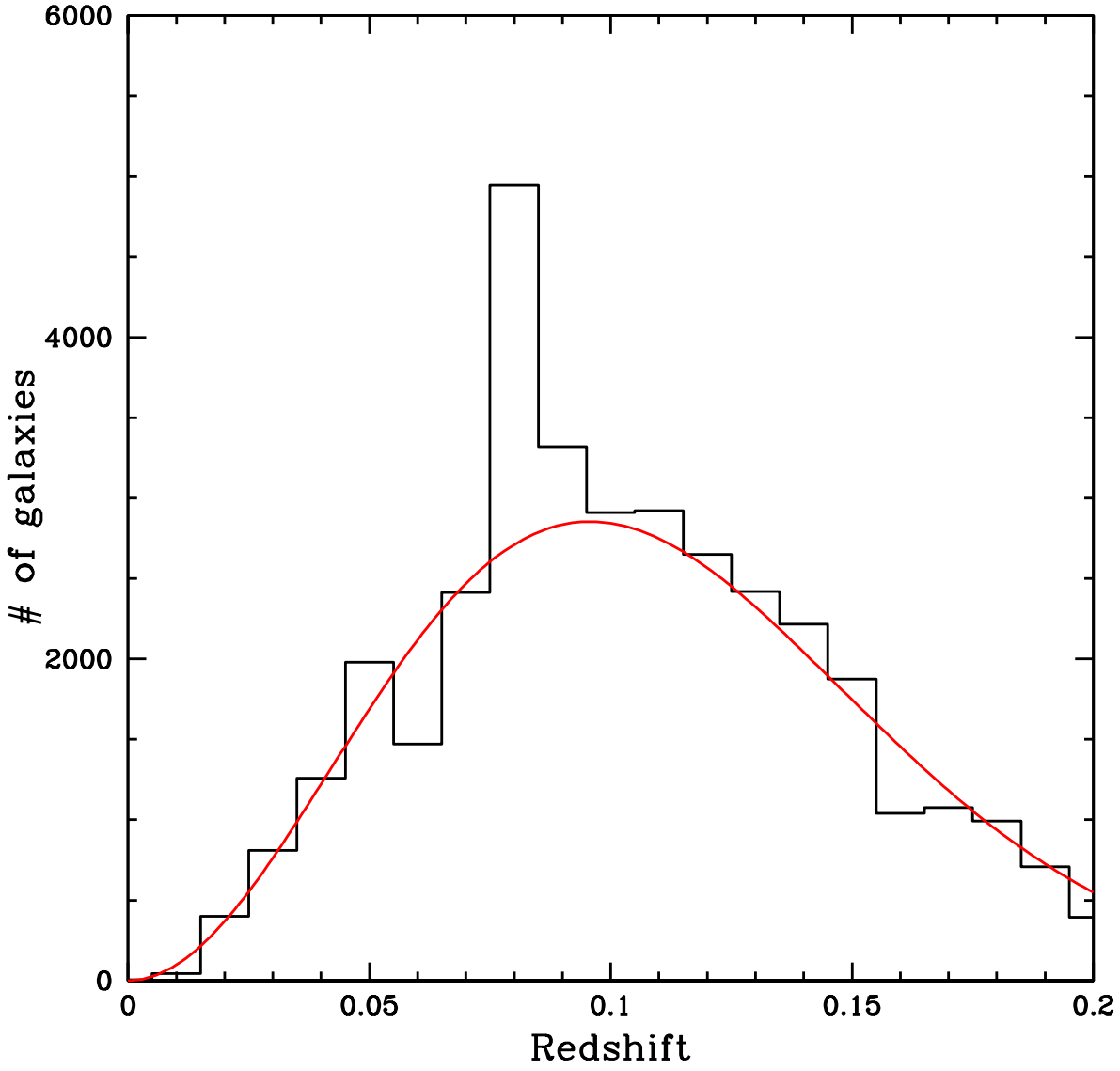


Figure 3.2: The redshift distribution of the full sample of SDSS galaxies which were used to find groups at low redshift. The red line is the Maxwellian fit to the data which was used to estimate the background.

(2006). They use a traditional friends-of-friends algorithm in position-redshift space to find groups in three different volume limited samples. We find that 12 out of 13 of our groups below z=0.1, the depth of the deepest Berlind sample, are also found in the Berlind catalogue, ie. the Berlind group centres are contained within our groups. Eighty-five of the 99 group members which make up the low redshift group sample in this chapter would also be group members if we were to use the Berlind catalogue as our group catalogue.

The low percentage of galaxies in groups in our sample seems in contradiction with other group catalogues based on local redshift surveys. For example, the 2dF Percolation Inferred Galaxy Groups (2PIGG) catalogue (Eke et al., 2004), which is based on the 2dF survey, finds that $\sim$ 55% of galaxies are in groups in the local universe. However, the fraction of 2PIGG groups with more than two members and within velocity dispersion limits of 100 km/s to 700 km/s (which are our criteria) is only 24%. The reduction of the sampling rate to match the CNOC2 completeness results in the non-detection of about half of these groups. A further 30% of galaxies are not found in groups because the Carlberg algorithm is not a strict friends-of-friends procedure: there is an additional step to check that candidate group galaxies are overdense with respect to the background. Accounting for these selection effects, we would only expect to find 9 % of galaxies satisfying our definition of a group. Finally, we also remove groups which are not fully contained within the very narrow MGC strip, i.e. the group centers are within $500h_{75}^{-1}$kpc of a survey edge. This step reduces the volume from which groups are selected from by $\sim$ 30 %. Our group catalogue is therefore incomplete relative to 2PIGG, but our sample is robust (see §3.4.3) and accurately reproduces the CNOC2 group-finding algorithm at higher redshift. The small number of group galaxies confirms, as suggested in §3.2.1, that our field sample is only slightly depleted in group galaxies when compared to the Universe as whole. Indeed, our results are unchanged if we include these group galaxies in our field population at this redshift, but for consistency with the CNOC2 groups, we do not.

### 3.2.3 Comparison of Surveys

The measurement of a galaxy's morphology can depend on a number of factors besides its intrinsic morphology, such as the imaging wavelength, angular resolution and surface brightness limit. Because of these systematic differences, direct measurement of morphological evolution is difficult. In this chapter, we largely concentrate on a direct comparison

between group and field galaxies at fixed redshift, which eliminates the effects of these systematic differences. Nonetheless, the MGC and CNOC2 are quite well matched in the key areas, which allows us to compare the differential group and field behavior between redshifts.

Specifically, the two surveys probe approximately the same restframe wavelength. The MGC survey is a rest frame B Band (observed frame $\sim$ 440 nm) survey, while our ACS images are in the rest frame V Band (observed frame $\sim$ 775 nm). Since disks tend to be bluer than bulges one might expect a lower B/T when measured in the B-band; however the intrinsic morphological differences are only significant at much wider wavelength separation (Taylor-Mager et al., 2007).

The apparent surface brightness limit of the MGC survey is 26 mag/arcsec$^2$ and that of the *HST* ACS images is 30 mag/arcsec$^2$. Figure 3.3 shows the absolute surface brightness limits of the two surveys as a function of redshift, including $(1+z)^4$ cosmological dimming. For the redshift ranges of interest, the absolute surface brightness limits are comparable.

The excellent angular resolution of our *HST* ACS images (point spread function (PSF) FWHM $\sim$ 0.1 arcsec) allows for morphological measurements of the CNOC2 sample. In fact, this gives a physical resolution which is somewhat better than the MGC survey (PSF FWHM $\sim$ 1 arcsec) in the redshift range of interest, as shown in Figure 3.4. Of greater concern is that the physical PSF of the MGC survey has a large variation within the sample itself, due to the redshift range spanned by the galaxies. Below we investigate the effect of the physical resolution on the morphological measurements. We find that the resolution differences have no effect on the bulge-to-total light measurements, but do affect the asymmetry parameter, causing the measured asymmetry to be higher in galaxies with better resolution. In this chapter, we only analyze asymmetry measures on matched samples of galaxies, which mitigates this effect.

The properties of galaxies vary with luminosity (eg., Baldry et al., 2004), so when comparing morphological properties between the two surveys we must use a common luminosity limit. Fukugita et al. (1995) have shown that late type galaxies (Scd to Sab) have B-V=0.5–0.78, while early type galaxies (S0 and E) have B-V=0.85–0.96. Thus, our $z = 0.4$ magnitude limit of $M_V$<-19 corresponds approximately to an MGC limit between $M_B = -18.5$ and $-18.0$, depending on type and neglecting any luminosity evolution. Therefore, when directly comparing the group and field behavior between the two surveys

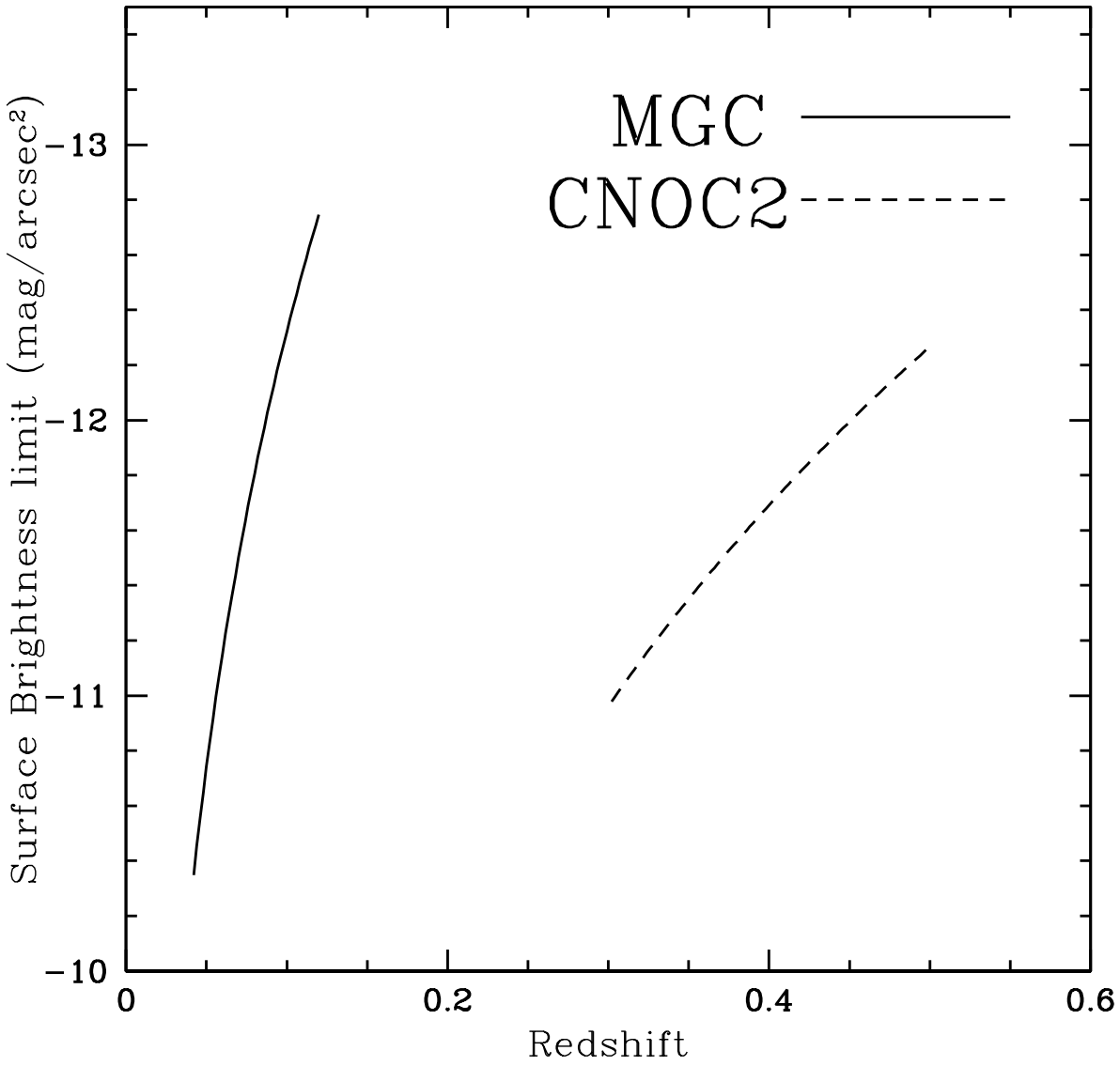


Figure 3.3: A comparison of the absolute surface brightness limits of our two samples of galaxies, as function of redshift. The solid line represents the MGC surface brightness (26 mag/arcsec$^2$), while the dashed line is the equivalent for the CNOC2 sample (30 mag/arcsec$^2$).

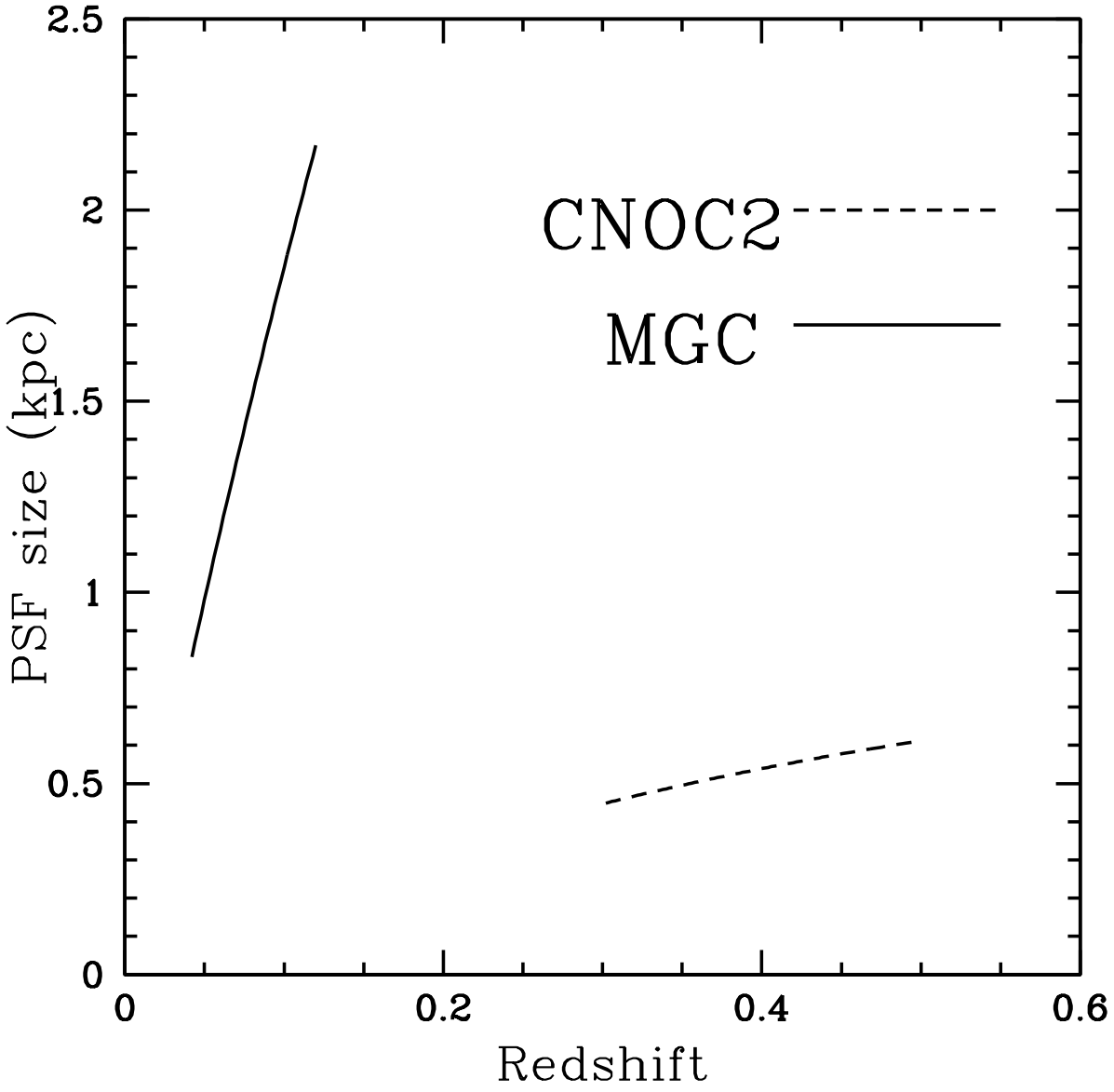


Figure 3.4: A comparison of the point spread function FWHM of our two samples of galaxies as a function of redshift. The solid line represents the ground-based MGC PSF (1 arcsec), while the dashed line corresponds to the *HST* resolution of the higher redshift CNOC2 sample (0.1 arcsec).

we only consider MGC galaxies brighter than $M_B \approx -18$ (except in Figure 3.8 which includes galaxies as faint as $M_B = -16$).

**Dependence of galaxy properties on PSF size**

As discussed in §3.2.3, the CNOC2 and MGC surveys compare well in absolute surface brightness limits, physical size of the PSF and the rest waveband used in the morphological decomposition. In fact, the biggest variation in these parameters is actually within the MGC sample itself. The PSF size is $\sim$ 3 kpc in size at z = 0.14 and just $\sim$ 1 kpc at z=0.05.

In this section, we investigate the redshift dependence of the key morphological indicators in three bins of redshift within the MGC sample. Some care must be taken because, as we have seen, the disk fraction changes rapidly with luminosity; therefore, without first matching on luminosity we would have a higher disk fraction in the lowest redshift bins. We have broken the sample into low ($0 < z <= 0.05$), medium ($0.05 < z <= 0.1$) and high ($0.1 < z < 0.15$) redshift bins. Each galaxy in the $0.05 < z <= 0.1$ bin was randomly matched to a galaxy in each of the other two redshift ranges with an absolute B magnitude within 0.03 magnitudes. The sample has 2169 galaxies in the $0.05 < z < 0.1$ range. They were matched to a unique sample of 266 galaxies in the $0 < z < 0.05$ range and 1354 galaxies in the $0.1 < z < 0.15$ range. Each galaxy was weighted by the number of times it was matched.

Figure 3.5 shows the B/T distribution of the three different redshift samples. These distributions are very similar in all redshift bins and our conclusions are unchanged if the field sample is taken as any of these bins.

In §3.3.3, we claim that the observed difference in the mean asymmetries between the CNOC2 sample and the MGC sample is due to the better physical resolution of the CNOC2 images. To test this we reduce the resolution of the original image and the residual image of a representative sample of 60 galaxies from our CNOC2 sample by convolving with a Gaussian with different widths. Figure 3.6 shows the asymmetry distribution of the original sample (thin, solid black line), and the asymmetries after broadening with a 1 kpc (black, dashed line) and 2 kpc PSF (thick, solid black line). Clearly the asymmetry is reduced with poorer physical resolution, which explains the higher asymmetries of the CNOC2 sample.

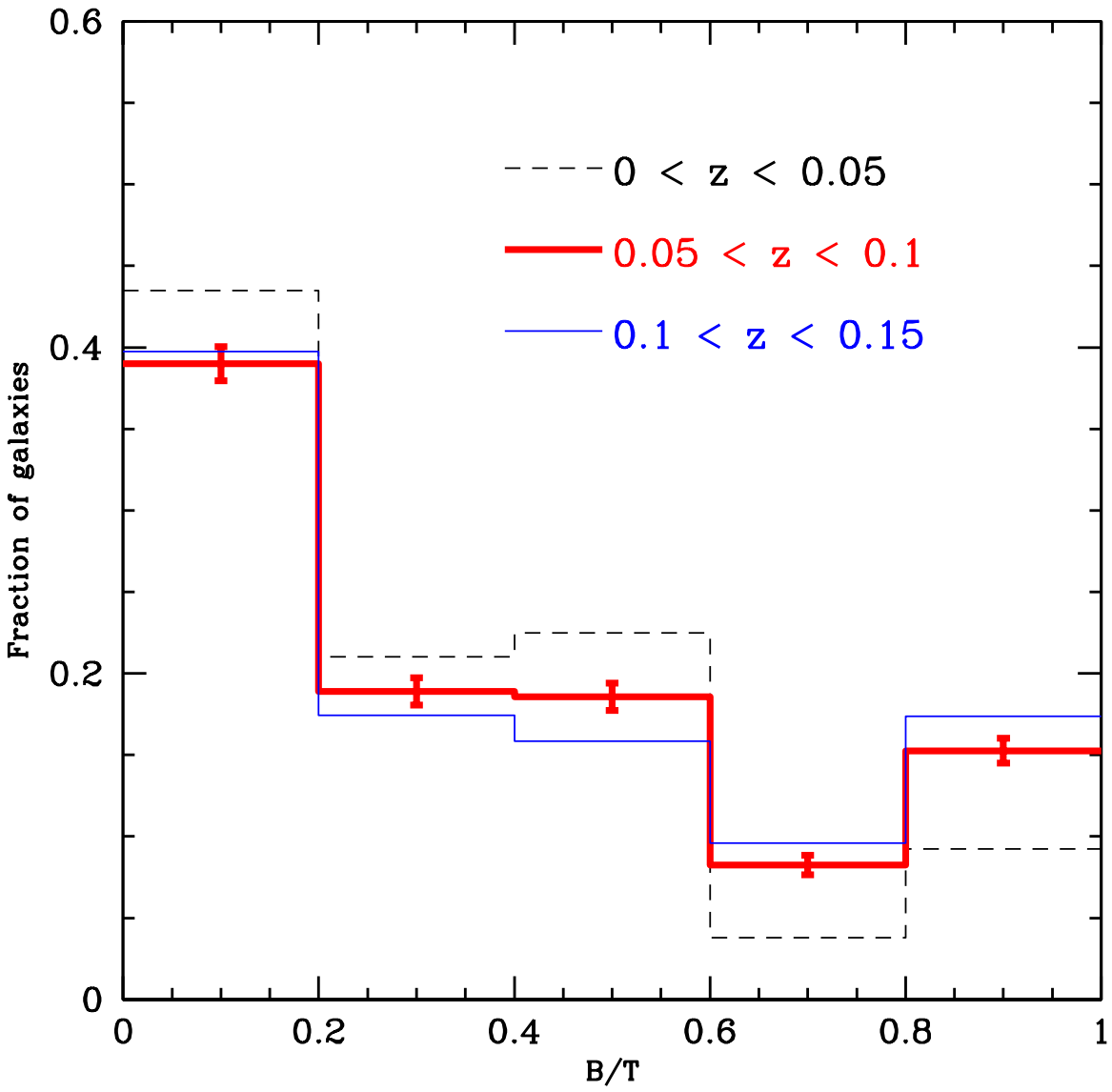


Figure 3.5: The B/T distribution of luminosity-matched samples of MGC galaxies in bins of redshift. The sample is divided into low ($0 < z < 0.05$; thin, dashed, black line), medium ($0.05 < z < 0.1$; thick red line) and high ($0.1 < z < 0.15$; thin, solid, blue line) redshift bins

For this reason, we do not compare the asymmetries between the two surveys and always use samples matched in redshift within a given survey.

### 3.2.4 Gim2d Morphological Measurements

Allen et al. (2006) have presented morphological measurements of the MGC and we follow their procedure to derive morphological parameters for the CNOC2 sample. We use the parametric IRAF package GIM2D (Simard et al., 2002; Marleau & Simard, 1998), which fits the sky-subtracted surface brightness distribution of each galaxy with up to 12 parameters describing a bulge and a disk component. GIM2D searches the large-parameter space of models using a Metropolis et al. (1953) algorithm, which is inefficient but does not easily get trapped in local minima. Häussler et al. (2007) have shown that GIM2D produces reliable fits with small systematic errors when the effective galaxy surface brightness is above the sky level, as it is for the galaxies in our sample. [1]

The GIM2D algorithm can fit single component (Sersic profile) or two component (Sersic + exponential disk) models to the galaxy profile. The Sersic profile is given by

$$I_b(R) = I_e \exp\left[-b_n[(R/R_e)^{1/n} - 1]\right], \tag{3.1}$$

where $I_e$ is the intensity at the radius, $R_e$, and $n$ is the Sersic index. The parameter $b_n$ is set to $1.9992n - 0.3271$ within GIM2D to ensure that $R_e$ is the projected radius which encloses half the total luminosity.

In a two component fit, the Sersic profile corresponds to the bulge model, and the disk is fit by an exponential model,

$$I_d(R) = I_0 \exp(-R/h), \tag{3.2}$$

where $I_0$ is the central intensity, $I_d(R)$ is the disk light profile as a function of radius $R$,and $h$ is the scale length.

[1] Haussler et al also show that another parametric galaxy fitting code, GALFIT (Peng et al., 2002), performs better than GIM2D in crowded fields. However, GALFIT uses a downhill gradient algorithm which, although very efficient, may not be as robust as the simulated annealing technique of GIM2D for problems with many local minima, like two- component fitting.

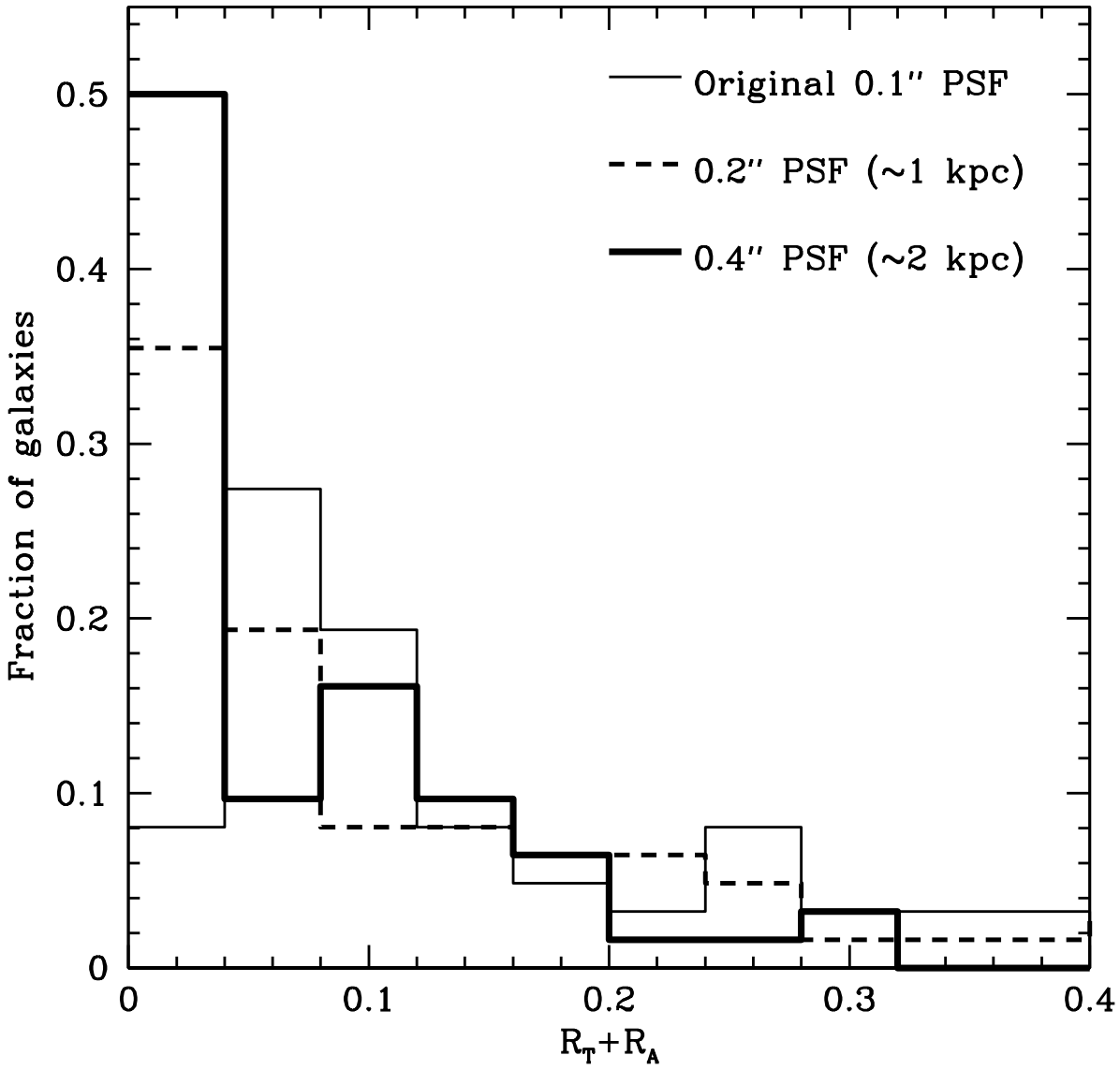


Figure 3.6: The distribution of asymmetries ($R_T$+$R_A$) measured within 2 halflight radii for different physical resolutions for a sample of 60 representative CNOC2 galaxies. The images were blurred with a Gaussian with a PSF of 1 (black, dashed line) and 2 kpc (thick, solid black line). The original, unblurred asymmetry is shown as the thin black line.

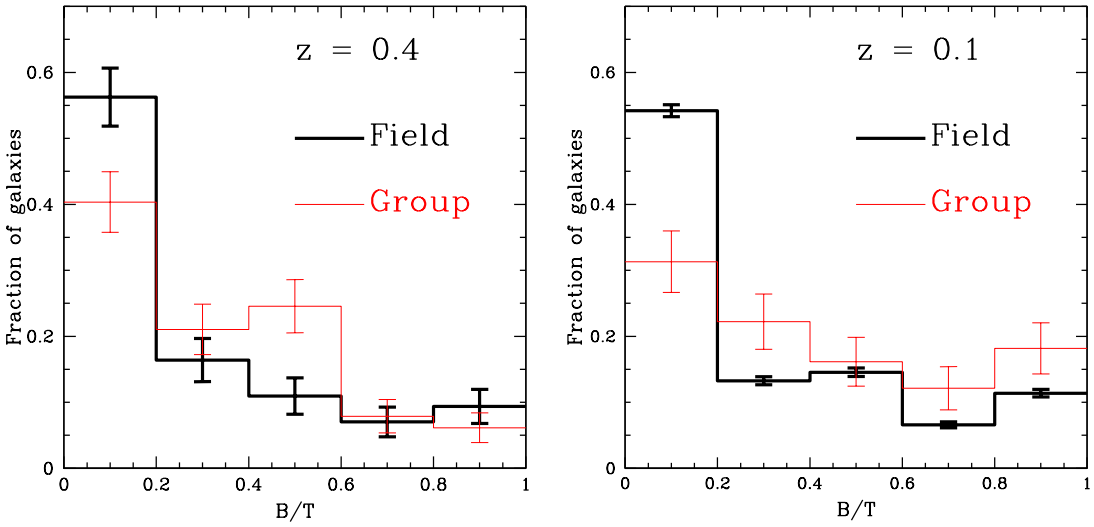


Figure 3.7: The histogram of relative bulge luminosity for the z $\sim$ 0.4 (left) and z $\sim$ 0.1 (right) samples. The thin red line in each plot indicates the stacked group at that redshift, and the thick black line is the field sample. Uncertainties are estimated with the jackknife technique.

Ideally, we would like to fit two components to all galaxies, but often galaxies do not have two resolvable components. It is for this reason that we follow the prescription of Allen et al. (2006), who have made a careful study of GIM2D output. They suggest a logical filtering system which initially fits a two-component model to the galaxy. For galaxies which have "normal" light profiles, this fit is kept, but for those galaxies which have perturbed profiles or are obviously better described by a single component, we fit a pure Sersic profile. In practice, this has little effect on our results.

### Residual Substructure

To quantify the substructure in the surface brightness profiles we use the residual parameter, R, as defined by Schade et al. (1995). This parameter is also known as the "asymmetry parameter, R" (Im et al., 2002) and the "residual substructure parameter, S" (McIntosh et al., 2004). It is defined as

$$R = R_T + R_A \tag{3.3}$$

with

$$R_T = \frac{\Sigma(|R_{ij} + R_{ij}^{180}|/2)}{\Sigma I_{ij}} - \frac{\Sigma(|B_{ij} + B_{ij}^{180}|/2)}{\Sigma I_{ij}} \tag{3.4}$$

$$R_A = \frac{\Sigma(|R_{ij} - R_{ij}^{180}|/2)}{\Sigma I_{ij}} - \frac{\Sigma(|B_{ij} - B_{ij}^{180}|/2)}{\Sigma I_{ij}} \tag{3.5}$$

where $R_T$ is the total residual parameter and $R_A$ is the asymmetric residual parameter. $R_{ij}$ is the flux at pixel position (i,j) in the residual image, $R_{ij}^{180}$ is the flux at (i,j) in the residual image rotated by $180^o$. $B_{ij}$ and $B_{ij}^{180}$ are the corresponding values in the background noise. Finally, $I_{ij}$ is defined as the flux at (i,j) in the object image. The sum is done over all pixels out to r= $2r_{hl}$, where $r_{hl}$ is the radius at which half the galaxy's light is enclosed.

## 3.3 Results

Although our data sample is comprised of a relatively large number of group galaxies (99 in the MGC sample and 114 in the CNOC2 sample), each group has typically less than ten spectroscopically confirmed members. Therefore, we stack the individual groups to maximize the signal of the bulk group galaxy proprieties. Weinmann et al. (2006a) have shown that the velocity dispersion of a group is a poor tracer of the mass of the group halo, especially for groups containing few confirmed members. Although our group velocity dispersions vary from 100 km/s to 700 km/s, Wilman et al. (2005b) has shown that the individual CNOC2 groups show no significant differences based on group type or velocity dispersion from a combined group. Thus we combine all the galaxies within $500h_{75}^{-1}$kpc of a group center at each redshift to form a stacked z$\sim$0.1 group and a stacked z$\sim$0.4 group. Because of the large uncertainties on the velocity dispersions we do not attempt to estimate a "virial radius" for each group, but instead simply require a group member to be within $500h_{75}^{-1}$kpc of the group center, corresponding approximately to the expected virial radius of a typical group in our sample, with a 360km/s velocity dispersion.

### 3.3.1 B/T Distribution

In Figure 3.7, we present the quantitative morphology distribution of the two samples. We compare field and group distributions of the ratio of the bulge luminosity to total luminosity (B/T) of each galaxy. Pure bulge galaxies have a B/T of 1, while pure disk

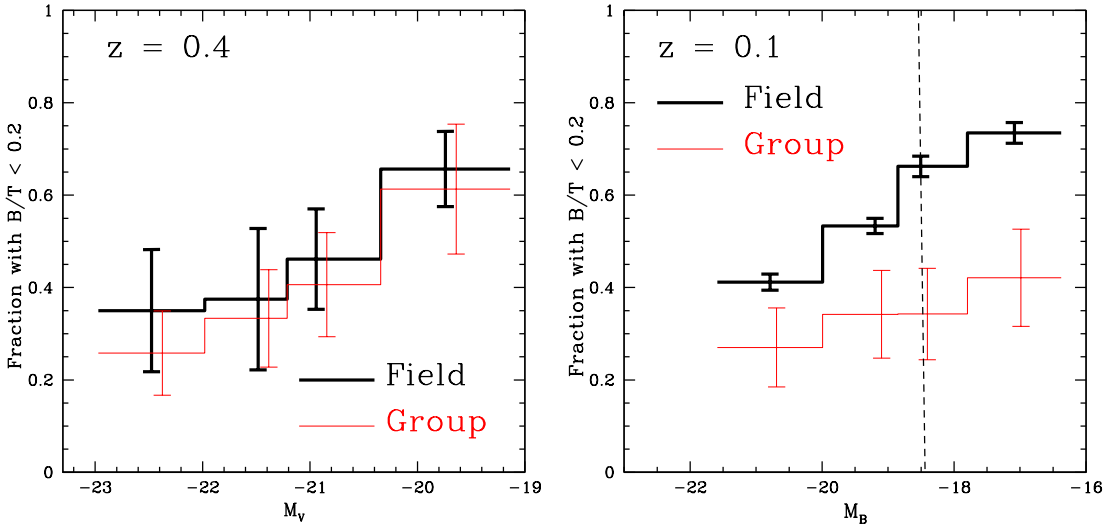


Figure 3.8: The fraction of galaxies with B/T<0.2 (disk-dominated) as a function of absolute magnitude. Left: The z $\sim$ 0.4 sample. Magnitudes are measured using the flux calculated by GIM2D and k-corrected to rest frame V band. Right: The z $\sim$ 0.1 sample, where magnitudes are measured in the B band. The field galaxies are represented by the thick black line and the group galaxies by the thin red line. The dashed vertical line indicates the equivalent B-band limit corresponding to the CNOC2 $M_V = -19$ magnitude limit, assuming a B-V color of 0.63. Uncertainties are measured using the jackknife technique.

galaxies have a B/T of 0. The left hand panel of Figure 3.7 shows the B/T distribution for the z $\sim$ 0.4 sample of galaxies. The red line represents the stacked group from the CNOC2 sample and the black line represents the field galaxies. A Kolmogorov-Smirnov (KS) test shows that the group and field sample are not drawn from a common parent distribution, with 98.4% confidence. The most significant difference within the CNOC2 sample is at B/T<0.2, where the fraction of galaxies in the field ($\sim 57 \pm 5\%$) is higher than that in groups ($\sim 41 \pm 5\%$). In the right hand panel of Figure 3.7, we present the B/T distribution for the z $\sim$ 0.1 sample. Similar to the CNOC2 sample, the fraction of B/T $< 0.2$ galaxies is much higher in the field ($\sim 54 \pm 1\%$) than in the groups ($\sim 32 \pm 6\%$). A KS test rules out a common origin for the group and field distributions of the MGC sample at greater than 99.9 % confidence.

In both plots we have seen evidence for the well-known morphology-density relation.

In this case, it is manifested as a deficit of disk dominated galaxies in the group samples when compared to the field. However, it is known that bright galaxies tend to be more frequently bulge-dominated than faint galaxies. Therefore, it is possible that this form of the morphology-density relation is related to different field and group luminosity distributions rather than any intrinsic difference between group and field galaxies at fixed luminosity. To explore this we present Figure 3.8, which shows the fraction of disk-dominated galaxies as a function of total galaxy magnitude. Studies of the B/T distribution of visually classified galaxies have shown that elliptical and S0 galaxies predominately have B/T>0.3-0.4 (Tran et al. 2001 and Wilman et al. 2009), but we chose to define "disk dominated" to indicate galaxies with B/T<0.2. This choice is made to isolate those galaxies in the bin with the most significant difference between the group and field samples, but our conclusions are unchanged even if we use B/T<0.4 to define disk-dominated galaxies.

The left hand panel of Figure 3.8 shows the z $\sim$ 0.4 sample, with the thick black line representing field galaxies and the thin red line representing the groups. In any one luminosity bin there is no significant difference (ie.> 1 $\sigma$) between the fraction of disk galaxies in the group and field; however, overall there is a systematic difference of 5.5 $\pm$ 2 %, in the sense that the fraction of disk-dominated galaxies in groups is always lower than in field galaxies of comparable luminosity.

The right hand panel of Figure 3.8 shows the disk fraction as a function of magnitude for the $z \sim 0.1$ sample. The magnitude is the rest frame B band, the waveband in which the B/T decomposition was done. In this figure, we show all galaxies in our redshift range to $M_B$=-16, fainter than our volume-limited sample of $M_B$<-18. The dashed vertical line indicates the equivalent B-band limit of the CNOC2 $M_V = -19$ magnitude limit, assuming a B-V color of 0.63, which is typical of a late-type galaxy (Fukugita et al., 1995). At this redshift there is clearly a significant difference in the fraction of disk-dominated systems between group and field galaxies of the same luminosity. This difference is 24 $\pm$ 6 % over the full magnitude range of the sample, and 19 $\pm$ 6 % brighter than the equivalent CNOC2 luminosity limit.

Although the B/T distributions of the group and field galaxies are different at both redshifts, this predominately reflects a difference in luminosity distributions at high redshifts, but an intrinsic difference in the fraction of disk galaxies of fixed luminosity at low redshift. It therefore appears that the morphological segregation in groups has increased significantly from z $\sim$ 0.4 to z $\sim$ 0.1. We recall that the z=0.1 sample is measured in the

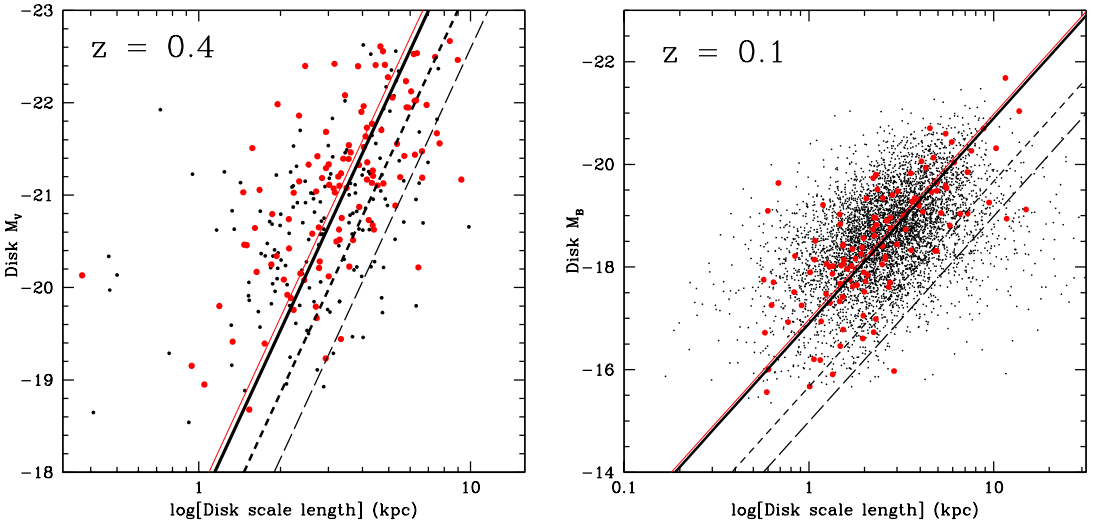


Figure 3.9: The distribution of disk magnitudes as a function of disk scalelength for non-bulge dominated galaxies (B/T <0.7). Left: z $\sim$ 0.4 sample. Right: z$\sim$ 0.1 sample. Large red points are group galaxies and small, black points are field galaxies. The thick solid black line is the best fit to the field, thin red line is the group best fit. The dotted (dashed) black line shows the effect of truncating star formation in field galaxies 1(3) Gyrs ago.

rest frame B band while the z=0.4 sample is measured in the rest frame V band. It would be possible to mimic our results if the disks of group galaxies were significantly redder than the disks of field galaxies. However, to create a B-band disk fraction consistent with the V band disk fraction, the disks of group galaxies must be B-V=2.07 redder than the disks of field galaxies. On average, in the MGC sample, pure disk (B/T=0) group galaxies are only B-V=0.01 redder than the pure disk field galaxies. Thus, it appears the evolution is real.

### 3.3.2 Structural Parameters

The evolution in morphological segregation suggests there is a change occurring within the group galaxies between z $\sim$ 0.4 and z $\sim$ 0.1. Here we focus on the possible causes of this evolution. We first look for structural differences between the group and field galaxies. If star formation in group galaxies is quenched, then the disk of the galaxy may slowly fade away, and we might expect to see a departure from the normal scaling relations between

disk size and luminosity.

In Figure 3.9 we plot the distribution of disk magnitudes as a function of the disk scalelength, excluding only the most bulge-dominated galaxies (B/T $> 0.7$). [2] The left hand panel shows the z $\sim 0.4$ sample, while the right hand panel shows the z $\sim 0.1$ sample. In both plots it is evident that there is a correlation between the disk size and its brightness, such that brighter disks have larger disk scale lengths. This is not surprising, but the fact that the group and field lie on the same relation (although with large scatter) is. The thick solid black line is the best fit to the scaling relation of the field galaxies. Best fit lines are determined using a robust biweight estimator which minimizes the effect of distant outliers. In principle, uniform fading of a perfectly exponential disk would result in a lower disk luminosity, but would leave the scalelength unchanged.[3] Therefore, an ideal population of faded disk galaxies would exhibit the same scaling relation, but with different normalization. Adopting this assumption, we fit only the normalization to the group galaxy relation, while maintaining the slope defined by the field galaxies, as shown by the thin red line. There is no statistically significant difference between the normalizations of the group and field populations (a difference of $0.086 \pm 0.134$ for the z=0.4 sample, and $0.103 \pm 0.151$ for the z=0.1 sample).

Since we do not see any significant difference in the disk scaling relations for group galaxies, it may be that the process of morphological transformation is instead dominated by a growing bulge (for example, through mergers). Again, if this were true, we might expect to see a deviation in the group and field bulge scaling relations. In Figure 3.10, we plot the distribution of bulge magnitudes as a function of the bulge half light radius, excluding the most disk–dominated galaxies (B/T $< 0.3$). The left hand panel shows the z $\sim 0.4$ sample and the right hand panel has the z$\sim$0.1 sample. The field and group distributions are again similar, at both redshifts. In §3.4, we examine the constraints these findings place on the amount of fading which is possible in the group sample.

[2] An occasional problem in modeling the surface brightness profile of galaxies with automated programs is the tendency to fit small disk (or bulge) components to galaxies which may have (e.g.) twisted isophotes. Thus we restrict our analysis to galaxies which have significant disk (or bulge) components when looking at their scaling properties.

[3] Häussler et al. (2007) have shown that the recovered scale length is underestimated for low S/N galaxies which are fit with a Sersic profile. However, our data are sufficiently deep to avoid this problem, typically reaching the surface brightness limiting isophotal radius at 3-5 disk scale lengths.

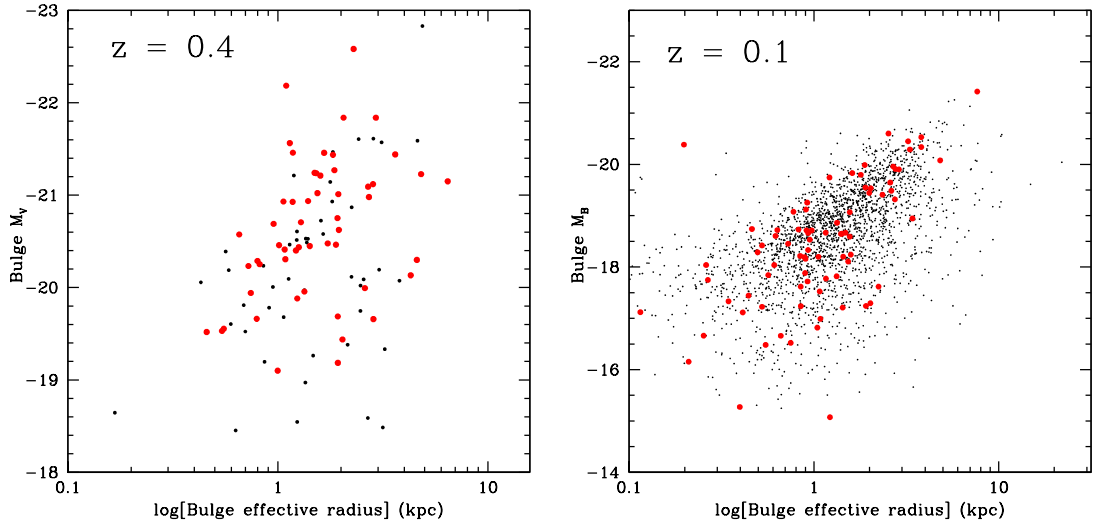


Figure 3.10: The distribution of bulge magnitude as a function of bulge half light radius for non-disk dominated (B/T $>$ 0.3) galaxies. Left: The z$\sim$ 0.4 sample. Large, red points are group galaxies and small, black points are field galaxies. Right: The z$\sim$ 0.1 sample. Red, filled points are group galaxies and black points are field galaxies.

### 3.3.3 Asymmetry

In this section we examine the asymmetries of the galaxies, to try to untangle a merger–driven transformation scenario from a gradual disk fading model. Galaxy mergers and harassment often produce noticeable asymmetric features, like tidal tails, which could manifest themselves as deviations from the smooth surface brightness profiles we have used for the morphological measurements. If galaxy mergers were enhanced in groups, we would expect to see an increase in the fraction of galaxies with large asymmetries. On the other hand, the cessation of star formation in the disk would likely result in the disappearance of bright clumps and spiral arms, thereby removing residual substructure, making the disks appear smoother.

We have seen that the fraction of disk galaxies depends on magnitude, and that the difference in the high redshift B/T distribution is partly due to different luminosity distributions in the field and group samples. For this reason, in the rest of this section, we match the field and group luminosity and redshift distributions. In the MGC sample, we match each group galaxy to the field galaxy with the closest magnitude and within 0.03

in redshift. The magnitude differences for these matched galaxies are all less than 0.02 because of the large number of available field galaxies in the sample. Similarly, for the CNOC2 sample, we match group galaxies to the nearest field galaxy in magnitude (within 0.2 mags) and within 0.05 in redshift. We match all 99 group galaxies in the MGC and 105 of the 114 CNOC2 group galaxies. The brightest CNOC2 group galaxies have no field counterpart, and so are effectively excluded from the remainder of this analysis.

To probe the substructure of the galaxies, we have calculated the asymmetry parameter according to the definitions given in §3.2.4. In Figure 3.11 we show the distribution in asymmetry for bulge dominated (B/T>0.5) and disk dominated (B/T<0.5) galaxies for both the CNOC2 and MGC surveys. The dashed vertical line indicates the lower limit for "highly asymmetric" galaxies ($R_T + R_A > 0.16$), as defined by Patton et al. (2005). Disk dominated galaxies have much higher median asymmetries than bulge dominated galaxies, as expected. However, there is no appreciable difference in the median asymmetry between the group and luminosity-matched field, in any of the samples. Although we can not resolve the disapperance of individual HII regions, visual inspection of disk dominated galaxies in Figures 3.12 and 3.13 clearly show that galaxies with low B/T and high asymmetries have strong asymmetric structures typical of star forming galaxies, ie. large spiral arms and lumpy regions. The lack of a systematic difference in the asymmetries of matched group and field disk-dominated galaxies means that we find no evidence for a mechanism that suppresses star formation in group disks.

We note that, as shown in Figure 3.4, the CNOC2 sample has a lower physical PSF than the MGC sample. We show below that galaxies which are blurred to have a lower physical resolution have lower asymmetry values. Therefore, we do not consider the change in median asymmetry between z $\sim$ 0.4 and z $\sim$ 0.1 as evidence of real evolution.

### 3.3.4 Images of a Sample of Group and Field galaxies at z=0.4

In this section, we show a representative sample of the group and field galaxies from our CNOC2 z=0.4 sample. As discussed in §3.2.3, the thumbnail images are from *HST* ACS observations. Each image is shown together with the GIM2D model and the residual of the *HST* image after the model was removed. We show the group galaxies in Figure 3.12, and the field galaxies in Figure 3.13. In Figure 3.14, we show images of the nine group galaxies

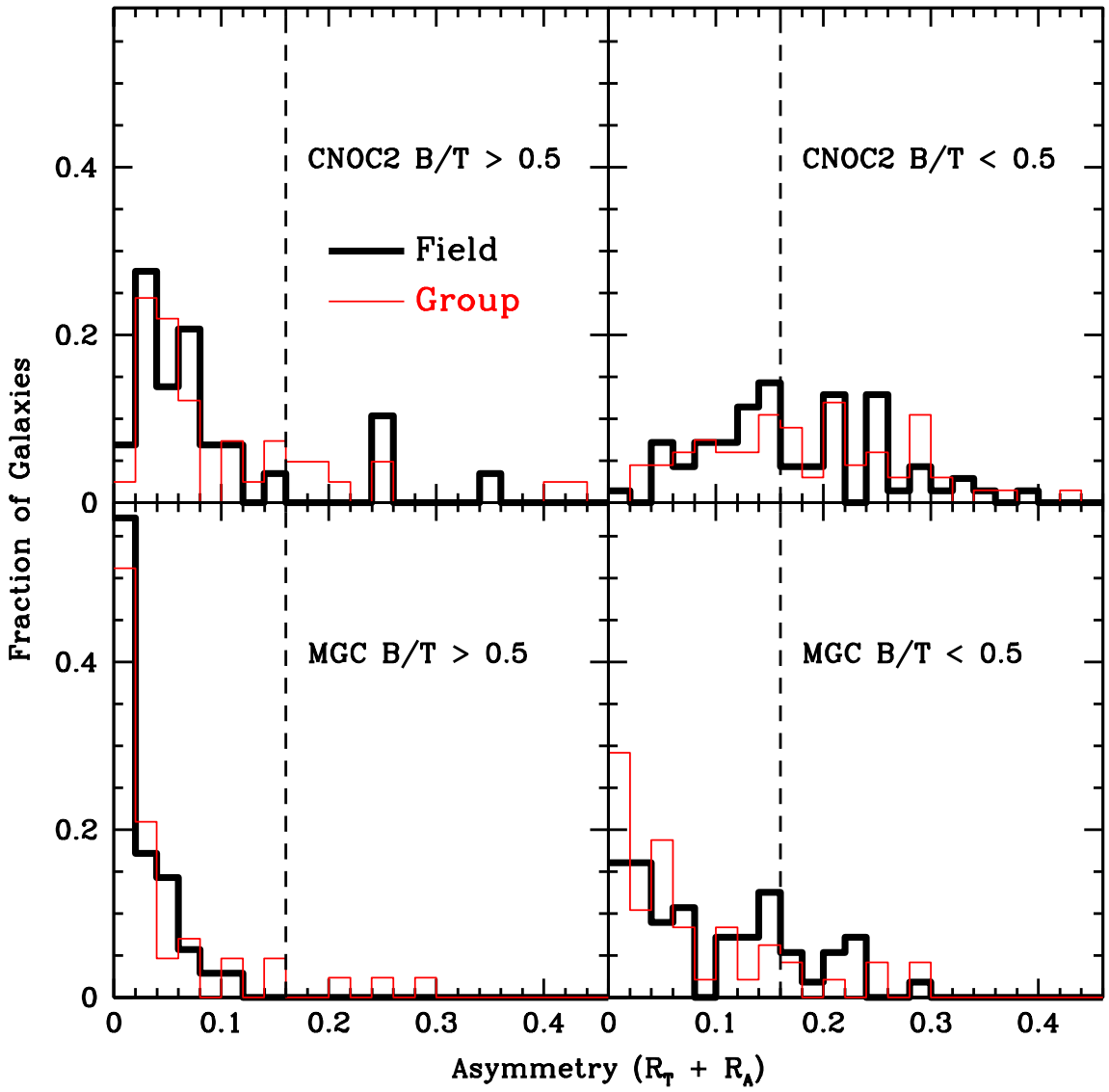


Figure 3.11: The distribution of asymmetries ($R_T$+$R_A$) for CNOC2 bulge dominated galaxies (top left), CNOC2 disk dominated galaxies (top right), MGC bulge dominated galaxies (bottom left), and MGC disk dominated galaxies (bottom right). In all plots group galaxies are represented by the thin red line and the luminosity matched field is the thick black line. The dashed vertical line indicates the lower limit for "highly asymmetric" galaxies ($R_T + R_A > 0.16$) as defined by Patton et al. (2005).

in the CNOC2 sample which are bulge dominated (B/T>0.5) and have high asymmetries ($R_T + R_A > 0.16$). The first four of these galaxies show interaction features.

## 3.4 Discussion

### 3.4.1 Galaxies in Transformation?

In this section we investigate how our results in §3.3 might constrain the number of galaxies that are in the process of transforming within the group environment. Specifically, we have shown in §3.3.2 that the bulge- and disk-components appear to obey scaling relations between size and luminosity that are independent of environment. This suggests that any transformation mechanism must either leave these scaling laws intact, or only affect a small number of galaxies at the epoch of observation. To investigate this, we consider a simple Bruzual & Charlot (2003) model with a constant star formation rate as appropriate for the disk components. If this star formation is suddenly truncated, within 1 Gyr it will have subsequently faded by 1.23 magnitudes in rest-$B$ (as measured for the MGC sample), or 0.68 magnitudes in rest-$V$ (appropriate for the higher-z CNOC2 sample). After 3 Gyr, the amount of fading expected is 1.91 mags (B) or 1.39 mags (V). However, such truncation should not affect the measured scale length of the disk. Therefore, if star formation were truncated in the entire population of group galaxies, we would expect the normalization of the scaling relation to change by these amounts. These relations are shown by the dotted (1 Gyr) and dashed (3 Gyr) black lines in Figure 3.9. These lines are significantly offset from the measured group relation (which is consistent with that of the field); therefore, we can easily rule out that star formation has been recently truncated in the entire disk population.

We would next like to establish what *fraction* of group galaxies could have undergone 1 (3) Gyr fading and still have a scaling relation that is consistent with the observed field scaling relation (ie. $< 2\ \sigma$ difference in the normalization, corresponding to a difference of 0.2 magnitudes for the MGC sample, and 0.18 magnitudes for CNOC2). To assess this we randomly choose a sample of group galaxies from Figure 3.9 and fade their disks for 1 (3) Gyrs according to the Bruzual & Charlot model described above. We recompute the B/T ratios of the sample, and impose our selection criteria on total magnitude and

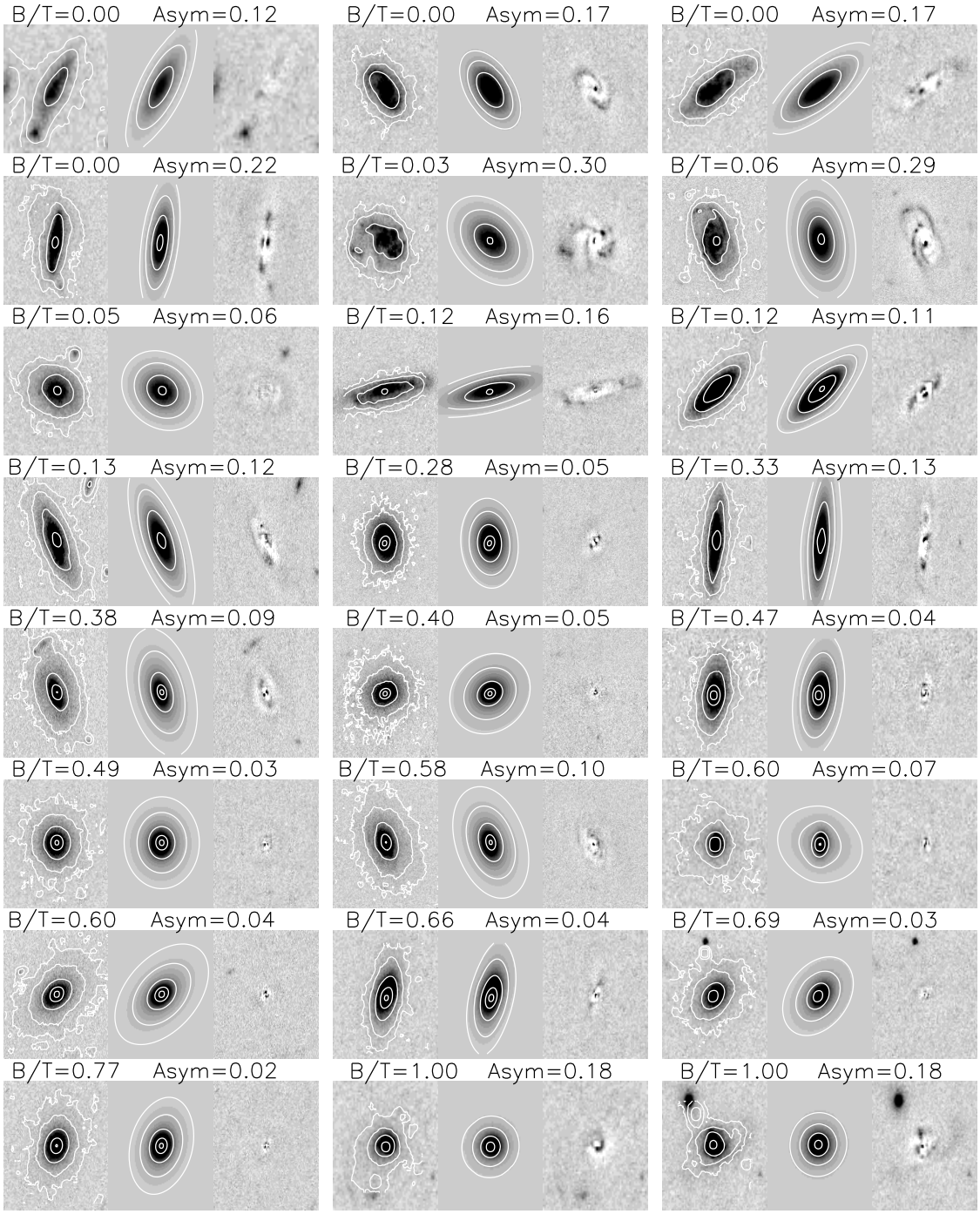


Figure 3.12: A representative sample of group galaxy images from the z=0.4 sample. For each of 24 galaxies is the *HST* ACS image (left panel), the GIM2D output model galaxy (middle panel), and the residual of the *HST* ACS image after the model is subtracted (right panel).

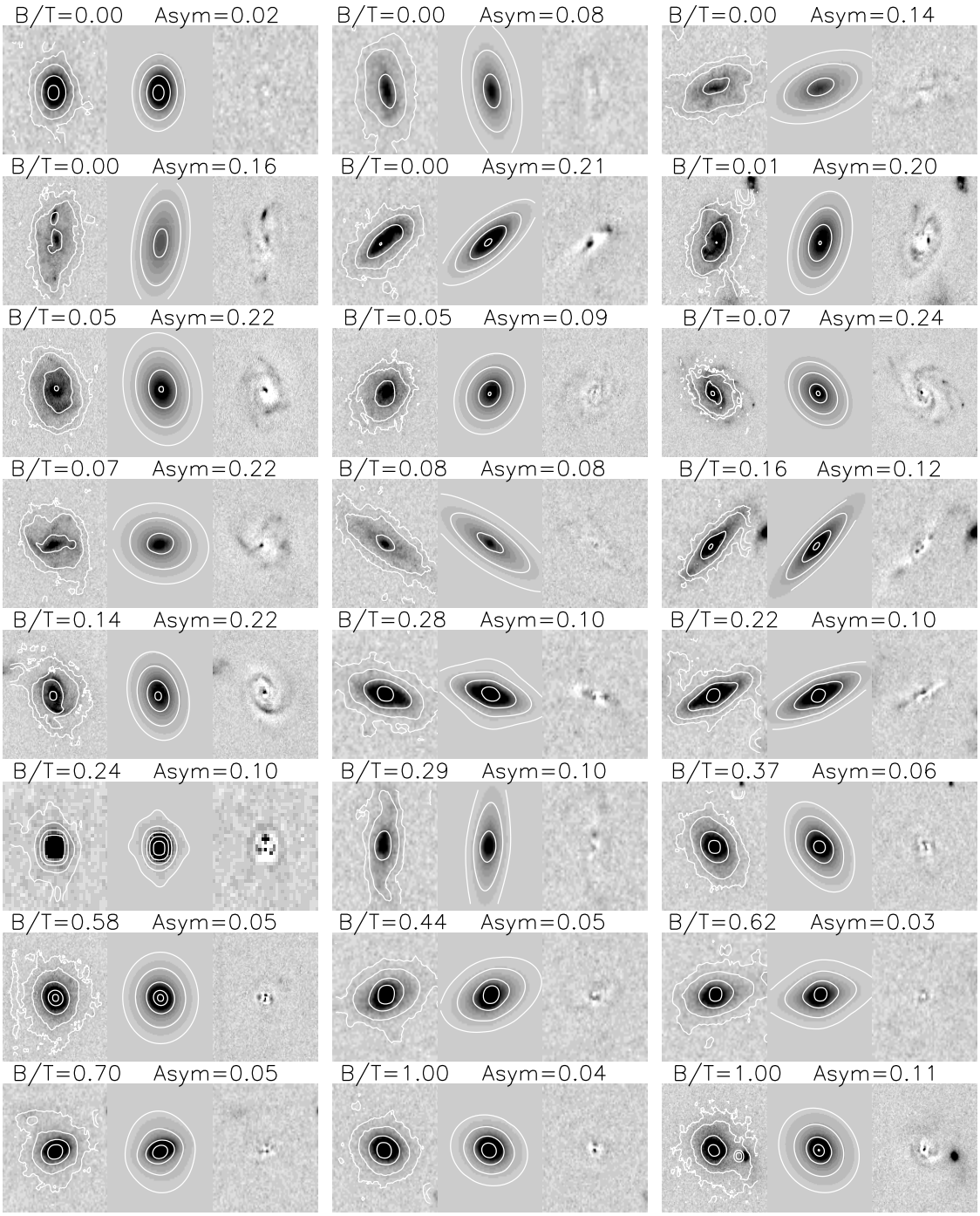


Figure 3.13: As in Figure 3.12, but for a representative sample of 24 field galaxies in the z=0.4 sample.

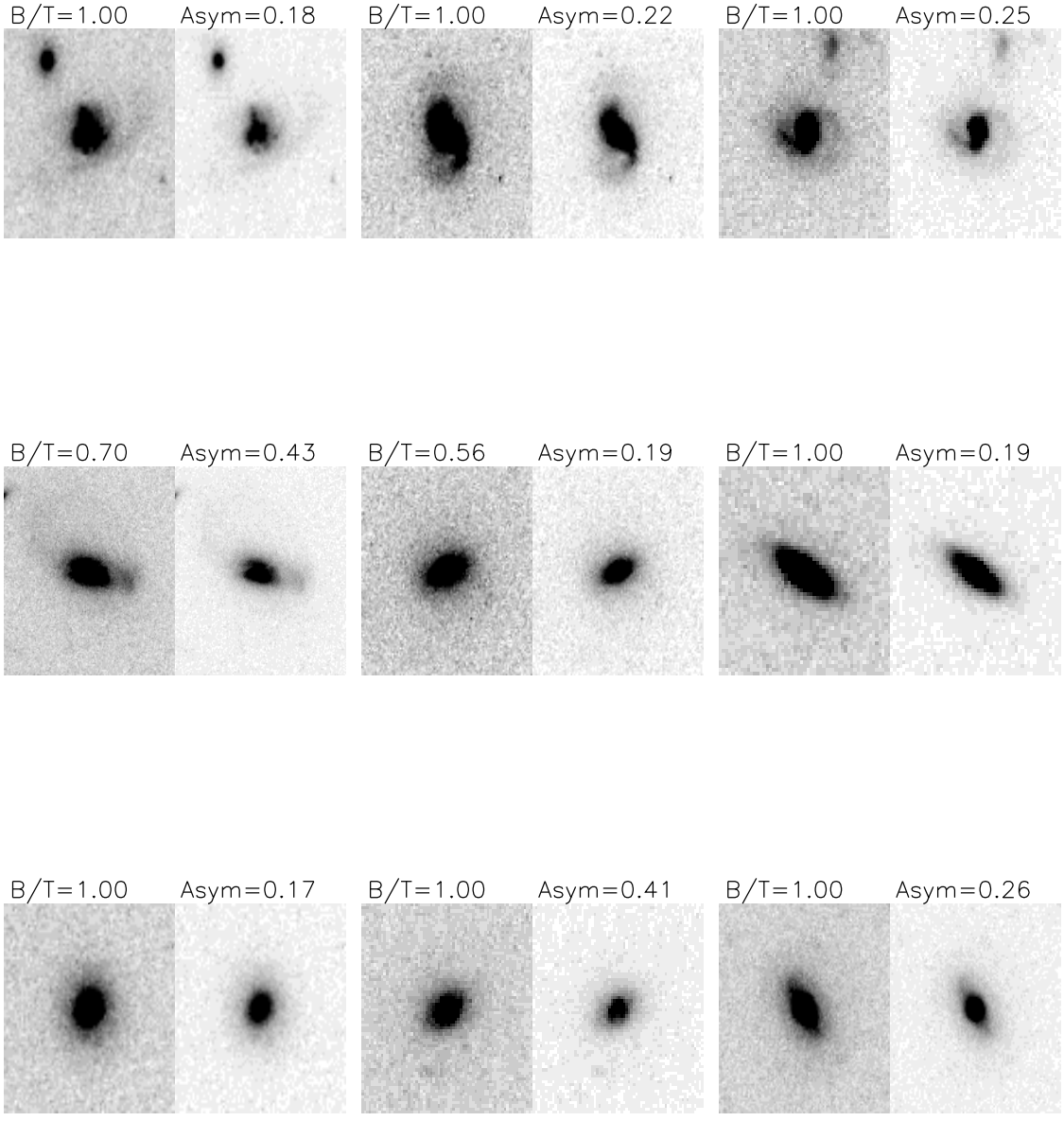


Figure 3.14: The nine group galaxies in the z=0.4 sample which are bulge dominated (B/T>0.5) and highly asymmetric ($R_T + R_A > 0.16$). The galaxies are shown with two stretches to show the interaction features. Prominent interaction features are seen in the first four of these galaxies.

B/T (recall we are excluding the most bulge–dominated galaxies from this analysis). The normalization of the scaling relation is then refit to the new set of data, keeping the slope fixed. We can then determine an upper limit on the fraction of galaxies which may have undergone such fading for 1 (3) Gyrs; these limits are $41 \pm 3$ % ($29 \pm 4$ %) for the CNOC2 sample, and $9 \pm 3$ % ($4 \pm 2$ %) for the MGC sample. The upper limit for the z=0.4 sample is quite high, as expected given the relatively small sample size. Therefore, based on these data alone, we cannot rule out the hypothesis that a substantial fraction of these galaxies are undergoing a significant change in their star formation rate. The upper limit for the $z = 0.1$ sample is much more restrictive, partly because of the sample size and partly because the rest-frame B-band is more sensitive to recent star formation. Our limits mean that any mechanism able to truncate star formation in disks is not dominant in present day groups.

Mergers are likely to be rare, but transformative events, so an increased merger history in groups would not be expected to increase the median asymmetry of group galaxies, but rather increase the fraction of highly asymmetric galaxies. By examining the fraction of galaxies with $R_T + R_A > 0.16$, we see that an extra $\sim 6 \pm 3$ % of group galaxies are highly asymmetric in the bulge-dominated samples at both redshifts, compared with the matched field sample (3.11). The fraction of highly asymmetric galaxies in the disk-dominated samples is similar for both the group and the luminosity-matched field. This may indicate that there is an increase of merging or interacting galaxies in groups. A visual inspection of the CNOC2 galaxies shows that 4 out of 9 of the "high-asymmetry" bulge dominated galaxies are indeed merging or interacting.

### 3.4.2 A comparison with X-ray selected groups

In §3.3.3, we have shown that the median asymmetry of group and field galaxies are statistically indistinguishable. These results are interesting because Tran et al. (2001) have shown that, in a sample of local X-ray selected groups, there is evidence for smoother disks in group galaxies than in the field. Studies of blue cluster galaxies have also shown that they have significantly lower asymmetry values than their blue field counterparts (McIntosh et al., 2004). Perhaps most intriguingly, Homeier et al. (2006) has recently shown that X-ray luminous clusters have galaxies with significantly lower average asymmetries than X-ray faint clusters. A related difference from our results comes from studies of X-ray group

galaxy morphology, which have shown that the fraction of early types is $\sim 0.7$ (Mulchaey et al., 2006; Jeltema et al., 2007) in the same magnitude and redshift range as our CNOC2 sample. To compare our data with this number we define early-type galaxies as those with B/T$> 0.4$, as Tran et al. (2001) has shown that this provides a good match with early type galaxies as classified on the Hubble-sequence. Using this definition, we find an early-type fraction of only $\sim 46$ % in the CNOC2 group sample, considerably lower than found in X-ray groups at this redshift. We revisit this issue in a follow-up paper when we consider and compare the results of Hubble-sequence morphological classification (Wilman et al., 2009). These results, combined with our result that the median asymmetry in optically selected group galaxies is not different from the luminosity matched field, point to the role that the hot intergalactic medium (IGM) may play in the smoothing of disk galaxies. Alternatively, the progenitors of optically selected groups may be different from the progenitors of X-ray selected ones.

### 3.4.3 Comparison with semi-analytic galaxy models

Recently, large dark matter simulations of large volumes have allowed theorists to produce usefully large catalogues of model galaxies, employing detailed modeling of galaxy formation based on relatively simple prescriptions for relevant physical processes. In this section we use the catalogues of one such "semi-analytic" galaxy formation model (Bower et al., 2006) to compare with our data. The Bower et al. model uses the dark matter Millennium simulation (Springel et al., 2005b), a $\Lambda$CDM cosmological box with $500/h$ Mpc sides, as the basis for the merger trees. The algorithm is based on the earlier GALFORM models of Benson et al. (2003) and Cole et al. (2000). The principal change from the Benson et al. model is a prescription for the quenching of star formation in massive halos by feedback powered by accretion onto a supermassive black hole. However, perhaps the most important change for our purposes is the modification of the method for computing disk instabilities. Disk instabilities are now the dominant mode of bulge formation in these models, although the brightest galaxies are still more often formed through mergers. Unlike older models, morphology is now sensitive to the baryonic physics of disks, rather than the (more robustly-predicted) merger history.

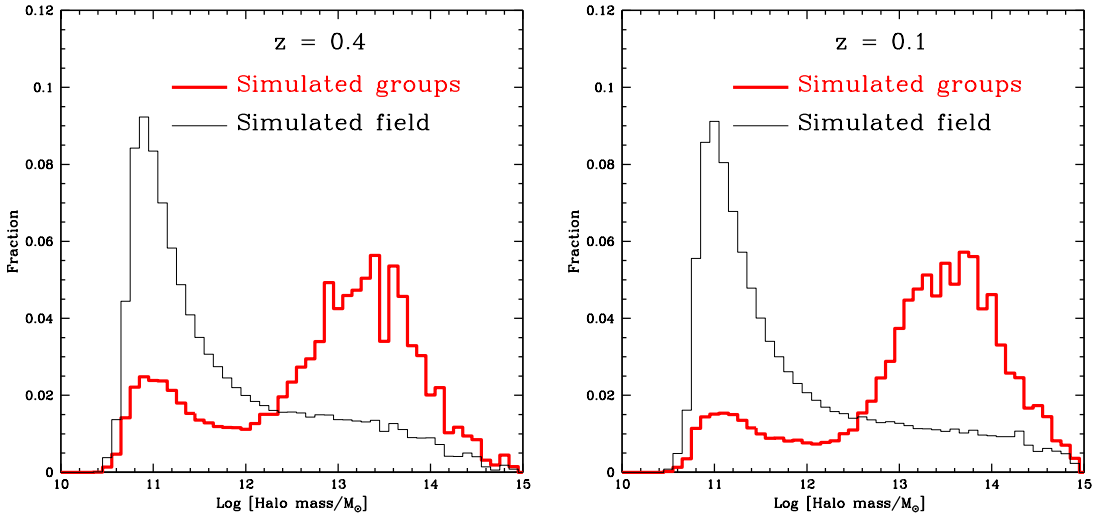


Figure 3.15: The distribution of halo masses for each galaxy in the Bower et al. (2006) model catalogue (thin, black line) and the distributions of galaxy halos in the simulated groups (thick, red line). The high redshift sample is on the left and the low redshift sample is on the right.

### Constructing a mock catalogue

We construct mock catalogues using the Bower et al. (2006) model for the z=0.1 and z=0.4 redshift time steps. Because of the large size of the Millennium simulation and the small spread in redshift of each of our samples, a single simulation box can be used for each epoch. Using the same group-finding procedure as described previously, we construct a stacked group sample to compare directly with our observations.

In Figure 3.15, we present the resulting distribution of galaxy halos in our group sample, compared with all halos in the Millennium simulation. We see that at both redshifts the group-finding algorithm selects predominately galaxies that are in halos with masses $5 \times 10^{12} < M_{\rm halo}/M_{\odot} < 10^{15}$. Both samples peak at $M_{\rm halo} \sim 6 \times 10^{13} M_{\odot}$, but the CNOC2 sample is somewhat biased toward lower masses than the MGC sample. Our algorithm finds a large percentage of groups that are made up principally of large dark matter halos: 76.4 % (85.1 %) of z=0.4 (z=0.1) galaxies are in halos with $M_{\rm halo} > 10^{12}$ $M_{\odot}$. In both plots there is a second peak – a distribution of low mass halos – which are contamination. However, we find that 79% (z=0.4) and 89% (z=0) of the $M_{\rm halo}$ $<10^{12}$

$M_\odot$ galaxies are within $500h_{75}^{-1}$kpc of a galaxy which resides in a halo with $M_{\rm halo}$ >$10^{12}$ $M_\odot$. Thus, the majority of our "contamination" is due to galaxies on the outskirts of a true group. This confirms that the Carlberg et al. (2001) algorithm selects groups which are real, and representative of massive dark matter halos, as also confirmed by previous weak lensing measurements (Parker et al., 2005) and our follow-up spectroscopy (Wilman et al., 2005b). Only 2.5 % (3.1 %) of our z=0.4 (z=0.1) galaxies are not associated with a massive ($M_{\rm halo} > 10^{12} M_\odot$) halo.

### B/T distribution

In Figure 3.16, we show the Bower et al. (2006) model predictions for the B/T distributions corresponding to our data samples. In all four panels the data are shown with a thick black line and the model predictions are shown with a thin, dashed, red line. The models are limited at $M_B < -18$ in the MGC comparisons, and by $M_v < -19$ for the CNOC2 comparison.

It is clear that there is remarkable agreement between the model and the data at z=0.1, especially considering that the model does not take into account any observational uncertainties associated with deriving B/T ratios from the surface brightness profile alone. However, the agreement between the models and the data at z=0.4 is not as good. In particular, the model underpredicts the fraction of B/T $< 0.2$ galaxies and overpredicts the fraction of B/T $> 0.8$ galaxies in both the groups and the field. Intriguingly, Figure 3.16 shows the models also predict that the fraction of disk dominated galaxies increases in the field between z=0.4 and z=0.1, but remains constant within the groups.

Given these predictions, we are now encouraged to investigate the time evolution of the disk fraction as a function of luminosity. From our data we have seen that the differences in the disk fraction as a function of magnitude are small at z=0.4 ($\sim 5.5 \pm 2$ %), but quite large in the local universe ($\sim 19 \pm 6$ %). To address this, we present Figure 3.17, which shows the relative disk (B/T $< 0.2$) deficiency between the field and the group samples, as a function of luminosity. The disk deficiency is the difference between the group and field disk fraction divided by the field disk fraction. This gives a measure of the fraction of field disks which are absent at a similar magnitude in the groups. In the left panel of Figure 3.17 we show the low redshift sample. The data from the MGC sample agrees well on average with the model predictions. In the right panel of Figure 3.17 we show the same

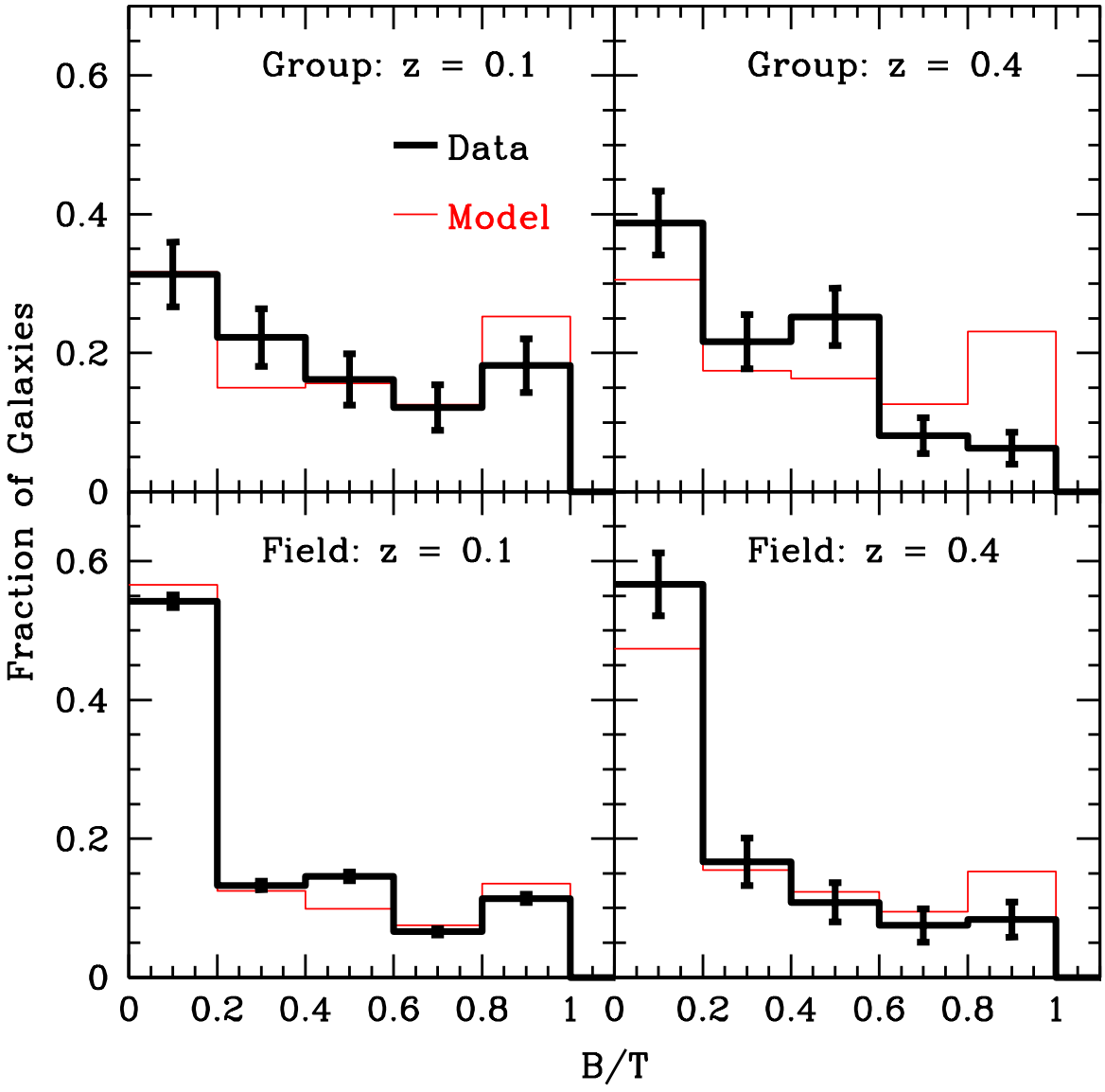


Figure 3.16: The B/T distributions of the Bower et al. (2006) model, compared with the observed group and field samples at z=0.1 and z=0.4. The model is the thin, red line in each panel and the data is the thick black line.

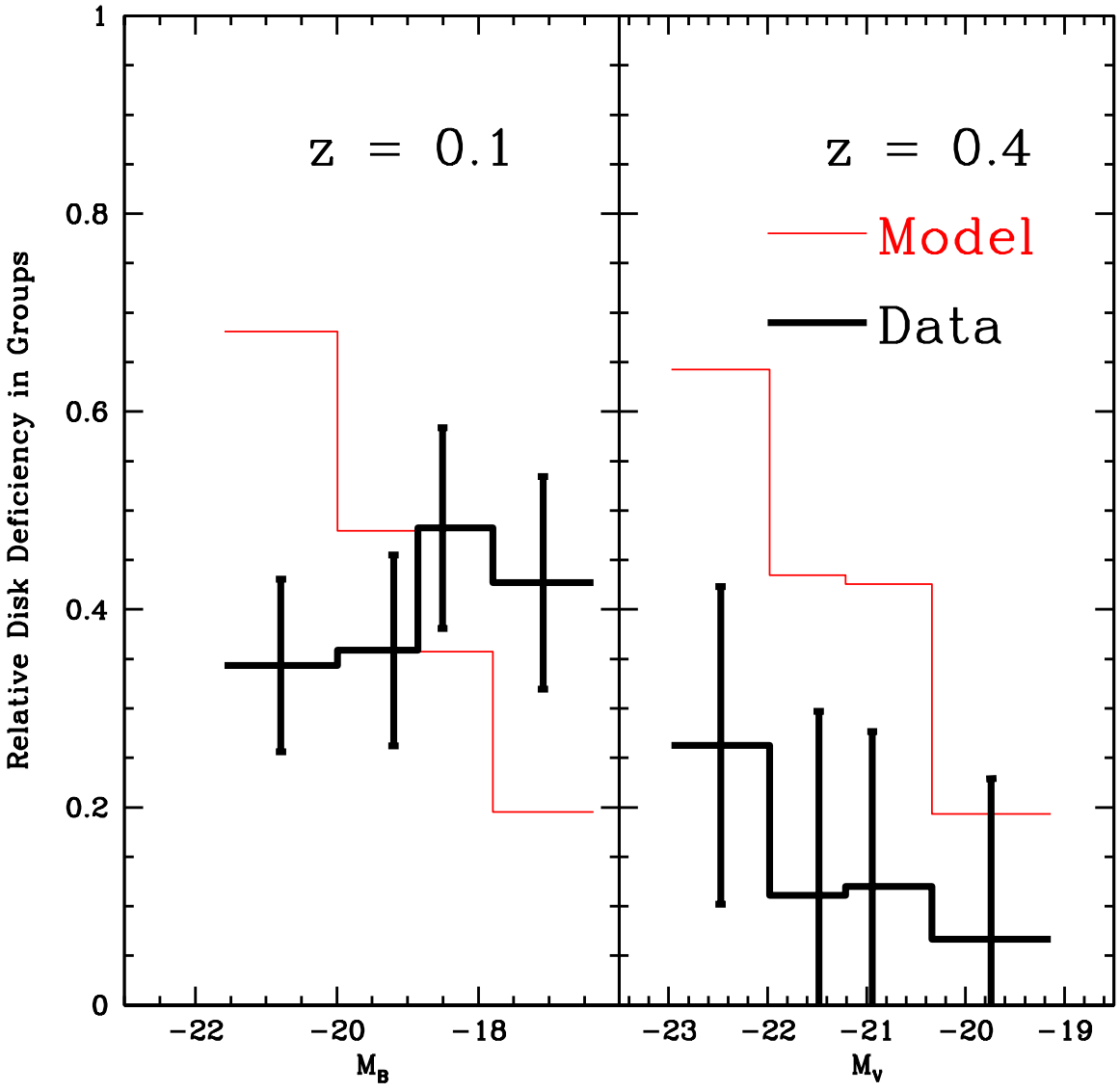


Figure 3.17: The relative disk deficiency in groups, parametrized as 1-group disk fraction/field disk fraction, where a disk has a B/T $< 0.2$. This is shown at z=0.4 (right panel) and z=0.1 (left panel) for both the Bower et al model (thin red line) and the data (thick black line).

comparison but for the high redshift sample. Although the average value of the group disk deficit is correctly predicted at z=0.1, the Bower et al. model predicts a group disk deficit which is much higher than the data at z=0.4. We note that, in the model, the predicted evolution is of a similar magnitude whether measured consistently in rest frame V or rest frame B, indirectly supporting our argument that the observed evolution is not driven by the difference in rest wavelength sampled by the two surveys.

We have seen in Figure 3.16 that the models underpredict the fraction of B/T $< 0.2$ at z=0.4 and that this leads to an overprediction of the disk deficiency in groups at the high redshift epoch. Intriguingly, inspection of Figure 3.16 shows that this is because the models predict that the fraction of disk dominated galaxies increases in the field between z=0.4 and z=0.1, but remains constant within the groups. While a direct comparison between the two epochs could be complicated by the different observed wavebands, we note that the same model predictions exist when considering only the underlying stellar mass. This is at odds with the data, which show that the B/T $< 0.2$ fraction *decreases* in the groups, and remains constant in the field.

## 3.5 Conclusions

We have presented a quantitative morphology study of optically-selected galaxy groups from two redshift surveys: CNOC2 (z$\sim$0.4), supplemented with significant additional Magellan spectroscopy, and MGC (z$\sim$0.1). We have compared these data with a similarly selected sample of groups drawn from the semi-analytic galaxy formation models of Bower et al. (2006). Our findings are:

- There is a significant difference, as indicated by a KS test, in the fractional bulge luminosity (B/T) distribution of group and field galaxies, in both the high and low redshift samples. The dominant difference is the deficit of disk–dominated (B/T $<$ 0.2) galaxies in the group samples.

- The difference in the disk fraction (B/T$<$0.2) of group galaxies relative to the field shows significant evolution between z=0.4 and z=0.1. At a given luminosity in the CNOC2 sample, the groups have $\sim 5.5 \pm 2$ % fewer B/T$<$0.2 galaxies than the field. By z=0.1 this difference has increased significantly, so that groups have $\sim 19 \pm 6$ %

fewer B/T<0.2 galaxies than the field in the same magnitude range. Although the z=0.1 sample traces rest frame B while the z=0.4 sample traces rest frame V, this difference is unlikely to be able to explain the differences.

- At neither redshift do we see any evidence that the bulk properties of the existing disks are significantly different for group galaxies than for field galaxies. They lie on similar scaling relations and show similar asymmetry distributions. There is no evidence that groups are actively perturbing or otherwise affecting a large fraction of the group disk population.

- We find that there is a small enhancement in the fraction of bulge-dominated group galaxies that are highly asymmetric, relative to bulge-dominated galaxies in the field. This may be consistent with enhanced merging in the group environment. Visual inspection of high asymmetry, bulge-dominated CNOC2 galaxies shows that 44% (4/9) exhibit clear evidence of interactions or merging.

- A sample of galaxies drawn from the semi-analytic galaxy catalogues of Bower et al. (2006) was shown to agree remarkably well with the B/T distribution of the field and group galaxies at z=0.1. However, our data have shown that time evolution of the B/T distributions predicted by the models is not seen in our data. In particular, the Bower et al. model underpredicts the fraction of disk dominated galaxies at $z \sim 0.4$.

The morphological difference between group and field galaxies at z=0.4 is mostly due to the tendency for group galaxies to be more luminous and, therefore, more bulge-dominated than field galaxies. This is consistent with our previous findings about group galaxies; namely, that their M/L ratios are consistent with the passive evolution of a predominately old population (Balogh et al., 2007), because the dominant difference in group galaxies is their pre-existing tendency to be bulge-dominated. This is also consistent with the fairly small difference in the emission-line fraction of group and field galaxies, at fixed stellar mass (Balogh et al., 2007) or magnitude (Wilman et al., 2005a).

The failure of the Bower et al. (2006) to reproduce the time evolution of the group disk deficit is interesting. These type of models predict a fairly rapid "strangulation" of galaxies once they enter larger halos, which causes the star formation rate to decrease on timescales of a few Gyr. This starts to play a large role at $\sim 10^{12}$ solar masses, significantly less massive than most of our groups. Weinmann et al. (2006a) have shown that this

mechanism is too effective, and produces a homogeneous, red satellite population at all magnitudes, in groups and clusters, which is not observed at z=0. Gilbank & Balogh (2008) have recently shown that this problem extends out to at least z=1. It is likely that the incorrect disk deficit evolution is another manifestation of the maximally efficient star formation quenching mechanism used by the models.

We have found that, in contrast to X-ray selected groups, our optically-selected group galaxies have median asymmetries that are similar to field galaxies. This may point to a possible role for galaxy interactions with the hot IGM. Alternatively, the progenitors of X-ray selected group galaxies may be fundamentally different from the progenitors of optically selected group galaxies. X-ray selected groups are more likely to be relaxed, virialized structures, suggesting that they were assembled earlier than optically selected groups. In the current models, the strangulation mechanism is assumed to operate efficiently in small haloes. Thus, little difference is expected in the population of different types of groups many Gyr later (i.e. at the epochs of interest here), since star formation has long ceased in most group members. However, recently it has been suggested that infalling galaxies may be able to retain a significant fraction of their gas (McCarthy et al., 2008b; Kawata & Mulchaey, 2008), significantly increasing the timescale for star formation to decrease. In this case, the headstart given to galaxies that fall into groups a little earlier may be better able to explain the difference between X-ray and optically selected groups.

# Chapter 4

# Evolution of star formation rates in galaxy groups since z=0.4

## 4.1 Introduction

The star formation history of a galaxy is a function of, at least, stellar mass, redshift and environment. In the local universe, a higher fraction of low mass galaxies are actively forming stars than more massive galaxies (Kauffmann et al., 2003b; Brinchmann et al., 2004). It has been known for some time that the star formation density of the universe has decreased by at least a factor of 10 in the last 8 or 10 Gyrs (Lilly et al., 1996; Madau et al., 1996; Hopkins, 2004). There is growing evidence that this reduction with redshift is seen, roughly equally, at all stellar masses (Gilbank et al., 2010b). Finally, at least in the local universe, the fraction of star forming galaxies in groups and clusters at fixed stellar mass is lower than the general field (Kauffmann et al., 2004; Kimm et al., 2009). Untangling why and to what extent each of stellar mass, redshift and environment drive a galaxy's star formation properties is a fundamental goal of galaxy formation and evolution research. Ultimately, we would hope to uncover the physical mechanisms responsible for each correlation.

The role of environment has been studied by Weinmann et al. (2006a), who separated galaxies based on colour and specific star formation rate (H$\alpha$ based) to find that the fraction of blue, star forming galaxies decreases with increasing halo mass at fixed luminosity. More

recently, using UV derived star formation rates and the same group catalogue, Kimm et al. (2009) finds that the fraction of passive satellites increases with halo mass. These studies were largely focused on the fraction of passive galaxies, rather than the actual star formation rates.

However, an important constraint on environmental mechanisms might be attained by examining how the star formation rates vary with environment. There is evidence that galaxies which are forming stars in groups have similar properties to those in the field, but that the fraction of those galaxies varies. Balogh et al. (2004b) finds that the two peaks of the bimodal distribution of red and blue galaxies change relative heights with environment at fixed luminosity. However, importantly, they find no difference in the location of the blue peak with environment. Recently, Peng et al. (2010) found that the relationship between star formation rate and stellar mass was the same in the highest and lowest density quartile of galaxies.

This behaviour may be expected if environmental correlations are largely driven by rare events such as ram pressure stripping of cold gas which would quickly increase the fraction of passive galaxies without changing the remaining star forming galaxies. However, Balogh & McGee (2010) found a homogeneity in the scatter of red fractions in individual galaxy groups and clusters. When directly compared to models for how galaxies are accreted into groups and subsequently into cluster, this homogeneity suggests that the halo mass threshold must be $\leq 10^{13}\ h^{-1}\ \mathrm{M}_{\odot}$(McGee et al., 2009). The efficiency of ram pressure stripping of cold gas in such low mass haloes is poor.

It is very difficult to obtain large collection of unbiased and well sampled galaxy groups at high and intermediate redshift and thus the majority of the previous work has been based in the local Universe. To combat this, our collaboration, the Group Environment Evolution Collaboration (GEEC), has undertaken a detailed, multi-wavelength study of galaxy groups at intermediate redshift ($0.3 < z < 0.55$) (Wilman et al., 2005b). We have shown that these are truly galaxy groups rather than clusters as the group sized velocity dispersions agree with stacked weak lensing and x-ray luminosities (Parker et al., 2005; Finoguenov et al., 2009). We have shown that the morphology-density relation, using either visual or quantitative morphologies, is in place at z=0.4 but also grows stronger to z=0 (Wilman et al., 2009; McGee et al., 2008). In addition the fraction of [OII] emitting galaxies, blue galaxies or infrared excess galaxies as a function of stellar mass is higher in the field than in the groups (Balogh et al., 2007, 2009).

[OII] emission can be effectively corrected to be a useful star formation tracer overall (Moustakas et al., 2006; Gilbank et al., 2010a). However, it is not clear that these corrections are effective for subsamples of galaxies, such as those which are affected by dense environments (Yan et al., 2006; Lemaux et al., 2010). In addition, to properly separate star forming from non-star forming galaxies, it is necessary to probe low star formation rates. It is difficult to attain this level of sensitivity with [OII], especially in low signal to noise spectra. In this chapter, we use SED-fit star formation rates, which are driven by UV data from *GALEX* , and stellar masses, which are driven by $K$ band data. This allows us to probe how star formation evolves as a function of environment and stellar mass since z=0.5.

In §4.2, we explain the two distinct surveys (GEEC and SDSS) used in the chapter as well as the wide array of photometric and spectroscopic data used in both. We will also detail the new *GALEX* and CFHT Wircam K band observations which will be used to fit detailed spectral energy distributions. In §4.3, we explain the SED fits used in this chapter including the fitting methodology, the sample of comparison stellar populations which are used to derive physical parameters. Further, we simulate a sample of galaxies which allow tests of the robustness and accuracy with which we recover physical parameters. Finally, we make direct comparisons with other methods of determining physical parameters. In §4.4, we examine the environmental dependence of the SSFR - $M_{\odot}$ diagram at both redshift epochs. In §4.5 we discuss the results and derive a plausible toy model for the truncation of star formation in group galaxies. Finally, in §4.6, we discuss the conclusions.

Throughout this chapter, we adopt a ΛCDM cosmology with the parameters; $\Omega_{\rm m} = 0.3$, $\Omega_{\Lambda} = 0.7$ and $h = H_0/(100\,{\rm km\,s^{-1}\,Mpc^{-1}}) = 0.75$. Also, in this chapter all magnitudes are stated within the AB magnitude system (Oke & Gunn, 1983).

## 4.2 The Data

To achieve our goal of studying the evolution of the star formation properties of galaxies and their dependence on environment requires a sample of galaxies at two redshift epochs and deep UV observations. For our z=0.4 sample, we use the sample of galaxies in the Group Environment Evolution Collaboration (GEEC) and deep *GALEX* observations made in Guest Observer mode. The low redshift sample of galaxies is derived from the Sloan

Digital Sky Survey (SDSS) and its overlap with the *GALEX* Medium Imaging Survey (MIS). Below we detail each sample, as well as the group finding algorithms used.

### 4.2.1 GEEC survey

The GEEC survey was designed to provide highly complete and deep spectroscopy in the fields of galaxy groups selected from an earlier, sparsely sample redshift survey. This backbone survey is the Canadian Network for Observational Cosmology (CNOC2) Field Galaxy Redshift Survey. It is a spectroscopic and photometric survey completed with the Multi-Object Spectroscopy (MOS) instrument at the 3.6m Canada France Hawaii telescope (CFHT) (Yee et al., 2000). The original survey targeted galaxies over four different patches of sky totaling about 1.5 square degrees. Spectroscopic redshifts of 6000 galaxies were obtained with an overall sampling rate of 48% to $R_C$=21.5. The survey used a band limiting filter which primarily limited successful redshifts to the range $0.1 < z < 0.6$, however, there was no colour pre-selection of targets.

Despite this relatively sparse sampling, Carlberg et al. (2001) was able to use a slightly modified friends of friends algorithm to define a sample of $\sim$ 200 galaxy groups. The only modification to the standard friends of friends algorithm, such as that described by Huchra & Geller (1982), is the requirement that the grouped galaxies are in a large scale overdensity. However, because of the sparse sampling of the survey, this step has no effect on the type of groups discovered.

These galaxy groups have been robustly characterized by both weak lensing (Parker et al., 2005), mock catalogues (McGee et al., 2008) and X-ray imaging (Finoguenov et al., 2009). The mass estimates from all of these approaches agree well with the expected mass based on the average velocity dispersions of the groups. The mock catalogue analysis also found that the fraction of galaxies not associated with real galaxy groups was only 2.5%.

The first step of the GEEC survey was presented in Wilman et al. (2005b), in which the collaboration obtained follow-up spectroscopy in 20 regions, each centered on a Carlberg et al. group at $0.3 < z < 0.55$. This spectroscopy was obtained using the Multi-Object Spectroscopy Low Dispersion Survey Spectrograph (LDSS2) at the 6.5m Baade telescope at Las Campanas Observatory (LCO) in Chile. This targeting greatly increased the sampling in these 20 targeted groups as well as 6 other Carlberg et al. groups which were partially

overlapping our targets on the sky. Thus, the completeness rose to $\sim 78\%$ to a statisical limit of $R_c$=22. This was a half magnitude deeper than the original CNOC2 survey.

In this chapter, we use data from both the targeted GEEC groups and the original Carlberg et al. groups, as well as making use of the full CNOC2 area from which to draw a comparison field sample.

### *GALEX* Observations

The Galaxy Evolution Explorer (*GALEX*) satellite is a NASA Small Explorer Class mission launched in 2003, which provides both imaging and grism capabilities in the ultraviolet (Martin et al., 2005; Morrissey et al., 2007). The *GALEX* satellite's dichroic beamsplitter feeds both a Near Ultraviolet (NUV; $\lambda_{\rm effective} = 2271$ $\mathring{A}$ ) and a Far Ultraviolet (FUV; $\lambda_{\rm effective} = 1528$ $\mathring{A}$) detector, thereby providing simultaneously imaging in both bands over a very large, circular area (1.°25 diameter). The *GALEX* satellite has been revolutionizing galaxy formation and evolution studies since its launch by providing such wide field imaging in the ultraviolet. This is a particularly important waveband to enable a characterization of the hot, massive and young stars which are indicative of recent star formation. Although, as we discuss, corrections must be made for both dust extinction and contributions from old stellar populations before robust star formation rates can be obtained.

We were awarded 9 orbits of *GALEX* observation time ($\sim$ 13.5 ks total) in Cycle 1 (PI: M. Balogh, ID: 037). This was intended to allow three orbits of observation time for each of three of the four CNOC2 patchs. However, early in the *GALEX* mission, intermittent problems with the FUV detector caused some observations to be obtained with only the NUV images passing image quality tests. Thus, further observations were undertaken to insure that the full compliment of FUV observing time was achieved. For this reason, the exposure time of the NUV images vary from 3 orbits per field (the 2 hour patch) to 6 orbits per field (the 14 hour patch). In Table 4.1, we detail the *GALEX* data of the three CNOC2 patchs. Because of the L-shaped geometry of the original CNOC2 patchs, the circular *GALEX* pointings do not cover the full patch. In this chapter we restrict our analysis to galaxies within 0.°6 of the center of the *GALEX* pointings.

We use the standard *GALEX* image reduction and calibrations obtained from the 2nd data release *GALEX* pipeline, as outlined in Morrissey et al. (2007). To provide a demonstration of the depth of our observations we present Figure 4.1, which shows the observed

| Patch | Central RA (J2000) | Central DEC (J2000) | NUV time (seconds) | FUV time (seconds) |
|---|---|---|---|---|
| 2h | 36.51625 | 0.35963889 | 5843 | 5676 |
| 14h | 222.40875 | 9.1826667 | 11739 | 5115 |
| 21h | 327.83479 | -5.5241111 | 8546 | 4682 |

Table 4.1: Details of the *GALEX* observations of the GEEC survey. Listed are the original CNOC2 patch name, the central right ascension (RA) and declination (DEC) of the *GALEX* pointings, as well as the combined FUV and NUV exposure time

NUV-r color as a function of observed r magnitude in four different redshift bins. In this Figure, we have matched sources that are individually detected on the NUV images to the nearest GEEC galaxy within $4''$. The faintest NUV sources which are matched to GEEC galaxies have magnitudes of $\sim 24.7$, as shown by the black line in the figure. This figure is shown only as an illustration of the *GALEX* pipeline processed data. For the remainder of the GEEC analysis we use psf-matched magnitudes as detailed in §4.2.1.

### CFHT Wircam K-band observations

In the 2009A observing season, we obtained observations in the K-band in the 14 and 21h fields using WIRCAM on the Canadian France Hawaii Telescope (CFHT). Four pointings, each with 33 minutes of exposure time, were made in each of the two fields. Thus, each field had a region $30'$ X $30'$ mapped out. Each pointing was divided into 80 exposures of 25 seconds each, and was dithered in a 5 point patter to fill in the chip gaps. The data was then reduced and processed by the Terapix pipeline.

### PSF matching and Photometry

There are at least two approaches to measuring accurate colours for sources in images with different psf's. One approach is to make a detailed model of the source in each image with the intent on measuring its "total" magnitude in each band. This is the approach we will use with the low redshift data, largely because of the availability of well understood "model" magnitudes in the SDSS. However, in the GEEC survey we take the second approach, that of the using aperture-based photometry after adjusting the images to have the same psf.

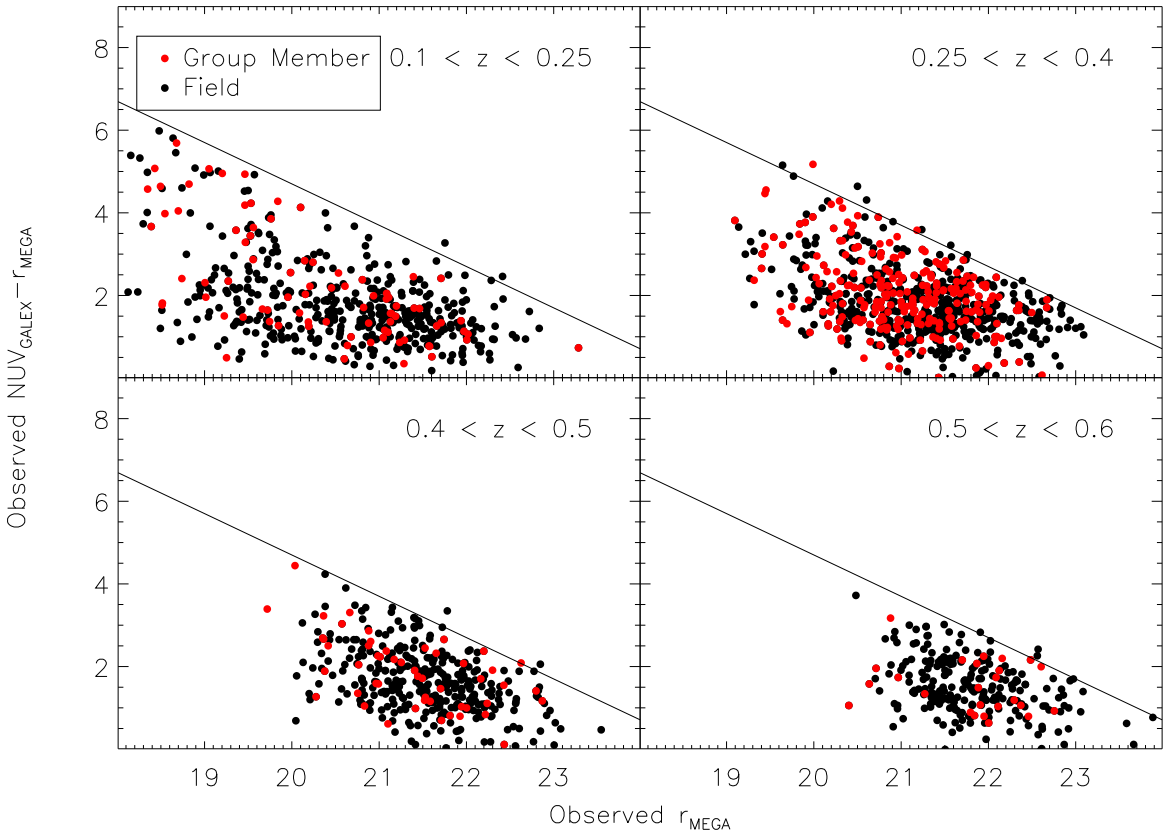


Figure 4.1: Observed colour magnitude in the *GALEX* NUV and CFHT Megacam r bands in four redshift bins within the GEEC survey. The black line is at NUV=24.7, which illustrates the limit of the faintest sources detected in the *GALEX* images. The red points are group members while the black points are field galaxies.

The original photometry of the CNOC2 survey was not accurate enough to allow detailed galaxy evolution measurements, such as SED-fitting. In Balogh et al. (2009), we presented the results of an extensive campaign to obtain new optical and near-infrared observations and photometry. In this chapter, we follow the same general scheme for making photometric measurements. While we briefly discuss this scheme below, we refer the reader to Balogh et al. (2009) for the full details.

The original GEEC object detection was done on a combined R(CFH12K) and $r$(Megacam) 'super' image for each of the CNOC2 patches. This image was used for detection as it allowed for the greatest depth and coverage, while closely resembling the original $R_C$ used in sample selection. We use this 'super' image only for object detection, and use each filter (including $r$ and $R$) separately for the photometry. All the photometric images, including the *GALEX* NUV, FUV and Wircam K-band images, were astrometrically aligned to the corresponding super image using SWARP (Bertin et al., 2002). In Table 4.2, we list each of the instruments and filters used in the chapter. We also list the fraction of galaxies in the GEEC sample which are covered by each filter. Notice that this simply measures the footprint of the data, rather than the detections.

The *GALEX* images have the largest psf's of any of our images ($\sim 4.7\,''$), so we convolve each of our images with a Gaussian appropriate to obtain a psf of $4.7\,''$. We then use SEXTRACTOR v2.5 (Bertin & Arnouts, 1996) in two-image mode on each image, with the 'super' $r$ image as the detection image. The photometry is then measured within 10"apertures, thus ensuring that we obtain psf-matched photometry for all the wavebands. It is this photometry we use for the rest of the GEEC analysis in the chapter. We do not apply Galactic extinction corrections directly to the photometry. We want to avoid adding extinction corrections to negative fluxes, which occasionally result from a non-detection. Instead, we apply a correction to each of the population synthesis models based on the measured extinction from Schlegel et al. (1998) for each patch of the survey. This essentially adds the reddening effect of Galactic extinction to the models, allowing a direct comparison with the photometry.

We restrict the analysis in this chapter to galaxies with $r < 22$ to allow an unbiased statistical sample to be generated. Due to this, the majority of our galaxies are well detected in all the photometric bands which have coverage in the area. However, it is important for our purposes to have well measured photometric errors. We do this by finding the standard deviation of the magnitude dependent difference between observations of the

| Instrument | Filter | Fraction covered |
|---|---|---|
| GALEX | $FUV$ | 1. |
| | $NUV$ | 1. |
| CFH12K | $B$ | 0.596 |
| | $V$ | 0.591 |
| | $R$ | 0.594 |
| | $I$ | 0.626 |
| Megacam | $u$ | 0.797 |
| | $g$ | 0.794 |
| | $r$ | 0.789 |
| | $i$ | 0.561 |
| | $z$ | 0.787 |
| INGRID | $K_s$ | 0.112 |
| SOFI | $K_s$ | 0.210 |
| WIRCAM | $K$ | 0.543 |

Table 4.2: The filters used for SED fitting of GEEC galaxies. The instrument in which the photometry was taken is listed along with the fraction of galaxies which are covered by this photometry.

same galaxy in two similar filters. This procedure will slightly overestimate the uncertainty because of real variation in galaxy types, which causes an intrinsic variation in the color. However, that variation is expected to be on the order of 0.05 magnitudes (Fukugita et al., 1995). We assume that the error is due to both filters equally when added in quadrature, however, we fit the results as a function of magnitude in each filter separately. This enables us to create, for each filter, a photometric error which depends only on observed magnitude. Thus, we do not have to create a photometric error for each galaxy individually. We also add zeropoint errors of 0.05 magnitudes to each of the filters in quadrature, except for NUV, INGRID and SOFI data for which we have zeropoint errors of 0.03, 0.17 and 0.1 mags, respectively.

#### Group finding

In order to maintain the unbiased properties of the survey, we restrict our discussion to galaxy groups which were pre-selected from the sample of Carlberg et al. (2001). However, we do redefine the galaxy groups using the Wilman et al. (2005) spectroscopy. We follow the redefinition scheme described extensively in McGee et al. (2008) and based on Wilman et al. (2005b). We define galaxy group members as those which are within 500 kpc of the luminosity weighted group centre and have a line of sight velocity within two velocity dispersions of the group redshift. Using this method our final sample of 2347 galaxies between z=0.3 and z=0.55 contains 335 group galaxies. Figure 4.2 shows the measured velocity dispersion of our galaxy groups as a function of redshift.

### 4.2.2 SDSS survey

The Sloan Digital Sky Survey (SDSS) is a five colour ($ugriz$) photometric and spectroscopic survey. In this chapter, we make use of the Data Release 6 (DR6), which contains over 790,000 galaxy spectra within approximately 7425 deg$^2$ (Adelman-McCarthy et al., 2008). We restrict our analysis to only galaxies within the main galaxy sample, which targets almost all galaxies with $r \leq 17.77$ (Strauss et al., 2002). Some galaxies are left unobserved because of the finite size of the fiber optic spectra plugs, which doesn't allow two galaxies to be observed when they are within 55″ of each other.

We use the $ugriz$ MODELMAG, which is designed to give the most accurate galaxy colour

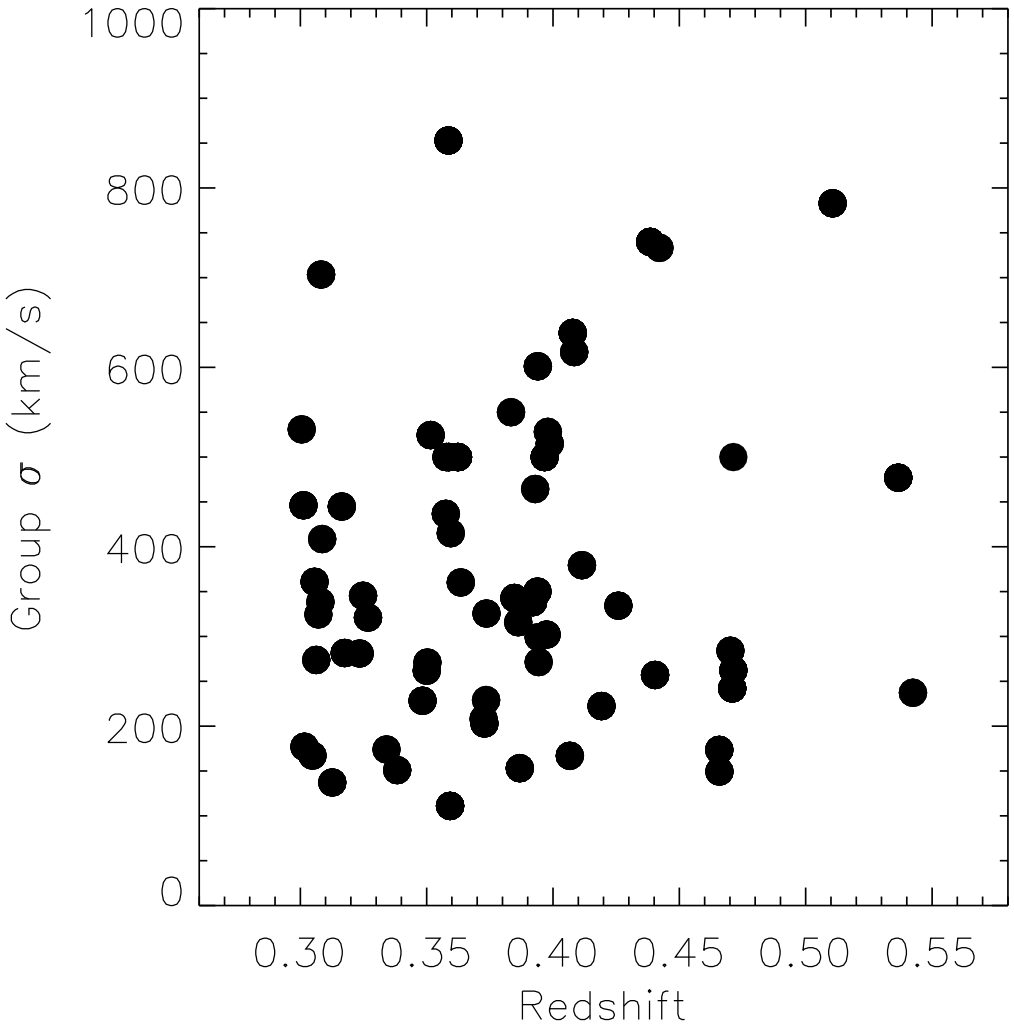


Figure 4.2: The velocity dispersion as a function of redshift for GEEC galaxy groups in our three fields with *GALEX* data. We restrict our sample to the groups shown, that is those between z=0.3 and z=0.55.

while still being close to a total magnitude (Stoughton et al., 2002). The SDSS photometry has zeropoint calibration errors of approximately 0.01 mag in $g$,$r$, and $i$, 0.02 mag in the z band and a slightly higher 0.03 in $u$ (Ivezić et al., 2004).

### *GALEX* data

The *GALEX* Medium Imaging survey (MIS) was designed to provide single orbit ($\sim$ 1500 second exposure) of approximately 1000 square degrees of the SDSS. We use 1017 tiles of the MIS which were released to the public via the 3rd General Release. We retain only objects with the central $0^{\circ}.6$ of each *GALEX* pointing, and resolve overlapping observations by keeping the one nearest the pointing center.

We follow the work of Budavári et al. (2009), who showed that an effective matching of SDSS galaxies and *GALEX* sources could be made by matching to the nearest source within $4''$. We use all galaxies within the main galaxy sample of the SDSS as our starting point. We reduce this sample to those galaxies within $0^{\circ}.6$ of a MIS tile and subsequent match to NUV/FUV sources from the *GALEX* sextractor catalogs. We use the MAG_AUTO photometry, which is close to a total magnitude. The final sample of galaxies in the SDSS/*GALEX* overlap between z=0.01 and z=0.15 is 49663. 87% of the sample is detected in *NUV* and 79% is detected in *FUV*.

### Group finding

In an attempt to compare the redshift evolution of group properties as fairly as possible, the primary goal of our low redshift group finder is to reproduce the selection of our GEEC groups. The method is very similar to the method used and described in Chapter 3 for low redshift groups.

GEEC groups were selected from a shallower and more sparsely sampled redshift survey than the SDSS. Thus, we apply two filters of the SDSS galaxies before applying the group finding algorithm. First, we apply the same absolute magnitude cut as the original CNOC2 group finder, $M_R$=-18.5 with an applied evolution correction of 1 mag per unit redshift. Secondly, we randomly remove half of the remaining galaxies to replicate the completeness of the CNOC2 redshift survey.

For all of the remaining galaxies, the local density was calculated by counting the galaxies within a cylinder of 0.33 $h_{75}^{-1}$ Mpc and $\pm$ 6.67 $h_{75}^{-1}$ Mpc line of sight depth centered on it. If the galaxy has fewer than three neighbours than the cylinder is expanded in every direction by 1.5 and the neighbours recounted. The galaxy is only available to become a grouped galaxy if its has a higher density than the background, which is estimated by Figure 3.2.

The groups are then compiled by beginning at the highest density galaxy and adding all the galaxies within its cylinders. Next all the galaxies in each of the cylinders centered on those galaxies are added. This continues until no more galaxies are added to the "proto-group". Members of this group are then used to calculate the geometric center, redshift and velocity dispersion. Using these quantities as starting points, galaxies are added or removed iteratively within $1.5R_{200}$ and three velocity dispersions. This process is repeated until convergence.

Using this sample of groups, we now add in all the galaxies which were randomly removed to reduce the completeness. This allows us to emulate the GEEC follow-up of the Carlberg et al groups. The geometric center, redshift and velocity dispersions were again re-computed, now using all available galaxies.

To avoid edge effects, we run the group finder on the entire SDSS DR6 main galaxy sample, and then subsequently restrict ourselves to groups within the SDSS/*GALEX* overlap region.

## 4.3 Fitting Spectral Energy Distributions

UV photometry, while extremely useful for measuring young stars, is sensitive to attenuation from dust. Early studies using UV photometry of star bursting and rapidly star forming galaxies found that the a reasonable dust correction could be made by assuming that the galaxy's spectral slope in the UV was proportional to the dust (Meurer et al., 1995; Calzetti et al., 2000). However, as ultra-violet light began to probe normal star forming galaxies, and even relatively quiescent galaxies, it was found that there is no universal relation between the UV slope and UV dust attenuation (Bell, 2002). In effect, the UV slope overestimates dust attenuation for galaxies with significant old populations. This

is particularly important when studying massive galaxies and those in groups because of their expected old populations.

To overcome these problems, we use all of the available photometry; optical, near-infrared and UV data to systematically compare against a sample of models created from the population synthesis code of Bruzual & Charlot (2003). This specific method we follow is that of Salim et al. (2007), who have earlier used a similar SDSS/*GALEX* overlap sample.

The general technique involves using a sample of template SEDs with known galaxy parameters. The templates are fit to the observational photometry and the galaxy parameters of the best fit model are adopted as the parameters of the observed galaxy. Below we discuss the template SEDs which we create using stellar population synthesis (§4.3.1) and then discuss the detailed methodology we use to find the best fitting parameters (§4.3.2).

### 4.3.1 Model Stellar Populations

All our galaxy templates are created using Bruzual & Charlot (2003) models with a Chabrier initial mass function. The model spectra are produced by randomly selecting values for a set of variables which control the model galaxy's age, metallicity, star formation history and dust obscuration. In particular, the age of the galaxy is randomly selected from a uniform logarithmic distribution between 0.1 Gyr and the age of the Universe at the epoch of observation. The metallicity is uniformly spaced between Z=0.0001 and 0.05, where the canonical solar metallicity is Z=0.02.

We assume that the star formation histories of these galaxies have a backbone of exponentially declining star formation rates, and superimposed onto this backbone histories are star formation bursts. In particular, the backbone rates are randomly chosen in a uniform distribution (SFR $\propto \exp(-\gamma t)$), where $\gamma$ is $0 \leq \gamma \leq 1$ Gyr$^{-1}$. On this backbone, we allow bursts which last some time randomly distributed in duration between 30 and 300 Myr. The strength of the bursts are also randomly chosen between 0.03 and 4 times the current stellar mass produced by the galaxy at the onset of the burst. These bursts are randomly assigned so that there is a 25% chance a galaxy will undergo at least one burst in a given Gyr.

We adopt the simple 2 component dust model of Charlot & Fall (2000). In this model, young stars are shrouded in the dust associated with their birth, which has an associated

optical depth to the observer of $\tau_v$. After birth these young stars gradually disrupt and or dissipate their dust clouds. This is modeled by assuming that only some fraction, $\mu_v$ of the original optical depth remains 10 Myr after the stars birth. The $\tau_v$ is drawn from a distribution which peaks at 1.2 magnitudes of attenuation and runs from 0 to 6 mags. The $\mu_v$ value runs from 0.1 to 1, peaking at 0.3.

We then create model magnitudes by convolving the Bruzual & Charlot (2003) resultant spectra with filter curves of *GALEX* NUV and FUV bands as well as the SDSS *ugriz* for the low redshift sample. The model magnitude catalogs are generated at each 0.03 redshift interval from z=0.02 to z=0.20. In the GEEC sample, we convolve the spectra with the expected transmission of *GALEX* NUV and FUV, CFH12K $BVRI$, Megacam $griz$, Wircam $K_s$, and 2MASS $K$. We use the 2MASS filter because both the Ingrid and SOFI $K$ band data were calibrated to give magnitudes on the 2MASS system. We generate catalogs every 0.05 redshift interval from z=0.3 to z=0.55.

### 4.3.2 Fitting Methodology

The set of model galaxies we have generated by randomly sampling the allowed parameter space acts as a Bayesian prior to the physical galaxies parameters. Our goal is to find a resultant probability distribution function (PDF) for each parameter and for each observed galaxy. For a given observed galaxy, we find the scale factor, $a_i$, which gives the minimum $\chi_i^2$ for each model galaxy, $i$, in Equation 4.1.

$$\chi_i^2 = \sum_X \left( \frac{F_{\mathrm{obs},X} - a_i F_{\mathrm{mod}_i,X}}{\sigma(F_{\mathrm{obs},X})} \right)^2 \tag{4.1}$$

In which, $X$ represents the sum over the 7 bands of low redshift photometry and the 12 bands of GEEC photometry. $F_{\mathrm{obs},X}$ then represents the flux in the Xth band of the observed galaxy, while, $F_{\mathrm{mod}_i,X}$ is the Xth band flux of the given model galaxy. $\sigma(F_{\mathrm{obs},X})$ is the sigma of flux in the $X$th observed band.

We use all available photometric bands for each galaxy. The only exception arises with GALEX NUV data, and only at low redshift, FUV. These are unique bands for two reasons. First, it is these bands which largely drive our star formation rates and are thus especially important. Secondly, these are the only bands for which there are a significant

number of non-detections. Therefore, for galaxies which are not detected in the original NUV or FUV imaging, we restrict the space of models to have NUV-r or FUV-r colours redder than the observed limits.

All of the SDSS photometry is deep enough to easily detect the spectroscopic sample. Similarly, with the GEEC photometry, except for the $z$ band data, all galaxies are brighter than the expected limits. However, at the faint end, the $z$ band photometric errors become large enough to encompass the models which are beyond the photometric limit, so we take no explicit action for these.

The minimum $\chi^2$ value of each model galaxy is then used to define a weight, $\exp(-\chi_i^2/2)$ for that model in fitting the given observed galaxy. The galaxy parameters of that model are then all given the weight, $w_i$. Once all models have been assigned a weight value, each galaxy parameter has a PDF constructed by compounding the associated weights at each parameter value range. We then obtain the parameter values which correspond to the median of the PDF. Also, we obtain $1\sigma$ error bars by using 1/4 of the 2.5-97.5 percentile range.

The models of Bruzual and Charlot that we use have time resolution of $10^7$ years. Therefore, the final galaxy parameters at any given epoch are representative only of the galaxy with the last $10^7$ years. However, UV star formation rates are sensitive to any star formation within the last 100 Myrs because this is the lifetime of the massive stars which produce UV emission. In other words, a burst of star formation will shine in the UV for 100 Myrs. Accordingly, we average the final 100 Myrs of any simulated Bruzual Charlot galaxy to produce a parameter which the UV is tracing. Thus, when we refer to star formation rates produces by this SED fitting, we are referring to the average star formation rate within the past 100 Myrs.

### 4.3.3 Understanding the physical parameters

In this section, we attempt to determine how well our SED fit galaxy parameters reproduce the values given by alternative methods. However, first we present Figure 4.3 as a type of sanity check. This figure shows the SED fit star formation rates for SDSS galaxies which are detected in the $NUV$ images as a function of $NUV$ magnitude and $r$ magnitude. This clearly shows that the star formation rates are driven by the $NUV$ data, and do not

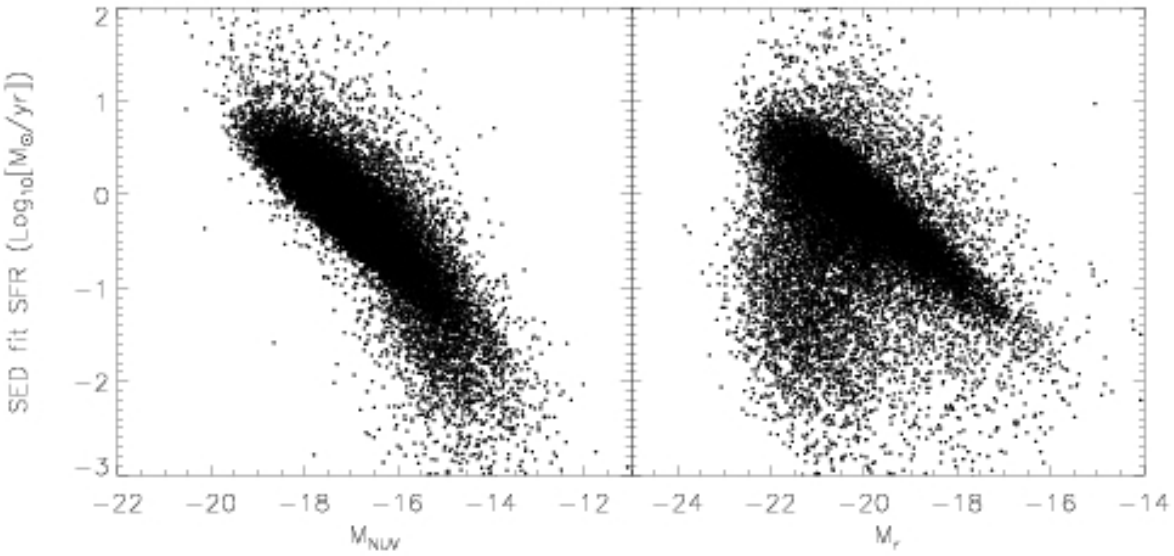


Figure 4.3: The SED fit star formation rate of SDSS galaxies as a function of *NUV* magnitude (left panel) and $r$ magnitude (right panel). These are shown only for *NUV* detected galaxies.

correlate well with the $r$ magnitude. Note that there is an artificial correlation created between $r$ magnitude and star formation rate, especially at fainter magnitudes, because we are only showing those galaxies which are detected in $NUV$.

Now, we will compare our SDSS stellar masses and star formation rates with the publicly available results of Kauffmann et al. (2003b, K03; for stellar masses) and Brinchmann et al. (2004, B04; for star formation rates). We also compare our GEEC stellar masses to those determined primarily from $K$ band data by Balogh et al. (2007).

**SDSS comparisons: Stellar Masses**

The method of fitting stellar masses used by Kauffmann et al. (2003b), in many ways is the philosophical forerunner of the Bayesian method we use here, with much of the formalism explained in that paper. The authors use a large suite of galaxy models created using stellar population synthesis, and find that they can constrain the $z$ band mass to light ratios using the 4000-$\AA$ break ($D_n(4000)$) and the Balmer absorption line index $H\delta_A$. By then scaling by the observed $z$ band photometry, they determine the galaxy's stellar mass. Thus, despite the similar methodology, the K03 stellar masses are largely determined by the spectral features, which determine the star formation history and thus the mass to light ratio. While our stellar masses are determined by using the UV light to constrain the star formation histories and then the photometry to scale to a stellar mass.

In Figure 4.4, we show the difference between our stellar masses and those of K03 as a function of our stellar mass. The K03 have been converted from a Kroupa (2001) to a Chabrier IMF by dividing by 1.04. The masses are well reproduced using our method, with a $\sigma$ that is smaller than the average of the uncertainties in either method. This likely means that despite our different methods, the uncertainties on each method are correlated. Nonetheless, our SED fitting seems to produce reliable results, notwithstanding systematic issues common in both methods (ie. evolving imf, stellar population synthesis uncertainties, etc.).

**SDSS comparisons: Star formation Rates**

One of the most common and robust methods of determining star formation rates of star forming galaxies is to use the recombination emission line $H\alpha$, which reemits the radiation

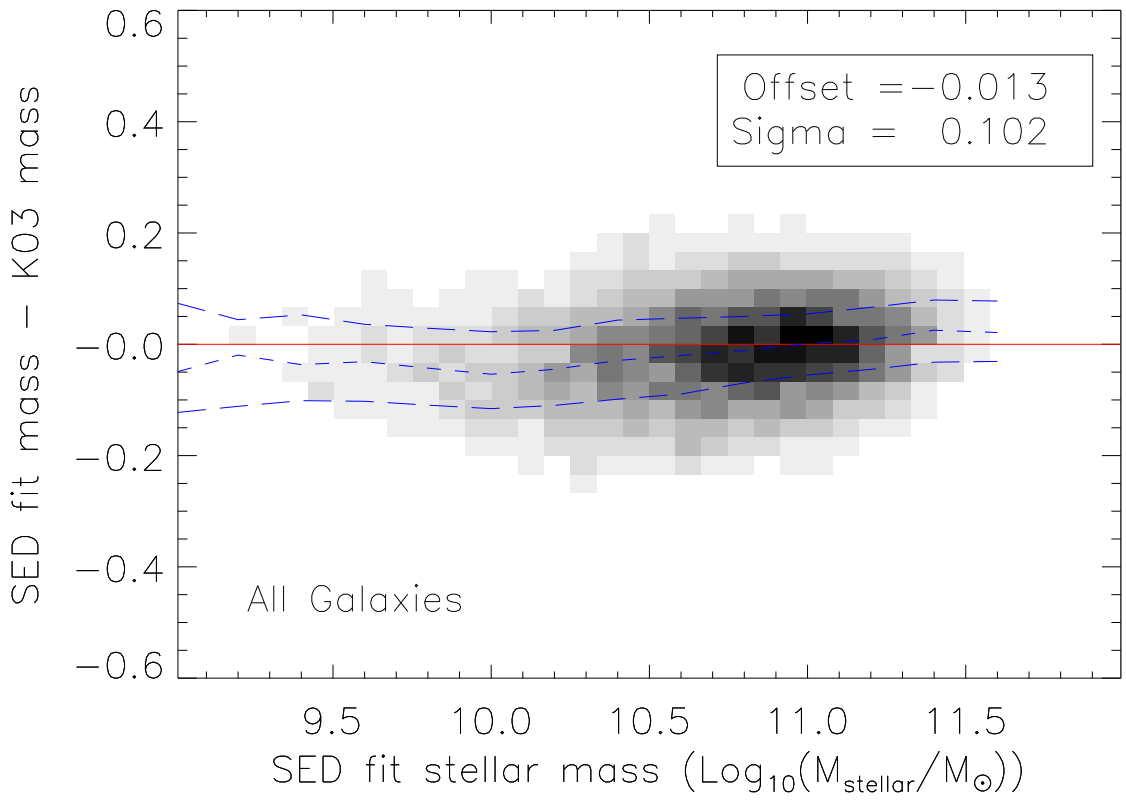


Figure 4.4: The difference between the SED fit masses presented in this chapter and those based on from Kauffmann et al. (2003b). The masses are well reproduced using our method. The red line represent the equality of the masses, while the blue dashed lines show the median and 1 sigma upper and lower bounds of the distribution.

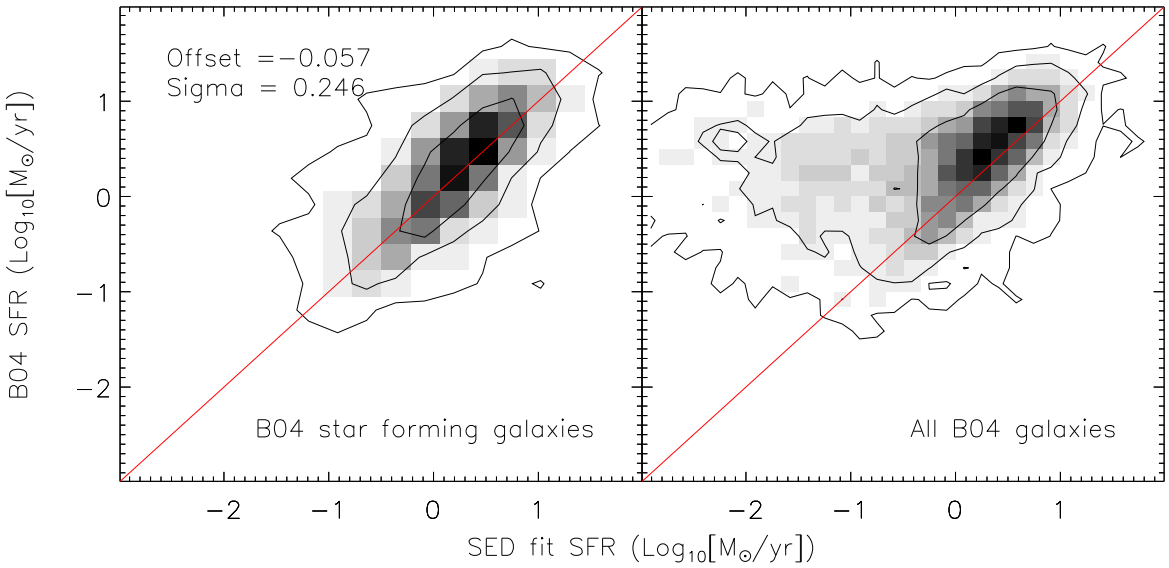


Figure 4.5: A comparison between the SED fit star formation rates in this paper and those found by Brinchmann et al. (2004). We show this for galaxies which B04 classifies as "star-forming" in the left panel and all galaxies in the right panel. The red line shows the equality between the B04 and SED fit star formation rates.

of massive young stars. To that end, Brinchmann et al. (2004, B04) use the emission lines of SDSS galaxies, to both classify the type of galaxy and to determine the star formation rates. As this method is completely based on spectral features this should give essentially an independent measurement to ours.

B04 classifies galaxies into several categories based on the position of the galaxy within the Baldwin et al. (1981, BPT) diagram and the quality of the spectra. The BPT diagram is used to determine whether a galaxy has AGN activity based on the ratios of four emission lines ([OIII]5007, H$\beta$, [NII]6584 and H$\alpha$). A galaxy with a high signal to noise ratio in each emission line and which lies in the star forming locus of the BPT diagram is defined as a

"star forming" galaxy. The other B04 categories are used to denote AGN or Composite galaxies, as well as low S/N categories of each.

The star formation rate of high signal to noise star forming galaxies is relatively straightforward to obtain from emission lines. Thus, it is this class of galaxies which we first compare our SED fit star formation rates to, as shown in the left panel of Figure 4.5. The B04 star formation rates were calculated assuming a Kroupa (2001) initial mass function. Following Salim et al. (2007), we have divided the B04 rates by 1.06 to account for this difference in IMF. Our measurement agrees very well, with only a negligible offset and a 1 $\sigma$ value which is consistent with our expected measurement errors. Importantly, some of this scatter is likely real, given that the B04 SFRs are based on H$\alpha$, which is sensitive to star formation within the last 10 Myrs, while our SFRs are based on $NUV$, which is sensitive star formation in the last 100 Myrs.

The right panel of Figure 4.5 shows the comparison of our SFR's with all of the galaxies for which B04 determined SFRs and are in the *GALEX* sample. While the SED fit high star formation rates still agree well with the B04 measurements, there is a long tail of SED fit determined low star formation rates which B04 believes are forming stars at much higher rates. Salim et al. (2007) also noted this behavior when comparing UV derived SFR with B04. Salim et al. extensively investigate this phenomenon and find that these galaxies are ones in which B04 used indirect SF indicators, either because of lack of H$\alpha$ emission or because of AGN contamination of the nebular emission lines. Thus, as Salim et al. conclude, the UV SED fit SFR are likely more accurate for these galaxies.

### GEEC comparisons: Stellar Masses

In Balogh et al. (2007), we determined stellar masses for a limited sample of GEEC galaxies based on the $K$ band data which was available at the time. These were determined by computing $K$ band mass to light ratios using simple stellar population modeling. The authors use a young, constantly star forming galaxy model to approximate the most blue galaxies ($B$ - $V < 0.4$) and a old, single stellar population model for the reddest galaxies ($B$ - $V > 1$). The mass to light ratios for intermediate galaxies are determined by a linear interpolation between these two extremes based on the galaxy's $B$-$V$ color.

In Figure 4.6, we present a comparison between our current SED fit stellar masses and those of B07. We have converted from a Salpeter IMF to a Chabrier IMF by subtracting

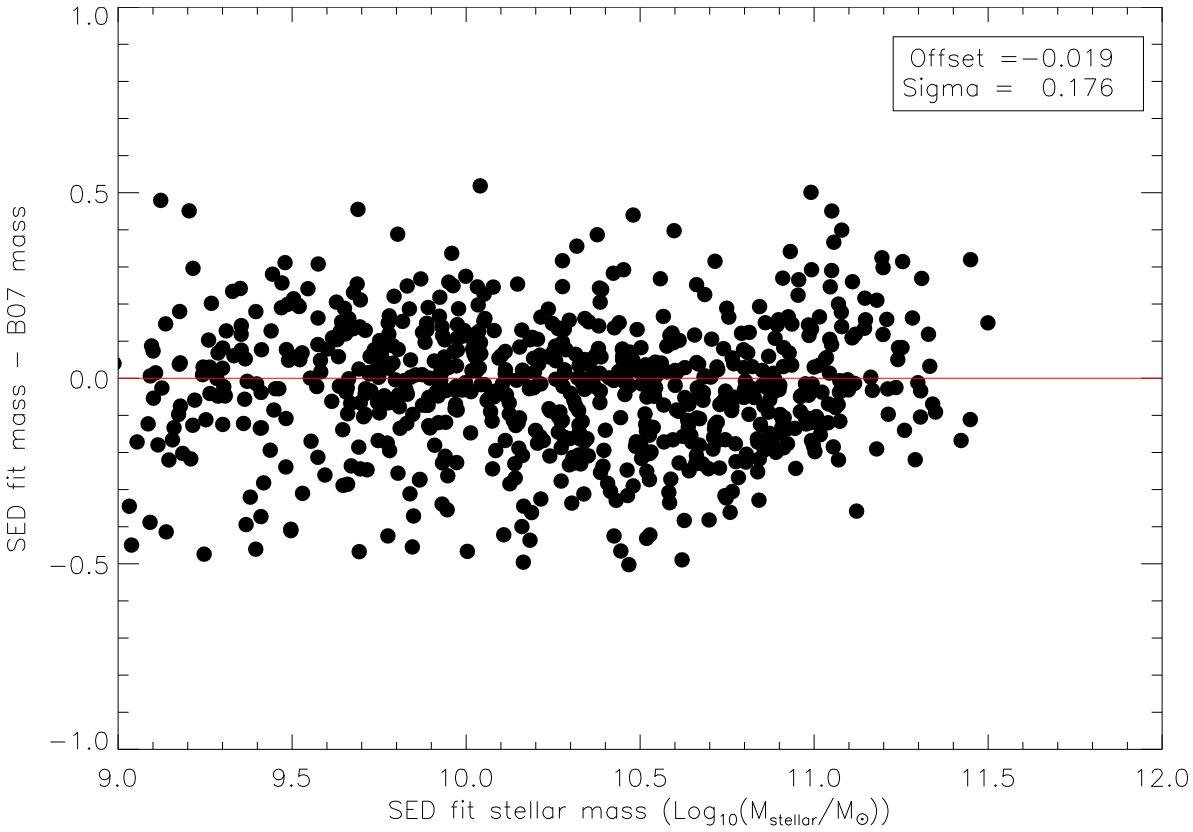


Figure 4.6: Comparison between the SED fit stellar masses in this paper and the $K$-band determined Balogh et al. (2007)(B07) masses for galaxies in both catalogs in the redshift range $0.1 < z < 0.55$. The 1 $\sigma$ scatter is 0.176 dex, and the SED fit stellar masses are systematically lower by 0.019 dex.

0.21 dex. Encouragingly, there is only a slight offset of -0.019 between the masses and the scatter is quite small 0.176 $\sigma$. This scatter is actually smaller than the formal errors of both mass measurements, but since they are, at least partially, using the same photometry, the errors are correlated.

### Dust enshrouded star formation

As we have shown, the SED-fit star formation rates agree very well with the rates inferred from star forming galaxies using dust corrected H$\alpha$. However, the possibility exists that

some star forming galaxies could be so optically thick that they would not emit significantly in H$\alpha$ or UV. Using star formation rates inferred from UV/optical photometry like ours and comparing to mid-infrared star formation indicators, Salim et al. (2009) found that indeed most of the star forming galaxies were not optically thick.

To obtain a star formation rate from mid-infrared photometry, such as that taken at 24 $\mu$m by the Spitzer Space Telescope, first involves a correction to obtain the total infrared emission emitted by the galaxy. In the standard manner, this correction is found by assuming a model, usually empirical, which constrains the SED in the infrared. There are a variety of models available and Salim et al. (2009) found that the UV SED fit star formation rates could reproduce the mid-IR derived star formation rates to within a factor of 2 using the UV/optical photometry alone when using the models of Chary & Elbaz (2001) and Dale & Helou (2002). However, when using the more recent templates of Rieke et al. (2009), the UV/optical photometry did not accurately reproduce the dust measured SFR. 24 $\mu$m photometry for GEEC galaxies is presented in Tyler et al. (in prep). However, we note that in that paper, which makes use of the Rieke et al. (2009) templates, the dust enshrouded star formation is similar in the groups and in the field. In other words, it is unlikely that we are missing a large population of optically thick star formation which only exists in one environment.

### 4.3.4 Simulating galaxy samples

The SED fit galaxy parameters which we use in this paper are principally, the specific star formation rate (SSFR) and the stellar mass. In §4.3.3, we have attempted to quantify the accuracy of these galaxy parameters by comparing them to other, largely independent, methods of obtaining them. However, this approach is not fully satisfactory, because the parameters can only be tested for limited cases, ie. H$\alpha$ measurements provided only solid constraints on the low redshift, star forming galaxies. In this section, we create a mock sample of observations of galaxies for which we know the "true" SSFR and stellar mass.

For each survey, we create a sample of 100,000 galaxies which are drawn from the same distribution of dust, metallicity, age and star formation parameters as described in §4.3.1. However, while this distribution of galaxy parameters is the same for both the mock galaxies and the fitting models, the specific models are not in both catalogs. The mock galaxies are normalized to have stellar masses between $10^8$ and $10^{12}$ $M_\odot$, and are

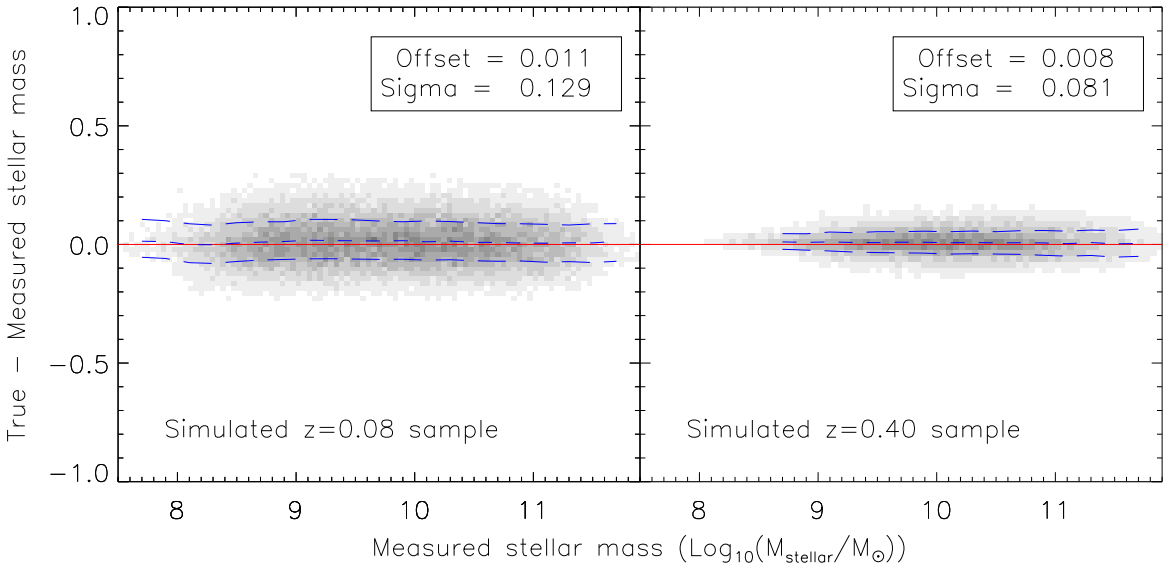


Figure 4.7: Comparison between the "true" stellar masses of a mock set of simulated galaxies and the SED fit stellar mass of the mock galaxies. This is shown for both the z=0.08 simulated sample (left panel) and the z=0.4 sample (right panel). The solid red line in both plots shows where the difference in measurements is 0. The blue, central dotted line represents the running median of the offset, while the two blue, dashed lines show the 1 $\sigma$ limits.

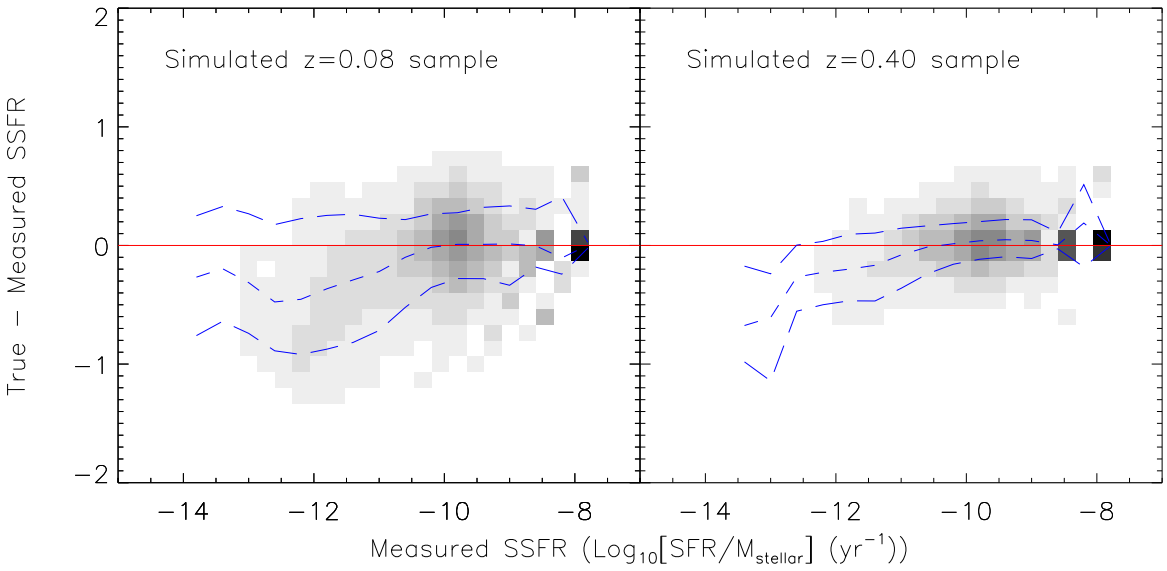


Figure 4.8: The difference between the "true" specific star formation rate of our mock galaxies and the results of the SED fitting as a function of the SED fit results. Again, this is shown for both samples, the z=0.08 (left panel) and the z=0.4 (right panel) simulated sample. The blue, central dotted line represents the running median of the offset, while the two blue, dashed lines show the 1 $\sigma$ limits.

then placed at z=0.08 (SDSS mock galaxies) and z=0.4 (GEEC mock galaxies). Mock observations are then created using the 7 filters of the SDSS sample and the 12 filters of the GEEC sample. For each mock galaxy, the photometry in each band is given a random Gaussian error consistent with the expectations of that bands measurement and zeropoint errors. In the GEEC sample, we also simulate the heterogeneous nature of the waveband coverage by removing observations in order to reproduce a sample with the same fraction of coverage in each band. However, as in the real method, we always have a minimum of 4 filters of coverage, including *GALEX* NUV and at least one band at $r$ or redder. Crucially, we also simulate the depth of the *GALEX* NUV and FUV data. When the mock NUV or FUV observation is beyond the magnitude limit of our real observations, we restrict to fitting only models with an NUV-$R$ and FUV-$R$ color greater than the color at the NUV and FUV observation limit.

In Figure 4.7, we present the stellar mass parameters which result from SED fitting the mock set of simulated galaxies in both surveys. We show the difference between the "true" stellar mass and those obtained by SED fitting the mock observations as a function of the SED masses. The fitting recovers very well the true stellar mass, with only a nominal systematic offset and no mass dependent deviations in the adequacy of the recovery. Note that the z=0.4 sample has a smaller scatter ($\sigma$ = 0.081 dex) than the z=0.08 sample ($\sigma$ = 0.129 dex). This is likely because we restrict the age of galaxies in the models to be less than the age of the Universe at that epoch, which means that the z=0.4 sample has less cosmic time for wide variations in star formation histories.

In Figure 4.8, we show the SSFR results produced from SED fitting the mock galaxies. Unlike the stellar mass comparison, we see a systematic deviation from the true SSFR which depends on the SSFR. At the star forming end, greater than $\mathrm{Log}_{10}$(SSFR) = -10.5 at z=0.08 and $\mathrm{Log}_{10}$(SSFR) = -11 at z=0.4, the SSFR is reproduced correctly with small $\sigma$ ($\sim$ 0.25 dex at low redshift and $\sim$ 0.2 dex at z=0.4). However, below these points, the SED fit SSFR seems to systematically overestimate the true SSFR by $\sim$ 0.3 dex. This behavior is a direct result of the depth of the *GALEX* NUV data. As we have mentioned, when the NUV magnitude is beyond our completeness, we simply restrict model space to those models which have NUV -$R$ colours redder than that. This leads to a slight overestimate of the SSFR because there is effectively no reasonable constraint on it. Thus, the SSFR is essentially an average of the remaining models. This is indicative that our priors for low star formation rate galaxies are not correct. However, since this has no impact for the

present analysis, we do not attempt to fix this problem.

Thus, our mock sample fitting has lead to two important points. First, as also evidenced by our comparisons with published stellar masses in §4.3.1, we are able to accurately recover stellar masses to the level of $\sigma = 0.2$ dex over the full range of mass. Second, we have shown that we can recover SSFR for star forming galaxies, but that we may be overestimating the SSFRs of non-star forming galaxies. This is an important point, since the B04 star formation rates did not allow us to estimate our accuracy at low SFR. With these findings in mind, in this paper, we avoid making a detailed analysis of the rates of low star forming galaxies.

## 4.4 Results

### 4.4.1 SSFR-$M_\odot$ plane

The star formation rate of a galaxy is a very useful quantity, but is hard to interpret by itself. Many authors have thus examined the specific star formation rate (SSFR) which is defined as the star formation rate normalized by the total stellar mass of the galaxy.

$$\mathrm{SSFR} \equiv \frac{\mathrm{SFR}}{\mathrm{M_{stellar}}} \tag{4.2}$$

This is a useful quantity because it quantifies the current SFR with respect to the past SFR. For instance, a value of SSFR of $10^{-9}$ yr$^{-1}$ means that if the galaxy maintains its current SFR for $10^9$ yr, then it will double its stellar mass. SSFR can then easily be converted into a "birthrate", $b$, defined as $b = \mathrm{SSFR} \times t$, where $t$ is the age of the universe. A value of $b$ greater than 1 means the galaxy is forming stars faster than it has in the past.

It is with this intuition, that we present Figure 4.9, which shows the SSFR as a function of the galaxy stellar mass for galaxies in the SDSS sample. We have two panels, one showing the field galaxies and one showing the group members. It should be noted that the points each represent individual galaxies, but that the galaxies have not been weighted to show either the $1/\mathrm{V_{max}}$ or the density weighting. Thus, especially galaxies in the bottom left corner, those of low mass and SSFR, are systematically underestimated. However, when fitting lines or defining other quantities we always account for these weights.

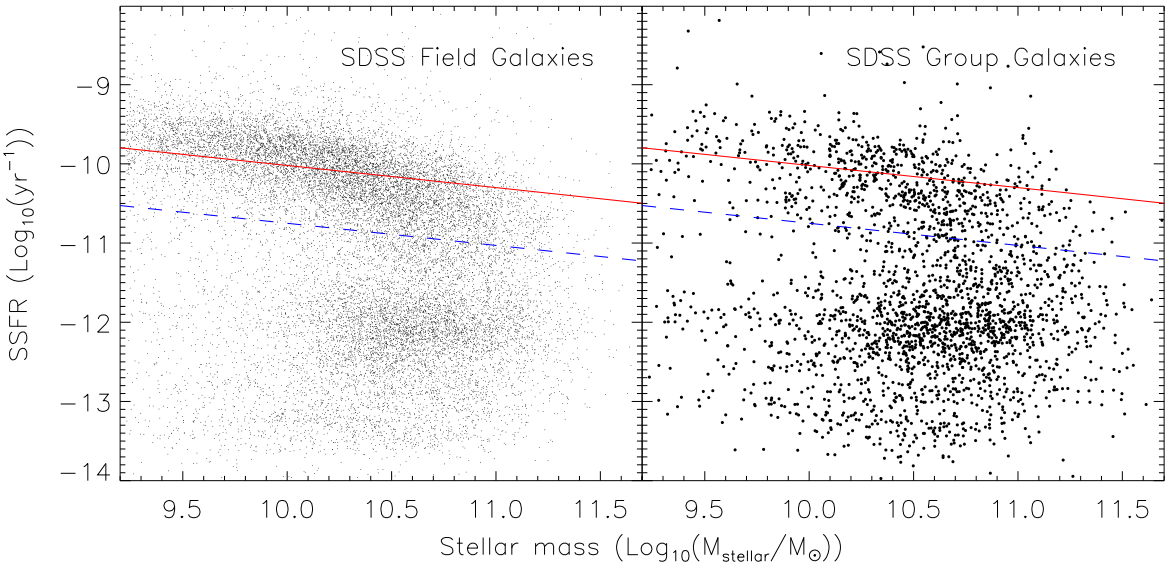


Figure 4.9: Specific star formation rates of both the group (right) and field (left) galaxies in the SDSS survey (median redshift 0.08). The thick red line is a fit to the SSFR star forming sequence of field galaxies. The dashed blue line is the 0.75 dex lower than the red line and represents our division between star forming and passive galaxies. We show both lines in the both panels, although they are determined by fitting only to the field galaxies.

Examining this figure, it is apparent that galaxies tend to cluster in either a group of passive galaxies at SSFR $\sim 10^{-12}$, or a group of star forming galaxies at SSFR $\sim 10^{-10}$. This behavior is obvious in both the group and field galaxies. But, as we have shown in §4.3.4 our measurement of low SSFR rates is not very accurate, and so we do not examine this behavior further.

The galaxies clustered at $\sim 10^{-10}$ has been called by other authors the "main sequence of star-forming galaxies" (Noeske et al., 2007). These galaxies have a birthrate, $b$, of approximately 1, which could suggest that they have been forming stars at about this rate for their lifetime. It is important to remember that our results showed that the low SSFR rates were actually overestimates, meaning that the cluster of points at SSFR $\sim 10^{-12}$ are essentially upper limits. In other words, this 'main sequence' is not due to an insensitivity to star formation rates just underneath the sequence. This is a crucial point as the work of Noeske et al. (2007) was based principally on emission lines, which are relatively insensitive to low star formation rates.

In an attempt to quantify this "main sequence", we fit a line, using the weighted data, to all field galaxies above SSFR=$10^{-11}$ subsequently removing galaxies which lie greater than 2 $\sigma$ from the ridgeline. This enables us to define the ridgeline of main sequence field galaxies to be

$$\mathrm{Log}_{10}(\mathrm{SSFR}) = -7.22 - 0.28 \times \mathrm{Log}_{10}(\mathrm{M}_{\mathrm{stellar}}/\mathrm{M}_{\odot}). \tag{4.3}$$

This relation has $\sigma = 0.21$ dex, which is consistent with our expected measurement error of SSFR. We show the ridgeline as a solid red line in Figure 4.9 for both the field and group panels, however, we have only fit the ridgeline to the field galaxies. The dashed blue line has the same slope as the ridgeline but is located 0.75 dex lower (SSFR=-7.97 - 0.28 $\times$ $\mathrm{M}_{\mathrm{stellar}}$). We use this as the division between passive and star forming galaxies in the SDSS survey.

The slope of the sequence of star forming galaxies is interesting. We find that the sequence is slightly mass dependent, with a slope of 0.28 units of SSFR per stellar mass. If we assume that this star forming sequence of galaxies have always been star forming, then the massive galaxies have either formed earlier than less massive galaxies or have declining star formation histories relative to less massive galaxies.

Peng et al. (2010) found, also using data from SDSS, that the slope of the ridgeline was flatter, at $\sim 0.10$. However, Peng et al. use Brinchmann et al. (2004) H$\alpha$ derived star formation rates for galaxies classified as blue and star forming. They are missing galaxies which are 'composite' or AGN. As was shown by Salim et al. (2007), this removes most of the massive galaxies. These are the galaxies which drive the tilt in the sequence, thus removing them leads to a flatter ridgeline.

We now move to higher redshift to examine the GEEC sample at z $\sim$ 0.4. In Figure 4.10, we show the SSFR-$M_{stellar}$ plot for GEEC galaxies, separated into group and field galaxies. We only plot the stellar mass region in which we can create a statistically complete sample by applying the spatial, magnitude and $1/V_{max}$ weights as described in §4.2.1. As in the previous figure, we see that it appears that the galaxies form an sequence of star forming galaxies. Using the same procedure as above, we fit the star forming ridgeline of GEEC field galaxies. We find that the SSFR sequence is defined by

$$\mathrm{Log}_{10}(\mathrm{SSFR}) = -6.93 - 0.29 \times \mathrm{Log}_{10}(\mathrm{M}_{\mathrm{stellar}}/\mathrm{M}_{\odot}). \tag{4.4}$$

Interestingly, the ridgeline is just shifted upwards by 0.29 dex, while maintaining approximately the same slope. Thus, at least for the star forming field galaxies, from z=0.4 to z=0.08, we see a general lowering of the level of star formation in galaxies with no apparent mass dependence. Notice that the group galaxies also appear to follow approximately the same star formation sequence. As in the case of the SDSS galaxies, we define a division between star forming and passive galaxies as 0.75 dex lower than the SSFR ridgeline. Thus at z=0.4, star forming galaxies are defined to have SSFRs larger than SSFR=-7.68 - 0.29 $\times$ $M_{stellar}$).

It does not appear, via visual inspection of Figures 4.9 and 4.10, that the specific star formation rates of star forming galaxies is wildly different in groups and the field at fixed redshift. To quantify this intuition, we present Figure 4.11 which shows the average SSFR of galaxies classified as star forming in both surveys. There is no apparent difference in the average SSFR of group and field galaxies at a given epoch, but there is a decline with redshift.

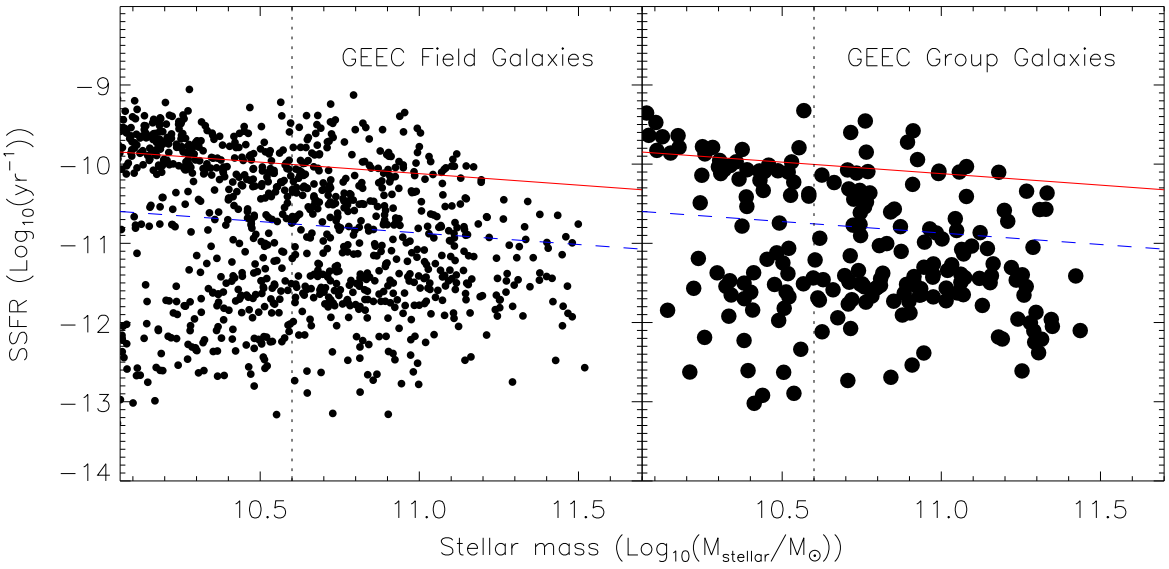


Figure 4.10: Specific star formation rates as a function of stellar mass for both the group (right) and field (left) galaxies in the GEEC survey (redshift = 0.4). The thick red line is a fit to the SSFR star forming sequence of field galaxies. The dashed blue line is the 0.75 dex lower than the red line and represents our division between star forming and passive galaxies. These are reproduced in the group galaxy panel, but are fit only to the field galaxies. The vertical, black, dotted line corresponds to the stellar mass limit ($M_{stellar}$ = $3.9 \times 10^{10}$) at the highest redshift of the sample (z=0.55). Using $1/V_{max}$ weighting, we can obtain a complete sample to $M_{stellar} = 1.44 \times 10^{10}$, but the scatter plot does not reflect these weightings.

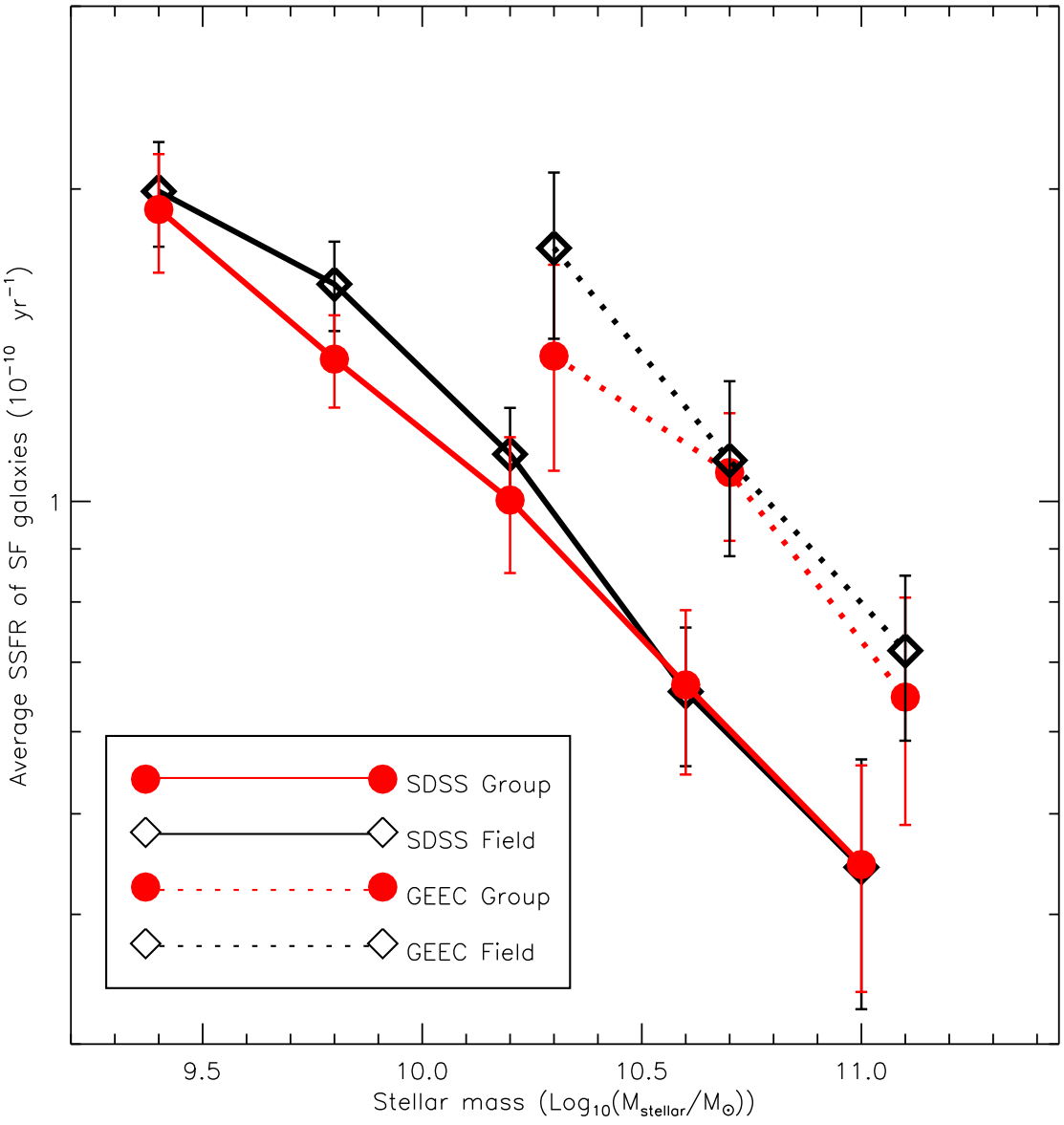


Figure 4.11: Average SSFR of star forming galaxies in the group and field of SDSS and GEEC surveys. Star forming galaxies are defined as being above the blue dashed line in Figures 4.9 and 4.10, which is 0.75 dex below the peak of the star forming sequence.

### 4.4.2 Fraction of passive galaxies

We have concentrated principally on the sequence of star forming galaxies and its position on the SSFR-$M_{\odot}$plot. We now shift to look at what fraction of galaxies are within the sequence. As detailed above, we define passive galaxies as those which are 0.75 dex, or approximately $3\sigma$, lower than the ridge line of the SF sequence.

Figure 4.12 shows the passive fractions as a function of stellar mass for the group and field galaxies in both the SDSS survey and the GEEC survey. At both redshifts, we see that at all stellar masses probed, groups have a higher fraction of passive galaxies than the field. Given that this is comparing group galaxies with field galaxies at fixed stellar mass and red shift, it is strong evidence that group galaxies have star formation prematurely truncated by the group environment.

To guide the eye in Figure 4.12, we have drawn an approximation to each of the group and field passive fraction in SDSS. These two lines have very different slopes, implying that there is a mass dependent difference in the truncation mechanisms in the group and the field. This is most interesting when comparing to the GEEC sample. The SDSS lines have been re-drawn on the GEEC panel as well. This shows that the group and field galaxies at z=0.4 have a mass dependent fraction with a similar slope to the SDSS field galaxies. Thus, the evolution in groups must be mass dependent to end with the correct fraction of passive galaxies in groups at z=0.

## 4.5 Discussion

### 4.5.1 Accretion model

In Chapter 2, we introduced a simple model for relating environmental effects to a galaxies accretion history. In this model, galaxies become 'environmentally affected' some time, $T_{\rm trunc}$, after they fall into a host halo with a mass greater than $M_{\rm trunc}$. This model is based on the semi-analytic model of Font et al. (2008a), but uses only the accretion history and stellar mass of it. In Figure 4.13, we show the results for a model where $T_{\rm trunc}$= 3 Gyrs and $M_{\rm trunc}$=$10^{13}$ $M_{\odot}$. This shows the predictions for the environmentally affected fraction at z=0.08 and z=0.4, as well as the observed group passive fractions at these redshifts. To

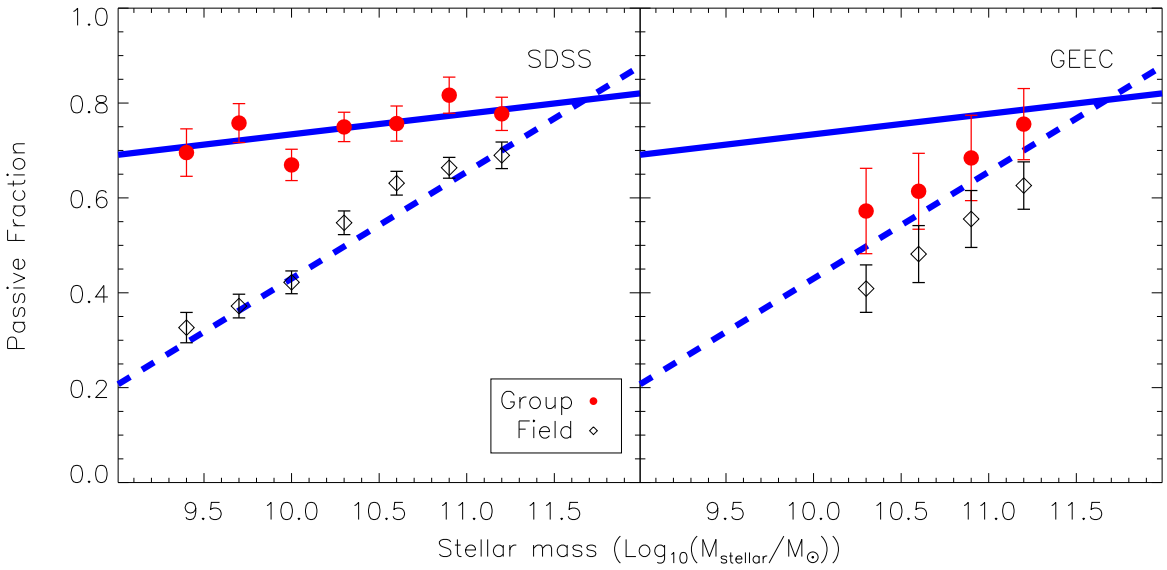


Figure 4.12: The fraction of passive galaxies in the group and field of SDSS (left panel) and GEEC (right panel) surveys. Passive galaxies have SSFRs at least 0.75 dex lower than the star forming sequence of galaxies. The solid blue line is an approximation to the mass dependence of the SDSS group galaxies, while the dashed blue line is an approximation to the SDSS field galaxies. For illustrative purposes, the same lines have also been reproduced in the GEEC panel.

match the overall SFR-determined passive fraction this model has a higher mass threshold than was shown previously in Figure 2.10, which had been determined to match optical 'red' fractions. However, as shown in Chapter 2, the rate of evolution in these models is principally determined by the $T_{\rm trunc}$. While this model is simple, it is interesting to note that it predicts approximately the correct evolution in the passive fraction. Notice that at $M_{stellar} = 10^{10.3}$ $M_{\odot}$, the evolution between the two redshift epochs in passive fractions is observed to be $\sim 0.18$. The model with a $T_{\rm trunc}$ of 3 Gyr agrees with this observed evolution. In contrast, a model with the same $M_{\rm trunc}$ but with $T_{\rm trunc}$= 1 Gyr predicts only an increase of 0.03. A timescale this short is clearly ruled out by the data. As we have argued in Chapter 2, the most powerful argument against a higher $M_{\rm trunc}$ is simply the observed difference in group and field passive fractions. A mechanism which occurs in the halo mass and timescale regime of our successful model could be strangulation, the relatively gentle process of removing the outer hot halo of infalling galaxies.

### 4.5.2 The nature of passive galaxies

We have seen that the sequence of star forming galaxies evolves with redshift, but that it is independent of environment. However, given that the fraction of star forming galaxies is so strongly environment dependent, we can ask the question: Are our results consistent with all passive galaxies residing in massive halos? The models of Font et al. (2008a) show that 42% of galaxies are in halos above $10^{12.75}$M$_{\odot}$at z=0 while at z=0.4, there are 26% of galaxies in these halos. Assuming that all of the galaxy groups have properties given by our sample, and the total population has the value of our 'field' data, we can infer the properties of 'isolated' galaxies. Then we can relate the group and field passive fractions ($f_{\rm passive,group}$, $f_{\rm passive,field}$) to the isolated passive fraction ($f_{\rm passive,isolated}$) using the group and isolated galaxy fraction at that redshift ($F_{\rm G}$, $F_{\rm I}$), as

$$f_{\rm passive,isolated} = \frac{f_{\rm passive,field} - F_{\rm G} * f_{\rm passive,group}}{F_{\rm I}} \tag{4.5}$$

In this way, we see that the implied isolated passive fraction at $M_{stellar} = 10^{11}$ $M_{\odot}$is 0.50 ($\frac{0.55-0.26*0.68}{0.74}$) at z=0.4 and is 0.54 ($\frac{0.66-0.42*0.82}{0.58}$) at z=0. In other words, there is an intrinsic high passive fraction at this mass in isolated galaxies, but most of the evolution in the field between z=0.4 and z=0 is driven by the evolving group passive fraction. At

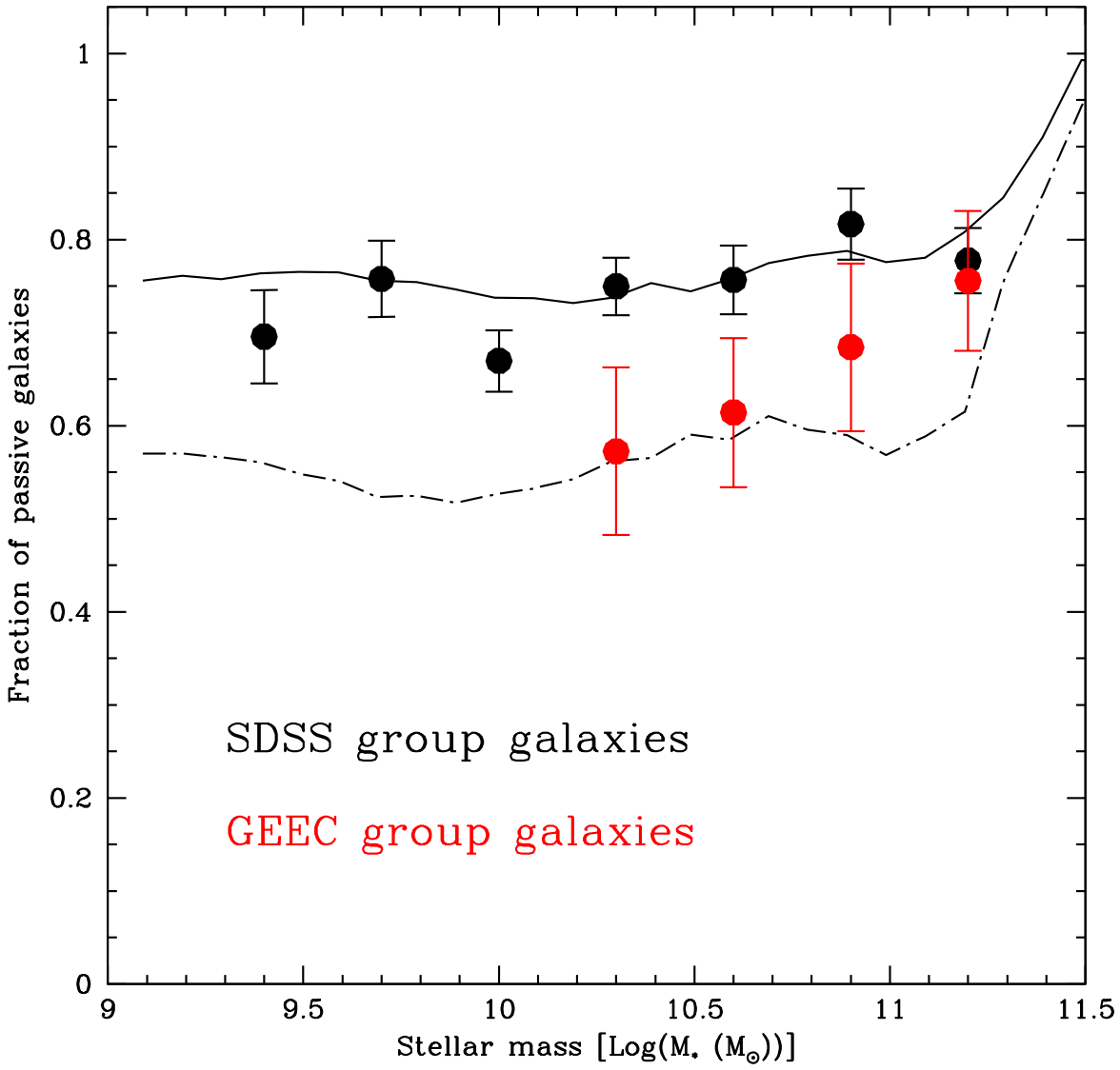


Figure 4.13: Comparison between the passive fraction of GEEC and SDSS group galaxies and a simple accretion model for environmental effects. Passive galaxies were determined via their specific star formation rates. The accretion model assumes that a galaxy become passive 3 Gyrs after it falls into a halo of at least $10^{13}$ $M_{\odot}$. The solid black line is the prediction at the median redshift of SDSS, z=0.08, while the dashed black line is the model at z=0.4.

$M_{stellar} = 10^{9.4}$ $M_{\odot}$, for which we only have data at z=0, the implied true isolated fraction is 0.06 ($\frac{0.33-0.42*0.7}{0.58}$). In other words, at lower mass, the field passive fraction appears to be almost entirely due to galaxy groups.

From this emerges a general picture in which massive galaxies have a high fraction of passive galaxies regardless of their environment, while low mass galaxies are essentially only passive in groups. This implies that massive galaxies must have an internal mechanism, or at least one that does not depend on environment, which plays a large role in the galaxy properties. On the other hand, low mass galaxies are essentially all star forming unless they are in a group or cluster environment. There have been models in which this internal mechanism is proposed to be the resultant heating caused by the fueling of active galactic nuclei (Springel et al., 2005a; Hopkins et al., 2008).

## 4.6 Conclusion

We have fit spectral energy distributions to galaxies in two surveys, SDSS and GEEC. These SEDs use high quality, space based ultraviolet imaging along with optical, and near infrared for GEEC, photometry. We have compared this photometry to large suites of stellar population synthesis models to determine star formation rates and stellar masses. This method nicely reproduced alternative methods of measuring both star formation rates and stellar masses. By examining the results, we conclude the following.

- Star forming galaxies of all environments undergo a systematic lowering of their star formation rate between z=0.4 and z=0.08 regardless of mass.
- The star formation properties of star forming galaxies, as measured by their average specific star formation rates, are the same in the group and field environment at fixed redshift.
- The fraction of passive galaxies is higher in groups than the field at both redshifts. However, the difference between the group and field grows with time and is mass dependent, in the sense the the difference is larger at low masses.
- Low mass galaxies at z=0 have group and field passive fractions which can be explained if passive galaxies only exist in groups.

- The evolution of passive fractions in groups between z=0.4 and z=0 is consistent with an accretion model in which galaxies are environmentally affected 3 Gyrs after falling into a $10^{13}$ $M_{\odot}$galaxy.

These results show a remarkable similarity to our measurements of morphology in Chapter 3. In that chapter, we showed that the fraction of disk galaxies is higher in the field at both redshift and the difference grows larger with time. Also, we found that there was no indication that the disks were different in the field or groups.

These results all suggest that only a fraction of galaxies in groups must be actively truncated at any given time. If the mechanism is quick enough, like ram pressure stripping, then the truncation time might be short enough that only a small fraction of group galaxies are affected at a given time. This would allow the bulk of the star forming galaxies to remain unchanged but still allow the observed evolution. However, as we have mentioned in Chapter 1, ram pressure stripping is likely not effective in galaxy groups.

Based on our accretion model, strangulation seems like a suitable candidate for environmental mechanisms. However, it is unclear if strangulation can allow galaxies to remain apparently unaffected for some time. In semi-analytic models, strangulation produces too many 'green' galaxies, which would likely alter the disk and star formation properties (Font et al., 2008a).

# Chapter 5

# Constraints on intragroup stellar mass from hostless Type Ia supernova

## 5.1 Introduction

Diffuse light in the halos of galaxy clusters has been extensively studied since the discovery of 'swarms of stars' between galaxies in the Coma cluster by Zwicky (1951). Although puzzling at the time, diffuse stellar light is now thought to be a natural consequence of hierarchical structure formation, which causes merging galaxies to shed some of their stellar material (Willman et al., 2004; Purcell et al., 2007). The diffuse light in individual massive clusters has been the focus of many observational studies,which find that the fraction of the total cluster light in this component is 10-30% (e.g., Thuan & Kormendy, 1977; Scheick & Kuhn, 1994). By stacking $\sim$ 700 clusters, Zibetti et al. (2005) was able to tightly constrain the diffuse light within 500 kpc of the cluster center to be 10.9 $\pm$ 5.0 % of the total cluster light.

At the other extreme, the diffuse light around galaxies like the Milky Way is similarly thought to arise from the tidal heating and stripping of infalling dwarf galaxies (e.g., Searle & Zinn, 1978; Bullock et al., 2001b; Font et al., 2008b). However, in this regime, the fraction is only $\sim$ 1-2 % of the total light in the halo (e.g., Chiba & Beers, 2000; Yanny

et al., 2000; Law et al., 2005). Probing the intermediate halo mass regime, that of galaxy groups, is important in order to reconcile these two extreme regimes.

Galaxy groups are difficult to observe in detail and thus, a study of the intragroup medium (IGM) in typical systems has not been done. Studies of the more extreme compact groups have found a large variation in the group to group diffuse light, ranging from 5% up to as much as 45 % of the total light (White et al., 2003; Da Rocha & Mendes de Oliveira, 2005; Da Rocha et al., 2008).

Galaxy groups have velocity dispersions comparable to that of the most massive galaxies within them, and as such are a prime location for the mergers, tidal stripping and shredding which is thought to give rise to the diffuse light. Thus, the amount of diffuse stellar mass in galaxy groups is a direct probe of the efficiency with which infalling galaxies are disrupted. This could have important implications for semi-analytic models, which produce too many faint red galaxies (Weinmann et al., 2006b; Gilbank & Balogh, 2008).

Type Ia supernova (SNe Ia) likely result when a carbon-oxygen white dwarf acquires additional mass from a companion star, which causes a thermonuclear explosion. However, the exact origin of the progenitor material is uncertain, which makes direct prediction of SN Ia rates from stellar population modeling difficult. It is typical to parametrize the rate and then measure the coefficients empirically. The most common model for the SN Ia rate is the so called A+B model, which assumes that SN Ia arise from two distinct channels. In this model, there is a "prompt" component which depends on the current star formation rate (SFR) of the host and a "delayed" component which traces the host's stellar mass (Scannapieco & Bildsten, 2005; Graham et al., 2008). This model was motivated by the observation that the SN Ia rate is $\sim$ 20-30 times higher in late type galaxies than in early type galaxies of the same mass (Mannucci et al., 2005).

Relatively little attention has been given to SNe which may be hosted by diffuse material within groups and clusters. But, Gal-Yam et al. (2003) found that 2 of the 7 cluster SNe Ia discovered during a survey of low redshift Abell clusters were not associated with galaxies. Recently, Sand et al. (2008) have begun a search of 60 X-ray selected galaxy clusters with the expectation of finding $\sim$ 10 intracluster SNe Ia. They identified three intracluster candidates in early data, all of which were actually outside of $R_{200}$, implying a relative deficit of intracluster mass at small cluster radii.

This study is complementary to these studies, as we constrain the diffuse stellar mass

in relatively low-mass galaxy groups, by correlating type Ia supernovae with a large group catalogue, to identify supernovae without a resolved galaxy host. In §6.2, we discuss our supernova and group sample, as well as introducing the derived galaxy properties we use. In §5.3, we discuss the procedure we use to identify the hosts or lack of hosts of the supernovae. Finally, in §5.4, we discuss the constraints this places on the diffuse stellar mass in galaxy groups. Throughout this chapter, we adopt, as was done during the assembly of the group catalogue, a ΛCDM cosmology with the parameters of the third year WMAP data, namely $\Omega_{\rm m} = 0.238$, $\Omega_\Lambda = 0.762$, $\Omega_{\rm b} = 0.042$, $n = 0.951$, $h = H_0/(100\,{\rm km\,s^{-1}\,Mpc^{-1}}) = 0.73$ and $\sigma_8 = 0.75$ (Spergel et al., 2007).

## 5.2 Data

In this chapter, we require a uniformly selected sample of SNe Ia and a large sample of galaxy groups over a large area of the sky to find enough hostless SNe Ia to constrain the diffuse stellar mass. Therefore, we will examine the region of Stripe 82 in the Sloan Digital Sky Survey (SDSS) which hosts the SDSS supernova survey.

### 5.2.1 SDSS supernova survey

The SDSS supernova survey was designed to identify SNe Ia at low redshift ($0.05 < z < 0.35$) by imaging an area of 300 sq. degrees multiple times over a period of 5 years (Frieman et al., 2008). Once identified, the SNe Ia candidates are spectroscopically followed up and classified (Sako et al., 2008; Zheng et al., 2008). This has resulted in the largest collection of supernova at low redshift. Crucially, for our purposes, the scanning throughout the 300 sq. degrees is very uniform, resulting in a consistent detection threshold. For the following, we restrict our analysis to the 368 confirmed SNe Ia within $0.1 < z < 0.2$. We note that the SDSS supernova survey also identifies type II SNe. However, despite being more numerous, they are are also much fainter (Bazin et al., 2009). Thus spectroscopic follow-up of type II SNe was limited to those at $z < 0.06$, which is below our redshift limit.

### 5.2.2 Group catalogue

Reliable and representative samples of galaxy groups can be found using friends of friends algorithms in large redshift surveys (e.g., Huchra & Geller, 1982; Carlberg et al., 2001; Berlind et al., 2006). We use a highly complete group sample defined by Yang et al. (2007), who have applied their 'friends of friends'-like algorithm to the SDSS fourth data release to produce a sample of $\sim$ 300,000 galaxy groups with masses as low as $10^{11.5}\ h^{-1}\ \mathrm{M}_{\odot}$. An important aspect in the construction of this group catalogue is the subsequent mass estimates, which are obtained by essentially ranking groups by their total luminosity or total stellar mass and associating these rankings with the expectations of a $\Lambda$CDM halo occupation model. We use "Sample I" from Yang et al. (2007), which exclusively uses galaxies with SDSS spectroscopic redshifts. We chose this sample, as opposed to the other samples, which add in existing redshifts from the literature, because we are principally concerned with obtaining a uniformly selected population of galaxy groups. In this chapter, we use the halo mass rankings obtained from the total group stellar mass and restrict our analysis to groups with masses greater than $10^{13}\ h^{-1}\ \mathrm{M}_{\odot}$, which leaves a final sample of 1401 groups between z=0.1 and z=0.2 within the SDSS supernova legacy survey area. The galaxy groups have a median halo mass of $1.98 \times 10^{13}\ h^{-1}\ \mathrm{M}_{\odot}$and a mean value of $3.86 \times 10^{13}\ h^{-1}\ \mathrm{M}_{\odot}$with a standard deviation of $3.16 \times 10^{13}\ h^{-1}\ \mathrm{M}_{\odot}$.

We make use of measurements of the stellar mass and star formation rates of the galaxies within the main galaxy spectroscopic sample of the SDSS. Our stellar masses are taken from Kauffmann et al. (2003b), and were determined by comparing large libraries of stellar population models with line indices and broad band photometry. The star formation rates we use were measured by Brinchmann et al. (2004) using principally H$\alpha$ emission along with continuum properties (e.g., 4000-$\mathring{A}$ break).

## 5.3 Hosted and hostless group SNe Ia

Our goal is to obtain a complete sample of SNe Ia which reside within galaxy groups in our sample. We define group membership as those SNe Ia which are within the projected group virial radius and which are $\pm$ 3000 km/s from the group redshift. This velocity range is larger than the typical velocity dispersion of our groups, but is chosen to be 2 sigma of the precision with which redshifts can be derived from SNe Ia spectral features

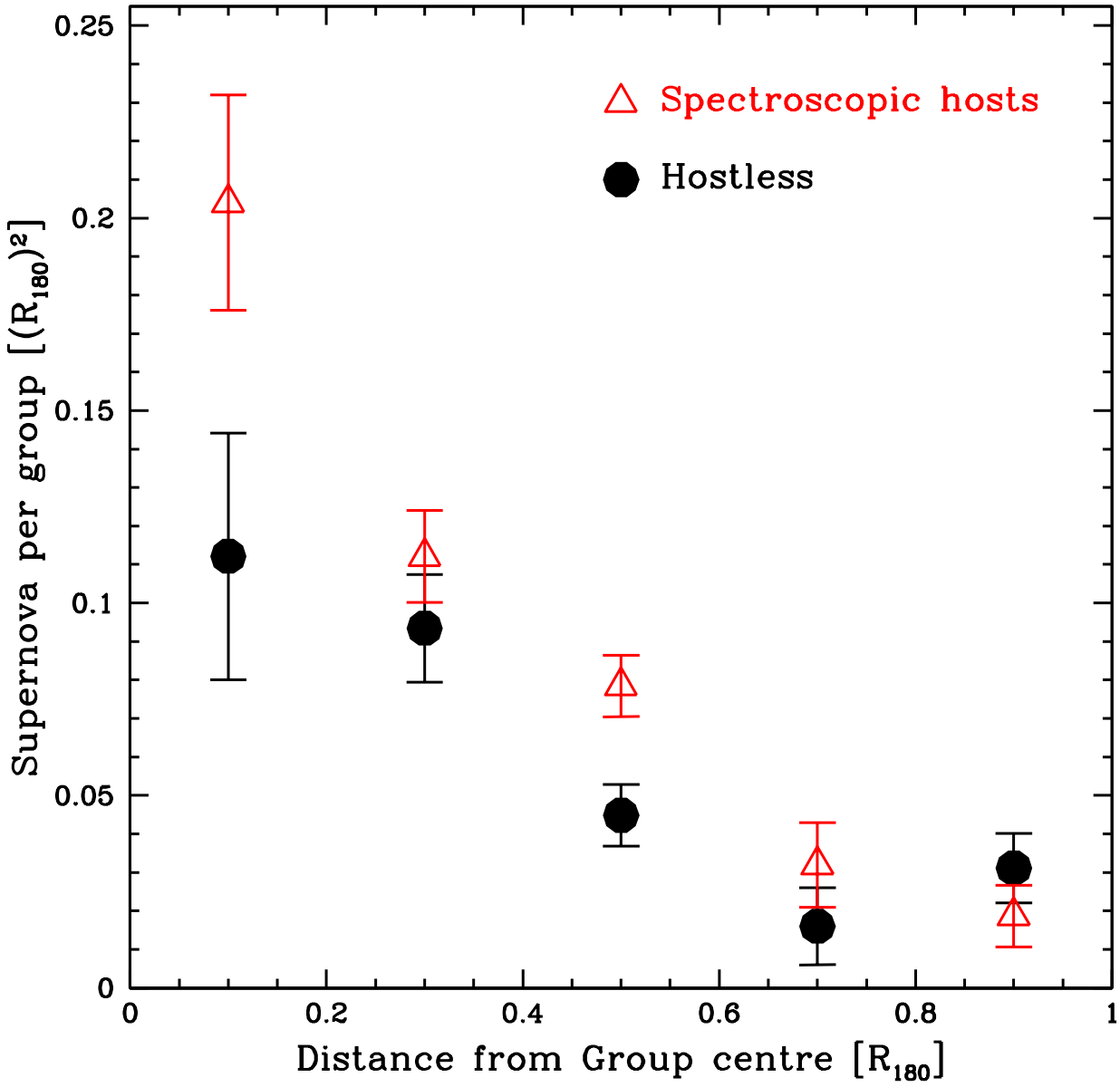


Figure 5.1: The distribution of type Ia supernovae as a function of distance from the group centre. The red triangles represent the rate of SNe Ia hosted by the sample of spectroscopic galaxies with the group, while black circles signify the rate of hostless SNe Ia within the group sample. $R_{180}$ corresponds to a distance of 0.79 $h^{-1}$ Mpc for a group with the mean mass of our sample ( $3.86 \times 10^{13}$ $h^{-1}$ $M_{\odot}$).

(ie. $\sim$ 1500 kms$^{-1}$, Frieman et al., 2008; Cooper et al., 2009). Of the 368 SNe Ia in our complete sample, 59 are matched to one of our galaxy groups.

We search for host galaxies of the 59 group SNe, by matching to all group galaxies in the main galaxy sample of SDSS. We assume a SN is hosted if it is within a distance equal to twice the size of the radius enclosing 90% of the galaxy's light. This radius corresponds to a physical scale of 9–14 kpc/h for most of the galaxies in the spectroscopic sample, and is slightly smaller for those in the photometric sample. However, for a few of the bright group/cluster galaxies this distance is much larger because of their extended haloes. For this reason we have capped the search radius to be a maximum of 40 kpc/h. In practise, this changes the membership of just one SNe, which is 78 kpc/h from a BCG. By matching within our search radius and a velocity window of $\pm$ 3000 km/s, we find that 23 of the 59 group SNe are hosted by galaxies within the main spectroscopic galaxy sample. The spectroscopic galaxy sample only reaches a magnitude limit of $r = 17.77$, so we must extend our search for the hosts of the remaining SNe to the photometric catalogues, which reach 95 % completeness at $r \sim 22.2$. This is an absolute magnitude of $M_r \approx -15$ to $-16$ in our sample. We search for hosts of the remaining SNe in the photometric catalogues again within our scaled radius, and now use the photometric redshifts supplied by the SDSS pipeline. Fourteen of the remaining 36 SNe were matched with host galaxies using this criteria. Finally, we relax the requirement that the galaxy photometric redshift is within the range of the SN spectroscopic redshift, and find an additional three galaxies are matched. This leaves us with a sample of 19 SNe with no host galaxy in the photometric catalogue. The images of these SNe, as with the entire sample, were visually inspected to confirm that they appeared as truly hostless SNe. Given the limit of our photometric catalog, we might expect that some of these 19 supernovae are actually hosted by galaxies which are below our detection threshold. Integrating the $r$-band luminosity function of SDSS at z $\sim$ 0.1 (Blanton et al., 2003b), only 3 % of the total galaxy luminosity is below our detection limit. If we adopt a luminosity function typical of rich galaxy clusters, which have a steep faint end slope (Milne et al., 2007), as much as 5 % of the total galaxy luminosity may go undetected in our images. Thus, if the number of supernova scale with luminosity, then it is likely that $\sim 2 \pm 1$ of the apparently hostless galaxies are actually hosted by very faint galaxies (all uncertainties are $1\sigma$). In summary, we find that of the 59 total group SNe, 23 are matched to spectroscopically confirmed galaxy, 14 are matched to galaxy via photometric redshift, and a further 3 appear associated with other galaxies.

This leaves a sample of 19 apparently hostless SNe.

## 5.4 Results

We are first interested in the distribution of the SNe Ia sample within our galaxy groups. This is presented in Figure 5.1, in which we show the SN Ia per area per group as a function of groupcentric distance in units of $R_{180}$ as calculated in Yang et al. (2007). The SN Ia counts per area decline steeply with groupcentric distance, which indicate they are associated with the galaxy group. Also shown is the rate of SN Ia hosted by group galaxies within the spectroscopic sample. Given the small numbers and uncertainty on each point, the distributions are similar. There is no evidence that the hostless SN, and thus the diffuse stellar mass, are distributed differently from the galaxy population.

Assuming that all 19 apparently hostless galaxies are truly hostless, and making the simplifying assumption that the stellar population in the intragroup medium is the same as within the group galaxies, our measurement immediately tells us the diffuse stellar mass represents $\sim 32^{+4}_{-3}$ per cent of the total stellar mass in these groups, where the quoted statistical uncertainty is the $1\sigma$ confidence limit. We now explore the systematic uncertainties and consequences associated with this measurement.

### 5.4.1 Upper limit on the diffuse group stellar mass

As discussed above, without a definite model of the origin of SNe Ia, the conversion of a SNe number count into the underlying stellar mass is uncertain. Therefore, we first try to derive the *maximum* diffuse stellar mass possible given the population of hostless SNe Ia. First, we will assume that the 22 supernova without a spectroscopic or photo-z confirmed host are true descendants of diffuse group stellar mass. This includes the 19 supernova with no apparent host as well as three which appear to be located within galaxies, but whose galaxies have photometric redshifts inconsistant with both the SN redshift and the redshift of the group. To obtain a robust upper limit we here further assume that there is no contribution from faint, undetected hosts. It is worth pointing out that this is also an upper limit because it is much easier to detect SNe Ia in hostless environments, where

the contrast is high, than it is for those which occur in galaxies. We will assume that the remaining 37 supernova occur within galaxies.

We now need to derive a relation between the stellar mass and the number of resulting "delayed" supernova. To do this, we must accurately know the stellar mass and star formation rate of a population of galaxies. We will use our sample of galaxies which are spectroscopically confirmed and which are within our groups. Using the stellar masses of Kauffmann et al. (2003b) we find that the spectroscopic sample of galaxies in our 1401 groups has a total stellar mass of $6.55 \times 10^{14}\ h^{-1}\ \mathrm{M}_{\odot}$and, using the star formation rates of Brinchmann et al. (2004), the total star formation rate is $2.62 \times 10^{4}\ h^{-1}\ \mathrm{M}_{\odot}$/yr. We can now use the empirical relation of Dilday et al. (2008), which was derived from the SDSS supernova survey, to find out how many of the 23 SNe in the spectroscopic sample are "prompt" SN and how many are "delayed". Dilday et al. finds that the supernova rate, r, is given by, r=A$\rho$+B$\dot{\rho}$, where $\rho$ is the stellar mass, $\dot{\rho}$ is the star formation rate, A=2.8$\pm$1.2 $\times\ 10^{-14}$ SNe $\mathrm{M}_{\odot}^{-1}$ $\mathrm{yr}^{-1}$ and B=$9.3^{+3.4}_{-3.1} \times 10^{-4}$ SNe $\mathrm{M}_{\odot}^{-1}$. Using this formula, we find that $43^{+18}_{-16}$ % of 23 SNe are "delayed" and 57 $^{+16}_{-18}$ % are "prompt". So, we see that there are $9.9^{+4.1}_{-3.9}$ "delayed" SNe (=$43^{+18}_{-16}$ % $\times$23), which arise from an underlying stellar mass of 6.55 $\times\ 10^{14}\ h^{-1}\ \mathrm{M}_{\odot}$. Thus, we have the relation that 1 delayed SN arises from an underlying stellar mass of $6.62^{+3.92}_{-3.54} \times 10^{13}\ h^{-1}\ \mathrm{M}_{\odot}$. We will us this relation throughout the rest of the chapter to relate the stellar mass to a quantity of delayed SNe.

The diffuse stellar mass is expected to be relatively old, as the intragroup mass is not expected to be able to form stars in-situ. Any star formation which results from the stripping of gas from galaxies will occur near the galaxy, and likely would appear as if it was hosted by that galaxy (Sun et al., 2007a, 2009). Indeed, the intracluster light observed to date has been universally old (Zibetti et al., 2005). So, it is reasonable to assume that there exist no "prompt" supernova in the intragroup mass, particularly since we are here after a robust upper limit on the diffuse stellar mass. Thus, we can conclude that the diffuse component hosts at most 22 "delayed" SN, and we can use the relation found above that 1 "delayed" SN arises from a stellar mass of $6.62^{+3.92}_{-3.54} \times 10^{13}\ h^{-1}\ \mathrm{M}_{\odot}$, to see that the total stellar mass in the diffuse component is $\leq 1.46^{+0.86}_{-0.73} \times 10^{15}\ h^{-1}\ \mathrm{M}_{\odot}$. Therefore, the total diffuse stellar mass per group is $\leq 1.04^{+0.61}_{-0.52} \times 10^{12} h^{-1}\ \mathrm{M}_{\odot}$, or $\leq 2.69^{+1.58}_{-1.34}$% of the halo mass, given the average halo mass per group of $3.86 \times 10^{13}\ h^{-1}\ \mathrm{M}_{\odot}$. Taking the upper limit allowed by the statistical uncertainty, our robust upper limit on the fraction of total mass that occurs in the diffuse stellar component is 4.3%. In Figure 5.2, we show these

upper limits in two bins of halo mass. We discuss the implications of this in Section 5.5.

### 5.4.2 Best estimate of the intragroup mass

We have presented a robust upper limit on the quantity of intragroup stellar mass in galaxy groups. We now attempt to make a more realistic calculation of the contribution from undetected host galaxies, to arrive at an estimate of the actual mass.

In the previous section, we assumed all 22 hostless SN were actually associated with the diffuse mass. However, three of these appear to be associated with photometric galaxies, which have inconsistent photometric redshifts. From their proximity to these galaxies we think it is more likely that the photometric redshift is incorrect, and these are really "hosted" SN, within the group. Moreover, we have argued that for typical groups up to 5 % of the group galaxy light is expected to be in unresolved hosts. Therefore, if stellar light scales as stellar mass, we would expect $\sim 2$ of the remaining 19 apparently hostless SNe to be "delayed" SNe hosted in unresolved galaxies.

However, while the "delayed" SN rate should only depend on the total stellar mass, galaxies which are strongly star forming will have a greater "prompt" component than galaxies within our spectroscopic sample. To estimate this effect, we must adopt a scaling between the stellar mass and star formation rate. As low mass galaxies are usually uniformly star forming, we assume that the low mass galaxies double their stellar mass in a Hubble time (e.g. SFR=$\frac{M/M_{\odot}}{10^{10}yr}$). Using the relation of Dilday et al., we find that the number of prompt SN is equal to $9.3/2.8 = 3.3$ times the number of delayed SN, so that $\sim$ 6 of the hostless SNe are likely due to "prompt" explosions in unresolved galaxies. Taken together, this means only $\sim 11$ of our hostless SNe are likely true intragroup SNe. Again, we assume that all true intragroup SNe are "delayed" SNe, because the intragroup mass is uniformly old. Therefore, we can use the previous scaling which stated that 1 "delayed" SN arises from a stellar mass of $6.62^{+3.92}_{-3.54} \times 10^{13}$ $h^{-1}$ $M_{\odot}$, to find that a total mass of $7.28^{+4.31}_{-3.89}$ $\times$ $10^{14}$ $h^{-1}$ $M_{\odot}$is in the diffuse component. On average, this corresponds to $5.20^{+3.08}_{-2.78}$ $\times$ $10^{11}$ $h^{-1}$ $M_{\odot}$per group, representing a fraction $1.32^{+0.78}_{-0.70}$ % of the total halo mass. The black points in Figure 5.2 shows the final best estimate of the diffuse stellar mass in two bins of halo mass, after all the corrections discussed above. The diffuse stellar fraction is statistically indistinguishable in the two mass bins, with $\sim 1.3^{+0.73}_{-0.65}$ % in the lowest mass groups, and $1.2^{+0.62}_{-0.56}$ % for the more massive systems.

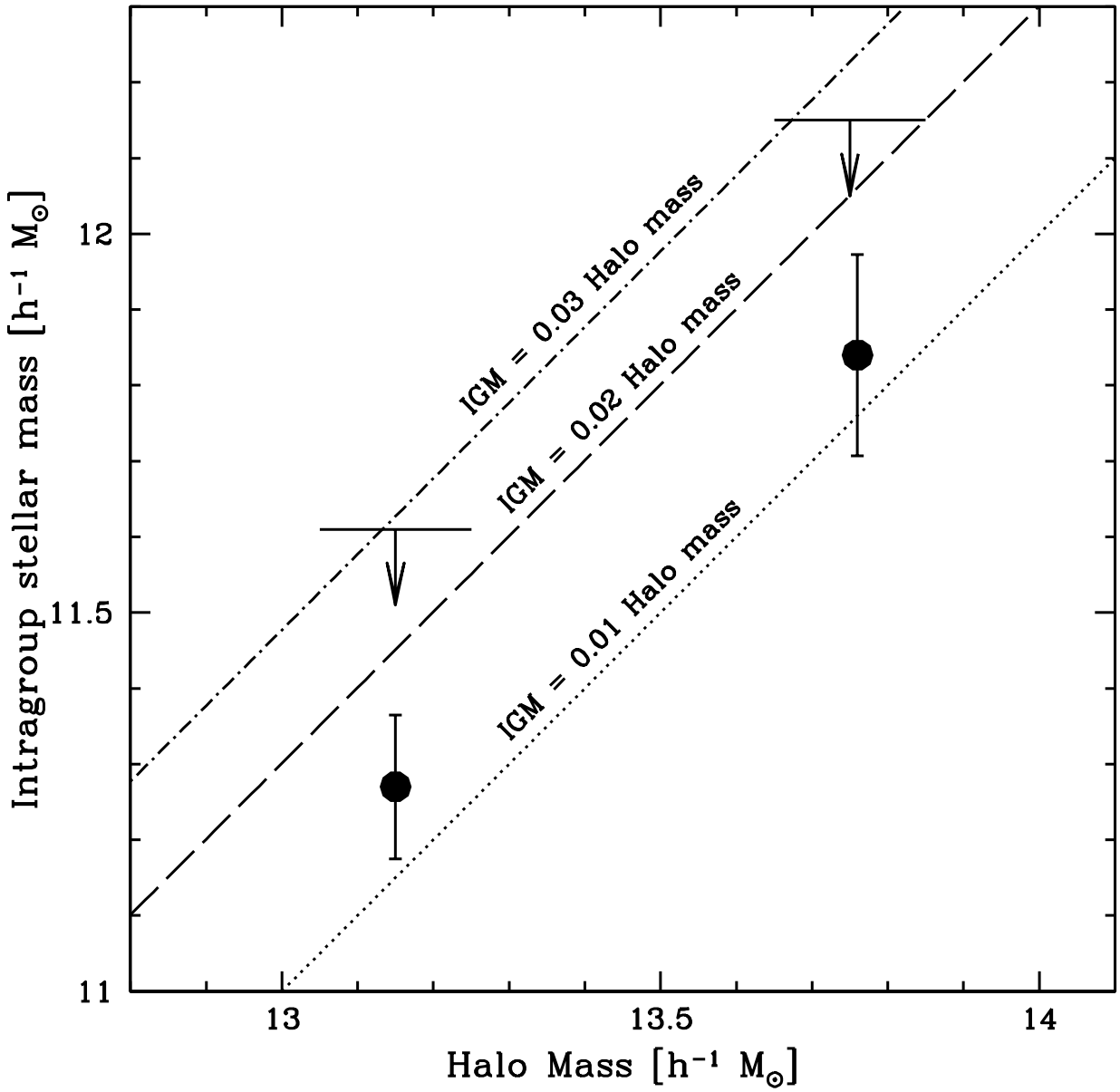


Figure 5.2: The measurements of intragroup stellar mass for our sample, assuming no prompt component of SN. The thick black line with the arrow represent our upper limits, while the dots are the best estimate after accounting for a contribution from possible host galaxies below the survey magnitude limit. Also shown are three equality lines where the intragroup stellar mass equals 0.03 (dot-dashed line), 0.02 (dashed line) or 0.01 (dotted line) of the total halo mass.

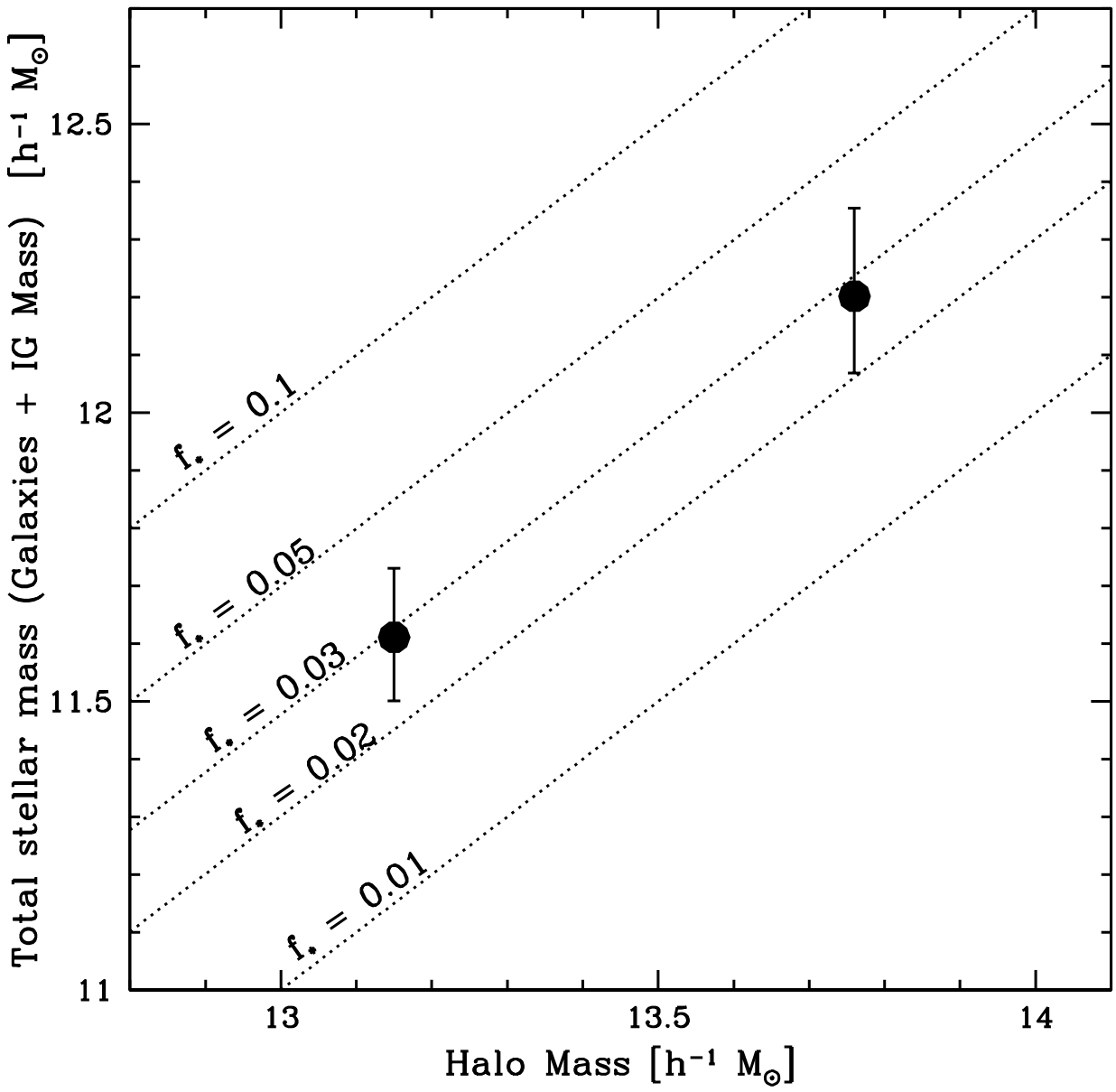


Figure 5.3: Total stellar mass in our sample of groups. This includes the diffuse intragroup mass measured in this chapter added to the stellar mass of galaxies in the same sample as determined by Yang et al. (2009). The dashed lines represent lines of constant total stellar fraction, $f_* = \frac{\text{Total Stellar Mass}}{\text{Total Halo Mass}}$. Our sample indicates the stellar fraction these groups is $\sim$ 0.02-0.04.

A potential systematic error in our results could occur if the SDSS supernova pipeline and/or spectroscopic follow-up is biased towards finding SNe without hosts. The first issue, that of the finding algorithm, was explored by Dilday et al. (2008), who found that the pipeline uncovers $> 98$ % of SNe Ia to a redshift of 0.2. Even if the completeness were only 95% and entirely biased toward hostless SN (i.e. assuming the 5% missed SN are associated with galaxies), our result on the amount of mass in diffuse form would only change from 1.32% to 1.17%. Regarding the spectroscopic follow-up, Sako et al. (2008) state that essentially all of the z<0.15 type Ia SNe were spectroscopically followed up, and our results are unchanged if we restrict just to this sample. Thus we conclude that neither of these selection affects have a significant affect on our results.

## 5.5 Discussion and Conclusions

We have measured the diffuse stellar mass in galaxy groups using the rate of hostless SNe Ia. We find that $1.32^{+0.78}_{-0.70}$ % of the total halo mass of a group is in the form of this diffuse intragroup stellar mass. Although many numerical predictions exist for the mass of the diffuse intragroup material, they are usually stated as a fraction of the total stellar mass. To obtain this measure we will use the stellar mass functions of Yang et al. (2009), which were measured for the same sample of groups we use. They find that the stellar mass function of the group galaxies is well approximated by a log-normal distribution for the central galaxy and a modified Schechter function for the satellite population. Integrating these functions over all galaxies reveals that the fraction of stars in galaxies is $\sim 1.5$ % of the halo mass for groups in our mass range[1]. Therefore, $\sim 47^{+16}_{-15}$ % of the stellar mass in our groups is in the diffuse component.This is significantly higher than the estimates of Purcell et al. (2007), who use Press-Schechter formalism along with analytic models for the disruption and stripping of halos to estimate that $\sim 20$ % of the stellar mass is in a diffuse form. It is also significantly larger than that seen in the most massive clusters, which is more typically about 10% (Zibetti et al., 2005).

In Figure 5.3, we show the total stellar mass as a function of halo mass for our sample. This shows that, with the uncertainty, the total stellar fraction in our groups is $0.028^{+0.011}_{-0.010}$,

[1]A very similar result is obtained if we use the total stellar mass within the spectroscopic sample, and include a small correction for the stellar mass below the spectroscopic limit.

with a robust upper limit of 0.058. We find some tension with a previous measurement by Gonzalez et al. (2007) of the stellar fraction in a few similar sized groups. They found $\sim$ 6% of the total halo mass was in some form of stars in these sized groups, while massive clusters have stellar fractions of only $\sim 0.02$. Our robust upper limit on the stellar fraction is actually just consistent with their measurement, but this conservative limit would imply that there is almost three times as much stellar mass in the IGM as in the galaxies; not only is this almost certainly unreasonable, it is also much higher than Gonzalez et al. (2007) themselves find. In fact, the fraction of stellar mass we find in the IGM ($\sim$ 47 per cent) is in reasonable agreement with their study; the difference in our result is in the stellar mass fractions themselves, as evident in Yang et al. (2009). Since it is expected that clusters are formed from the buildup of groups (Berrier et al., 2009; McGee et al., 2009) and given that mergers do not destroy stellar mass, Balogh et al. (2008) showed that a group stellar fraction as high as found by Gonzalez et al. (2007) was incompatible with the low stellar fractions in clusters, and argued that the halo masses of the Gonzalez et al. (2007) groups were underestimated. The lower measurement of the group stellar fraction from this work and Yang et al. (2009) supports this conclusion.

We conclude, therefore, that despite the significant contribution from intragroup stars, the stellar mass fraction in groups is not significantly larger than in massive clusters. This suggests that the low gas fraction in groups (e.g. Vikhlinin et al., 2006; Sun et al., 2008) cannot likely be explained via an extraordinarily high star formation efficiency.

This technique will be very interesting to apply to higher redshift data sets, because the redshift evolution of the intragroup stellar mass will be an important clue in unraveling its origin.

# Chapter 6

# Dust accretion and destruction in galaxy groups and clusters

## 6.1 Introduction

Dust grains have long been known to play an important role in the interstellar medium and the star formation which occurs within a galaxy. Further, because dust grains can absorb and redden background sources, an accurate knowledge of the large scale distribution of these grains is crucial. Groups and clusters of galaxies present a unique opportunity to study this large scale distribution as well as the processes important in dust evolution. Dust within massive clusters is thought to sputter on timescales of $10^7$ - $10^9$ years (Draine & Salpeter, 1979), depending on the density and temperatures of the environment. This is caused by the ejection of atoms from the dust grain by the collision with sufficiently energetic gas particles. Given the presence of a distributed, hot plasma in groups and clusters, the short timescale for sputtering means that dust observed in these systems must have been accreted recently. This potentially gives a probe of the relevant dust creation processes.

Recently Ménard et al. (2009b) have shown that dust excesses exist out to Mpc scales around i<21 galaxies. There are a variety of mechanisms by which dust may escape from galaxies and become distributed on such large scales. Star-forming galaxies are often seen to have large outflows of gas and dust which are blown out by the power from supernova

feedback (Heckman et al., 1990; Tremonti et al., 2007). In addition, active galactic nuclei (AGN) can have significant power, and the jets they induce may be able to remove gas and dust from galaxies and redistribute it within the larger environment (e.g. McNamara & Nulsen, 2007). During galaxy-galaxy mergers a significant amount of the gas and dust may be removed due to collisional processes, or subsequently blown out by the induced star-formation or AGN power (Hopkins et al., 2006). Observations of galaxies falling into massive clusters show gas and dust being stripped from the galaxy and incorporated into the surrounding environments (Crowl et al., 2005; Domainko et al., 2006).

The temperatures and densities of the large scale environments of groups and clusters are difficult to probe observationally. While X-ray observatories have allowed the determination of the temperatures and densities of massive clusters to near the virial radius (e.g. Vikhlinin et al., 2005), analysis of the detailed properties of representative samples of groups has largely relied on stacking large samples (Dai et al., 2007) and/or been limited to measuring total X-ray luminosities (Rykoff et al., 2008a). As a result, the densities and temperatures of the environments outside the virial radius are largely inferred from simulations alone (Pfrommer et al., 2006; Kay et al., 2007). Indeed, the non-detection of significant amounts of baryonic material in the local universe has given rise to the postulate that this material is contained in overdense gas with temperatures of $10^5$-$10^7$, dubbed the warm-hot intergalactic medium (WHIM) (see Bregman, 2007). The expected temperature and density of the WHIM are likely able to destroy dust through thermal sputtering. Therefore, measuring the large scale dust distribution is a potentially powerful probe of the large scale temperatures and densities.

Previous attempts to measure the dust centered on clusters has focused on the inner regions, largely within the virial radius. Observations of typical groups ($< 10^{13.5}\ h^{-1}\ \mathrm{M}_\odot$) have not yet been done. The first attempts to quantify the dust content of clusters involved the counting of relative deficiency of background sources. These attempts generally agreed that the $V-$band attenuation is on the order of 0.2-0.4 (Zwicky, 1951; Bogart & Wagoner, 1973; Boyle et al., 1988; Romani & Maoz, 1992). However, early infrared observations of clusters attempting to detect direct emission from this dust largely led to non or marginal detections, implying dust masses much lower than that implied by background counts (Annis & Jewitt, 1993; Wise et al., 1993; Stickel et al., 2002; Montier & Giard, 2005). Similarly, recent observations with Spitzer have also failed to show dust masses implied by 0.2-0.4 magnitudes of attenuation (Bai et al., 2007).

Recently, large, uniform surveys have made detecting statistical colour excesses of background sources of large samples of clusters feasible. Chelouche et al. (2007) have correlated background quasars with intervening galaxy clusters and found that, for massive clusters, the excess reddening, E(B-V), is on the order of 0.004 magnitudes in the central Mpc. Bovy et al. (2008), using the spectra of early type galaxies, found an upper limit on the extinction within 2 Mpc of massive clusters to be $A_V < 0.003$ magnitudes. Similar results were obtained by Muller et al. (2008), who found, using photometric redshifts to identify background galaxies, a similar result of $A_V = 0.004 \pm 0.010$ mag of attenuation. However, these type of measurements are differential measurements and, as such, are dependent on the control sample of sources with which the colour excess is measured. Since it is known that clusters of this halo mass have significant excess mass out to at least 20 $h^{-1}$ Mpc (Sheldon et al., 2007b), and indeed Chelouche et al. (2007) has shown that the colour excess varies at least out to 5 Mpc from the cluster center, then the presence of dust on these larger scales may bias the measurement of the central regions.

In this chapter, by measuring the reddening effect on background quasars, we examine the large scale ($\sim 50\ h^{-1}$ Mpc ) radial profile of dust centered on groups and clusters. This is the first measurement of such large scales and the first to probe such low mass groups. The large scale is important to separate the cluster/group dust from the dust expected to be associated with individual galaxies. We discuss the data in §6.2 and present the method and the measurement in §6.3. We discuss the implications of the measurement in §6.4 and summarize our findings in §6.5. Throughout this chapter, we adopt, as was done during the assembly of the group catalogue, a ΛCDM cosmology with the parameters of the third year WMAP data, namely $\Omega_{\rm m} = 0.238$, $\Omega_\Lambda = 0.762$, $\Omega_{\rm b} = 0.042$, $n = 0.951$, $h = H_0/(100\,{\rm km\,s^{-1}\,Mpc^{-1}}) = 0.73$ and $\sigma_8 = 0.75$ (Spergel et al., 2007).

## 6.2 Data

The technique we use to examine the dust content of galaxy groups and clusters is conceptually simple. Our approach relies on measuring the change in the mean colour of background sources as a function of their projected distance from groups and clusters. It is expected that the change in the mean colour will be small, and thus we must stack the signal from many clusters together to measure the effect on the distribution of background

sources. Therefore, we require a large sample of groups and clusters, which are uniformly selected and have well defined masses. We also require that we have a large number of background sources with an intrinsic colour distribution with little scatter and which do not vary with sky position. The background sources must also be at high redshift, so that they are not physically associated with the clusters we are examining. For these purposes, the best publicly available data is derived from the the Fourth Data Release (DR4) of the Sloan Digital Sky Survey, a five colour (*ugriz*) photometric and spectroscopic survey covering over 4780 deg$^2$ and containing $\sim$ 670,000 spectra of galaxies, quasars and stars (Adelman-McCarthy et al., 2006). Below we discuss the group sample and the sample of background objects drawn from this survey which are used in this chapter.

### 6.2.1 Galaxy group catalogue

The majority of galaxies in the local universe reside in some kind of association with at least one other galaxy (Eke et al., 2004). However, quantifying the mass of a large sample of those associations is difficult. In particular, X-ray temperature or luminosity, often used as a mass indicator in galaxy clusters (Reiprich & Böhringer, 2002), is too low or faint in galaxy groups to determine mass for a survey the size of the SDSS. Also, the velocity dispersions of galaxies, which are often used as tracers of the potential well of clusters or massive groups, is ineffective when the groups contain only a handful of spectroscopically confirmed galaxies. Recently, Yang et al. (2005) showed that an effective mass estimate of galaxy groups can be obtained by essentially ranking groups by their total luminosity and associating these rankings with the expectations of a ΛCDM halo occupation model.

Yang et al. (2007) have applied their algorithm to the SDSS DR4 to produce a sample of $\sim$ 300,000 galaxy groups with masses as low as $10^{11.5}$ $h^{-1}$ $M_\odot$. In this chapter we use "Sample I" from Yang et al. (2007), which exclusively uses galaxies with SDSS spectroscopic redshifts. We chose this sample, as opposed to the other samples, which add in existing redshifts from the literature, because we are principally concerned with obtaining a uniformly selected population of galaxy groups. In the most recent galaxy group catalogue of Yang et al., the authors rank the galaxy groups both by total luminosity in the $r-$band as well as the total stellar mass of the group. In this chapter, we will use the group masses obtained by the ranking the total stellar mass, with the goal of minimizing the effect of a particular group's recent star formation history. However, we note that because we must

stack many groups in relatively wide mass bins, this choice has no effect on the results. Finally, we restrict our analysis to galaxy groups with masses greater than $10^{12.5}$ $h^{-1}$ $M_{\odot}$, which leaves a final sample of 75947 groups between z=0 and z=0.2. Figure 6.1 shows the halo mass distribution of our group sample broken into three mass bins which we use later in the chapter.

### 6.2.2 Background objects: spectroscopically identified quasars

Our principal concerns when choosing a sample of background objects to examine are that the sources are at sufficiently high redshift that they are not physically associated with the group, that they represent a relatively uniform population, with a small dispersion about their average properties, and that their colours are well calibrated. For all these reasons we have chosen to examine the photometric properties of spectroscopically identified quasars drawn from the fourth edition of the SDSS quasar catalog (Schneider et al., 2007). This catalog contains $\sim$ 77,000 quasars brighter than $M_i = -22$ drawn from the fifth SDSS data release, and are targeted based on their photometric properties and/or the presence of an unresolved radio source (Richards & others., 2002). We reduce this sample to contain only quasars within DR4, ie. those for which we have an identified group sample. The SDSS quasar catalog contains *psf* magnitudes for each of the five bands of SDSS photometry (*ugriz*), with typical errors of 0.03 mag. The colours have been corrected for galactic extinction using the dust maps of Schlegel et al. (1998). We only examine quasars with redshifts between z = 1 and z = 3 in order to avoid quasars physically associated with the target groups, or extreme objects at high redshift.

## 6.3 Analysis

Our first goal is to measure the change in the mean colour of the background quasars as a function of their position from foreground clusters. This change in the mean colour is also known as the excess reddening because interstellar dust is observed to extinguish light more readily at the blue end of visible light, causing the light to redden.

We parametrize the excess reddening, $E(i-j)$, of a source, $k$, as

$$E(i-j)^k = m_i^k - m_j^k - \langle m_i - m_j \rangle_{control} \tag{6.1}$$

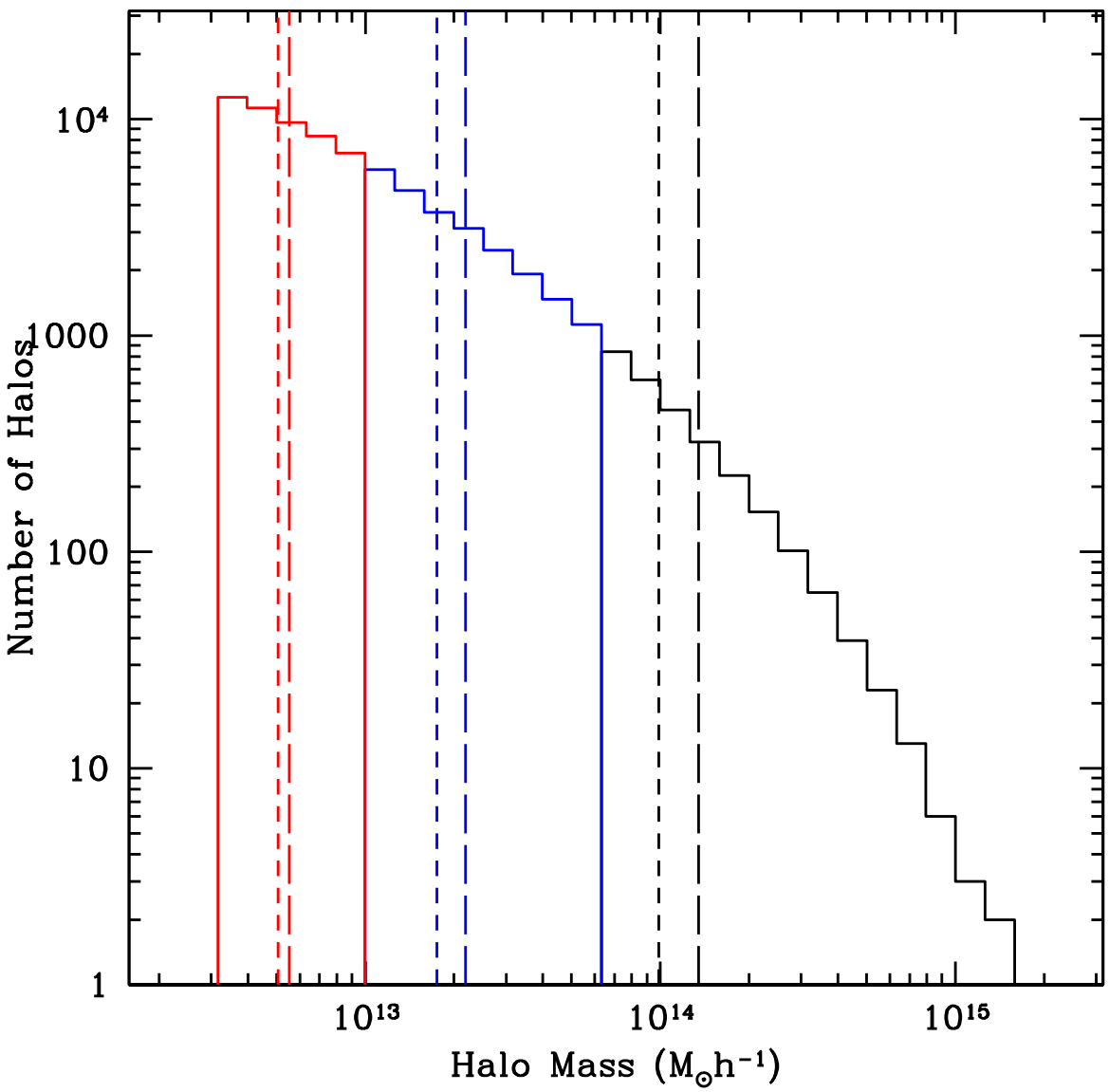


Figure 6.1: The halo mass distribution of the galaxy group and cluster sample. The sample is shown in three groups of halo mass, from $10^{12.5}$ to $10^{13}$ $h^{-1}$ $M_{\odot}$(red), $10^{13}$ to $10^{13.8}$ $h^{-1}$ $M_{\odot}$(blue), and $10^{13.8}$ to $10^{15.3}$ $h^{-1}$ $M_{\odot}$(black). The short dashed (long dashed) line in each bin represents the median (mean) halo mass of the bin.

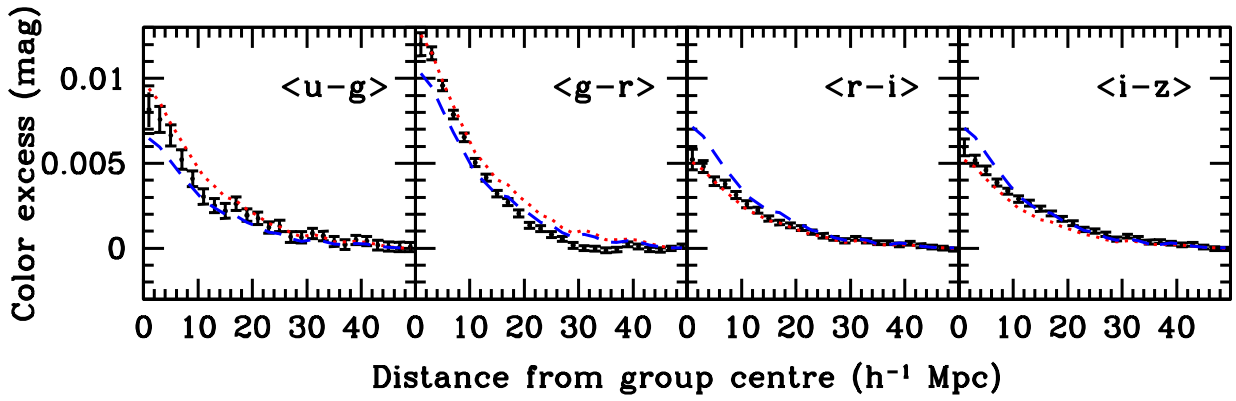


Figure 6.2: The excess colour of four independent colours as a function of distance from the group center. The excess colour is measured with respect to the colour of quasars at a projected distance of 46 to 50 $h^{-1}$ Mpc . The error bars are 1 sigma errors from Monte Carlo estimation. The blue, dashed line (red, dotted line) represents the $R_V$=2.0(5.0) dust reddening law which minimizes the chi-square for $A_V$ as a function of radius.

where $m_i$ and $m_j$ are the magnitudes in the $i$ and $j$ bands of the source for which the excess reddening is measured. The final term in this expression is the mean colour of the control sample of objects. In practise, the excess reddening measured in this way of a single background source is dominated by the intrinsic distribution width of colours of that source. However, with the assumption that the background sources have a well defined mean colour we can stack large numbers of sources to measure a mean excess colour, $\langle E(i-j)\rangle$. Therefore, by stacking many backgrounds sources in bins of projected distance, $r$, from the centre of our group and cluster samples, we can obtain an excess colour profile of the groups and clusters, $\langle E(i-j)\rangle(r)$.

A key feature of this type of measurement is the control sample of sources. Unless the unobscured mean colour of the background sources is known, it must be made as a differential measurement with respect to a control sample of background sources. In the literature, the control sample is not well defined. Bovy et al. (2008) use a control sample of all background sources greater than 2 $h^{-1}$ Mpc from the center of a cluster, while Chelouche et al. (2007) defines the control sample to be background sources which are greater than $7R_{200}$ from the cluster center. We have, by trial and error, found that the differential dust signal approaches zero only at >40 $h^{-1}$ Mpc from the center of the cluster. So, the control sample of background sources must be taken from large radius. The control

sample of quasars are defined as those which have projected clustercentric distances, $r$, of 46 $h^{-1}$ Mpc $< r <$ 50 $h^{-1}$ Mpc from a given cluster in the sample.

Notice that, similar to the weak lensing or cluster correlation measures, our dust measurement is a correlation measurement. A given quasar can have a small projected distance from cluster A, but still be counted as a control quasar if it is in the control range of cluster B. In other words, each quasar is in many clustercentric radial bins. Because of the much larger area covered by the control sample of quasars, the number of quasars in the control sample greatly outnumber the number of quasars in any of the other samples. This enables us to do a Monte Carlo estimation of the error in the excess colour by selecting 200 independent samples of control quasars which have the same number as a given target bin. The error bars are then the 1 sigma limits of the excess color from the 200 trials for each bin.

### 6.3.1 Large scale distribution

We begin by examining the total colour excess from a stacked set of all the groups in our sample. We measure the mean colour of the background quasars within clustercentric annuli in projected radius bins of 2 $h^{-1}$ Mpc , out to 50 $h^{-1}$ Mpc from the cluster center. The five band photometry of the SDSS quasar sample allows for the measurement of four independent excess reddening signals. Figure 6.2 shows the colour excess for each of the four sets of independent colours.

As Figure 6.2 shows, a significant colour excess is measured in all four independent colours as far out as 30 $h^{-1}$ Mpc from the group and cluster centre. The typical projected virial radius of a group or cluster of this mass (M $\sim 10^{13.5}$ $h^{-1}$ $M_{\odot}$) is less than 1 $h^{-1}$ Mpc . Thus, such a significant large scale distribution of reddening is initially surprising. However, studies of the cluster correlation function (Bahcall & Soneira, 1983), and the weak lensing profile of similar clusters (Sheldon et al., 2007b; Johnston et al., 2007) shows that there is a significant excess of matter out to similar distances from clusters. We expect that the dust excess to such large scales is just a result of this excess matter, although we will address this further in §6.4.2.

While the size of the measured excess reddening shown in Figure 6.2 is quite small ($< 0.015$ mag), if it is due to the presence of dust then it corresponds to a large and

extended dust distribution. However, there are some systematic effects which must be accounted for before we can be sure the reddening is due to dust. In particular, galaxy groups and clusters have significant mass, and therefore sources behind this mass will be gravitationally magnified. A sample of sources which is chosen by a fixed flux limit will lead to more high redshift sources, and a lower absolute luminosity limit at fixed redshift behind the cluster, than for a patch of sky far from the cluster. Thus this measurement is potentially affected when the intrinsic mean colour of the background sources is luminosity or redshift dependent.

We can estimate the size of the magnification effect of our groups and clusters. We would expect this effect to trace the mass distribution, so it would be most pronounced close to the cluster. Johnston et al. (2007) measured the mass profile of a large sample of galaxy clusters and found that at a distance of 1 $h^{-1}$ Mpc from the most massive clusters the surface mass density is $\sim 10^2\ h\ \mathrm{M}_\odot/\mathrm{pc}^2$. This corresponds to a magnification of $\sim$ 0.02 magnitudes — a minute change in the effective limiting magnitude of our quasar sample. Given this, we see that for our <g-r> measurement of $\sim 0.011$ at 1 $h^{-1}$ Mpc to be completely explained by magnification of a quasar sample with varying mean colour, the intrinsic *cumulative* $g-r$ colour of our quasar sample would have to vary by 0.55 per magnitude near the magnitude limit. However, we find that the cumulative $g-r$ colour of the control sample of quasars only varies by 0.005 magnitudes from i=19 to i=20.2, the magnitude limit of our sample. In other words, as it is for all four independent colours, the size of the magnification-induced reddening effect is two orders of magnitude smaller than required to explain our results.

We note that the possibility of having foreground emission from the group or cluster contribute to the the reddening signal is not physical, given that the local background subtraction used in the quasar photometry will remove this component.

### 6.3.2 Wavelength dependence of reddening

Here we consider the wavelength dependence of the reddening, to gain some indication of the nature of the dust. The wavelength dependence, $R_V$ is commonly parametrized by linking the absolute extinction in the $V$ band, $A_V$ to the excess $B-V$ colour as

$$R_V = \frac{A_V}{E(B-V)}. \tag{6.2}$$

A value of $R_V = 3.1$ is generally used based on studies of interstellar Milky Way dust, but values in the range from 2.5 to 5 have been measured for the Magellanic clouds (Prevot et al., 1984) and starbursting galaxies (Calzetti et al., 2000). In contrast, the emission from a typical collection of cluster galaxies would have a negative $R_V$. Unfortunately, we can not directly determine $R_V$ because we do not have $B$ and $V$ magnitudes. However, using the fitting functions of O'Donnell (1994), we can transform our excess colours to determine $A_V$ and to determine whether the shape of the expected reddening curve is consistent with the known properties of interstellar dust.

In Figure 6.2, we also show the predictions of two dust reddening laws, one with $R_V$ =2.0 and one with $R_V$=5.0. To do this we must find the $A_V$ value at each radial bin from the combination of the four independent colours. We do this by minimizing the chi square value at each step given the errors on each colour. For the majority of the colours and radii, these two dust laws essentially bracket the data. This seems to suggest that the colour profile is very similar to that expected from known dust laws. However, we would like to make a more precise measurement, which we do by stacking the data in radial bins.

In Figure 6.3, we show the reddening of background quasars in two radial bins for each photometric band with respect to the r band. The solid black line in each panel is the extinction curve expected from an interstellar dust law with $R_V$=3.1. The dust attenuation, $A_V$, is 0.0223 in the panel showing the inner 10 $h^{-1}$ Mpc , while it is 0.0097 for the $10 > r > 20$ $h^{-1}$ Mpc bin. While the $R_V$=3.1 law shows reasonable agreement with the wavelength dependence of the reddening, we also allow $R_V$ to be fit simultaneously with $A_V$. These results are shown with the dotted line and correspond to best fitting $R_V$ values of 3.3 and 3.5 in the two radial bins respectively. Thus, the reddening is very similar to the expectations of a Milky Way dust law.

### 6.3.3 Halo mass dependence

We now explore how this dust distribution depends on the mass of the host halo. In Figure 6.4 we show the qso <g-i> colour excess as a function of distance from the group center in three bins of total group mass. The <g-i> colour is chosen as our principle measure of the dust reddening in the remainder of the chapter. These two photometric bands are the best calibrated, and have been recently used in the literature. Conveniently, the <g-i> is

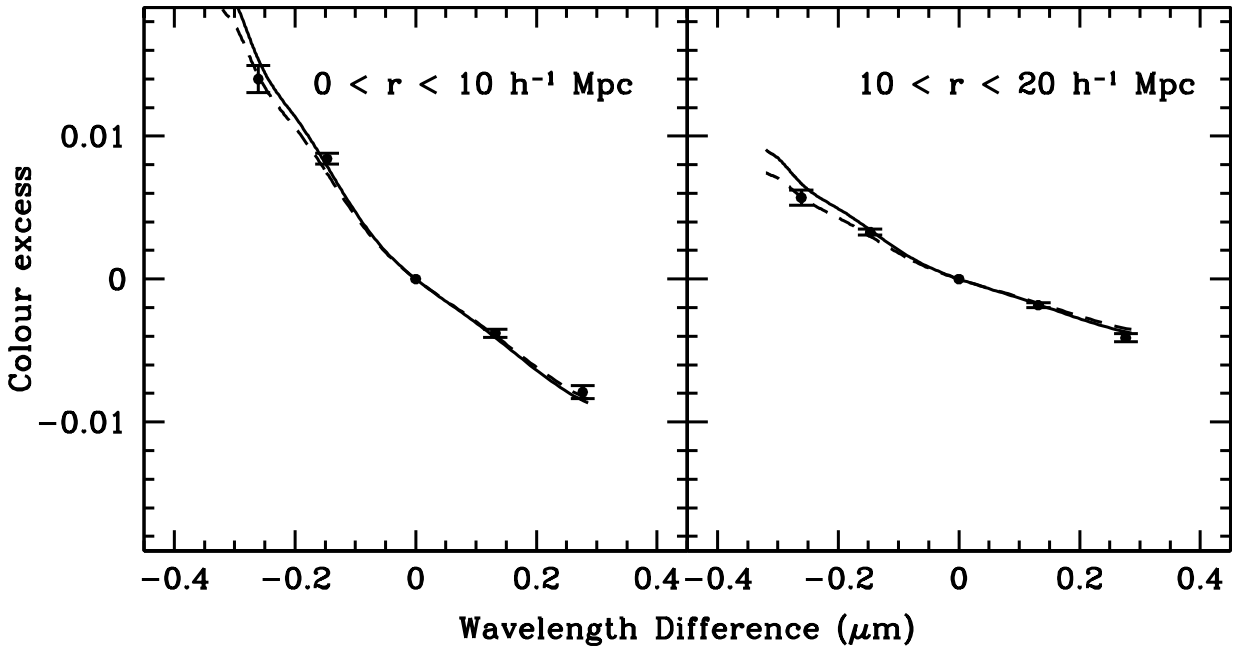


Figure 6.3: The colour excess in two bins of radial distance from the group centres. The solid black line is the expectations from a $R_V$=3.1 dust law, using the expansion of (O'Donnell, 1994), with a attenuation of $A_V = 0.0223$ and 0.0097 for the $0 > r > 10$ $h^{-1}$ Mpc and $10 > r > 20$ $h^{-1}$ Mpc bins respectively. The dotted line is the result of simultaneously fitting for $R_V$ and $A_V$, which results in ($R_V$,$A_V$) = (3.3, 0.0220) and (3.5, 0.0094) in the two radial bins, respectively. The data points are for the colours u-r, g-r, r-r, i-r, z-r respectively.

most closely related to the more commonly used $B-V$ dust colour as (Prevot et al., 1984; Ménard et al., 2008)

$$E(g-i) = \frac{\lambda_g^{-1.2} - \lambda_i^{-1.2}}{\lambda_B^{-1.2} - \lambda_V^{-1.2}} E(B-V) \quad (6.3)$$

$$= 1.55E(B-V). \quad (6.4)$$

Using this transformation, and assuming $R_V$=3.1, we show the corresponding dust attenuation in the $V$ band, $A_V$, on the right ordinate axis. Quite strikingly we see that the centers of the clusters have dust attenuations of $A_V \sim$ 0.03-0.04, when measured with respect to quasars $\sim 45\ h^{-1}$ Mpc away. In comparison, the disk of a spiral galaxy at a similar redshift has a dust attenuation of $A_V \sim 0.25$ mag (Holwerda et al., 2009). This suggests that the dust signal cannot be localized to disks within the line of sight alone, because the covering fraction of such group and cluster members is much less than $(0.03/0.25) = 0.12$. In other words, there must be a significant component of dust which is not localized within the disks of $\sim 0.1$L* galaxies alone. A similar conclusion was reached recently by Ménard et al. (2009b), who showed that the dust attenuation around galaxies extends well beyond the radius expected if the dust was confined to the disk. We examine this further in §6.3.4.

It is also noticeable that the dust distribution shows a relatively small halo-mass dependence, in that the most massive bin shows a larger colour excess than the lowest mass bin at each position out to 20 $h^{-1}$ Mpc . However, except at the inner most bins, the measured colour excess in each of the three mass bins is always within $\sim$ 0.001–0.002 magnitudes, a much smaller range than the range of their values as a function of group centric distance. A possible explanation for such a small dependence on the halo mass could be that the halo masses themselves are uncertain, so that perhaps the wide halo mass bins actually contain roughly the same size groups. However, it is worth noting that the fraction of red galaxies within these same groups show a significant halo mass dependence. 50% of the $L_*$ galaxies in $10^{14}\ h^{-1}$ $M_\odot$ are "early type" while only 20% of the same galaxies are "early type" in $10^{12.5}\ h^{-1}$ $M_\odot$haloes (Weinmann et al., 2006a). This argues that the masses are well defined for a statistical study such as this.

In the bottom panel of Figure 6.4, we show the same <g-i> colour excess but now as a function of scaled radius, namely $R_{180}$. For this plot we have used the individual $R_{180}$ of

each cluster, rather than using the median $R_{180}$ of each bin. This is an important point, as simply scaling physical distance in the top panel by the median $R_{180}$ would result in lower mass groups actually have a higher reddening than higher mass groups. However, because there is a range of $R_{180}$ in each bin, the result is to almost completely remove the halo mass dependence, especially at distances far from the cluster. It appears that the dust reddening is similar at a given scaled radius far from the cluster. We will return to the interesting behavior at small scales in §6.4.2.

### 6.3.4 Spatial distribution of the dust

By measuring the quasar colour excess as the difference in the mean value of the quasars, our results are insensitive to the spatial distribution of the dust. If the dust exists in concentrated clumps with a small covering fraction, then the colour excess could be driven by relatively few objects with large reddening values. However, if the dust is uniformly distributed we would expect each quasar to be reddened by the mean value.

In an attempt to address this question, we explore the color excess as a function of the percentiles of the quasar color distributions. In order to determine what fraction of quasars contribute to the signal, we sort the quasars in a particular radial bin and those in the "control" background sample by their measured *g*-*i* colours. We bin each sample by percentile and measure the mean *g*-*i* colour in that percentile bin, and then subtract the measured mean *g*-*i* percentile colour of the cluster quasars from the measure mean *g*-*i* colour of the "control" sample for in the corresponding percentile. This leaves us with the $\langle g - i \rangle$ colour excess in percentile bins.

Admittedly, this measure is difficult to interpret physically, so we first attempt to develop a framework in which to interpret the results by using simulated reddening on background quasars. We take as our control sample of quasars those which are the control sample of the $10^{13.5}$-$10^{13}$ mass bin. We then add an amount of reddening to some fraction of the background quasars ($F_{red}$) such that the mean colour excess is 0.01; for instance, all quasars can be reddened by 0.01 magnitudes, or 1/3 of the quasars can be reddened by 0.03 magnitudes. The results are shown in Figure 6.5, where $F_{red}$ is varied to be 1, 0.15, 0.05 and 0.01. As expected, the color excess as a function of color percentile is flat for $F_{red}$=1 and becomes more dominated by a high percentile peak with lowered $F_{red}$.

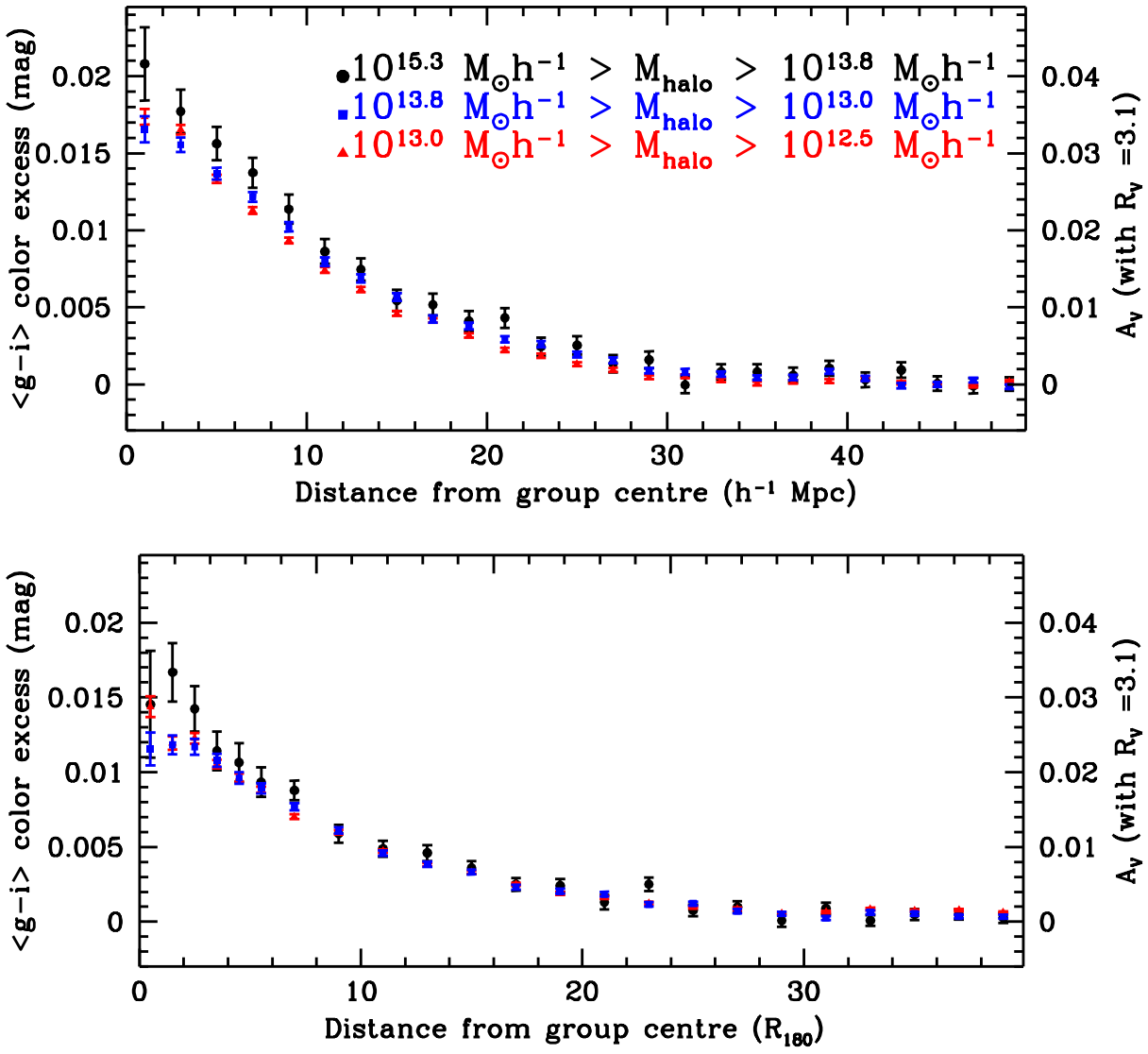


Figure 6.4: The $g-i$ colour excess in three samples of galaxy groups as a function of distance from the group center. The V band attenuation $A_V$ is plotted on the right ordinate axis assuming $R_V$=3.1. This is shown as a function of physical distance (top panel) and in $R_{180}$ (bottom panel).

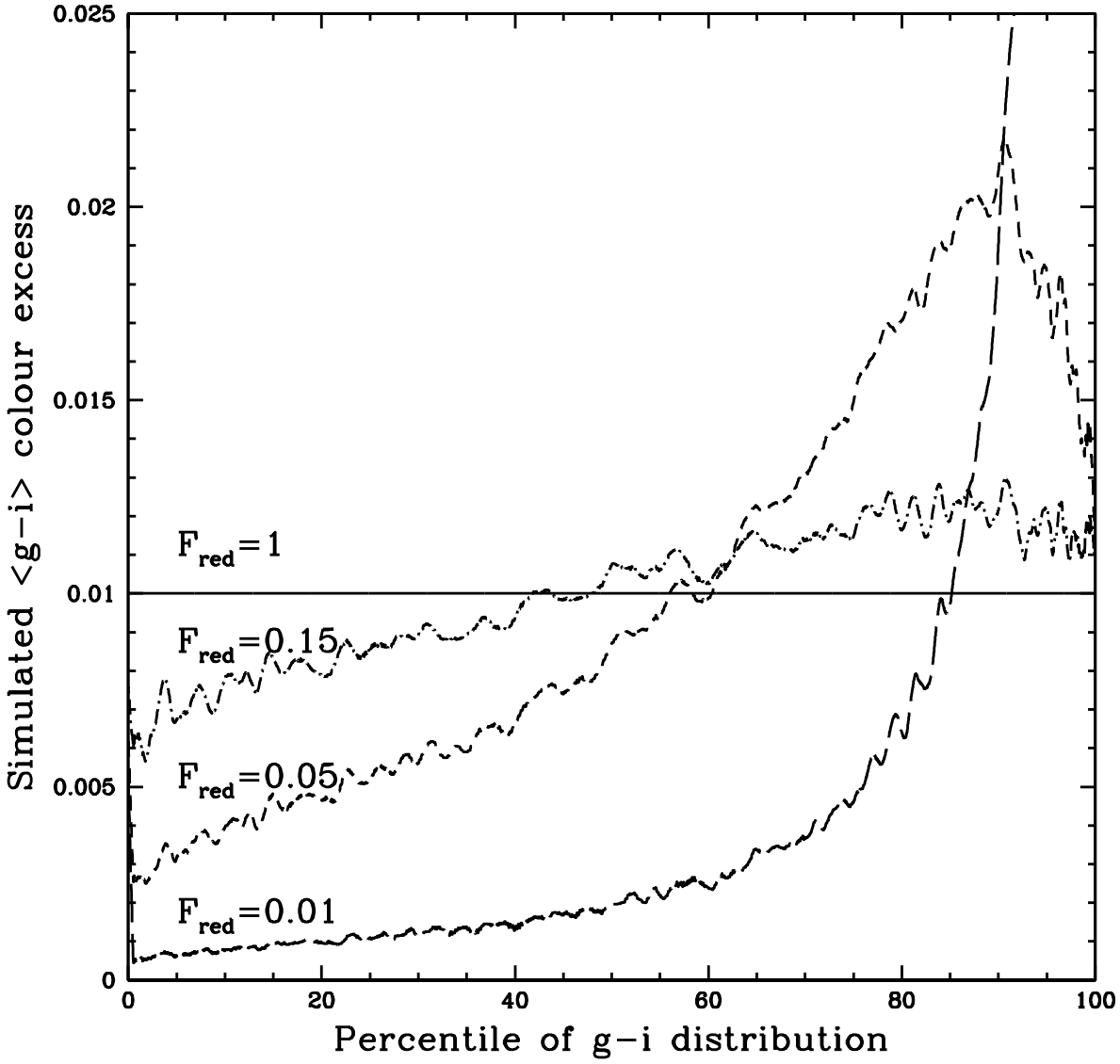


Figure 6.5: The simulated $g - i$ colour excess as a function of percentile for four different reddening models. The model is set to have a mean color excess of 0.01 and $F_{red}$ determines the fraction of objects which are reddened.

We now present Figure 6.6, which shows the color excess as a function of the percentiles of the real quasar color distributions. This is shown for several radial bins and for each halo mass range. We notice that for the majority of the radial bins the quasar color excess is relatively constant, never more than $\sim$ 50 % away from the mean value in that bin. Comparing these with the results of our simulated data suggest that $\sim$ 15 % of the quasars are causing this signal. Further, we see that the color excess curves become progressively steeper with decreasing radius, implying that the bulk of the signal is coming from fewer objects as we get near to the cluster. In the inner-most bin the reddening can be explained with 5–15% of the quasars dominating the signal.

As we will see in section §6.4.1, there are $\sim$ 20 galaxies ($i < 21$) in the central 2 $h^{-1}$ Mpc of our most massive clusters. Thus, assuming that the reddening signal is concentrated uniformly in "bubbles" around these galaxies, a 10% covering fraction requires the "bubbles" to have radii of $\sim$ 140 $h^{-1}$ kpc . These bubbles are significantly larger than the typical size of the stellar mass in a galaxy (Shen et al., 2003; McGee et al., 2008) . So, while this excess dust is not isotropically distributed throughout the groups, it also is not confined to massive galaxies.

The results of Figure 6.6 are also relevant in understanding a possible selection effect on our results. Our colour excess measurement are based on samples from a magnitude limited survey, and thus dust extinction may move quasars out of our sample, thereby leaving a relatively reduced color excess. However, examining Figure 6.6 we see that there does not exist any significant population of highly extincted quasars. Further, this result exists even when the sample is reduced to different magnitude bins. The lack of a highly extincted population suggests that this is not a significant effect for the bulk properties of the sample.

## 6.4 Discussion

We have shown that there is a significant distribution of dust centered on galaxy groups and clusters and, in this section, we would like to measure some of its physical properties. This requires more information about the physical nature of the dust and, while we were able to show that the reddening is consistent with that expected from local interstellar dust, our measurements are somewhat crude. In what follows we will therefore make the

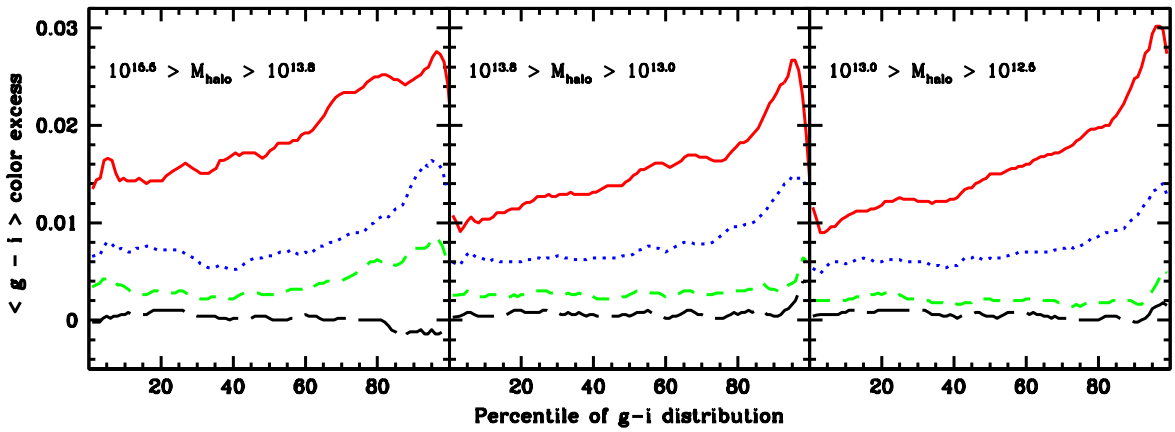


Figure 6.6: The relative color excess at a given percentile of the quasar color distribution. This is shown in several radial bins for each halo mass range. The color excess is measured with respect to the color at a given percentile of the control quasars. The red, solid line is for quasars within the central 2 $h^{-1}$ Mpc , while the blue, dotted line is for quasars within $9 <$ r ($h^{-1}$ Mpc ) $< 11$. The green, dashed (black, long dashed) line is for quasars within $19 <$ r ($h^{-1}$ Mpc ) $< 21$ ($29 <$ r ($h^{-1}$ Mpc ) $< 31$).

assumption that the dust is similar to Milky Way interstellar dust with an $R_V$=3.1.

We are most interested in converting the $A_V$ values we have measured into a dust mass surface density. To do this we need an estimate of $K_{ext}$, the extinction cross section for a given mass of dust:

$$\Sigma M_{dust} = \frac{A_V}{K_{ext}} \tag{6.5}$$

For this, we use the carbonaceous-silicate dust grain model developed by Weingartner & Draine (2001) and Li & Draine (2001) and subsequently tweaked by Draine (2003). These models have been shown to successfully reproduced the observed infrared emission, scattering properties and extinction properties of local interstellar dust. The value of $K_{ext}$ is wavelength dependent, but in the $V$ band it is $K_{ext} = 1.54 \times 10^4 cm^2/g$. With this assumption we can now directly show the surface mass density of dust which is responsible for the reddening signal. We plot this in Figure 6.7 for each of the three halo mass bins.

From this we conclude that the dust mass located within 1 $h^{-1}$ Mpc of the cluster center is on the order of $10^{10}$ $h^{-1}$ $M_\odot$, with little dependence on halo mass. If we assume that the gas fractions of these clusters are equal to the universal baryon fraction this implies that, for a $10^{14}$ $h^{-1}$ $M_\odot$ cluster, the dust-to-gas ratio is $\sim 0.0003$, or 3% of the interstellar medium ratio (Pei, 1992). However, for a $10^{12.5}$ $h^{-1}$ $M_\odot$ group, the ratio is $\sim 0.0055$, approximately 50% of the interstellar medium ratio.

Here it is worth examining the theoretical expectations of thermal sputtering. Draine & Salpeter (1979) have shown that, for dust grains principally composed of graphite, silicate or iron, collisions with gas of $10^6 < T < 10^9$ K can destroy them. Then, for gas of this temperature dust grains can have a typical lifetime $\tau$ of

$$\tau \approx 2 \times 10^4 \mathrm{yr} \left(\frac{\mathrm{cm}^{-3}}{\mathrm{n_H}}\right) \left(\frac{\mathrm{a}}{0.01 \mu \mathrm{m}}\right) \tag{6.6}$$

where $n_H$ is the gas density and $a$ is the radius of the typical dust grain. For the more massive clusters, a typical gas density is a few $10^{-3}$ cm$^{-3}$ while interstellar grains are smaller than 0.5 $\mu m$ (Mathis et al., 1977). Therefore, dust grains in this gas will only survive for $\sim$ 1 Gyr. So any dust which exists in the more massive clusters must have been accreted within the last Gyr. McGee et al. (2009) have shown, using semi-analytic merger trees, that local galaxy clusters accrete $\sim$ 5% of their final galaxies per Gyr from otherwise isolated halos. This suggests that only 5% of the total accreted dust should exist

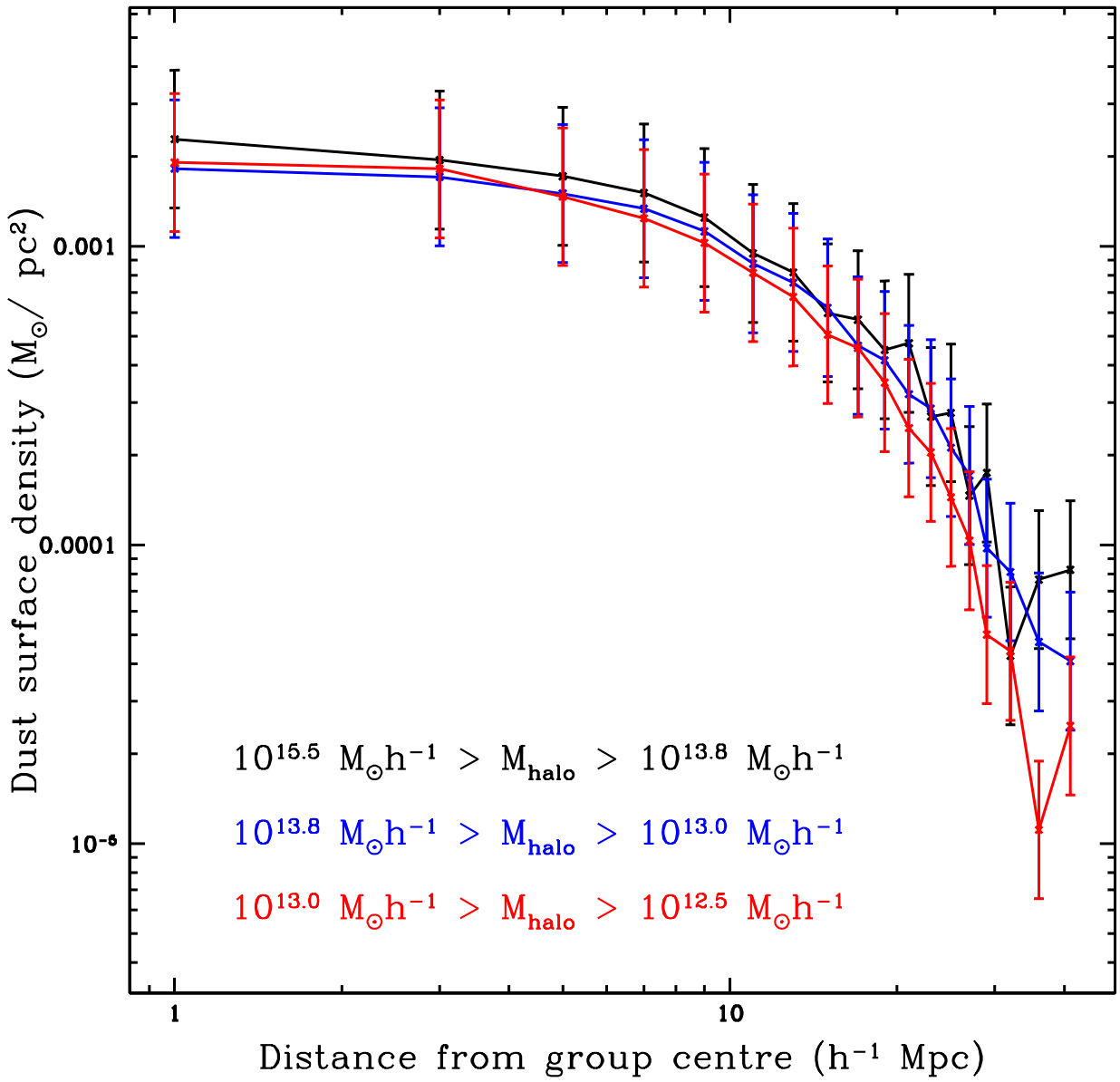


Figure 6.7: The excess dust surface mass density, in units of $h$ $M_\odot/pc^2$, as a function of group-centric distance. This is shown for three different bins of group mass.

in massive clusters today. This is remarkably similar to the implied dust-to-gas ratio of the most massive clusters.

### 6.4.1 Excess galaxy profile

Ménard et al. (2009b) have recently shown that the dust-to-total mass ratio is approximately constant to a distance of 10 Mpc from individual galaxies. Similarly, they have shown that the dust-to-galaxy ratio is constant, except within the inner 20 kpc of the galaxy, where it's expected the signal is due to the galactic disk. We would like to explore similar ratios as a function of group centric radii. Unfortunately, we do not have available weak lensing mass profiles for our groups and clusters. However, we are able to correlate the excess number of galaxies in the SDSS photometry catalogues with the positions of our groups and clusters. Additionally, it is worth pointing out that Sheldon et al. (2007a) has found that, for clusters similar to ours, the weak lensing mass to light ratio is approximately constant from 1 Mpc to $\sim$ 20 Mpc. Therefore, we would expect that the galaxy/dust ratio should show similar trends to the mass/dust ratios.

In Figure 6.8, we present the excess number of galaxies as a function of cluster-centric position for each of the three bins of halo mass. This measurement was made by correlating the position of all SDSS galaxies with a galactic de-reddened $i$ magnitude of $< 21$, where special care was taken with survey edges by using the SDSSpix code.[1] We choose to use the magnitude limit of $i < 21$ because this limit was used by Ménard et al. (2009b). This figure demonstrates that the excess number of galaxies has a steeper slope in the inner 10 $h^{-1}$ Mpc than the similar excess dust mass plot. The figure also shows that there are significantly more galaxies in the higher halo mass bins, which again argues that the halo masses are well defined for large statistical samples.

### 6.4.2 Dust mass associated with each galaxy

Now that we have compiled the excess dust mass distribution around the clusters and the excess galaxy number around the clusters, we can examine their ratio. We show this in Figure 6.9. There are a number of striking aspects of this plot. In particular, we see that

[1] http://dls.physics.ucdavis.edu/~scranton/SDSSPix/

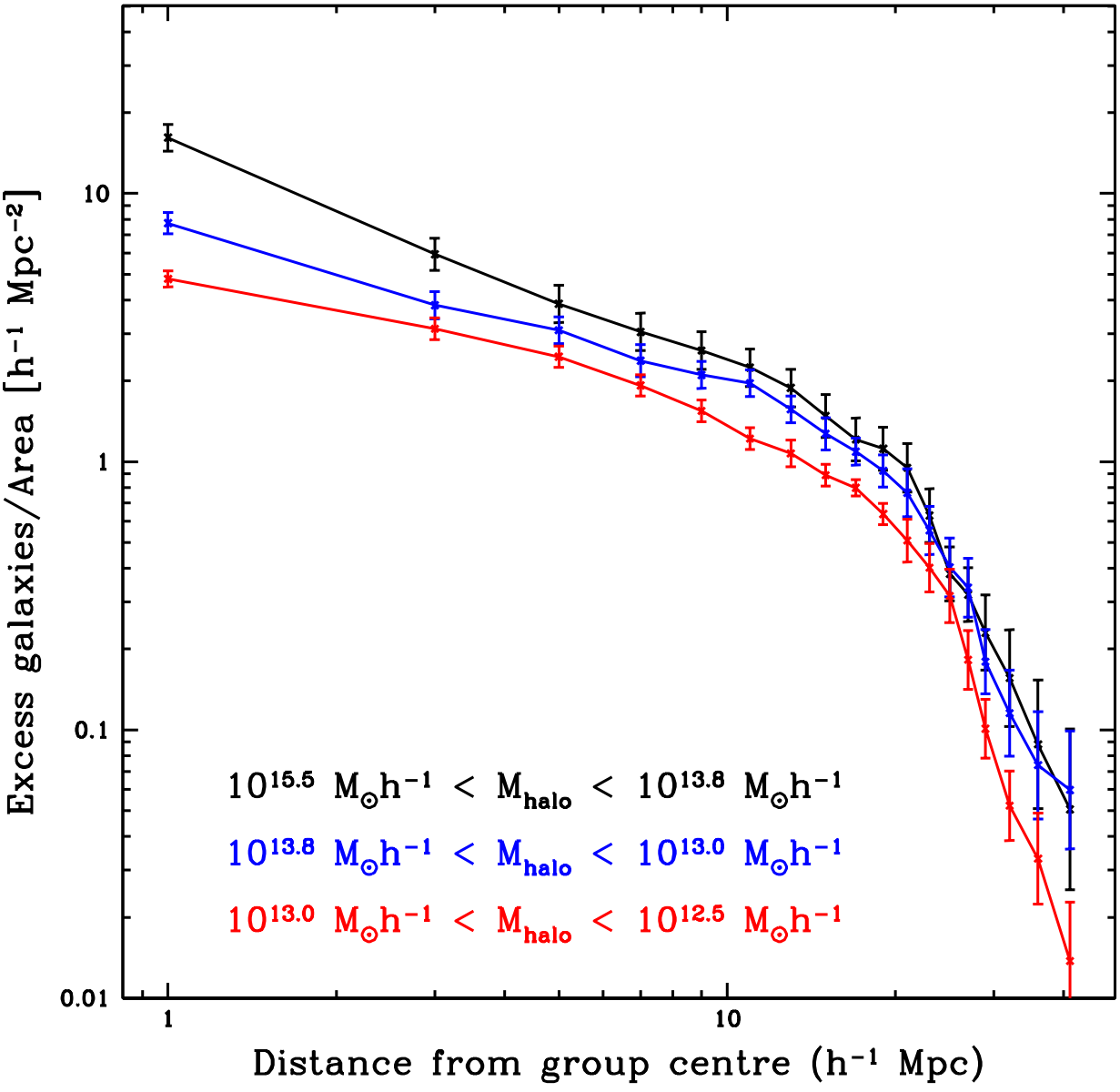


Figure 6.8: The excess number of galaxies ($i < 21$) as a function of cluster-centric position for three bins of halo mass. The excess number was determined by statistical background subtraction. The uncertainties are 1 sigma expectations from the Jackknife method.

for the bulk of the galaxies, those which are $> 7\ h^{-1}$ Mpc away, the excess dust mass per galaxy is on the order of $10^9$ $M_\odot$. This is approximately equal to the stellar mass of the median excess galaxy, and roughly agrees with supernova feedback models, which imply that up to 50% of metals produced are blown out of the galaxy (Finlator & Davé, 2008). The constant dust per galaxy fraction also confirms our earlier suggestion that the dust excess seen out to large radii ($> 30\ h^{-1}$ Mpc ) is simply due to excess halo clustering around galaxy groups and clusters.

However, the most obvious feature of this plot is the significant drop in dust mass per galaxy at small groupcentric radii, especially for the more massive cluster bin. The most massive clusters have dust to galaxy ratios $\sim 15$ % of the value far from the cluster, while small groups have $\sim 80$ % of the value. These numbers are not significantly different from the dust to gas ratios we found earlier.

There are two explanations for this reduction in the dust to galaxy ratio. First, as we have discussed, the dust could be destroyed by thermal sputtering in hot gas. Within a fixed physical radius, this sputtering would be more effective in clusters than in groups, since the average density of the hot gas is substantially higher. Second, it is also possible that galaxies near clusters and groups may be fundamentally different in their dust creation properties. It is expected that most of the dust creation occurs in supernova, and it has been shown through extensive observations that groups and clusters have significantly lower star formation rates than isolated environments (Gómez et al., 2003; Balogh et al., 2004a; Weinmann et al., 2006a; Pasquali et al., 2009) and that difference extends to at least z=1 (Wilman et al., 2005a; Gerke et al., 2007; Balogh et al., 2009).

Unfortunately, the star formation rates in the large scale environments around groups and clusters have not been studied as extensively, especially at higher redshift. Lewis et al. (2002) have attempted to quantify this in the low redshift universe using a sample of massive clusters. They find that the mean star formation rate of galaxies is below the field value as far out as $\sim$ 7-10 virial radii. Further, they see that the average star formation rate at 1 virial radius is 70 % the isolated value. However, even despite this, the key to the amount of dust created is actually the stellar mass, which is essentially the integrated star formation rate. Since galaxy groups are actually quite efficient at producing stellar mass (Parker et al., 2005; Balogh et al., 2007), this suggests that the main driver of lower dust to galaxy ratios near clusters is not due to reduced dust creation. In effect, because the bulk of star formation/dust creation occurs at higher redshift the current cluster and

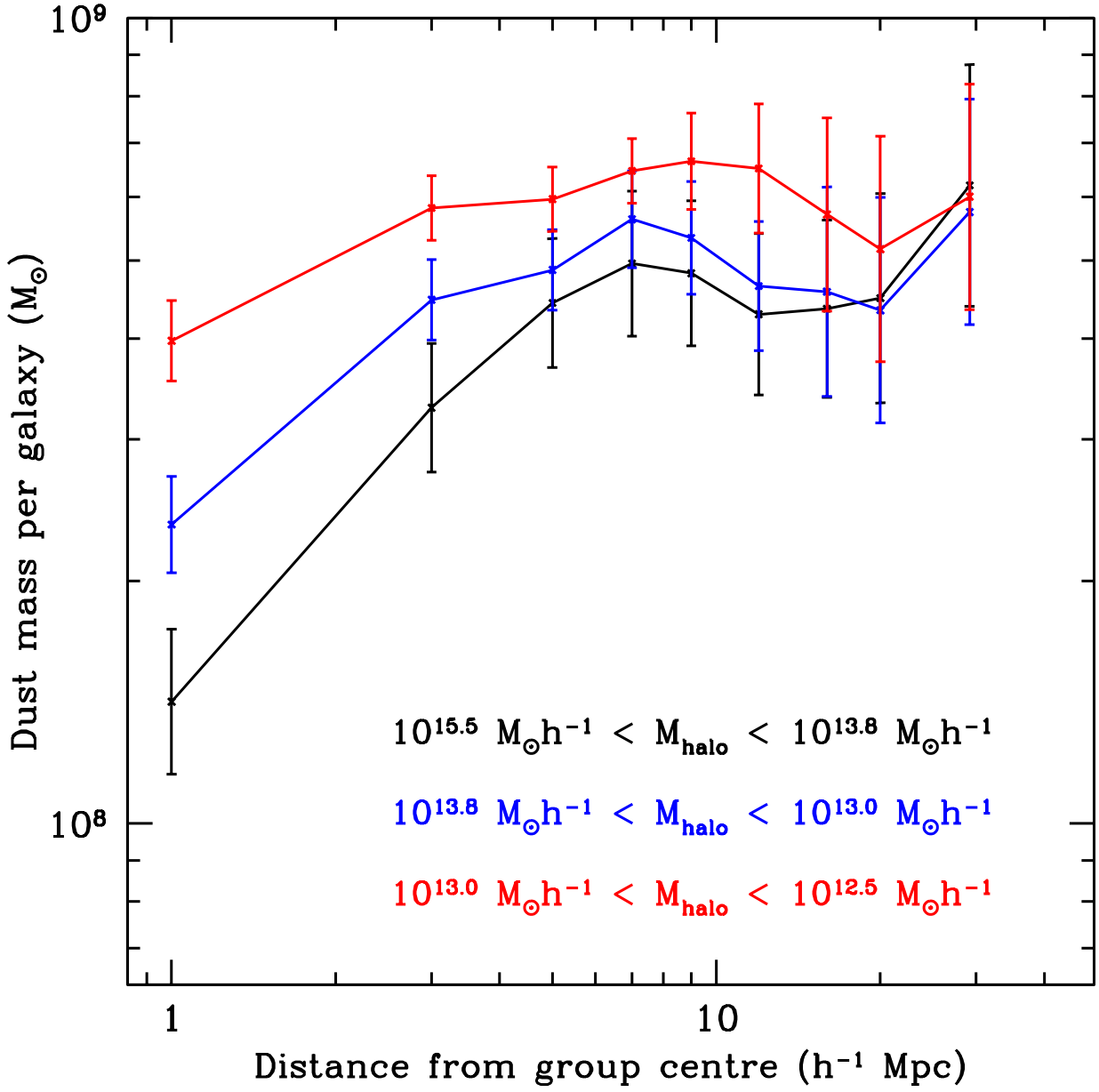


Figure 6.9: The excess surface dust mass per excess galaxy as a function of distance from the group centre.

field star formation rates are not as relevant.

### 6.4.3 Impact on other science

We have shown that there is a significant and large scale variation in the dust reddening associated with galaxy groups and clusters. Although studying the properties of this dust and its implications for dust creation and destruction properties was the main goal of the chapter, in this section we briefly assess the impact this reddening and attenuation of light might have on other studies.

Ménard et al. (2009a) have shown that not correcting for the impact of dust on background "standard candle" supernova can bias the measurement of $\Omega_{\rm m}$ at the few percent level. Here we point out an additional concern in the measuring of cosmological parameters. Our measurements imply that variations in attenuation by dust can be as high as 0.04 magnitudes in the $V$ band (and higher in bluer bands). The next generation of large scale photometric surveys, such as LSST and DES, which principally are driven by the desire to probe the cosmological parameters, have design goals of 0.01 magnitude zeropoint stability from field to field (e.g. Ivezic et al., 2008; Tucker et al., 2007). Our measurements suggest this will not be possible to achieve without accounting for the dust in and around groups and clusters.

The dust attenuation may also be a problem for very low surface brightness features in clusters, such as the intra-cluster and -group medium. Zackrisson et al. (2009) have shown that because the dust extinguishes background light, measuring the sky background, of which the extragalactic background is a small part, some annulus from the cluster would lead to an over-subtraction. Crucially, this can lead to an underestimate of the intracluster light by as much as 1.3 magnitudes at an observed surface brightness of 30 magnitudes/arcsec$^2$ for attenuations of $A_V$=0.05. 30 magnitudes/arcsec$^2$ is close to the faint limit of the measurements of intracluster light by Zibetti et al. (2005). While an attenuation of $A_V$=0.05 is not unreasonable given our results, as we have shown, the dust attenuation is dependent on the cluster-centric radius. Zibetti et al. (2005) et al. measured the sky background in a 100-kpc thick ring with an inner radius of 1 Mpc centered on their clusters. Although this is below the spatial resolution of our measurements, we do note that our most massive cluster varies only from $A_V \sim 0.042$ at 1 $h^{-1}$ Mpc to $\sim 0.034$ at 3 $h^{-1}$ Mpc . In other words, we would expect that the variation in dust attenuations is

not large ($< 0.005$ mag), and therefore does not induce a significant underestimate in the intracluster light.

## 6.5 Conclusions

We have used a sample of spectroscopically identified high redshift quasars to probe the dust content of 70,000 uniformly selected galaxy groups and clusters. We have used the resulting colour excesses, in conjugation with synthetic dust models, to estimate the excess surface mass density around these clusters. Finally we have compared the resulting dust distribution with the excess galaxies around the same groups and clusters. Our findings are as follows.

- We have shown that there exists a large scale distribution of dust centered on groups and clusters with masses as low as M $\sim 10^{12.5}$ $h^{-1}$ $M_{\odot}$, and which extends 30 $h^{-1}$ Mpc from the group centre. The wavelength-dependence of this extinction is consistent with that expected for interstellar dust.

- We find that the dust must be distributed relatively uniformly, with a covering fraction on the order of 10 % to explain the excess color as a function of percentile of the color distribution.

- We find that the halo mass dependence of the dust content is much smaller than would be expected by a simple scaling, implying that the dust-to-gas ratio of the most massive clusters ($\sim 10^{14}$ $h^{-1}$ $M_{\odot}$) is $\sim 3\%$ of the local ISM value, while in small groups ($\sim 10^{12.7}$ $h^{-1}$ $M_{\odot}$) it is $\sim 55\%$ of the local ISM value.

- We find that the implied dust-to-galaxy ratio falls significantly closer to the group and cluster center. This reduction in the dust to galaxy ratio has a significant halo mass dependence, such that the more massive groups and clusters show a stronger reduction. This suggests that either dust is destroyed by thermal sputtering of the dust grains by the hot, dense gas or the intrinsic dust production is reduced in these galaxies.

# Chapter 7

# Conclusions

It has long been known that, in the local Universe, the environment of a galaxy correlates with its properties, such that denser environments host a higher fraction of galaxies which are not forming stars and appear spheroidal. However, despite numerous confirmations of this phenomenon through the years, several key questions have remained unanswered. This thesis attempts to address two of the most important of these questions. First; are the properties of galaxies in dense environments the result of 'Nature' or 'Nurture'? That is, are a higher fraction of galaxies in groups and clusters 'born' spheroidal and passive (Nature), or is there a physical mechanism which transforms galaxies from disk-like and star-forming to spheroidal and passive (Nurture)? Secondly, if the answer is 'Nurture', what is the physical mechanism which causes this transformation?

We attempt to address these questions principally by examining the evolution of morphology and star formation rates of group galaxies within the last five Gyrs. Our data are drawn from two surveys: SDSS at low redshift ($z \sim 0$) and CNOC2/GEEC at intermediate redshift ($z \sim 0.4$). Our set of galaxy groups at z=0.4 are unique, as they are one of the first samples which are based on a redshift survey and contain no colour pre-selection. This means that the groups we obtain are typical, and not selected to have significant populations of red galaxies, x-ray emission or to be visually striking.

To assess morphology, we use the quantitative bulge and disk decomposition software, GIM2D. This allows a direct comparison of the properties of the bulge and disk components of each galaxy. An important measure of the overall morphology is the bulge to total luminosity fraction (B/T). We determine star formation rates by fitting a large suite of

stellar population models to UV and optical photometry of SDSS and GEEC galaxies. This reproduces star formation rates and stellar masses to high accuracy in the regions of interest.

The studies in this thesis have resulted in four general conclusions which we now summarize.

1. **The fraction of passive/bulge dominated galaxies is larger in groups than in the field at both redshifts, but the relative difference grows.** At fixed luminosity, galaxy groups contain on the order of 6% fewer disk dominated galaxies than the field. By z=0, this difference has more than tripled to 19%. Similarly, we have seen that the fraction of passive galaxies is larger in groups than in the field at both redshifts, and the relative difference in the group and field passive fraction grows with redshift. The observation that the relative difference grows with redshift is strong evidence that there is a transforming mechanism which affects galaxies in groups (ie. a Nurture scenario).

2. **Disk dominated/star forming galaxies in groups appear no different than those in the field at the same redshift.** Despite this strong evolution between z=0.4 and z=0, there is no evidence that the disks in the groups are appreciably different from the field disks at either redshift. Both the group and field disks seem to have similar scaling relations. That is, they have similar luminosities at fixed size. Further, they have similar asymmetry distributions, contrary to expectations if star forming regions were being destroyed in group disks. Interestingly, we find that at both redshifts there is a noticeable 'main sequence of star forming galaxies' which have birthrate parameters of about 1. The location of this main sequence is redshift dependent, in the sense that galaxies were forming stars at higher rates at z=0.4, but it shows no difference between the group and the field at fixed redshift.

3. **A significant fraction of the stellar mass in low redshift groups is in the form of diffuse intra-group mass.** We used a novel approach to probe the difficult to observe intragroup stellar mass by correlating supernova type Ia with galaxy groups. This is the first measurement in typical galaxy groups. The intragroup stellar mass is an important clue to the mechanisms responsible for environmental trends, as it is expected to arise from galaxy shredding, stripping or harassment. We found

a surprisingly large fraction ($\sim$ 47 %) of the stellar mass of a galaxy group is in this diffuse form.

4. **The relative rise of passive galaxies is matched by a model in which environmental effects occur 3 Gyr after falling into a group halo.** By tracking the accretion histories of galaxies into groups and clusters we were able to test simple models of environmental effects for their expected redshift evolutions. One such model assumes that a galaxy is 'environmentally affected' some time, $T_{\rm trunc}$, after becoming a member of a halo with a mass above a truncation mass, $M_{\rm trunc}$. Interestingly, approximately independently of $M_{\rm trunc}$, a $T_{\rm trunc}$ of $\sim$ 1 Gyr produces only little evolution in the environmentally affected fraction with redshift. The observations described in our conclusion 1, leads to the determination that the truncation timescale is at least $>$ 2 Gyr. In addition, the remarkably low scatter in the fraction of environmentally affected galaxies means that $M_{\rm trunc}$ is $\leq 10^{13}\ h^{-1}\ {\rm M}_{\odot}$. This model also leads to the interesting prediction that typical galaxy groups and clusters at a redshift of 1.5 will have essentially no environmentally affected galaxies. Indeed, observations of a significant environmental effect at high redshift may mean that gravitational interactions, which scale as the density, are a driving process.

## 7.1 Physical explanation

The four conclusions detailed in the previous section are important clues to the role of galaxy groups in galaxy evolution. Any feasible model for the physical mechanism which causes environmental transformations must satisfy each of these four conclusions. The first is perhaps the strongest evidence, save direct observations of transforming galaxies, that 'Nurture' is the cause of the environmental correlations. That is, that a physical mechanism actively transforms galaxies.

Conclusion 2 and 4 are perhaps the strongest constraints on this mechanism. There are two different scenarios in which both of these constraints could be met. In the first scenario, it could be that a process like 'strangulation' occurs on every galaxy which falls into a group-sized halo. However, this mechanism is so gentle that it leaves the galaxy relatively unaffected for essentially 3 Gyr. This will allow the properties of star forming galaxies in the group and in the field to remain the same, but will allow for the evolution

we see with redshift. However, semi-analytic models which attempt to implement realistic strangulation prescriptions have proven not 'gentle' enough (Font et al., 2008a; Balogh et al., 2009). As soon as these galaxies fall into group halos they begin to have their star formation properties altered, which is inconsistent with conclusion 2. Further, the large fraction of stellar mass which we have measured in the intragroup medium seems hard to reconcile with a gentle transformation mechanism. Diffuse stellar mass is thought to arise from aggressive mechanisms like harassment and stripping.

In the second scenario, environmental effects are not felt immediately upon falling into a group-sized halo, but rather depend on their orbit. Numerical simulations have shown that the bulk of the environmental influence on a galaxy occurs at pericentre, and strongly depends on the depth of the orbit (McCarthy et al., 2008b). In this case, the transforming population can be relatively small owing to a quick truncation in these galaxies. The wide array of orbits leads to the appearance that it takes 3 Gyr for entire population to transform. This scenario would likely also give rise to a significant population of diffuse stellar mass. This second scenario is the most consistent explanation of our current observations. However, there is some future work that needs to be undertaken to confirm this explanation.

## 7.2 Future work

- **Orbit tracking:** Current semi-analytic models of galaxy formation do not track the orbits of galaxies after they fall into more massive halos. The realistic strangulation models are applied to each galaxy based on a drawing an orbit from a distribution of orbital parameters that were measured in dark matter simulations (Benson, 2005; Font et al., 2008a). This leads to a large number of unsatisfactory approximations, such as randomly drawing a new orbit when the host halo doubles in size. A detailed study of galaxy trajectories in groups is clearly needed in order to test the feasibility of our suggested scenario for environmental effects.

- **Numerical simulations of halo stripping:** Despite its ubiquity in galaxy environment literature, simulations of 'strangulation' are quite limited. The only attempt to implement this model into a complete galaxy formation model is based on a prescription of a limited number of simulations, which have not explored the full range

of mass ratios, gas distributions or orbital parameters. Great progress can be made by expanding this range of simulations as well as studying full numerical simulations of galaxy formation.

- **Higher redshift galaxy groups:** The bulk of the constraints we have placed on the physical mechanism responsible for environmental effects have arisen due to observations of evolution in the properties of galaxy groups within the last 4 Gyrs. However, there is still much to be gained from probing back even further in cosmic history. In this effort, we have identified a sample of low mass galaxy groups at z $\sim$ 0.9 (7 Gyrs ago) in the COSMOS field. As GEEC2, we have begun an extensive spectroscopic follow-up campaign to improve the completeness and depth of the group membership. As shown in Chapter 2, the timescale on which environmental affects are displayed is probed very effectively at z=1. This is largely due to the very high galaxy infall rates which are characteristic of this redshift. These high infall rates also allows our best chance yet of catching an elusive 'transition' population of galaxies, which are essentially the 'holy grail' of environmental studies.

- **Gas content and spatial distribution:** In the coming years we will be entering a golden age for studies of the gas content of typical galaxies at all redshifts. ALMA and SKA will map the spatial distribution of gas in galaxies at an epoch when environmental affects are first being displayed. This will tell us directly if galaxies in groups have their cold gas stripped or is simply used up in a 'strangulation' type scenario.

- **Evolution of intragroup stellar mass:** Large scale photometric surveys such as PanStarrs and LSST will allow the direct measurement of stacked samples of groups and clusters at a range of redshifts. This will be a probe of the role that shredding, harassment and tidal stripping play in environmental effects.

# Bibliography


Abadi, M. G., Moore, B., & Bower, R. G. 1999, MNRAS, 308, 947

Abell, G. O. 1958, ApJS, 3, 211

Abraham, R. G., Crawford, C. S., & McHardy, I. M. 1991, MNRAS, 252, 482

Abraham, R. G., Smecker-Hane, T. A., Hutchings, J. B., Carlberg, R. G., Yee, H. K. C., Ellingson, E., Morris, S., Oke, J. B., & Rigler, M. 1996, ApJ, 471, 694

Abraham, R. G., van den Bergh, S., & Nair, P. 2003, ApJ, 588, 218

Adelman-McCarthy, J. K. et al. 2006, ApJS, 162, 38

—. 2008, ApJS, 175, 297

Allen, P. D., Driver, S. P., Graham, A. W., Cameron, E., Liske, J., & de Propris, R. 2006, MNRAS, 371, 2

Annis, J. & Jewitt, D. 1993, MNRAS, 264, 593

Bahcall, N. A. & Soneira, R. M. 1983, ApJ, 270, 20

Bai, L., Rieke, G. H., & Rieke, M. J. 2007, ApJL, 668, L5

Baldry, I. K., Balogh, M. L., Bower, R. G., Glazebrook, K., Nichol, R. C., Bamford, S. P., & Budavari, T. 2006, MNRAS, 373, 469

Baldry, I. K., Glazebrook, K., Brinkmann, J., Ivezić, Ž., Lupton, R. H., Nichol, R. C., & Szalay, A. S. 2004, ApJ, 600, 681

Baldwin, J. A., Phillips, M. M., & Terlevich, R. 1981, PASP, 93, 5

Balogh, M., Eke, V., Miller, C., Lewis, I., Bower, R., Couch, W., Nichol, R., Bland-Hawthorn, J., Baldry, I. K., Baugh, C., Bridges, T., Cannon, R., Cole, S., Colless, M., Collins, C., Cross, N., Dalton, G., de Propris, R., Driver, S. P., Efstathiou, G., Ellis, R. S., Frenk, C. S., Glazebrook, K., Gomez, P., Gray, A., Hawkins, E., Jackson, C., Lahav, O., Lumsden, S., Maddox, S., Madgwick, D., Norberg, P., Peacock, J. A., Percival, W., Peterson, B. A., Sutherland, W., & Taylor, K. 2004a, MNRAS, 348, 1355

Balogh, M. L., Babul, A., Voit, G. M., McCarthy, I. G., Jones, L. R., Lewis, G. F., & Ebeling, H. 2006, MNRAS, 366, 624

Balogh, M. L., Baldry, I. K., Nichol, R., Miller, C., Bower, R., & Glazebrook, K. 2004b, ApJL, 615, L101

Balogh, M. L., Christlein, D., Zabludoff, A. I., & Zaritsky, D. 2001, ApJ, 557, 117

Balogh, M. L., McCarthy, I. G., Bower, R. G., & Eke, V. R. 2008, MNRAS, 385, 1003

Balogh, M. L. & McGee, S. L. 2010, MNRAS, 402, L59

Balogh, M. L., McGee, S. L., Wilman, D., Bower, R. G., Hau, G., Morris, S. L., Mulchaey, J. S., Oemler, Jr., A., Parker, L., & Gwyn, S. 2009, ArXiv e-prints, 0905.3401

Balogh, M. L., Morris, S. L., Yee, H. K. C., Carlberg, R. G., & Ellingson, E. 1999, ApJ, 527, 54

Balogh, M. L., Navarro, J. F., & Morris, S. L. 2000, ApJ, 540, 113

Balogh, M. L., Wilman, D., Henderson, R. D. E., Bower, R. G., Gilbank, D., Whitaker, R., Morris, S. L., Hau, G., Mulchaey, J. S., Oemler, A., & Carlberg, R. G. 2007, MNRAS, 374, 1169

Bamford, S. P., Nichol, R. C., Baldry, I. K., Land, K., Lintott, C. J., Schawinski, K., Slosar, A., Szalay, A. S., Thomas, D., Torki, M., Andreescu, D., Edmondson, E. M., Miller, C. J., Murray, P., Raddick, M. J., & Vandenberg, J. 2009, MNRAS, 393, 1324

Barnes, J. E. & Hernquist, L. 1992, ARA&A, 30, 705

—. 1996, ApJ, 471, 115

Bazin, G. et al. 2009, A&A, 499, 653

Becker, M. R., McKay, T. A., Koester, B., Wechsler, R. H., Rozo, E., Evrard, A., Johnston, D., Sheldon, E., Annis, J., Lau, E., Nichol, R., & Miller, C. 2007, ApJ, 669, 905

Beers, T. C., Flynn, K., & Gebhardt, K. 1990, AJ, 100, 32

Bell, E. F. 2002, ApJ, 577, 150

Bell, E. F., Wolf, C., Meisenheimer, K., Rix, H.-W., Borch, A., Dye, S., Kleinheinrich, M., Wisotzki, L., & McIntosh, D. H. 2004, ApJ, 608, 752

Bell, E. F., Zheng, X. Z., Papovich, C., Borch, A., Wolf, C., & Meisenheimer, K. 2007, ApJ, 663, 834

Benson, A. J. 2005, MNRAS, 358, 551

Benson, A. J., Bower, R. G., Frenk, C. S., Lacey, C. G., Baugh, C. M., & Cole, S. 2003, ApJ, 599, 38

Benson, A. J., Kamionkowski, M., & Hassani, S. H. 2005, MNRAS, 357, 847

Berlind, A. A., Frieman, J., Weinberg, D. H., Blanton, M. R., Warren, M. S., Abazajian, K., Scranton, R., Hogg, D. W., Scoccimarro, R., Bahcall, N. A., Brinkmann, J., Gott, J. R. I., Kleinman, S. J., Krzesinski, J., Lee, B. C., Miller, C. J., Nitta, A., Schneider, D. P., Tucker, D. L., & Zehavi, I. 2006, ApJS, 167, 1

Berrier, J. C., Stewart, K. R., Bullock, J. S., Purcell, C. W., Barton, E. J., & Wechsler, R. H. 2009, ApJ, 690, 1292

Bertin, E. & Arnouts, S. 1996, A&AS, 117, 393

Bertin, E., Mellier, Y., Radovich, M., Missonnier, G., Didelon, P., & Morin, B. 2002, in Astronomical Society of the Pacific Conference Series, Vol. 281, Astronomical Data Analysis Software and Systems XI, ed. D. A. Bohlender, D. Durand, & T. H. Handley, 228–+

Blanton, M. R., Hogg, D. W., Bahcall, N. A., Baldry, I. K., Brinkmann, J., Csabai, I., Eisenstein, D., Fukugita, M., Gunn, J. E., Ivezić, Ž., Lamb, D. Q., Lupton, R. H.,

Loveday, J., Munn, J. A., Nichol, R. C., Okamura, S., Schlegel, D. J., Shimasaku, K., Strauss, M. A., Vogeley, M. S., & Weinberg, D. H. 2003a, ApJ, 594, 186

Blanton, M. R., Hogg, D. W., Bahcall, N. A., Brinkmann, J., Britton, M., Connolly, A. J., Csabai, I., Fukugita, M., Loveday, J., Meiksin, A., Munn, J. A., Nichol, R. C., Okamura, S., Quinn, T., Schneider, D. P., Shimasaku, K., Strauss, M. A., Tegmark, M., Vogeley, M. S., & Weinberg, D. H. 2003b, ApJ, 592, 819

Blanton, M. R. & Moustakas, J. 2009, ARA&A, 47, 159

Bogart, R. S. & Wagoner, R. V. 1973, ApJ, 181, 609

Bond, J. R., Cole, S., Efstathiou, G., & Kaiser, N. 1991, ApJ, 379, 440

Bouwens, R. J., Illingworth, G. D., Franx, M., Chary, R., Meurer, G. R., Conselice, C. J., Ford, H., Giavalisco, M., & van Dokkum, P. 2009, ApJ, 705, 936

Bovy, J., Hogg, D. W., & Moustakas, J. 2008, ApJ, 688, 198

Bower, R. G. 1991, MNRAS, 248, 332

Bower, R. G. & Balogh, M. L. 2004, in Clusters of Galaxies: Probes of Cosmological Structure and Galaxy Evolution, ed. J. S. Mulchaey, A. Dressler, & A. Oemler, 325–+

Bower, R. G., Benson, A. J., Malbon, R., Helly, J. C., Frenk, C. S., Baugh, C. M., Cole, S., & Lacey, C. G. 2006, MNRAS, 370, 645

Bower, R. G., McCarthy, I. G., & Benson, A. J. 2008, MNRAS, 390, 1399

Boyle, B. J., Fong, R., & Shanks, T. 1988, MNRAS, 231, 897

Bregman, J. N. 2007, ARA&A, 45, 221

Brinchmann, J. et al. 2004, MNRAS, 351, 1151

Broadhurst, T., Takada, M., Umetsu, K., Kong, X., Arimoto, N., Chiba, M., & Futamase, T. 2005, ApJL, 619, L143

Bruzual, G. & Charlot, S. 2003, MNRAS, 344, 1000

Budavári, T., Heinis, S., Szalay, A. S., Nieto-Santisteban, M., Gupchup, J., Shiao, B., Smith, M., Chang, R., Kauffmann, G., Morrissey, P., Schiminovich, D., Milliard, B., Wyder, T. K., Martin, D. C., Barlow, T. A., Seibert, M., Forster, K., Bianchi, L., Donas, J., Friedman, P. G., Heckman, T. M., Lee, Y., Madore, B. F., Neff, S. G., Rich, R. M., & Welsh, B. Y. 2009, ApJ, 694, 1281

Bullock, J. S., Kolatt, T. S., Sigad, Y., Somerville, R. S., Kravtsov, A. V., Klypin, A. A., Primack, J. R., & Dekel, A. 2001a, MNRAS, 321, 559

Bullock, J. S., Kravtsov, A. V., & Weinberg, D. H. 2001b, ApJ, 548, 33

Bundy, K., Fukugita, M., Ellis, R. S., Targett, T. A., Belli, S., & Kodama, T. 2009, ApJ, 697, 1369

Butcher, H. & Oemler, Jr., A. 1978a, ApJ, 219, 18

—. 1978b, ApJ, 226, 559

Cabanac, R. A., Alard, C., Dantel-Fort, M., Fort, B., Gavazzi, R., Gomez, P., Kneib, J. P., Le Fèvre, O., Mellier, Y., Pello, R., Soucail, G., Sygnet, J. F., & Valls-Gabaud, D. 2007, A&A, 461, 813

Calzetti, D., Armus, L., Bohlin, R. C., Kinney, A. L., Koornneef, J., & Storchi-Bergmann, T. 2000, ApJ, 533, 682

Carlberg, R. G., Yee, H. K. C., Ellingson, E., Abraham, R., Gravel, P., Morris, S., & Pritchet, C. J. 1996, ApJ, 462, 32

Carlberg, R. G., Yee, H. K. C., Morris, S. L., Lin, H., Hall, P. B., Patton, D. R., Sawicki, M., & Shepherd, C. W. 2001, ApJ, 552, 427

Cavaliere, A. & Fusco-Femiano, R. 1976, A&A, 49, 137

Charlot, S. & Fall, S. M. 2000, ApJ, 539, 718

Chary, R. & Elbaz, D. 2001, ApJ, 556, 562

Chelouche, D., Koester, B. P., & Bowen, D. V. 2007, ApJL, 671, L97

Chiba, M. & Beers, T. C. 2000, AJ, 119, 2843

Cole, S., Lacey, C. G., Baugh, C. M., & Frenk, C. S. 2000, MNRAS, 319, 168

Cooper, M. C., Newman, J. A., Coil, A. L., Croton, D. J., Gerke, B. F., Yan, R., Davis, M., Faber, S. M., Guhathakurta, P., Koo, D. C., Weiner, B. J., & Willmer, C. N. A. 2007, MNRAS, 376, 1445

Cooper, M. C., Newman, J. A., & Yan, R. 2009, ArXiv e-prints

Couch, W. J. & Sharples, R. M. 1987, MNRAS, 229, 423

Crain, R. A., Theuns, T., Dalla Vecchia, C., Eke, V. R., Frenk, C. S., Jenkins, A., Kay, S. T., Peacock, J. A., Pearce, F. R., Schaye, J., Springel, V., Thomas, P. A., White, S. D. M., & Wiersma, R. P. C. 2009, ArXiv e-prints,0906.4350

Croton, D. J., Springel, V., White, S. D. M., De Lucia, G., Frenk, C. S., Gao, L., Jenkins, A., Kauffmann, G., Navarro, J. F., & Yoshida, N. 2006, MNRAS, 365, 11

Crowl, H. H., Kenney, J. D. P., van Gorkom, J. H., & Vollmer, B. 2005, AJ, 130, 65

Da Rocha, C. & Mendes de Oliveira, C. 2005, MNRAS, 364, 1069

Da Rocha, C., Ziegler, B. L., & Mendes de Oliveira, C. 2008, MNRAS, 388, 1433

Dai, X., Kochanek, C. S., & Morgan, N. D. 2007, ApJ, 658, 917

Dale, D. A. & Helou, G. 2002, ApJ, 576, 159

Dariush, A. A., Raychaudhury, S., Ponman, T. J., Khosroshahi, H. G., Benson, A. J., Bower, R. G., & Pearce, F. 2010, MNRAS, 559

Davis, M., Efstathiou, G., Frenk, C. S., & White, S. D. M. 1985, ApJ, 292, 371

Dilday, B. et al. 2008, ApJ, 682, 262

Domainko, W., Mair, M., Kapferer, W., van Kampen, E., Kronberger, T., Schindler, S., Kimeswenger, S., Ruffert, M., & Mangete, O. E. 2006, A&A, 452, 795

Draine, B. T. 2003, ARA&A, 41, 241

Draine, B. T. & Salpeter, E. E. 1979, ApJ, 231, 77

Dressler, A. 1980, ApJ, 236, 351

Dressler, A., Oemler, A. J., Couch, W. J., Smail, I., Ellis, R. S., Barger, A., Butcher, H., Poggianti, B. M., & Sharples, R. M. 1997, ApJ, 490, 577

Driver, S. P., Liske, J., Cross, N. J. G., De Propris, R., & Allen, P. D. 2005, MNRAS, 360, 81

Eke, V. R., Baugh, C. M., Cole, S., Frenk, C. S., Norberg, P., Peacock, J. A., Baldry, I. K., Bland-Hawthorn, J., Bridges, T., Cannon, R., Colless, M., Collins, C., Couch, W., Dalton, G., de Propris, R., Driver, S. P., Efstathiou, G., Ellis, R. S., Glazebrook, K., Jackson, C., Lahav, O., Lewis, I., Lumsden, S., Maddox, S., Madgwick, D., Peterson, B. A., Sutherland, W., & Taylor, K. 2004, MNRAS, 348, 866

Ellingson, E., Lin, H., Yee, H. K. C., & Carlberg, R. G. 2001, ApJ, 547, 609

Faber, S. M., Willmer, C. N. A., Wolf, C., Koo, D. C., Weiner, B. J., Newman, J. A., Im, M., Coil, A. L., Conroy, C., Cooper, M. C., Davis, M., Finkbeiner, D. P., Gerke, B. F., Gebhardt, K., Groth, E. J., Guhathakurta, P., Harker, J., Kaiser, N., Kassin, S., Kleinheinrich, M., Konidaris, N. P., Kron, R. G., Lin, L., Luppino, G., Madgwick, D. S., Meisenheimer, K., Noeske, K. G., Phillips, A. C., Sarajedini, V. L., Schiavon, R. P., Simard, L., Szalay, A. S., Vogt, N. P., & Yan, R. 2007, ApJ, 665, 265

Fabian, A. C., Sanders, J. S., Ettori, S., Taylor, G. B., Allen, S. W., Crawford, C. S., Iwasawa, K., Johnstone, R. M., & Ogle, P. M. 2000, MNRAS, 318, L65

Fakhouri, O. & Ma, C. 2009, MNRAS, 394, 1825

Ferrarese, L. & Merritt, D. 2000, ApJL, 539, L9

Finlator, K. & Davé, R. 2008, MNRAS, 385, 2181

Finn, R. A., Balogh, M. L., Zaritsky, D., Miller, C. J., & Nichol, R. C. 2008, ApJ, 679, 279

Finoguenov, A., Connelly, J. L., Parker, L. C., Wilman, D. J., Mulchaey, J. S., Saglia, R. P., Balogh, M. L., Bower, R. G., & McGee, S. L. 2009, ApJ, 704, 564

Font, A. S., Bower, R. G., McCarthy, I. G., Benson, A. J., Frenk, C. S., Helly, J. C., Lacey, C. G., Baugh, C. M., & Cole, S. 2008a, MNRAS, 389, 1619

Font, A. S. et al. 2008b, ApJ, 673, 215

Forman, W., Kellogg, E., Gursky, H., Tananbaum, H., & Giacconi, R. 1972, ApJ, 178, 309

Frieman, J. A. et al. 2008, AJ, 135, 338

Fukugita, M., Shimasaku, K., & Ichikawa, T. 1995, PASP, 107, 945

Gal-Yam, A., Maoz, D., Guhathakurta, P., & Filippenko, A. V. 2003, AJ, 125, 1087

Gerke, B. F., Newman, J. A., Faber, S. M., Cooper, M. C., Croton, D. J., Davis, M., Willmer, C. N. A., Yan, R., Coil, A. L., Guhathakurta, P., Koo, D. C., & Weiner, B. J. 2007, MNRAS, 376, 1425

Gilbank, D. G., Baldry, I. K., Balogh, M. L., Glazebrook, K., & Bower, R. G. 2010a, MNRAS, 626

Gilbank, D. G. & Balogh, M. L. 2008, MNRAS, 385, L116

Gilbank, D. G., Balogh, M. L., Glazebrook, K., Bower, R. G., Baldry, I. K., Davies, G. T., Hau, G. K. T., Li, I. H., & McCarthy, P. 2010b, MNRAS, 704

Gladders, M. D. & Yee, H. K. C. 2000, AJ, 120, 2148

Gómez, P. L., Nichol, R. C., Miller, C. J., Balogh, M. L., Goto, T., Zabludoff, A. I., Romer, A. K., Bernardi, M., Sheth, R., Hopkins, A. M., Castander, F. J., Connolly, A. J., Schneider, D. P., Brinkmann, J., Lamb, D. Q., SubbaRao, M., & York, D. G. 2003, ApJ, 584, 210

Gonzalez, A. H., Zaritsky, D., & Zabludoff, A. I. 2007, ApJ, 666, 147

Gottlöber, S., Klypin, A., & Kravtsov, A. V. 2001, ApJ, 546, 223

Graham, M. L. et al. 2008, AJ, 135, 1343

Gunn, J. E. & Gott, III, J. R. 1972, ApJ, 176, 1

Haines, C. P., La Barbera, F., Mercurio, A., Merluzzi, P., & Busarello, G. 2006, ApJL, 647, L21

Hansen, S. M., Sheldon, E. S., Wechsler, R. H., & Koester, B. P. 2007, ArXiv e-prints,0710.3780, 710

Harker, G., Cole, S., Helly, J., Frenk, C., & Jenkins, A. 2006, MNRAS, 367, 1039

Hau, G. K. T., Bower, R. G., Kilborn, V., Forbes, D. A., Balogh, M. L., & Oosterloo, T. 2008, MNRAS, 385, 1965

Häussler, B., McIntosh, D. H., Barden, M., Bell, E. F., Rix, H.-W., Borch, A., Beckwith, S. V. W., Caldwell, J. A. R., Heymans, C., Jahnke, K., Jogee, S., Koposov, S. E., Meisenheimer, K., Sánchez, S. F., Somerville, R. S., Wisotzki, L., & Wolf, C. 2007, ApJS, 172, 615

Heckman, T. M., Armus, L., & Miley, G. K. 1990, ApJS, 74, 833

Helly, J. C., Cole, S., Frenk, C. S., Baugh, C. M., Benson, A., & Lacey, C. 2003, MNRAS, 338, 903

Hetterscheidt, M., Erben, T., Schneider, P., Maoli, R., van Waerbeke, L., & Mellier, Y. 2005, A&A, 442, 43

Holder, G. P., McCarthy, I. G., & Babul, A. 2007, MNRAS, 382, 1697

Holwerda, B. W., Keel, W. C., Williams, B., Dalcanton, J. J., & de Jong, R. S. 2009, AJ, 137, 3000

Homeier, N. L., Postman, M., Menanteau, F., Blakeslee, J. P., Mei, S., Demarco, R., Ford, H. C., Illingworth, G. D., & Zirm, A. 2006, AJ, 131, 143

Hopkins, A. M. 2004, ApJ, 615, 209

Hopkins, P. F., Bundy, K., Hernquist, L., & Ellis, R. S. 2007, ApJ, 659, 976

Hopkins, P. F., Cox, T. J., Kereš, D., & Hernquist, L. 2008, ApJS, 175, 390

Hopkins, P. F., Cox, T. J., Younger, J. D., & Hernquist, L. 2009, ApJ, 691, 1168

Hopkins, P. F., Hernquist, L., Cox, T. J., Di Matteo, T., Robertson, B., & Springel, V. 2006, ApJS, 163, 1

Huchra, J. P. & Geller, M. J. 1982, ApJ, 257, 423

Humason, M. L. 1936, ApJ, 83, 10

Im, M., Simard, L., Faber, S. M., Koo, D. C., Gebhardt, K., Willmer, C. N. A., Phillips, A. C., Illingworth, G. D., Vogt, N. P., & Sarajedini, V. L. 2002, ApJ, 571, 136

Ivezić, Ž., Lupton, R. H., Schlegel, D., Boroski, B., Adelman-McCarthy, J., Yanny, B., Kent, S., Stoughton, C., Finkbeiner, D., Padmanabhan, N., Rockosi, C. M., Gunn, J. E., Knapp, G. R., Strauss, M. A., Richards, G. T., Eisenstein, D., Nicinski, T., Kleinman, S. J., Krzesinski, J., Newman, P. R., Snedden, S., Thakar, A. R., Szalay, A., Munn, J. A., Smith, J. A., Tucker, D., & Lee, B. C. 2004, Astronomische Nachrichten, 325, 583

Ivezic, Z., Tyson, J. A., Allsman, R., Andrew, J., Angel, R., & for the LSST Collaboration. 2008, ArXiv e-prints

Jeltema, T. E., Binder, B., & Mulchaey, J. S. 2008, ApJ, 679, 1162

Jeltema, T. E., Mulchaey, J. S., Lubin, L. M., & Fassnacht, C. D. 2007, ApJ, 658, 865

Jenkins, A., Frenk, C. S., White, S. D. M., Colberg, J. M., Cole, S., Evrard, A. E., Couchman, H. M. P., & Yoshida, N. 2001, MNRAS, 321, 372

Johnston, D. E., Sheldon, E. S., Wechsler, R. H., Rozo, E., Koester, B. P., Frieman, J. A., McKay, T. A., Evrard, A. E., Becker, M. R., & Annis, J. 2007, ArXiv e-prints

Kaiser, N. 1984, ApJL, 284, L9

Kannappan, S. J., Guie, J. M., & Baker, A. J. 2009, AJ, 138, 579

Kauffmann, G. 1995, MNRAS, 274, 161

Kauffmann, G. & Haehnelt, M. 2000, MNRAS, 311, 576

Kauffmann, G., Heckman, T. M., Tremonti, C., Brinchmann, J., Charlot, S., White, S. D. M., Ridgway, S. E., Brinkmann, J., Fukugita, M., Hall, P. B., Ivezić, Ž., Richards, G. T., & Schneider, D. P. 2003a, MNRAS, 346, 1055

Kauffmann, G., White, S. D. M., & Guiderdoni, B. 1993, MNRAS, 264, 201

Kauffmann, G., White, S. D. M., Heckman, T. M., Ménard, B., Brinchmann, J., Charlot, S., Tremonti, C., & Brinkmann, J. 2004, MNRAS, 353, 713

Kauffmann, G. et al. 2003b, MNRAS, 341, 33

Kawata, D. & Mulchaey, J. S. 2008, ApJL, 672, L103

Kay, S. T., da Silva, A. C., Aghanim, N., Blanchard, A., Liddle, A. R., Puget, J.-L., Sadat, R., & Thomas, P. A. 2007, MNRAS, 377, 317

Kenney, J. D. P. & Koopmann, R. A. 1999, AJ, 117, 181

Kenney, J. D. P., van Gorkom, J. H., & Vollmer, B. 2004, AJ, 127, 3361

Kennicutt, Jr., R. C. 1998, ApJ, 498, 541

Kimm, T., Somerville, R. S., Yi, S. K., van den Bosch, F. C., Salim, S., Fontanot, F., Monaco, P., Mo, H., Pasquali, A., Rich, R. M., & Yang, X. 2009, MNRAS, 394, 1131

Kodama, T. & Bower, R. G. 2001, MNRAS, 321, 18

Komatsu, E., Dunkley, J., Nolta, M. R., Bennett, C. L., Gold, B., Hinshaw, G., Jarosik, N., Larson, D., Limon, M., Page, L., Spergel, D. N., Halpern, M., Hill, R. S., Kogut, A., Meyer, S. S., Tucker, G. S., Weiland, J. L., Wollack, E., & Wright, E. L. 2009, ApJS, 180, 330

Kovac, K. et al. 2009, ArXiv e-prints

Kroupa, P. 2001, MNRAS, 322, 231

Kubo, J. M., Stebbins, A., Annis, J., Dell'Antonio, I. P., Lin, H., Khiabanian, H., & Frieman, J. A. 2007, ApJ, 671, 1466

Lacey, C. & Cole, S. 1993, MNRAS, 262, 627

Larson, R. B., Tinsley, B. M., & Caldwell, C. N. 1980, ApJ, 237, 692

Lavery, R. J. & Henry, J. P. 1986, ApJL, 304, L5

Law, D. R., Johnston, K. V., & Majewski, S. R. 2005, ApJ, 619, 807

Lemaux, B. C., Lubin, L. M., Shapley, A., Kocevski, D., Gal, R. R., & Squires, G. K. 2010, ApJ, 716, 970

Lewis, I., Balogh, M., De Propris, R., Couch, W., Bower, R., Offer, A., Bland-Hawthorn, J., Baldry, I. K., Baugh, C., Bridges, T., Cannon, R., Cole, S., Colless, M., Collins, C., Cross, N., Dalton, G., Driver, S. P., Efstathiou, G., Ellis, R. S., Frenk, C. S., Glazebrook, K., Hawkins, E., Jackson, C., Lahav, O., Lumsden, S., Maddox, S., Madgwick, D., Norberg, P., Peacock, J. A., Percival, W., Peterson, B. A., Sutherland, W., & Taylor, K. 2002, MNRAS, 334, 673

Li, A. & Draine, B. T. 2001, ApJ, 554, 778

Li, Y., Mo, H. J., & Gao, L. 2008, MNRAS, 389, 1419

Lilly, S. J., Le Fevre, O., Hammer, F., & Crampton, D. 1996, ApJL, 460, L1+

Lin, L., Cooper, M. C., Jian, H., Koo, D. C., Patton, D. R., Yan, R., Willmer, C. N. A., Coil, A. L., Chiueh, T., Croton, D. J., Gerke, B. F., Lotz, J., Guhathakurta, P., & Newman, J. A. 2010, ArXiv e-prints

Lin, Y., Mohr, J. J., & Stanford, S. A. 2004, ApJ, 610, 745

Liske, J., Lemon, D. J., Driver, S. P., Cross, N. J. G., & Couch, W. J. 2003, MNRAS, 344, 307

Lotz, J. M., Primack, J., & Madau, P. 2004, AJ, 128, 163

Lu, T., Gilbank, D. G., Balogh, M. L., & Bognat, A. 2009, ArXiv e-prints, 0905.3392

Madau, P., Ferguson, H. C., Dickinson, M. E., Giavalisco, M., Steidel, C. C., & Fruchter, A. 1996, MNRAS, 283, 1388

Magorrian, J., Tremaine, S., Richstone, D., Bender, R., Bower, G., Dressler, A., Faber, S. M., Gebhardt, K., Green, R., Grillmair, C., Kormendy, J., & Lauer, T. 1998, AJ, 115, 2285

Mannucci, F. et al. 2005, A&A, 433, 807

Marleau, F. R. & Simard, L. 1998, ApJ, 507, 585

Martin, D. C., Fanson, J., Schiminovich, D., Morrissey, P., Friedman, P. G., Barlow, T. A., Conrow, T., Grange, R., Jelinsky, P. N., Milliard, B., Siegmund, O. H. W., Bianchi, L., Byun, Y., Donas, J., Forster, K., Heckman, T. M., Lee, Y., Madore, B. F., Malina, R. F., Neff, S. G., Rich, R. M., Small, T., Surber, F., Szalay, A. S., Welsh, B., & Wyder, T. K. 2005, ApJL, 619, L1

Mathis, J. S., Rumpl, W., & Nordsieck, K. H. 1977, ApJ, 217, 425

McCarthy, I. G., Babul, A., Bower, R. G., & Balogh, M. L. 2008a, MNRAS, 386, 1309

McCarthy, I. G., Balogh, M. L., Babul, A., Poole, G. B., & Horner, D. J. 2004, ApJ, 613, 811

McCarthy, I. G., Bower, R. G., & Balogh, M. L. 2007, MNRAS, 377, 1457

McCarthy, I. G., Frenk, C. S., Font, A. S., Lacey, C. G., Bower, R. G., Mitchell, N. L., Balogh, M. L., & Theuns, T. 2008b, MNRAS, 383, 593

McGee, S. L. & Balogh, M. L. 2010a, MNRAS, 403, L79

—. 2010b, MNRAS, 607

McGee, S. L., Balogh, M. L., Bower, R. G., Font, A. S., & McCarthy, I. G. 2009, MNRAS, 400, 937

McGee, S. L., Balogh, M. L., Henderson, R. D. E., Wilman, D. J., Bower, R. G., Mulchaey, J. S., & Oemler, A. J. 2008, MNRAS, 387, 1605

McIntosh, D., Rix, H.-W., & Caldwell, N. 2004, ApJ, 610, 161

McNamara, B. R. & Nulsen, P. E. J. 2007, ARA&A, 45, 117

McNamara, B. R., Wise, M., Nulsen, P. E. J., David, L. P., Sarazin, C. L., Bautz, M., Markevitch, M., Vikhlinin, A., Forman, W. R., Jones, C., & Harris, D. E. 2000, ApJL, 534, L135

Menanteau, F., Ford, H. C., Motta, V., Benítez, N., Martel, A. R., Blakeslee, J. P., & Infante, L. 2006, AJ, 131, 208

Ménard, B., Kilbinger, M., & Scranton, R. 2009a, ArXiv e-prints

Ménard, B., Nestor, D., Turnshek, D., Quider, A., Richards, G., Chelouche, D., & Rao, S. 2008, MNRAS, 385, 1053

Ménard, B., Scranton, R., Fukugita, M., & Richards, G. 2009b, ArXiv e-prints

Metropolis, N., Rosenbluth, A., Rosenbluth, M., Teller, A., & Teller, E. 1953, Journal of Chemical Physics, 21, 1087

Meurer, G. R., Heckman, T. M., Leitherer, C., Kinney, A., Robert, C., & Garnett, D. R. 1995, AJ, 110, 2665

Mihos, J. C. & Hernquist, L. 1996, ApJ, 464, 641

Miller, C. J., Nichol, R. C., Reichart, D., Wechsler, R. H., Evrard, A. E., Annis, J., McKay, T. A., Bahcall, N. A., Bernardi, M., Boehringer, H., Connolly, A. J., Goto, T., Kniazev, A., Lamb, D., Postman, M., Schneider, D. P., Sheth, R. K., & Voges, W. 2005, AJ, 130, 968

Milne, M. L. et al. 2007, AJ, 133, 177

Miyazaki, S., Hamana, T., Ellis, R. S., Kashikawa, N., Massey, R. J., Taylor, J., & Refregier, A. 2007, ApJ, 669, 714

Momcheva, I., Williams, K., Keeton, C., & Zabludoff, A. 2006, ApJ, 641, 169

Montier, L. A. & Giard, M. 2005, A&A, 439, 35

Moore, B., Katz, N., Lake, G., Dressler, A., & Oemler, A. 1996, Nature, 379, 613

Moore, B., Lake, G., & Katz, N. 1998, ApJ, 495, 139

Morrissey, P., Conrow, T., Barlow, T. A., Small, T., Seibert, M., Wyder, T. K., Budavári, T., Arnouts, S., Friedman, P. G., Forster, K., Martin, D. C., Neff, S. G., Schiminovich, D., Bianchi, L., Donas, J., Heckman, T. M., Lee, Y., Madore, B. F., Milliard, B., Rich, R. M., Szalay, A. S., Welsh, B. Y., & Yi, S. K. 2007, ApJS, 173, 682

Moustakas, J., Kennicutt, Jr., R. C., & Tremonti, C. A. 2006, ApJ, 642, 775

Mulchaey, J. S., Lubin, L. M., Fassnacht, C., Rosati, P., & Jeltema, T. E. 2006, ApJ, 646, 133

Muller, S., Wu, S.-Y., Hsieh, B.-C., González, R. A., Loinard, L., Yee, H. K. C., & Gladders, M. D. 2008, ApJ, 680, 975

Natarajan, P., Kneib, J.-P., Smail, I., Treu, T., Ellis, R., Moran, S., Limousin, M., & Czoske, O. 2007, ArXiv e-prints, 0711.4587

Noeske, K. G., Weiner, B. J., Faber, S. M., Papovich, C., Koo, D. C., Somerville, R. S., Bundy, K., Conselice, C. J., Newman, J. A., Schiminovich, D., Le Floc'h, E., Coil, A. L., Rieke, G. H., Lotz, J. M., Primack, J. R., Barmby, P., Cooper, M. C., Davis, M., Ellis, R. S., Fazio, G. G., Guhathakurta, P., Huang, J., Kassin, S. A., Martin, D. C., Phillips, A. C., Rich, R. M., Small, T. A., Willmer, C. N. A., & Wilson, G. 2007, ApJL, 660, L43

O'Donnell, J. E. 1994, ApJ, 422, 158

Oemler, Jr., A. 1974, ApJ, 194, 1

Oguri, M., Hennawi, J. F., Gladders, M. D., Dahle, H., Natarajan, P., Dalal, N., Koester, B. P., Sharon, K., & Bayliss, M. 2009, ApJ, 699, 1038

Oke, J. B. & Gunn, J. E. 1983, ApJ, 266, 713

Oosterloo, T. & van Gorkom, J. 2005, A&A, 437, L19

Parker, L. C., Hudson, M. J., Carlberg, R. G., & Hoekstra, H. 2005, ApJ, 634, 806

Pasquali, A., van den Bosch, F. C., Mo, H. J., Yang, X., & Somerville, R. 2009, MNRAS, 394, 38

Patton, D. R., Grant, J. K., Simard, L., Pritchet, C. J., Carlberg, R. G., & Borne, K. D. 2005, AJ, 130, 2043

Pavlovsky et. al, C. 2005, ACS Data Handbook, Version 4.0 (Baltimore: STScI)

Pei, Y. C. 1992, ApJ, 395, 130

Peng, C. Y., Ho, L. C., Impey, C. D., & Rix, H.-W. 2002, AJ, 124, 266

Peng, Y. et al. 2010, ArXiv e-prints

Perlmutter, S., Aldering, G., Goldhaber, G., Knop, R. A., Nugent, P., Castro, P. G., Deustua, S., Fabbro, S., Goobar, A., Groom, D. E., Hook, I. M., Kim, A. G., Kim, M. Y., Lee, J. C., Nunes, N. J., Pain, R., Pennypacker, C. R., Quimby, R., Lidman, C., Ellis, R. S., Irwin, M., McMahon, R. G., Ruiz-Lapuente, P., Walton, N., Schaefer, B., Boyle, B. J., Filippenko, A. V., Matheson, T., Fruchter, A. S., Panagia, N., Newberg, H. J. M., Couch, W. J., & The Supernova Cosmology Project. 1999, ApJ, 517, 565

Pfrommer, C., Springel, V., Enßlin, T. A., & Jubelgas, M. 2006, MNRAS, 367, 113

Poggianti, B. M., Smail, I., Dressler, A., Couch, W. J., Barger, A. J., Butcher, H., Ellis, R. S., & Oemler, A. J. 1999, ApJ, 518, 576

Poggianti, B. M., von der Linden, A., De Lucia, G., Desai, V., Simard, L., Halliday, C., Aragón-Salamanca, A., Bower, R., Varela, J., Best, P., Clowe, D. I., Dalcanton, J., Jablonka, P., Milvang-Jensen, B., Pello, R., Rudnick, G., Saglia, R., White, S. D. M., & Zaritsky, D. 2006, ApJ, 642, 188

Postman, M. & Geller, M. J. 1984, ApJ, 281, 95

Press, W. H. & Schechter, P. 1974, ApJ, 187, 425

Prevot, M. L., Lequeux, J., Prevot, L., Maurice, E., & Rocca-Volmerange, B. 1984, A&A, 132, 389

Purcell, C. W., Bullock, J. S., & Zentner, A. R. 2007, ApJ, 666, 20

Quilis, V., Moore, B., & Bower, R. 2000, Science, 288, 1617

Rasmussen, J., Ponman, T. J., Mulchaey, J. S., Miles, T. A., & Raychaudhury, S. 2006, MNRAS, 373, 653

Reiprich, T. H. & Böhringer, H. 2002, ApJ, 567, 716

Richards, G. T. & others. 2002, AJ, 123, 2945

Rieke, G. H., Alonso-Herrero, A., Weiner, B. J., Pérez-González, P. G., Blaylock, M., Donley, J. L., & Marcillac, D. 2009, ApJ, 692, 556

Riess, A. G., Filippenko, A. V., Challis, P., Clocchiatti, A., Diercks, A., Garnavich, P. M., Gilliland, R. L., Hogan, C. J., Jha, S., Kirshner, R. P., Leibundgut, B., Phillips, M. M., Reiss, D., Schmidt, B. P., Schommer, R. A., Smith, R. C., Spyromilio, J., Stubbs, C., Suntzeff, N. B., & Tonry, J. 1998, AJ, 116, 1009

Romani, R. W. & Maoz, D. 1992, ApJ, 386, 36

Rykoff, E. S., Evrard, A. E., McKay, T. A., Becker, M. R., Johnston, D. E., Koester, B. P., Nord, B., Rozo, E., Sheldon, E. S., Stanek, R., & Wechsler, R. H. 2008a, MNRAS, 387, L28

Rykoff, E. S., McKay, T. A., Becker, M. R., Evrard, A., Johnston, D. E., Koester, B. P., Rozo, E., Sheldon, E. S., & Wechsler, R. H. 2008b, ApJ, 675, 1106

Sako, M. et al. 2008, AJ, 135, 348

Salim, S., Dickinson, M., Michael Rich, R., Charlot, S., Lee, J. C., Schiminovich, D., Pérez-González, P. G., Ashby, M. L. N., Papovich, C., Faber, S. M., Ivison, R. J., Frayer, D. T., Walton, J. M., Weiner, B. J., Chary, R., Bundy, K., Noeske, K., & Koekemoer, A. M. 2009, ApJ, 700, 161

Salim, S., Rich, R. M., Charlot, S., Brinchmann, J., Johnson, B. D., Schiminovich, D., Seibert, M., Mallery, R., Heckman, T. M., Forster, K., Friedman, P. G., Martin, D. C., Morrissey, P., Neff, S. G., Small, T., Wyder, T. K., Bianchi, L., Donas, J., Lee, Y., Madore, B. F., Milliard, B., Szalay, A. S., Welsh, B. Y., & Yi, S. K. 2007, ApJS, 173, 267

Sand, D. J. et al. 2008, AJ, 135, 1917

Scannapieco, E. & Bildsten, L. 2005, ApJL, 629, L85

Schade, D., Lilly, S. J., Crampton, D., LeFèvre, O., Hammer, F., & Tresse, L. 1995, ApJ, 451, 1

Scheick, X. & Kuhn, J. R. 1994, ApJ, 423, 566

Schlegel, D. J., Finkbeiner, D. P., & Davis, M. 1998, ApJ, 500, 525

Schneider, D. P. et al. 2007, AJ, 134, 102

Searle, L. & Zinn, R. 1978, ApJ, 225, 357

Seljak, U. & Zaldarriaga, M. 1996, ApJ, 469, 437

Sheldon, E. S., Johnston, D. E., Masjedi, M., McKay, T. A., Blanton, M. R., Scranton, R., Wechsler, R. H., Koester, B. P., Hansen, S. M., Frieman, J. A., & Annis, J. 2007a, ArXiv e-prints

Sheldon, E. S., Johnston, D. E., Scranton, R., Koester, B. P., McKay, T. A., Oyaizu, H., Cunha, C., Lima, M., Lin, H., Frieman, J. A., Wechsler, R. H., Annis, J., Mandelbaum, R., Bahcall, N. A., & Fukugita, M. 2007b, ArXiv e-prints

Shen, S., Mo, H. J., White, S. D. M., Blanton, M. R., Kauffmann, G., Voges, W., Brinkmann, J., & Csabai, I. 2003, MNRAS, 343, 978

Sheth, R. K. & Tormen, G. 2002, MNRAS, 329, 61

Simard, L., Willmer, C. N. A., Vogt, N. P., Sarajedini, V. L., Phillips, A. C., Weiner, B. J., Koo, D. C., Im, M., Illingworth, G. D., & Faber, S. M. 2002, ApJS, 142, 1

Simha, V., Weinberg, D. H., Dave, R., Gnedin, O. Y., Katz, N., & Keres, D. 2008, ArXiv e-prints, 0809.2999

Smith, G. P. & Taylor, J. E. 2008, ApJL, 682, L73

Somerville, R. S. & Primack, J. R. 1999, MNRAS, 310, 1087

Spergel, D. N. et al. 2007, ApJS, 170, 377

Spitzer, Jr., L. 1958, ApJ, 127, 17

Springel, V. 2005, MNRAS, 364, 1105

Springel, V., Di Matteo, T., & Hernquist, L. 2005a, MNRAS, 361, 776

Springel, V., White, S. D. M., Jenkins, A., Frenk, C. S., Yoshida, N., Gao, L., Navarro, J., Thacker, R., Croton, D., Helly, J., Peacock, J. A., Cole, S., Thomas, P., Couchman, H., Evrard, A., Colberg, J., & Pearce, F. 2005b, Nature, 435, 629

Staniszewski, Z. et al. 2009, ApJ, 701, 32

Stewart, K. R., Bullock, J. S., Wechsler, R. H., & Maller, A. H. 2009, ApJ, 702, 307

Stewart, K. R., Bullock, J. S., Wechsler, R. H., Maller, A. H., & Zentner, A. R. 2008, ApJ, 683, 597

Stickel, M., Klaas, U., Lemke, D., & Mattila, K. 2002, A&A, 383, 367

Stoughton, C. et al. 2002, AJ, 123, 485

Strateva, I. et al. 2001, AJ, 122, 1861

Strauss, M. A. et al. 2002, AJ, 124, 1810

Sun, M., Donahue, M., & Voit, G. M. 2007a, ApJ, 671, 190

Sun, M., Jones, C., Forman, W., Vikhlinin, A., Donahue, M., & Voit, M. 2007b, ApJ, 657, 197

Sun, M., Voit, G. M., Donahue, M., Jones, C., Forman, W., & Vikhlinin, A. 2008, ArXiv e-prints, 0805.2320

Sun, M. et al. 2009, ArXiv e-prints

Sunyaev, R. A. & Zeldovich, Y. B. 1972, Comments on Astrophysics and Space Physics, 4, 173

Taylor-Mager, V. A., Conselice, C. J., Windhorst, R. A., & Jansen, R. A. 2007, ApJ, 659, 162

Tegmark, M. et al. 2004, Phys. Rev. D, 69, 103501

Thanjavur, K., Crampton, D., & Willis, J. 2010, ApJ, 714, 1355

Thuan, T. X. & Kormendy, J. 1977, PASP, 89, 466

Toomre, A. & Toomre, J. 1972, ApJ, 178, 623

Tran, K.-V. H., Simard, L., Zabludoff, A. I., & Mulchaey, J. S. 2001, ApJ, 549, 172

Tremonti, C. A., Moustakas, J., & Diamond-Stanic, A. M. 2007, ApJL, 663, L77

Tucker, D. L., Annis, J. T., Lin, H., Kent, S., Stoughton, C., Peoples, J., Allam, S. S., Mohr, J. J., Barkhouse, W. A., Ngeow, C., Alam, T., Beldica, C., Cai, D., Daues, G., Plante, R., Miller, C., Smith, C., & Suntzeff, N. B. 2007, in Astronomical Society of the Pacific Conference Series, Vol. 364, The Future of Photometric, Spectrophotometric and Polarimetric Standardization, ed. C. Sterken, 187–+

van den Bosch, F. C. 2002, MNRAS, 331, 98

van der Wel, A., Bell, E. F., Holden, B. P., Skibba, R. A., & Rix, H. 2010, ApJ, 714, 1779

van Dokkum, P. G., Franx, M., Fabricant, D., Kelson, D. D., & Illingworth, G. D. 1999, ApJL, 520, L95

Vikhlinin, A., Markevitch, M., Murray, S. S., Jones, C., Forman, W., & Van Speybroeck, L. 2005, ApJ, 628, 655

Vikhlinin, A. et al. 2006, ApJ, 640, 691

Vollmer, B., Balkowski, C., Cayatte, V., van Driel, W., & Huchtmeier, W. 2004, A&A, 419, 35

Warren, M. S., Abazajian, K., Holz, D. E., & Teodoro, L. 2006, ApJ, 646, 881

Weingartner, J. C. & Draine, B. T. 2001, ApJ, 548, 296

Weinmann, S. M., van den Bosch, F. C., Yang, X., & Mo, H. J. 2006a, MNRAS, 366, 2

Weinmann, S. M., van den Bosch, F. C., Yang, X., Mo, H. J., Croton, D. J., & Moore, B. 2006b, MNRAS, 372, 1161

White, P. M. et al. 2003, ApJ, 585, 739

White, S. D. M. & Frenk, C. S. 1991, ApJ, 379, 52

White, S. D. M., Navarro, J. F., Evrard, A. E., & Frenk, C. S. 1993, Nature, 366, 429

White, S. D. M. & Rees, M. J. 1978, MNRAS, 183, 341

Willman, B., Governato, F., Wadsley, J., & Quinn, T. 2004, MNRAS, 355, 159

Wilman, D. J., Balogh, M. L., Bower, R. G., Mulchaey, J. S., Oemler, A., Carlberg, R. G., Eke, V. R., Lewis, I., Morris, S. L., & Whitaker, R. J. 2005a, MNRAS, 358, 88

Wilman, D. J., Balogh, M. L., Bower, R. G., Mulchaey, J. S., Oemler, A., Carlberg, R. G., Morris, S. L., & Whitaker, R. J. 2005b, MNRAS, 358, 71

Wilman, D. J., Oemler, A., Mulchaey, J. S., McGee, S. L., Balogh, M. L., & Bower, R. G. 2009, ApJ, 692, 298

Wilman, D. J., Pierini, D., Tyler, K., McGee, S. L., Oemler, Jr., A., Morris, S. L., Balogh, M. L., Bower, R. G., & Mulchaey, J. S. 2008, ApJ, 680, 1009

Wise, M. W., O'Connell, R. W., Bregman, J. N., & Roberts, M. S. 1993, ApJ, 405, 94

Wittman, D., Tyson, J. A., Margoniner, V. E., Cohen, J. G., & Dell'Antonio, I. P. 2001, ApJL, 557, L89

Wolf, C., Aragón-Salamanca, A., Balogh, M., Barden, M., Bell, E. F., Gray, M. E., Peng, C. Y., Bacon, D., Barazza, F. D., Böhm, A., Caldwell, J. A. R., Gallazzi, A., Häußler, B., Heymans, C., Jahnke, K., Jogee, S., van Kampen, E., Lane, K., McIntosh, D. H., Meisenheimer, K., Papovich, C., Sánchez, S. F., Taylor, A., Wisotzki, L., & Zheng, X. 2009, MNRAS, 393, 1302

Wolf, C., Bell, E. F., McIntosh, D. H., Rix, H.-W., Barden, M., Beckwith, S. V. W., Borch, A., Caldwell, J. A. R., Häussler, B., Heymans, C., Jahnke, K., Jogee, S., Meisenheimer, K., Peng, C. Y., Sánchez, S. F., Somerville, R. S., & Wisotzki, L. 2005, ApJ, 630, 771

Yan, R., Newman, J. A., Faber, S. M., Konidaris, N., Koo, D., & Davis, M. 2006, ApJ, 648, 281

Yang, X., Mo, H. J., & van den Bosch, F. C. 2009, ApJ, 695, 900

Yang, X., Mo, H. J., van den Bosch, F. C., & Jing, Y. P. 2005, MNRAS, 356, 1293

Yang, X. et al. 2007, ApJ, 671, 153

Yanny, B. et al. 2000, ApJ, 540, 825

Yee, H. K. C., Morris, S. L., Lin, H., Carlberg, R. G., Hall, P. B., Sawicki, M., Patton, D. R., Wirth, G. D., Ellingson, E., & Shepherd, C. W. 2000, ApJS, 129, 475

Zabludoff, A. I. & Mulchaey, J. S. 1998, ApJ, 496, 39

Zackrisson, E., Micheva, G., & Ostlin, G. 2009, ArXiv e-prints

Zheng, C. et al. 2008, AJ, 135, 1766

Zibetti, S., White, S. D. M., Schneider, D. P., & Brinkmann, J. 2005, MNRAS, 358, 949

Zwicky, F. 1938, PASP, 50, 218

—. 1939, Proceedings of the National Academy of Science, 25, 604

—. 1951, PASP, 63, 61